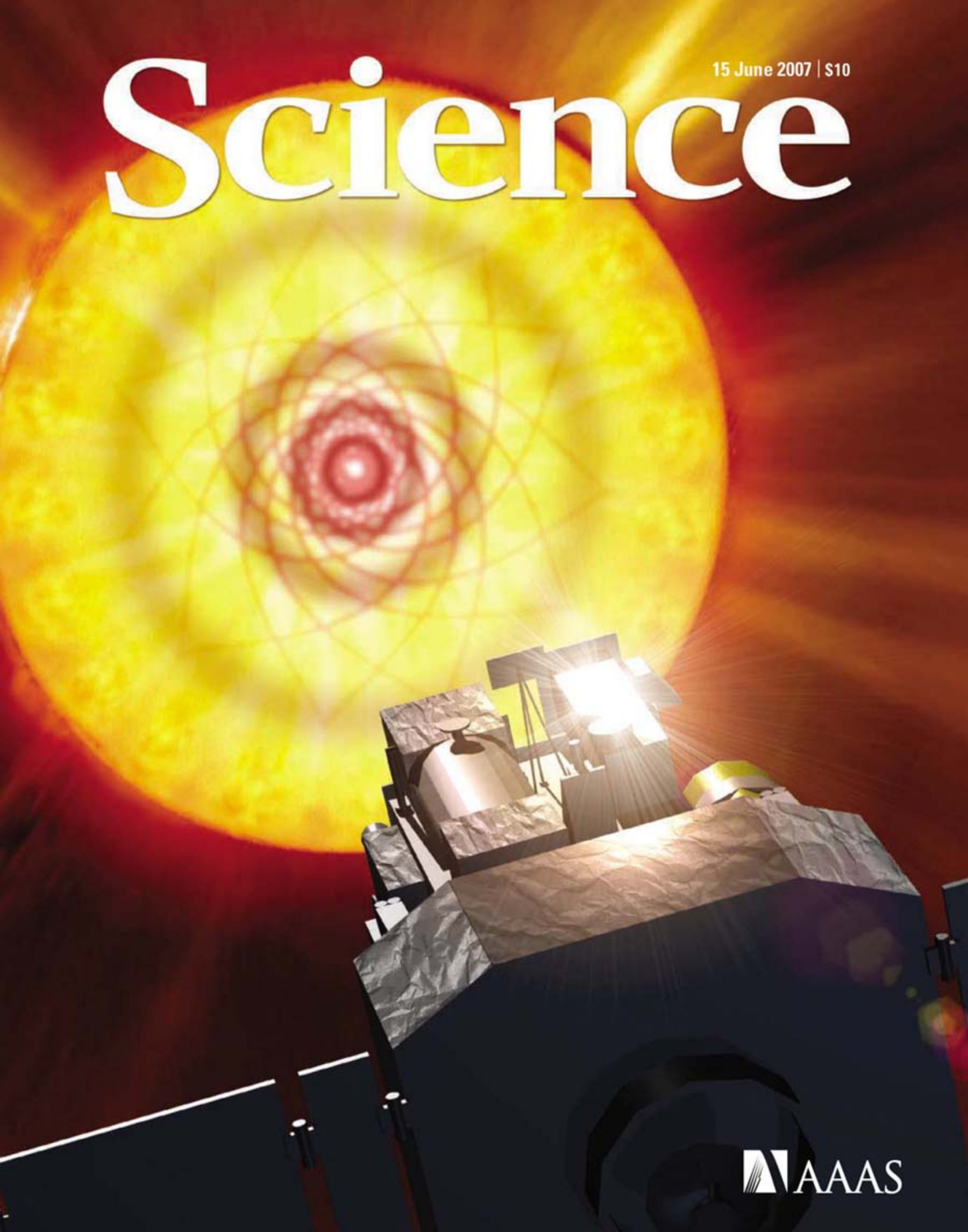


15 June 2007 | S10

Science



 AAAS



Brilliant Combination.

Stratagene Mx™ QPCR systems + next generation Brilliant® II reagents = the perfect pair.

Our complete quantitative PCR portfolio features products that include sample preparation, cDNA synthesis, QPCR amplification and detection, and powerful data analysis software to meet today's research needs as well as tomorrow's future applications. Couple our Mx™ line of high performance real-time QPCR systems with our next generation Brilliant® II QPCR reagents and there's no need to look any further than Stratagene for your QPCR research needs.

- **Brilliant® II reagents are designed for earlier Ct detection, improved reproducibility, and dynamic range**
- **Four- or five-color Mx™ QPCR systems with powerful MxPro™ QPCR Software**
- **Complete QPCR portfolio of instruments, reagents, service, and support**

For more information about our Brilliant® II QPCR reagents or Mx™ QPCR systems, please visit www.stratagene.com/MxQPCR.

Brilliant® is a registered trademark of Stratagene in the United States.
Mx™ and MxPro™ are trademarks of Stratagene in the United States.

Stratagene US and Canada

Order: 800-424-5444 x3
Technical Service: 800-894-1304 x2

Stratagene Europe

Order: 00800-7000-7000
Technical Service: 00800-7400-7400

Stratagene Japan K.K.

Order: 3-5821-8077
Technical Service: 3-5821-8076





Cytokine Center

Browse our web site with over 1300 proteins, including recombinant cytokines, growth factors, chemokines and neurotrophins. Daily shipping and competitive pricing are offered. Bulk quantities of many proteins available.

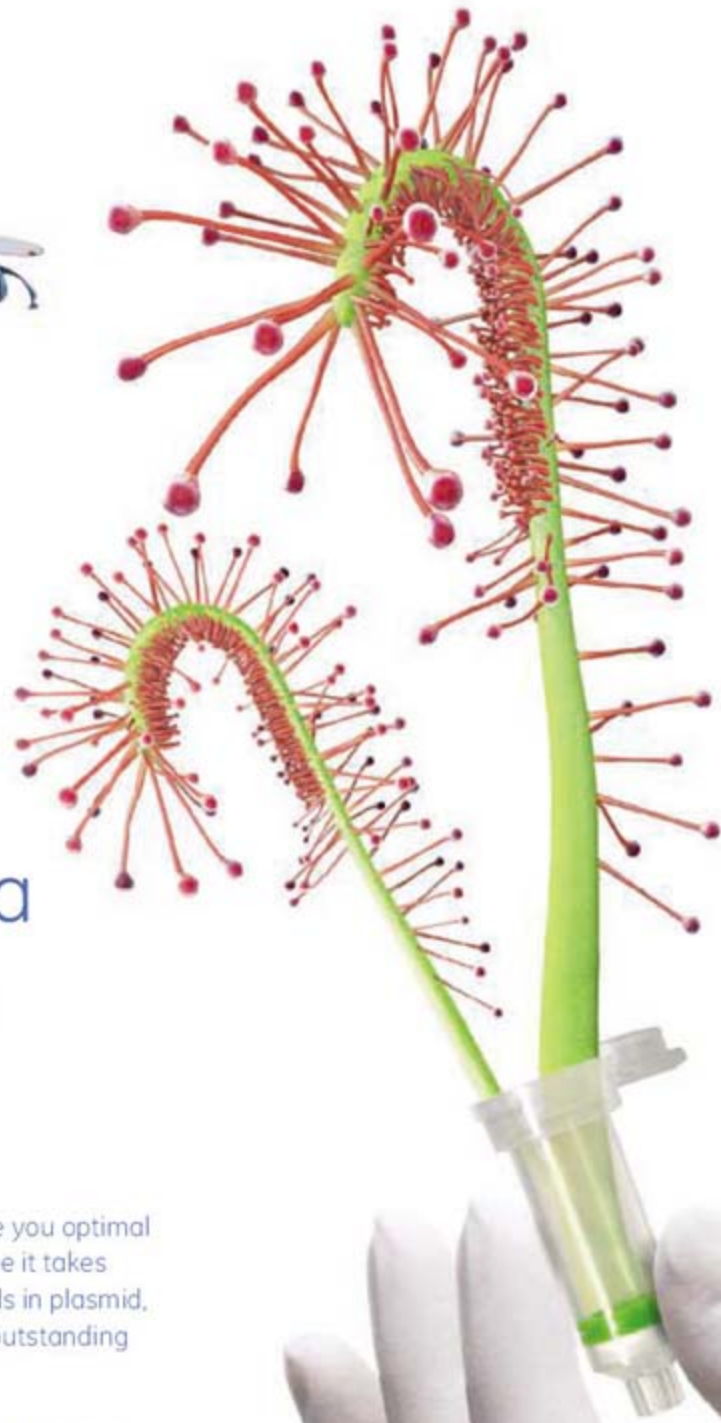


- IL-17E
- IL-17F
- IL-19
- IL-20
- IL-21
- IL-22
- IL-31
- Insulin
- IP-10
- JE
- JNK2a1
- JNK2a2
- KC / CXCL1
- KGF
- L-asparaginase
- LAG-1
- LALF Peptide
- LAR-PTP
- LBP
- LC-1
- LD-78β
- LDH
- LEC / NCC-4
- Leptin
- LIGHT
- LIX
- LKM
- LL-37
- Lungkine / CXCL15
- Lymphotactin
- sLYVE-1
- M-CSF
- MCP-1 (MCAF)
- MCP-2
- MCP-3
- MCP-4
- MCP-5
- MDC (67 a.a.)
- MDC (69 a.a.)
- MDH
- MEC
- Mek-1
- MIA
- Midkine
- MIG / CXCL9
- MIP-1α / CCL3
- MIP-1β / CCL4
- MIP-3 / CCL23
- MIP-3α / CCL20
- MIP-3β / CCL19
- MIP-4 (PARC) / CCL18
- MIP-5 / CCL15
- MMP-3
- MMP-7
- MMP-13
- Myostatin
- Nanog
- NAP-2
- Neurturin
- NFAT-1
- β-NGF
- NOGGIN
- NOV
- NP-1
- NT-1/BCSF-3
- NT-3
- NT-4
- Ocreotide
- Oncostatin M
- Osteoprotegerin (OPG)
- OTOR
- Oxytocin
- p38-α
- PAI-1
- Parathyroid Hormone
- PDGF-AA
- PDGF-AB
- PDGF-BB
- PDGF-CC
- Persephin
- PF-4
- PIGF-1
- PIGF-2
- PKA α-subunit
- PKC-α
- PKC-γ
- Pleiotrophin
- PLGF-1
- Polymyxin B (PMB)
- PRAS40
- PRL-1
- PRL-2
- PRL-3
- Prokineticin-2
- Prolactin
- Protirelin
- PTHrP
- PTP1B
- PTP-IA2
- PTP-MEG2
- PTP-PEST
- sRANK
- sRANKL
- RANTES
- RELM-α
- RELM-β
- Resistin
- RPTPβ
- RPTPγ
- RPTPμ
- SCF
- SCGF-α
- SCGF-β
- SDF-1α
- SDF-1β
- Secretin
- SF20
- SHP-2
- STAT1
- c-Src
- TACI
- TARC
- TC-PTP
- TECK
- TFF2
- TGF-α
- TGF-β1
- TGF-β2
- TGF-β3
- Thymosin α1
- sTIE-1/Fc Chimera
- sTIE-2/Fc Chimera
- TL-1A
- TNF-α
- TNF-β
- sTNF-receptor Type I
- sTNF-receptor Type II
- TPO
- sTRAIL R-1 (DR4)
- sTRAIL R-2 (DR5)
- TRAIL/Apo2L
- TSG
- TSH
- TSLP
- TWEAK
- TWEAK Receptor
- Urokinase
- EG-VEGF
- VEGF121
- VEGF145
- VEGF165
- VEGF-C
- VEGF-C I125
- VEGF-E
- HB-VEGF-E
- sVEGFR-1
- sVEGFR-2
- sVEGFR-3
- Visfatin
- WISP-1
- WISP-2
- WISP-3
- WNT-1

PROTEINS

- 4-1BBL
- 4-1BB Receptor
- 6 Ckine
- ACAD8
- ACAT2
- gAcrp30/Adipolean
- Activin A
- Activin B
- ACY1
- ADAT1
- Adiponectin
- ADRP
- AITRL
- Akt1
- Alpha-Feto Protein (AFP)
- Alpha-Galactosidase A
- Angiopoietin-1 (Ang-1)
- Angiopoietin-2 (Ang-2)
- Angiostatin K1-3
- Annexin-V
- apo-SAA
- Apolipoprotein A-1
- Apolipoprotein E2
- Apolipoprotein E3
- Apolipoprotein E4
- APRIL
- Artemin
- ATF2
- Aurora A
- Aurora B
- BAFF
- BAFF Receptor
- BCA-1 / BLC / CXCL13
- BCMA
- BD-1
- BD-2
- BD-3
- BDNF
- Betacellulin
- Bivalirudin
- BMP-2
- BMP-4
- BMP-6
- BMP-7
- BMP-13
- sBMPR-1A
- Brain Natriuretic Protein
- BRAK
- Breast Tumor Antigen
- C5a
- C5L2 Peptide
- C-10
- C-Reactive Protein
- C-Src
- Calbindin D-9K
- Calbindin D-28K
- Calbindin D-29K
- Calmodulin
- Calcitonin Acetate
- Carbonic Anhydrase III
- Carcino-embryonic Antigen
- Cardiotrophin-1
- Caspase-3
- Caspase-6
- CD4
- CD14
- CD22
- CD40 Ligand / TRAP
- CD95 / sFas Ligand
- CD105 / Endoglin
- CHIPS
- CNTF
- Collagen
- CREB
- CTACK / CCL27
- CTGF
- CTGFL / WISP-2
- CTLA-4 / Fc
- CXCL16
- CYR61
- Cytokeratin 8
- DEP-1
- Desmopressin
- Disulfide Oxidoreductase
- E-selectin
- ECGF
- EGF
- Elafin / SKALP
- EMAP-II
- ENA-78 / CXCL5
- Endostatin
- Enteropeptidase
- Eotaxin / CCL11
- Eotaxin-2
- Eotaxin-3 (TSC)
- EPHB2
- EPHB4
- Epigen
- Epiregulin
- Eptifibatide
- Erk-2
- Erythropoietin (EPO)
- Exodus-2
- Fas Ligand
- Fas Receptor
- FGF-1 (acidic)
- FGF-2 (basic)
- FGF-4
- FGF-5
- FGF-6
- FGF-7 / KGF
- FGF-8
- FGF-9
- FGF-10
- FGF-16
- FGF-17
- FGF-18
- FGF-19
- FGF-20
- sFGFR-1 (IIIc) / Fc Chimera
- sFGFR-2 (IIIc) / Fc Chimera
- sFGFR-3 / Fc Chimera
- sFGFR-4 / Fc Chimera
- sFlt-1 (native)
- sFlt-1 (D3)
- sFlt-1 (D4)
- sFlt-1 (D5)
- sFlt-1 (D7)
- Flt3-Ligand
- sFlt-4
- sFlt-4 / Fc Chimera
- Follistatin
- FSH
- Fractalkine / CX3C
- G-CSF
- α-Galactosidase A
- Galectin-1

- Galectin-3
- Gastrointestinal CA
- GCP-2
- GDF-3
- GDF-9
- GDF-11
- GDNF
- GLP-1
- Glucagon
- GM-CSF
- Goserelin
- GPBB
- Granzyme B
- GROα
- GROβ
- GROγ
- GRO/MGSA
- Growth Hormone
- Growth Hormone BP
- GST-p21/WAF-1
- HB-EGF
- HCC-1
- HGF
- Histidyl-tRNA synthetase
- Histrelin
- HRG1-β1
- I-309
- I-TAC
- IFN-α
- IFN-α A
- IFN-α 2a
- IFN-α 2b
- IFN-β
- IFN-γ
- IFN-Omega
- IGF-I
- IGF-II
- proIGF-II
- IGFBP-1
- IGFBP-2
- IGFBP-3
- IGFBP-4
- IGFBP-5
- IGFBP-6
- IGFBP-7
- IL-1α
- IL-1β
- IL-2
- IL-3
- IL-4
- sIL-4 Receptor
- IL-5
- IL-6
- sIL-6 Receptor
- IL-7
- IL-8 (72 a.a.)
- IL-8 (77 a.a.)
- IL-9
- IL-10
- IL-11
- IL-12
- IL-13
- IL-13 analog
- IL-15
- IL-16 (121 a.a.)
- IL-16 (130 a.a.)
- IL-17
- IL-17B
- IL-17D



Get attached to illustra for faster nucleic acid sample prep.

New illustra™ nucleic acid sample prep kits from GE Healthcare give you optimal yield and purity. What's more, they do this in as little as half the time it takes the best competing products. Whether you're purifying nucleic acids in plasmid, blood, tissue, cells or bacteria, you'll find that superior results and outstanding reproducibility come easily with illustra mini and midi kits.

With more than 20 years' experience in nucleic acid research, we're bringing science to life and helping transform healthcare. We call it Life Science Re-imagined.

www.gelifesciences.com/illustra

Speed is crucial to the sundew plant's success.
It reacts rapidly, bending its tentacles to bind its prey.
Some species can do this in just tenths of a second.





COVER

Artist's view of the Sun's core, showing gravity waves inferred from observations with the Global Oscillation at Low Frequency instrument aboard the Solar and Heliospheric Observatory. These signatures of solar gravity provide clues about the rotation rate of the solar core. See [page 1591](#).

Image: G. Pérez, SMM/IAC

DEPARTMENTS

- 1535 [Science Online](#)
- 1537 [This Week in Science](#)
- 1542 [Editors' Choice](#)
- 1544 [Contact Science](#)
- 1547 [Random Samples](#)
- 1549 [Newsmakers](#)
- 1635 [New Products](#)
- 1636 [Science Careers](#)

EDITORIAL

- 1541 [Nuclear Weapons Nonproliferation](#)
by Raymond Jeanloz

NEWS OF THE WEEK

- Heart Attack Risk Overshadows a Popular Diabetes Therapy 1550
- Delay in Europe Could Mean Extra Year for U.S. Collider 1551
- Bush Boosts AIDS Relief: Cause for Applause and Pause 1552
- Initiative Aims to Merge Animal and Human Health Science to Benefit Both 1553

SCIENCE SCOPE

- AIDSTruth.org Web Site Takes Aim at 'Denialists' 1554
- River-Level Forecasting Shows No Detectable Progress in 2 Decades 1555
- DNA Study Forces Rethink of What It Means to Be a Gene 1556
- Attempt to Patent Artificial Organism Draws a Protest 1556

NEWS FOCUS

- Food for Thought 1558
Swapping Guts for Brains
- Florida Red Tide Brews Up Drug Lead for Cystic Fibrosis 1561
- Stalking a Volcanic Torrent 1562



1558

LETTERS

- Culture, Conflict, and... Climate? 1564
M. D. Drapeau and B. K. Mignone
- Better Use of Existing Knowledge C. Batich
- Grazing and "Degradation" C. Hamblin et al.
- Response L. Gillson and M. T. Hoffman
- A Brief History of the FFAG Accelerator
L. W. Jones, A. M. Sessler, K. R. Symon

BOOKS ET AL.

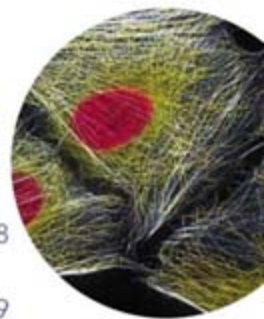
- [Culturing Life](#) How Cells Became Technologies 1568
H. Landecker, reviewed by M. S. Lindee
- [Folsom](#) New Archaeological Investigations of a Classic Paleoindian Bison Kill 1569
D. J. Meltzer, reviewed by D. Stanford

POLICY FORUM

- Sustainable Development of the Agricultural Bio-Economy 1570
N. Jordan et al.

PERSPECTIVES

- Recent Progress and Continuing Puzzles in Electrostatics 1572
L. B. Schein
- Waves in the Sun's Core 1573
F. Hill >> [Report p. 1591](#)
- [The Shape of Things to Come](#) 1574
K. A. Fitzgerald and D. T. Golenbock
>> [Reports pp. 1628 and 1632](#)
- [How Will the Stratosphere Affect Climate Change?](#) 1576
M. P. Baldwin, M. Dameris, T. G. Shepherd
- [Neural Networks Debunk Phrenology](#) 1578
R. T. Knight >> [Reports pp. 1609 and 1612](#)
- [Food Pathogen Detection](#) 1579
C. A. Batt



1568

QIAcube — pure efficiency

New



Winner of the New Product Award (NPA)
Designation of the Association for
Laboratory Automation (ALA) 2007



reddot design award
winner 2007

reddot design award
product design 2007



- Eliminate manual processing steps
- Continue to use trusted QIAGEN spin-column kits
- Free up your time with affordable, automated sample preparation
- Purify DNA, RNA, or proteins from up to 12 samples per run
- Standardize your results and increase your productivity

Contact QIAGEN today or visit www.qiagen.com/MyQIAcube.



Sample & Assay Technologies

SCIENCE EXPRESS

www.sciencexpress.org

IMMUNOLOGY

Reciprocal Th-17 and Regulatory T Cell Differentiation Mediated by Retinoic Acid

D. Mucida et al.

During development, a metabolite of vitamin A directs progenitor immune cells to become cells that prevent inflammation rather than ones that promote it.

[10.1126/science.1145697](https://doi.org/10.1126/science.1145697)

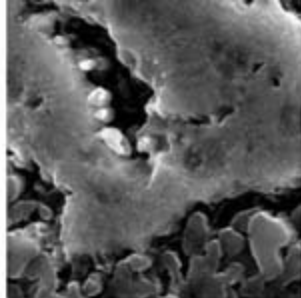
DEVELOPMENTAL BIOLOGY

Noise in Gene Expression Determines Cell Fate in *Bacillus subtilis*

H. Maamar, A. Raj, D. Dubnau

Bacteria that show more random fluctuations in gene expression are more likely to switch to an alternative phenotype in which they can take up foreign genetic material.

[10.1126/science.1140818](https://doi.org/10.1126/science.1140818)



GEOCHEMISTRY

Remnants of the Early Solar System Water Enriched in Heavy Oxygen Isotopes

N. Sakamoto et al.

Material extremely enriched in the heavy isotopes of oxygen is abundant in the matrix of a primitive meteorite, identifying a distinct water reservoir in the early solar system.

[10.1126/science.1142021](https://doi.org/10.1126/science.1142021)

PERSPECTIVE: Strange Water in the Solar System

E. D. Young

[10.1126/science.1145055](https://doi.org/10.1126/science.1145055)

CLIMATE CHANGE

Four Climate Cycles of Recurring Deep and Surface Water Destabilizations on the Iberian Margin

B. Martrat et al.

Alternating penetration of deep ocean waters from southern and northern poles into low latitudes drove century-to-millennial climate changes for at least the past 400,000 years.

[10.1126/science.1139994](https://doi.org/10.1126/science.1139994)

TECHNICAL COMMENT ABSTRACTS

ECOLOGY

Comment on "Carbon-Negative Biofuels from Low-Input High-Diversity Grassland Biomass" 1567

M. P. Russelle et al.

[full text at www.sciencemag.org/cgi/content/full/316/5831/1567b](http://www.sciencemag.org/cgi/content/full/316/5831/1567b)

Response to Comment on "Carbon-Negative Biofuels from Low-Input High-Diversity Grassland Biomass"

D. Tilman, J. Hill, C. Lehman

[full text at www.sciencemag.org/cgi/content/full/316/5831/1567c](http://www.sciencemag.org/cgi/content/full/316/5831/1567c)

REVIEW

ECOLOGY

The Macroecological Contribution to Global Change Solutions 1581

J. T. Kerr, H. M. Kharouba, D. J. Currie

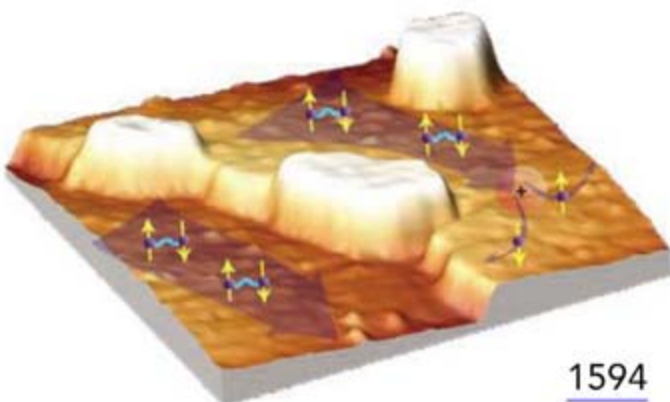
BREVIA

PLANETARY SCIENCE

The Mass of Dwarf Planet Eris 1585

M. E. Brown and E. L. Schaller

Observations of the orbit of dwarf planet Eris' satellite *Dysnomia* indicates that Eris has a density similar to Pluto's, but is about 1.27 times as large.



[1594](https://doi.org/10.1126/science.1145697)

RESEARCH ARTICLE

GENETICS

The Release 5.1 Annotation of *Drosophila melanogaster* Heterochromatin 1586

C. D. Smith, S. Shu, C. J. Mungall, G. H. Karpen

DNA near the centromeres of *Drosophila* chromosomes is repetitive and consists of transposons, tandem and satellite repeats, and over 200 coding and noncoding genes. >> *Report p. 1625*

REPORTS

ASTRONOMY

Tracking Solar Gravity Modes: The Dynamics of the Solar Core 1591

R. A. García et al.

Satellite detection of deep buoyancy-driven oscillations within the Sun implies that the solar core is spinning faster than the surrounding radiative zone. >> *Perspective p. 1573*

PHYSICS

Tuning the Quantum Stability and Superconductivity of Ultrathin Metal Alloys 1594

M. M. Özer et al.

Incorporating small amounts of bismuth into thin lead films adds extra electrons to the film, allowing control of its mechanical stability and superconducting behavior.

CHEMISTRY

Metal Chlorides in Ionic Liquid Solvents Convert Sugars to 5-Hydroxymethylfurfural 1597

H. Zhao, J. E. Holladay, H. Brown, Z. C. Zhang

A chromium catalyst efficiently converts glucose, which can be obtained renewably, to a versatile intermediate feedstock usually derived from petroleum.

GEOPHYSICS

Extracellular Proteins Limit the Dispersal of Biogenic Nanoparticles 1600

J. W. Moreau et al.

Cysteine-rich proteins from sulfate-reducing bacteria help aggregate metal-containing nanoparticles, retarding their mobility in the environment.



1581

[CONTENTS continued >>](#)

THE
DR. PAUL JANSSEN AWARD
FOR BIOMEDICAL RESEARCH

THE SELECTION COMMITTEE

OF

THE DR. PAUL JANSSEN AWARD
FOR BIOMEDICAL RESEARCH

INVITES NOMINATIONS FOR
THE 2008 AWARD



2006 WINNER:

DR. CRAIG MELLO

FOR HIS ROLE IN THE DISCOVERY OF RNA INTERFERENCE (RNAi)
AND THE ELUCIDATION OF ITS BIOLOGICAL FUNCTIONS

Please go to www.pauljanssenaward.com for more information
Deadline for nominations is December 1, 2007

2008 Selection Committee

Dr. Solomon Snyder
Chairman

Dr. Linda Buck

Dr. Jean-Marie Lehn

Dr. Craig Mello

Dr. Hartmut Michel

Dr. Edward Scolnick

Sir Richard Sykes

Johnson & Johnson

©Johnson & Johnson Pharmaceutical Services, LLC 2007

REPORTS CONTINUED...

GEOPHYSICS

Origin of the Low Rigidity of the Earth's Inner Core 1603

A. B. Belonoshko et al.

Molecular simulations suggest that crystal defects, rather than melting, may explain the low rigidity and shear wave velocities of the Earth's inner core.

ECOLOGY

Frequent Long-Distance Plant Colonization in the Changing Arctic 1606

I. G. Alsos et al.

Arctic islands have been colonized repeatedly by plant species from distant sources, suggesting that plant ranges can shift rapidly northward in response to global warming.

NEUROSCIENCE

Modulation of Neuronal Interactions Through Neuronal Synchronization 1609

T. Womelsdorf et al.

The interaction of two neuronal groups in the visual systems of cats and monkeys depends on the phase relation between their rhythmic activities.

>> *Perspective p. 1578*

NEUROSCIENCE

Neural Mechanisms of Visual Attention: How Top-Down Feedback Highlights Relevant Locations 1612

Y. B. Saalmann, I. N. Pigarev, T. R. Vidyasagar

As visual information flows from the retina to the cortex, feedback to neurons farther down the pathway increases activity in specific upstream areas to enable focused spatial attention.

>> *Perspective p. 1578*

CELL BIOLOGY

α -Klotho as a Regulator of Calcium Homeostasis 1615

A. Imura

A protein with several reported functions may also influence calcium metabolism by modulating the abundance of the sodium-potassium pump at the plasma membrane.

CELL BIOLOGY

Wnt Induces LRP6 Signalosomes and Promotes Dishevelled-Dependent LRP6 Phosphorylation 1619

J. Bilić et al.

Large, ribosome-sized protein complexes containing receptor and adapter proteins assemble at cell membranes to detect and transduce a critical developmental signal.



PSYCHOLOGY

Neural Responses to Taxation and Voluntary Giving Reveal Motives for Charitable Donations 1622

W. T. Harbaugh, U. Mayr, D. R. Burghart

Seeing one's taxes spent on public services is not as rewarding as paying for them oneself.

GENETICS

Sequence Finishing and Mapping of *Drosophila melanogaster* Heterochromatin 1625

R. A. Hoskins et al.

DNA near the centromeres of *Drosophila* chromosomes is repetitive and consists of transposons, tandem and satellite repeats, and over 200 coding and noncoding genes. >> *Research Article p. 1586*

IMMUNOLOGY

The Vaccine Adjuvant Monophosphoryl Lipid A as a TRIF-Biased Agonist of TLR4 1628

V. Mata-Haro et al.

A bacterial lipid that can be added to vaccines to boost effectiveness is less toxic than current versions, probably because it selectively stimulates only one immune pathway.

>> *Perspective p. 1574*

BIOCHEMISTRY

Crystal Structures of Human MD-2 and Its Complex with Antiendotoxic Lipid IVa 1632

U. Ohto, K. Fukase, K. Miyake, Y. Satow

The structure of a membrane protein bound to bacterial lipopolysaccharide reveals the first step in how the innate immune system senses the presence of invading bacteria.

>> *Perspective p. 1574*



ADVANCING SCIENCE. SERVING SOCIETY

SCIENCE (ISSN 0036-8075) is published weekly on Friday, except the last week in December, by the American Association for the Advancement of Science, 1200 New York Avenue, NW, Washington, DC 20005. Periodicals Mail postage (publication No. 484460) paid at Washington, DC, and additional mailing offices. Copyright © 2007 by the American Association for the Advancement of Science. The title SCIENCE is a registered trademark of the AAAS. Domestic individual membership and subscription (51 issues): \$142 (\$74 allocated to subscription). Domestic institutional subscription (51 issues): \$710; Foreign postage extra: Mexico, Caribbean (surface mail) \$55; other countries (air assist delivery) \$85. First class, airmail, student, and emeritus rates on request. Canadian rates with GST available upon request, GST #R1254 88122. Publications Mail Agreement Number 1069624. Printed in the U.S.A.

Change of address: Allow 4 weeks, giving old and new addresses and 8-digit account number. Postmaster: Send change of address to AAAS, P.O. Box 96178, Washington, DC 20090-6178. Single-copy sales: \$10.00 current issue, \$15.00 back issue prepaid includes surface postage; bulk rates on request. Authorization to photocopy material for internal or personal use under circumstances not falling within the fair use provisions of the Copyright Act is granted by AAAS to libraries and other users registered with the Copyright Clearance Center (CCC) Transactional Reporting Service, provided that \$18.00 per article is paid directly to CCC, 222 Rosewood Drive, Danvers, MA 01923. The identification code for Science is 0036-8075. Science is indexed in the Reader's Guide to Periodical Literature and in several specialized indexes.

CONTENTS continued >>>

Europe's most important interdisciplinary forum

Learn about new trends and directions in research, business, science policy and funding

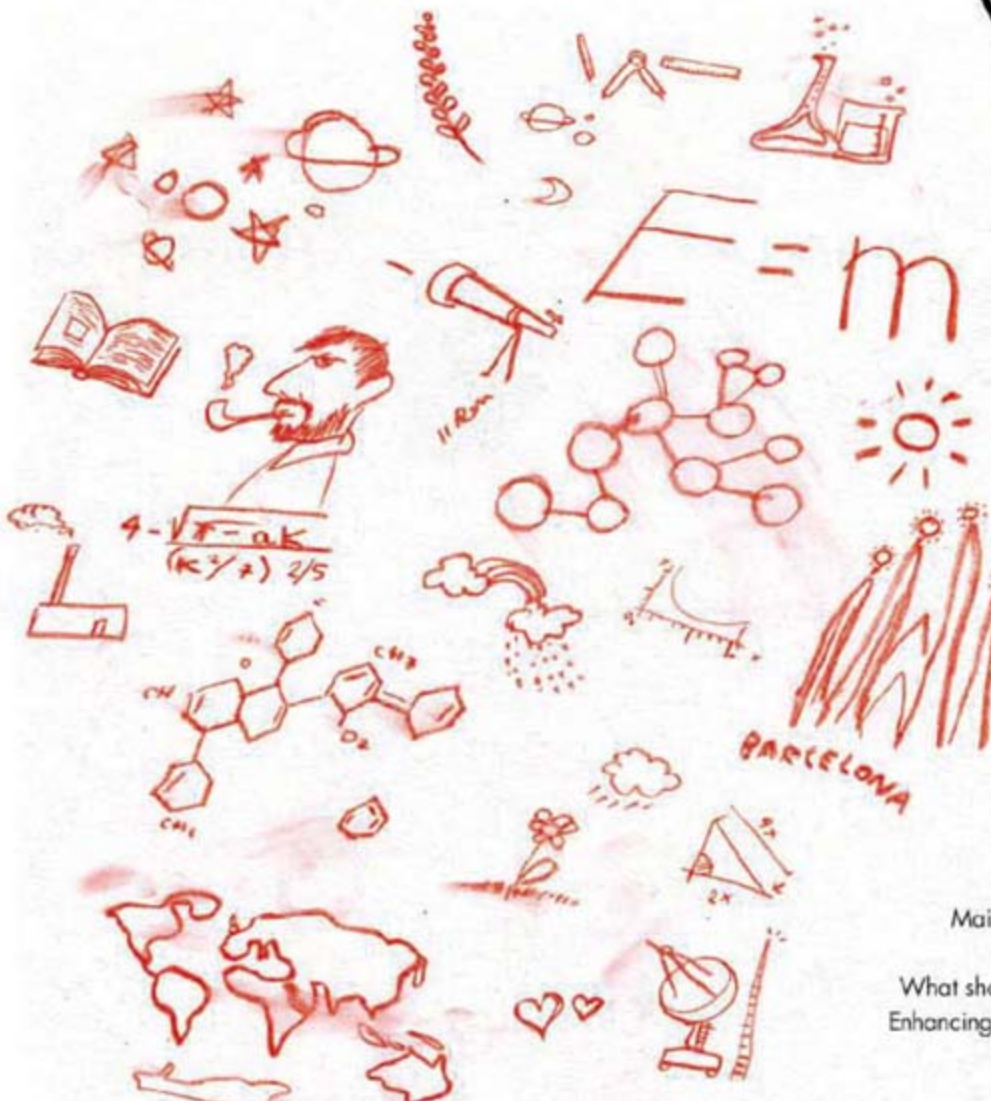
Network with the leaders of the world science community

Communicate your leading research and ideas to an international audience

Participate in the debate, the discussion and the excitement of European science and technology

Meet and talk to scientific journalists from Europe and around the world

Develop your career, your future projects, your horizons and your contacts



ANSWER THE CALL!
www.esof2008.org
SUBMIT A PROPOSAL



Scientific themes

- The human mind and behaviour
- The very big and the very small
- Maintaining an open society through science
- Engineering the body
- What should we eat and how should we look like?
- Enhancing energy security, fighting global warming
- Science policy
- Science and art
- Demography in an ageing Europe
- Screening: burdens and benefits

A FORUM FOR LEADING SCIENTISTS, YOUNG RESEARCHERS, POLICY MAKERS, BUSINESS PEOPLE AND JOURNALISTS

EUROSCIENCE OPEN FORUM

ESOF 2008

SCIENCE FOR A BETTER LIFE

BARCELONA, JULY 18-22

SCIENCE NOW

www.sciencenow.org DAILY NEWS COVERAGE

New Earth or Planetary Hothouse?

Scientists challenge the livability of the first potentially habitable extrasolar planet.

Work Out, Chow Down

There's no easy explanation for why we eat more after exercise.

Heavyweight From the Distant Past

Astronomers find one of the universe's oldest black holes.



Opportunities for scientists in pharmacy.

SCIENCE CAREERS

www.sciencecareers.org CAREER RESOURCES FOR SCIENTISTS

SPECIAL FEATURE: Careers in Pharmacy

K. Travis

Science Careers explores careers for pharmacists from the research bench to the corner pharmacy.

US: Behind the Scenes, Pharmacists Play a Key Role in Clinical Research

K. Hede

Demand for pharmacists trained in clinical research is growing at organizations involved in drug development.

FRANCE: French Pharmacist Finds Regulatory Niche

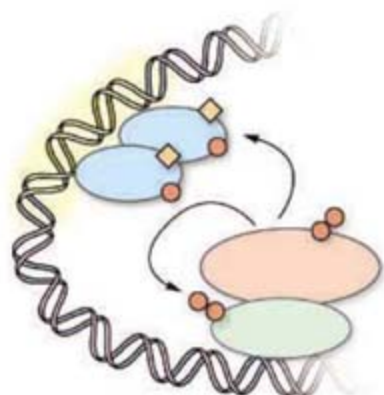
E. Pain

Franck Diafouka tried several pharmacy jobs before finding a good fit in public health.

US: Pharmacists Working in the Community

A. Fazekas

Community pharmacists say their jobs extend beyond being drug managers.



BRCA and estrogen receptor ubiquitination.

SCIENCE'S STKE

www.stke.org SIGNAL TRANSDUCTION KNOWLEDGE ENVIRONMENT

PERSPECTIVE: Double Duty for Rac1 in Epidermal Wound Healing

C. M. DiPersio

Rac1 has roles in promoting both the proliferation and migration of keratinocytes during wound healing.

PERSPECTIVE: BRCA1 Control of Steroid Receptor Ubiquitination

G. F. Heine and J. D. Parvin

Ubiquitination of the estrogen receptor by BRCA1 complex links the ubiquitin ligase activity of BRCA1 to its role as a tissue-specific tumor suppressor.

SCIENCE PODCAST



Listen to the 15 June *Science* Podcast to hear about neural insights into motives for charitable donations, the possible role of cooking in human evolution, sustainable development of a U.S. "bio-economy," and more.

www.sciencemag.org/about/podcast.dtl

Separate individual or institutional subscriptions to these products may be required for full-text access.

Perfecting qPCR

Quanta
BIO SCIENCES

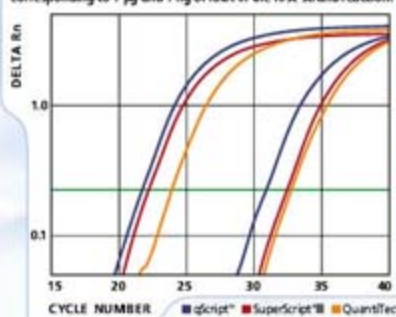
cDNA Synthesis for qPCR

Exceptional representation from less starting material every time.

Introducing qScript™, from Quanta BioSciences, the new standard for reproducibility, specificity, speed, and sensitivity in cDNA synthesis for qPCR. No other product delivers better sample representation, faster, and easier. qScript™ is available in several formats:

- qScript™ cDNA Supermix: The first and only optimized one-tube 1st strand cDNA synthesis for 2-step RT-PCR.
- qScript™ cDNA Synthesis Kit: Broad reproducibility for 2-step RT-PCR.

qRT-PCR of 5' end of TRRAP gene. 100 ng and 100 pg input levels corresponding to 1 µg and 1 ng of RNA in the first-strand reaction.



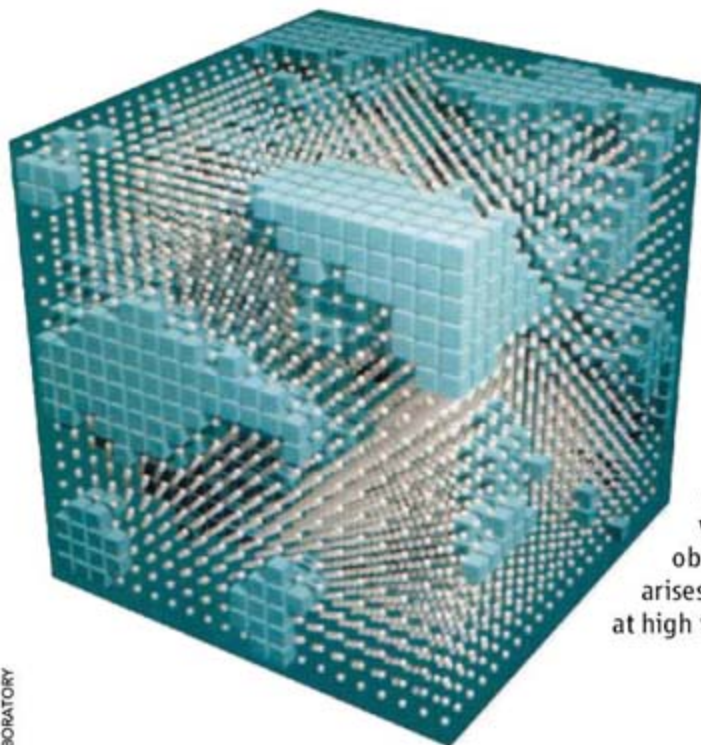
- qScript™ Flex cDNA Kit: Priming flexibility and sensitivity for 1st strand cDNA synthesis.
- qScript™ One-Step qRT-PCR Kit: Maximum RT-PCR efficiency, sensitivity, and specificity.

The founders of Quanta Biosciences have a legacy of leading the development of pioneering reagents including SuperScript® 1-Step RT-PCR kits, Platinum® Taq, iScript™, and iQ™ Supermix. qScript™ is their latest industry-defining product. To learn more about qScript™ visit quantabio.com

qScript™ is a trademark of Quanta BioSciences, Inc. SuperScript® and Platinum® Taq are registered trademarks of Invitrogen Corporation. Quantitect® is a registered trademark of Qiagen N.V. iScript™ and iQ™ are trademarks of Bio-Rad Laboratories, Inc. Quanta BioSciences is licensed for qPCR. See quantabio.com for details.

Order in North America through:

VWR  vwr.com
1.800.932.5000



<< Imperfect Inner Core

The Earth's inner core is not as stiff as would be expected for a solid-iron alloy, and one explanation for the deviation is that the inner core is partially molten. **Belonoshko *et al.*** (p. 1603) performed molecular dynamics simulations, which show that crystal defects could also reduce the inner core's rigidity and decrease its shear wave velocity. Their results, which are in closer agreement with seismic observations, suggest that the low rigidity of the Earth's inner core arises from viscous grain boundaries and high diffusion within iron crystals at high temperature.

Signatures of the Sun's Center

The Sun's vibrations can reveal details of its inner structure. Pressure-driven modes have long been observed, but they provide only limited information about the center of the Sun, which contains more than half the Sun's mass and is the region where fusion occurs. Gravity-driven modes can potentially reveal more about changes in buoyancy of the Sun's dense inner core but are very weak at the Sun's surface and have been hard to detect. **Garcia *et al.*** (p. 1591, published online 3 May; see the cover, the 4 May news story by **Kerr**, and the Perspective by **Hill**) report the observation of a periodic structure in the solar power spectrum that is characteristic of gravity modes in 10 years of data taken with the Global Oscillation at Low Frequency (GOLF) instrument aboard the Solar and Heliospheric Observatory (SOHO). These signatures suggest that the Sun's core rotates faster than in the rest of the radiative zone.

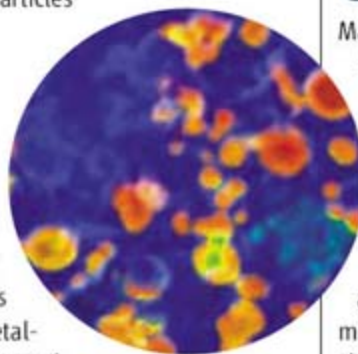
Controlling Quantum Stability

When films undergo thinning, they often break up into droplets as this change in morphology decreases surface tension. However, recent work has shown that for metallic films there are thicknesses, counted in a sequential odd-even integer number of monolayers, where the films are remarkably stable. This quantum stability is thought to arise from the competing effects of surface tension and the energy of the electrons confined to the layer. Such quantum confinement effects can also affect properties such as superconducting transition temperatures. **Özer *et al.*** (p. 1594) show that quantum stability and

the superconducting behavior can both be controlled by varying the electron density in the lead films by forming alloys with bismuth.

Limiting Nanoparticle Dispersal

Sulfate-reducing bacteria are known to produce metal-derived nanoparticles as part of the reduction process that helps reduce metal concentrations in anoxic waters, but the extent to which the resulting nanoparticles move about in the environment is uncertain. **Moreau *et al.*** (p. 1600) study the role of microbially derived proteins on the formation of zinc sulfide particles in a biofilm. The metal-binding polypeptides and proteins are important factors in extracellular metal-sulfide biomineralization, and they may play an important role in aggregation processes that limit the spread of nanoparticles in natural environments.



Arctic Plant Dispersal

Understanding of how the distributions of plant species might shift in response to climate change is hampered by the difficulty of obtaining good quantitative estimates of the frequency of long-distance dispersal. By analyzing the genetic variation of more than 4000 plant samples representing nine different flowering plant species from the arctic archipelago Svalbard and neighboring regions, **Alsos *et al.*** (p. 1606) show that

long-distance dispersal has occurred from various source regions in the Arctic during plant colonization of the Svalbard archipelago since the Last Glacial Maximum. Long-distance dispersal appears to have been much more common than previously believed, which in turn suggests that northward range shifts could occur rapidly following global warming.

From Local to Global Ecology

Macroecology aims to build quantitative predictions about the distribution and abundance of organisms at the scale of regions and even continents, and is relevant to the understanding of biotic changes that may take place as a result of shifting climates. **Kerr *et al.*** (p. 1581) review recent progress in the macroecological research program and assess its potential practical benefits to the management of the consequences of global change.

Focus on Fly Heterochromatin

The DNA of eukaryotic genomes is packaged into chromatin. Euchromatin marks regions that are generally gene-rich and transcriptionally active, whereas heterochromatin (encompassing roughly 30% of the genome in flies and humans) includes regions that are generally transcriptionally repressed and often include densely repeated sequences. Such repetitive regions are intrinsically difficult to analyze with current DNA mapping and sequencing methods. **Smith *et al.*** (p. 1586) and **Hoskins *et al.*** (p. 1625) describe

Continued on page 1539

Deadline extended
to August 1.

Get published in *Science*, win a trip to Stockholm, \$25,000 – and earn the respect of Nobel laureates

Established in 1995, the GE & *Science* Prize for Young Life Scientists seeks to bring science to life by recognizing outstanding Ph.D.s from around the world and rewarding their research in the field of molecular biology.

This is your chance to gain international acclaim and recognition for yourself and your faculty, and to turn your scientific ideas into reality. If you were awarded your Ph.D. in molecular biology* during 2006, describe your work in a 1000-word essay. Then submit it for the 2007 GE & *Science* Prize for Young Life Scientists. A panel of distinguished scientists selects one Grand Prize winner and four regional winners. **Deadline extended to August 1.**

There are few awards more rewarding in science than the *Science*/AAAS and GE Healthcare-sponsored prize – just ask the Grand Prize winner for 2006. In addition to having her essay published in *Science*, Irene Chen received \$25,000, was flown to the awards ceremony in Stockholm, Sweden, and got to pick the brains of Nobel laureates Andrew Fire and Craig Mello.**

GE & *Science* Prize for Young Life Scientists:
Life Science Re-imagined.

For more information, go to
www.gehealthcare.com/science



Grand Prize winner Irene Chen presents her research to a captivated audience



Chen and fellow Prizewinner Ron Milo find common ground with Nobel laureate Craig Mello

Established and presented by:



* For the purpose of this prize, molecular biology is defined as "that part of biology which attempts to interpret biological events in terms of the physico-chemical properties of molecules in a cell" (*McGraw-Hill Dictionary of Scientific and Technical Terms*, 4th Edition).

** Nobel Prize 2006 winners in Physiology or Medicine for their discovery of RNA interference – gene silencing by double-stranded RNA.

Continued from page 1537

a tour de force analysis of roughly 15 to 25 megabases of heterochromatic DNA from pericentromeric regions in the fruit fly *Drosophila melanogaster*. Mapping, sequencing, and annotation of the regions reveals that the great majority of the sequences is repetitive, consisting of retrotransposons, DNA transposons, tandem repeats, and satellite repeats, with ~9% of a unique sequence housing several hundred protein-coding genes and a smaller number of non-protein-coding genes.

Attention and Rhythm in Perception

How does the nervous system enable communication between different brain areas or different neuronal groups? (See the Perspective by Knight.) Saalman *et al.* (p. 1612) simultaneously recorded from two areas in the dorsal stream of the visual pathway, the lateral intraparietal area (LIP) and the medial temporal area (MT), while monkeys performed a delayed match-to-sample memory task. Activity in LIP predicted activity in MT when the receptive fields of the LIP and MT neurons were in the same place and when the monkey was attending to that place. LIP feedback can thus account for attention-enhanced MT responses. Womelsdorf *et al.* (p. 1609) combined multielectrode recording data from three different experimental preparations to test the hypothesis that the phase relation between the rhythmic activity of groups of neurons determines the strength of their mutual influence and found a heavy dependence of the correlation on phase. These results suggest a mechanism by which signals are matched and coupled during complex perceptual and cognitive operations.



The Gift of Giving

In Europe, taxation rates are high, and services are funded by government spending, whereas in the United States, low taxes and higher philanthropic donations are the norm. Harbaugh *et al.* (p. 1622) have carried out a neuroeconomic study to assess the degree of personal reward (as indexed by neural activation of reward-related brain

areas) in response to mandatory (via taxation) and voluntary contributions to charity. Subjects experienced a hedonic reaction when tax revenues were transferred to a charity, and subjects who showed greater neural activation under this regime were more generous when charitable contributions were made voluntary. The sense of well-being in the voluntary giving condition surpassed that seen when subjects were taxed.

Tuning Immune Stimulation

During vaccination, an additional stimulus to the immune response is often needed and is provided by a material called an adjuvant. Lipopolysaccharide (LPS) in the outer membrane of Gram-negative bacteria is a potent stimulant of the innate immune response, but the potential for toxic shock does not allow for its use in humans. A recently approved adjuvant, monophosphoryl lipid A (MPLA), has limited side effects compared to LPS from which it is derived (see the Perspective by Fitzgerald and Golenbock). Mata-Haro *et al.* (p. 1628) show that MPLA activates only a specific signaling component of the Toll-like receptor 4 (TLR4) pathway and avoids the myeloid differentiation factor 88 arm of TLR4 signaling, which can account for the much higher toxicity associated with LPS. Ohto *et al.* (p. 1632) determined crystal structures of the TLR4 co-receptor MD-2 alone and in complex with the antiendotoxic tetra-acylated lipid A core of LPS. MD-2 has a deep hydrophobic cavity that accommodates the four acyl chains of the lipid core.

Signaling Central

Wnt growth factors activate a signaling cascade that plays a key role in animal development, stem cell biology, and human cancer. Although many of the cascade components have been identified, how they come together to transmit the signal from the plasma membrane inside the cell is not clear. Bilic *et al.* (p. 1619) show that Wnt ligands induce formation of large, ribosome-sized complexes, termed the low-density lipoprotein receptor-related protein 6 (LRP6) signalosome at the plasma membrane. The large protein assemblies contain activated Wnt receptors and cytoplasmic adapter proteins. The scaffold protein Dishevelled and the Wnt co-receptor LRP6 play a central role in LRP6-signalosome formation, triggering subsequent molecular interactions that regulate the level of nuclear β -catenin.

CREDIT: HARBAUGH ET AL.

What does a first-class news writer need?

Constance Holden
2004 National Mental
Health Association:
Media Award



A first-class journal.

Award-winning journalists write for *Science*—with 12 top awards in the last four years. That's why we have the most compelling stories, and the biggest readership of any general scientific publication. To see the complete list of awards go to:

sciencemag.org/newsawards



Building

Your Drug Pipeline

***Faster, Better and Cheaper from
Discovery to Clinical Proof-of-Concept***

IBC's 12th Annual World Congress



**Drug
DISCOVERY
& DEVELOPMENT
of Innovative THERAPEUTICS**

New Name, New Content, New Focus

**Conference: August 6-9, 2007 • Exhibition: August 7-8, 2007
World Trade Center/Seaport Hotel • Boston, MA**

www.drugdisc.com/pipeline/sciencead

Register Early and Save!

Mention Priority Code **SCIENCEAD**
and get an additional \$50 off your registration
when registering online or by calling 800-390-4078



Raymond Jeanloz is a professor in the Departments of Earth and Planetary Science and of Astronomy at the University of California, Berkeley, and chairs the U.S. National Academy of Sciences' Committee on International Security and Arms Control.

Nuclear Weapons Nonproliferation

THE UNITED STATES IS CONSIDERING THE DEVELOPMENT AND DEPLOYMENT OF new nuclear weapon designs, the objective being to sustain the nation's ultimate deterrent for the foreseeable future.* These initiatives are presented as supporting the highest U.S. security priorities, which include countering the threats of terrorism and the proliferation of nuclear weapons—priorities that are widely shared internationally.

Proponents argue that the United States discussing, let alone deploying, new weapon designs has no significant impact on proliferation. Officials responsible for the U.S. nuclear weapons enterprise have made this point by considering the impact on three groups internationally: existing nuclear powers, rogue states, and terrorists. According to this characterization, rogue states and terrorists pursue their own interests, disregarding international influence to the degree they can. And the balance of power remains essentially unchanged among existing nuclear powers. As a senior Chinese colleague put it, our nations remain effectively deterred whether or not the United States introduces new weapons into its nuclear arsenal.

But the proponents' argument is flawed because it ignores the vast majority of nations around the world: nonnuclear powers that do conform to international norms. To the degree that it considers deploying new weapons, many of these countries view the United States as remaining aloof from its obligations under the Nuclear Non-Proliferation Treaty. Indeed, many of the acknowledged nuclear powers also express grave concerns that the United States' statements and actions may erode the nonproliferation regime by influencing the nonnuclear nations.

Of course, we cannot be certain how deploying new warhead types will affect the nonproliferation regime; after all, science provides only part of the expertise required to inform policy, so this issue has to be approached with humility and care. But countering the proliferation of nuclear weapons remains one of our highest priorities, and there is the real potential of undermining that goal. Simply stating, without evidence, that U.S. actions have no significant impact on proliferation amounts to ignoring the issue.

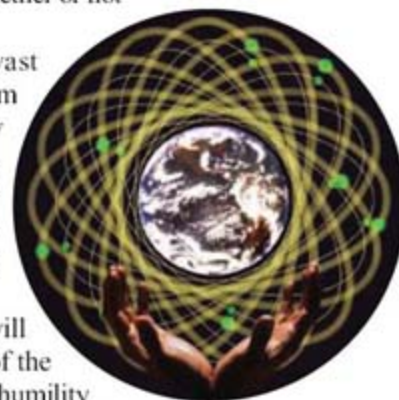
This is especially the case given that the United States has exceptional technical talent in areas relevant to nonproliferation. The national laboratories have vast expertise in assessing nuclear programs of all kinds; in tracking nuclear materials and supporting their protection, control, and accounting; and in applying nuclear forensics. They provide training for international inspectors, participating in inspections as appropriate, and maintain collaborations with counterparts worldwide. Moreover, they have the analytic tools of the scientific method and can evaluate competing hypotheses about what does or does not contribute to enhanced proliferation. Yet rather than benefiting from this national capability, their expertise remains essentially untapped as different options for U.S. policy are assessed. This is an unnecessary oversight and a missed opportunity. The existing national capabilities should be explicitly charged to evaluate the international impacts of different nuclear weapons options being considered.

It is all the more urgent that we do better as technical developments heighten, rather than diminish, the prospects for nuclear weapons proliferation. The knowledge, people, and materials associated with nuclear programs are spreading relentlessly. Indeed, a central reason why nonproliferation is among the highest security priorities for many countries is that there is already an enormous source of materials and expertise that can contribute to proliferation. Moreover, the community of latent nuclear states has greatly expanded over the years and will continue to do so.

It is therefore urgent that we collectively focus on the most effective means to counter the proliferation of nuclear weapons, including fully using the United States' relevant technical capabilities. Doing so will call more for intelligence and law enforcement—that is, for cooperative measures—than for traditional deterrence or military coercion. Partnering with nations around the world currently offers the most promising approach to the growing threat of nuclear arms.†

— Raymond Jeanloz

**The United States Nuclear Weapons Program: The Role of the Reliable Replacement Warhead* (www.aaas.org/news/releases/2007/media/trw_report_2007.pdf). †This editorial is adapted from R. Jeanloz, *Nonproliferation Threat of Nuclear Weapon Programs* (presentation at the AAAS Symposium on Ethical Issues in Nuclear Weapon Programs, Washington, DC, 16 February 2007) (www.sciencemag.org/cgi/content/full/316/5831/1541/DC1).



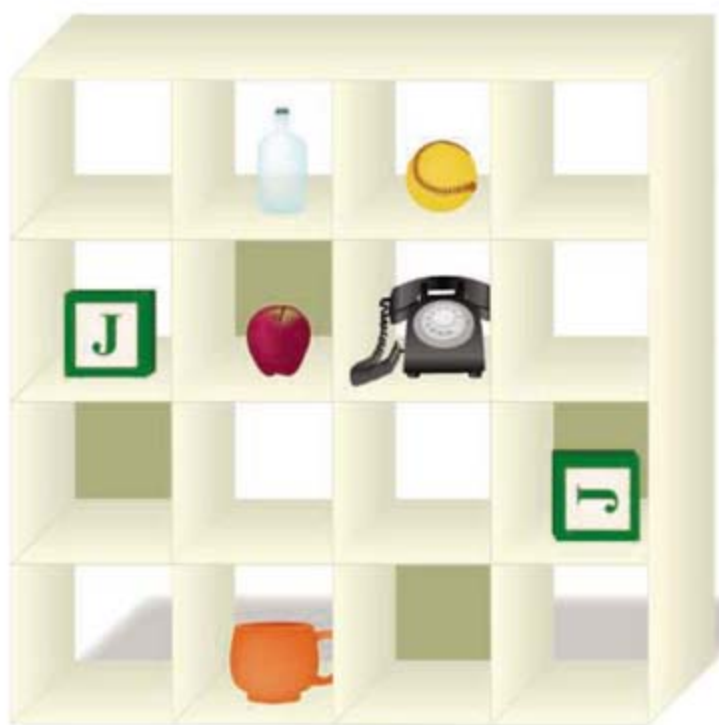
PSYCHOLOGY

Thinking Unselfishly

Problems that appear fiendishly challenging at first glance can seem childishly simple if viewed from the perspective of another. The capacity to infer the mental states of others—theory of mind—is known to develop at approximately the same age in children raised in different cultures, but the ease with which adults access these mind-reading abilities has been suggested to vary across countries, from the collectivism of East Asia to the individualism of the United States.

Wu and Keysar use a two-player game based on a 4-by-4 array of pigeonholes containing mundane objects, some of which are visible to both players and some only to the second. Directions (to move an object) that are completely unambiguous from the vantage point of the first player can, in fact, cause the second player to hesitate in choosing between two identical objects (only one of which is visible to the first player). They find, by tracking visual gaze and reaching movements, that Chinese reacted more quickly than Americans (non-Asians) and were almost never distracted by the second object that they could see but that their playing partner could not. These results favor the proposal that cultures with greater emphasis on interdependence induce a greater readiness to adopt or acknowledge the perspective of the other. — GJC

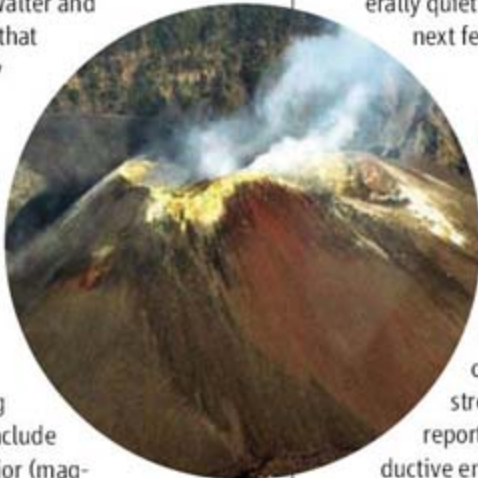
Psychol. Sci. **18**, 600 (2007).



GEOLOGY

Volcanic Shakeup

The powerful Sumatra Andaman earthquakes of 2004 (magnitude 9.3) and a few months later in 2005 (8.7) caused considerable devastation in Indonesia and, as a result of a huge tsunami, the surrounding regions. Walter and Amelung now suggest that these earthquakes may trigger an additional hazard. Such large subduction-zone earthquakes have been followed within a few years by eruptions in the neighboring volcanic arc, in some cases from dormant or rarely erupting volcanoes; examples include eruptions after the major (magnitude 9.0 or higher) earthquakes of Kamchatka in 1952, Chili in 1960, and Alaska in 1964. Two volcanoes (Talang and Barren Island) erupted in Indonesia soon after the nearby 2005 quake. Although the overall incidents are few, the pattern for large quakes is consistent and, according to the authors' analysis, statistically significant. Their numerical modeling shows that gener-



ally such large earthquakes in subduction zones, which are produced by large oceanward slip of the overlying plate, induce some extension in the volcanic arc further landward. Such extension can lower the pressure on trapped magma, inducing or hastening eruptions or leading to further melting. The authors recommend a close watch of generally quiet volcanoes in Indonesia over the next few years. — BH

Geology **35**, 539 (2007).

ENVIRONMENTAL SCIENCE

Fish Fatalities in the Field

Municipal wastewaters contain an enormous variety of chemicals, and fish located in downstream waterways have been reported to show alterations in reproductive endocrine function. Such male fish express proteins, such as vitellogenin, that are naturally found in the female reproductive system, and these males have been shown to develop early-stage eggs. It has been proposed that natural or synthetic estrogens in the water may contribute to the feminization of male fish, and controlled laboratory studies support this claim. Kidd *et al.* describe in detail a whole-lake analysis of

wild fathead minnows that have been exposed to low concentrations of estrogens. The results, which span seven years, reveal that when the synthetic estrogen 17 α -ethynylestradiol (as used in contraceptive pills) was added to a lake in northwestern Ontario, levels of vitellogenin mRNA and protein increased, and male fish showed arrested testicular development in comparison to fish in nearby untreated lakes. Intersex fish—that is, males with primary stage oocytes—were observed, and female fish showed elevated vitellogenin and displayed delayed ovarian development. Furthermore, though it is common to see fluctuations in wild fathead minnow populations, the experimental population collapsed after the second season of estrogen addition. This work demonstrates that chemicals like those that are detected in municipal wastewaters can affect wild fish reproduction and population sustainability. — BAP

Proc. Natl. Acad. Sci. U.S.A. **104**, 8897 (2007).

MICROBIOLOGY

Circumventing Host Mismatches

For many human pathogens, the molecular features of host specificity have not been defined, and this presents a hindrance to developing faithful animal models for diseases. A notable exception is the foodborne bacterium *Listeria monocytogenes*, in which the virulence factors internalin A and B

CREDITS (TOP TO BOTTOM): (ILLUSTRATION) N. KEVITYAGALA/SCIENCE (SOURCE) WU AND KEYSAR, *PSYCHOL. SCI.* **18**, 600 (2007); AP PHOTO

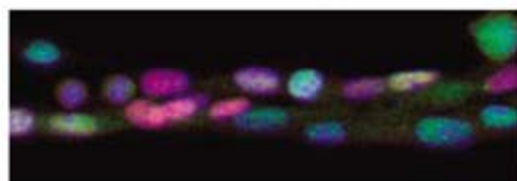
and their host targets (E-cadherin and hepatocyte growth factor receptor, respectively) are known to promote adherence (the first step in infection) to nonphagocytic host cells. One successful way of making a laboratory model for listeriosis has been to humanize mouse gut epithelium by introducing human E-cadherin, but this can add unexpected variables to experimentation. Wollert *et al.* have taken the obverse approach and adapted the pathogen to the mouse by using structure-based design to make individual amino acid substitutions in internalin A. Substitution of the proline at position 16 by glutamate together with a second substitution of a glutamate by a glutamine appears to equalize the binding affinities of internalin A for human and mouse E-cadherins. In vivo experiments confirmed that the engineered bacteria were competent to colonize the villi of mouse guts and cause systemic listeriosis. — CA

Cell **129**, 891 (2007).

DEVELOPMENT

Staying in Touch with Satellites

Adult skeletal muscle is remarkably proficient at repairing itself after bouts of intense exercise or injury, thanks to a population of satellite cells that are located in between the outer sheath (the basal lamina) and the inner muscle fiber. Satellite cells are normally quiescent, but in response to stress they begin dividing to generate new



Satellite cells (fuchsia) and muscle fiber (green).

muscle tissue and to restore the pool of satellite cells. An unresolved question is whether satellite cells are already-committed muscle progenitors, true stem cells, or a mixture of the two. Using genetically manipulated mice and in vivo tracking of satellite cells, Kuang *et al.* found that this population is in fact heterogeneous. Satellite cells that coexpress the molecular markers Pax7 and Myf5 preferentially differentiate into muscle cells, whereas those that express only Pax7 (about 1 in 10) undergo self-renewal, thereby replenishing the satellite cell reservoir. Notably, Myf5-deficient satellite cells produced Myf5-expressing daughter cells when cell division was asymmetric; that is, when the mitotic spindle was oriented perpendicularly to the axis of the muscle fiber. In these instances, the daughter cell that remained attached to the basal lamina became a new satellite stem cell, but the daughter cell that lost contact with the basal lamina became committed to the muscle cell lineage. The authors speculate

that a perturbation of the balance between stem cell renewal and commitment to differentiation within the satellite cell population may be a contributing factor in human diseases such as Duchenne muscular dystrophy. — PAK

Cell **129**, 999 (2007).

APPLIED PHYSICS

Clean Up on Graphene

Graphene, which comprises exfoliated sheets of graphite that are often supported on a dielectric substrate, can display unusual electronic properties that arise through two-dimensional confinement, and in device configurations, biasing of the dielectric can be used to control its conductivity. Although these materials are often assumed to be nearly ideal, in practice the dielectric layer could have trapped charges, and materials used in processing could remain on the graphene. Ishigami *et al.* present atomic-resolution scanning tunneling microscopy studies of graphene devices supported on silica. The as-processed graphene surfaces are covered with photoresist and could not be atomically imaged, even after solvent cleaning. Exposure to an argon-hydrogen atmosphere at 400°C removes the photoresist layer and reveals the influence of the dielectric layer: In addition to the expected hexagonal patterns, a triangular lattice is observed, either from film curvature or the effect of trapped charges. The graphene layer exhibits corrugations that follow the underlying substrate's roughness. — PDS

Nano Lett. **7**, 10.1021/nl070613a (2007).

CHEMISTRY

Whole Numbers for Half Cells?

Electrochemical reduction potentials in solution are generally measured and tabulated relative to a chosen reference reaction at the opposite electrode. Leib *et al.* have taken a step toward formulation of an absolute scale through gas-phase cluster experiments. They induced collisions between electrons and aqueous clusters of Ru³⁺ hexaammine ions, mass-selected to correspond to a bulk concentration of 1 M, and then they measured the energy dissipated upon electron capture by tracking how many water molecules evaporated from the cluster. This value in turn could be corrected for solvation free energies of reactant, product, and free electron to yield an estimate of solution-phase reduction energy. The authors note that although a solvated electron may still differ substantially from a charge transferred directly through a metal electrode, the cluster method includes molecular solvent-solute interactions that are otherwise very challenging to model. — JSY

J. Am. Chem. Soc. **129**, 10.1021/ja067794n (2007).

Institutional Site
License Available

Q

What can *Science*
STKE give me?



A

The definitive
resource on cellular
regulation

STKE – Signal Transduction
Knowledge Environment offers:

- A weekly electronic journal
- Information management tools
- A lab manual to help you organize your research
- An interactive database of signaling pathways

STKE gives you essential tools to power your understanding of cell signaling. It is also a vibrant virtual community, where researchers from around the world come together to exchange information and ideas. For more information go to www.stke.org

To sign up today, visit promo.aaas.org/stkeas

Sitewide access is available for institutions. To find out more e-mail stklicense@aaas.org



1200 New York Avenue, NW
Washington, DC 20005

Editorial: 202-326-6550, FAX 202-289-7562
News: 202-326-6581, FAX 202-371-9227

Bateman House, 82-88 Hills Road
Cambridge, UK CB2 1LQ

+44 (0) 1223 326500, FAX +44 (0) 1223 326501

SUBSCRIPTION SERVICES For change of address, missing issues, new orders and renewals, and payment questions: 866-434-AAAS (2227) or 202-326-6417, FAX 202-842-1065. Mailing addresses: AAAS, P.O. Box 96178, Washington, DC 20090-6178 or AAAS Member Services, 1200 New York Avenue, NW, Washington, DC 20005

INSTITUTIONAL SITE LICENSES please call 202-326-6755 for any questions or information

REPRINTS: Author Inquiries 800-635-7181

Commercial Inquiries 803-359-4578

PERMISSIONS 202-326-7074, FAX 202-682-0816

MEMBER BENEFITS Bookstore: AAAS/BarnesandNoble.com bookstore www.aaas.org/bn; Car purchase discount: Subaru VIP Program 202-326-6417; Credit Card: MBNA 800-847-7378; Car Rentals: Hertz 800-654-2200 CDP#343457, Dollar 800-800-4000 #AA1115; AAAS Travels: Bethchart Expeditions 800-252-4910; Life Insurance: Seabury & Smith 800-424-9883; Other Benefits: AAAS Member Services 202-326-6417 or www.aaasmember.org.

science_editors@aaas.org (for general editorial queries)

science_letters@aaas.org (for queries about letters)

science_reviews@aaas.org (for returning manuscript reviews)

science_bookrevs@aaas.org (for book review queries)

Published by the American Association for the Advancement of Science (AAAS), *Science* serves its readers as a forum for the presentation and discussion of important issues related to the advancement of science, including the presentation of minority or conflicting points of view, rather than by publishing only material on which a consensus has been reached. Accordingly, all articles published in *Science*—including editorials, news and comment, and book reviews—are signed and reflect the individual views of the authors and not official points of view adopted by the AAAS or the institutions with which the authors are affiliated.

AAAS was founded in 1848 and incorporated in 1874. Its mission is to advance science and innovation throughout the world for the benefit of all people. The goals of the association are to: foster communication among scientists, engineers and the public; enhance international cooperation in science and its applications; promote the responsible conduct and use of science and technology; foster education in science and technology for everyone; enhance the science and technology workforce and infrastructure; increase public understanding and appreciation of science and technology; and strengthen support for the science and technology enterprise.

INFORMATION FOR AUTHORS

See pages 120 and 121 of the 5 January 2007 issue or access www.sciencemag.org/feature/contribinfo/home.shtml

EDITOR-IN-CHIEF **Donald Kennedy**

EXECUTIVE EDITOR **Monica M. Bradford**

DEPUTY EDITORS **R. Brooks Hanson, Barbara R. Jasny,**

Katrina L. Kelen

NEWS EDITOR **Colin Norman**

EDITORIAL SUPERVISORY SENIOR EDITOR Phillip D. Szurmi; **SENIOR EDITOR/PERSPECTIVES** Lisa D. Chong; **SENIOR EDITORS** Gilbert J. Chin, Pamela J. Hines, Paula A. Kiberstis (Boston), Marc S. Lavine (Toronto), Beverly A. Purnell, L. Bryan Ray, Guy Riddihough, H. Jesse Smith, Valda Vinson, David Voss; **ASSOCIATE EDITORS** Jake S. Yeston, Laura M. Zahn; **ONLINE EDITOR** Stewart Wills; **ASSOCIATE ONLINE EDITOR** Tara S. Marathe; **BOOK REVIEW EDITOR** Sherman J. Suter; **ASSOCIATE LETTERS EDITOR** Etta Kavanagh; **EDITORIAL MANAGER** Cara Tate; **SENIOR COPY EDITORS** Jeffrey E. Cook, Cynthia Howe, Harry Jach, Barbara P. Ordway, Jennifer Silis, Trista Wagoner; **COPY EDITORS** Lauren Kmec, Peter Mooreside; **EDITORIAL COORDINATORS** Carolyn Kyle, Beverly Shields; **PUBLICATIONS ASSISTANTS** Ramatoulaye Diop, Chris Filiatreau, Joi S. Granger, Jeffrey Hearn, Lisa Johnson, Scott Miller, Jerry Richardson, Brian White, Anita Wynn; **EDITORIAL ASSISTANTS** Maris M. Bish, Emily Guise, Patricia M. Moore, Jennifer A. Seibert; **EXECUTIVE ASSISTANT** Sylvia S. Kihara; **ADMINISTRATIVE SUPPORT** Maryrose Madrid

NEWS SENIOR CORRESPONDENT Jean Marx; **DEPUTY NEWS EDITORS** Robert Coontz, Eliot Marshall, Jeffrey Mervis, Leslie Roberts; **CONTRIBUTING EDITORS** Elizabeth Colutta, Polly Shulman; **NEWS WRITERS** Yudhijit Bhattacharjee, Adrian Cho, Jennifer Couzin, David Grimm, Constance Holden, Jocelyn Kaiser, Richard A. Kerr, Eli Kintisch, Andrew Lawler (New England), Greg Miller, Elizabeth Pennisi, Robert F. Service (Pacific NW), Erik Stokstad; **INTERN** John Simpson; **CONTRIBUTING CORRESPONDENTS** Barry A. Cipra, Jon Cohen (San Diego, CA), Daniel Ferber, Ann Gibbons, Robert Irion, Mitch Leslie, Charles C. Mann, Evelyn Strauss, Gary Taubes; **COPY EDITORS** Linda B. Felaco, Rachel Curran, Sean Richardson; **ADMINISTRATIVE SUPPORT** Scherraine Mack, Fannie Groom; **BUREAUS** Berkeley, CA: 510-652-0302, FAX 510-652-1867, New England: 207-549-7755, San Diego, CA: 760-942-3252, FAX 760-942-4979, Pacific Northwest: 503-963-1940

PRODUCTION DIRECTOR James Landry; **SENIOR MANAGER** Wendy K. Shank; **ASSISTANT MANAGER** Rebecca Doshi; **SENIOR SPECIALISTS** Jay Covert, Chris Redwood; **SPECIALIST** Steve Forrester; **PREFLIGHT DIRECTOR** David M. Tompkins; **MANAGER** Marcus Spiegler; **SPECIALIST** Jessie Mudjtaba

ART DIRECTOR Kelly Buckheit Krause; **ASSOCIATE ART DIRECTOR** Aaron Morales; **ILLUSTRATORS** Chris Bickel, Katharine Suttif, **SENIOR ART ASSOCIATES** Holly Bishop, Laura Creveling, Preston Huey, Nayomi Kevitiyagala; **ASSOCIATE** Jessica Newfield; **PHOTO EDITOR** Leslie Blizard

SCIENCE INTERNATIONAL

EUROPE (science@science-int.co.uk) **EDITORIAL: INTERNATIONAL MANAGING EDITOR** Andrew M. Sugden; **SENIOR EDITOR/PERSPECTIVES** Julia Fahrenkamp-Uppenbrink; **SENIOR EDITORS** Caroline Ash (Geneva: +41 (0) 222 346 3106), Stella M. Hurlley, Ian S. Osborne, Stephen J. Simpson, Peter Stern; **ASSOCIATE EDITOR** Jonathan Baker; **EDITORIAL SUPPORT** Deborah Dennison, Rachel Roberts, Alice Whaley; **ADMINISTRATIVE SUPPORT** Janet Clements, Jill White; **NEWS: EUROPE NEWS EDITOR** John Travis; **DEPUTY NEWS EDITOR** Daniel Clery; **CORRESPONDENT** Gretchen Vogel (Berlin: +49 (0) 30 2809 3902, FAX +49 (0) 30 2809 8365); **CONTRIBUTING CORRESPONDENTS** Michael Balter (Paris), Martin Enserink (Amsterdam and Paris), John Bohannon (Vienna); **INTERN** Krista Zala

ASIA Japan Office: Asca Corporation, Eiko Ishioka, Fusako Tamura, 1-8-13, Hirano-cho, Chuo-ku, Osaka-shi, Osaka, 541-0046 Japan; +81 (0) 6 2022 6272, FAX +81 (0) 6 2022 6271; asca@os.gulf.or.jp; **ASIA NEWS EDITOR** Richard Stone +66 2 662 5818 (rstone@aaas.org); **CONTRIBUTING CORRESPONDENTS** Dennis Normile (Japan: +81 (0) 3 3391 0630, FAX 81 (0) 3 5936 3531; dnormile@gol.com); Hao Xin (China: +86 (0) 10 6307 4439 or 6307 3676, FAX +86 (0) 10 6307 4358; cindyhao@gmail.com); Pallava Bagla (South Asia: +91 (0) 11 2271 2896; pbagla@vsnl.com)

AFRICA Robert Koenig (contributing correspondent, rob.koenig@gmail.com)

EXECUTIVE PUBLISHER **Alan I. Leshner**

PUBLISHER **Beth Rosner**

FULFILLMENT & MEMBERSHIP SERVICES (membership@aaas.org) **DIRECTOR** Marlene Zendell; **MANAGER** Waylon Butler; **SYSTEMS SPECIALIST** Andrew Vargo; **CUSTOMER SERVICE SUPERVISOR** Pat Butler; **SPECIALISTS** Tamara Alfson, Laurie Baker, Latoya Casteel, Vicki Linton; **DATA ENTRY SUPERVISOR** Cynthia Johnson; **SPECIALISTS** Tomeka Diggs, Tarrika Hill, Erin Layne

BUSINESS OPERATIONS AND ADMINISTRATION DIRECTOR Deborah Rivera-Wienhold; **BUSINESS MANAGER** Randy Yi; **SENIOR BUSINESS ANALYST** Lisa Donovan; **BUSINESS ANALYST** Jessica Tierney; **FINANCIAL ANALYSTS** Michael LoBue, Farida Yeasmin; **RIGHTS AND PERMISSIONS: ADMINISTRATOR** Emilie David; **ASSOCIATE** Elizabeth Sandler; **MARKETING DIRECTOR** John Meyers; **MARKETING MANAGERS** Darryl Walter, Allison Pritchard; **MARKETING ASSOCIATES** Julianne Wielga, Mary Ellen Crowley, Catherine Featherston, Alison Chandler, Lauren Lamoureux; **INTERNATIONAL MARKETING MANAGER** Wendy Sturley; **MARKETING EXECUTIVE** Jennifer Reeves; **MARKETING/MEMBER SERVICES EXECUTIVE** Linda Rusz; **JAPAN SALES** Jason Hannaford; **SITE LICENSE SALES DIRECTOR** Tom Ryan; **SALES AND CUSTOMER SERVICE** Mehan Dossani, Kiki Forsythe, Catherine Holland, Wendy Wise; **ELECTRONIC MEDIA: MANAGER** Lizbeth Harman; **PROJECT MANAGER** Trista Snyder; **ASSISTANT MANAGER** Lisa Stanford; **PRODUCTION SPECIALISTS** Nichele Johnston, Kimberly Oster

ADVERTISING DIRECTOR WORLDWIDE AD SALES Bill Moran

PRODUCT (science_advertising@aaas.org); **CONSUMER & SPONSORSHIP SALES MANAGER** Tina Morra: 202-326-6542 **MIDWEST** Rick Bongiovanni: 330-405-7080, FAX 330-405-7081 • **WEST COAST/ CANADA** Teola Young: 650-964-2266 **EAST COAST/ CANADA** Christopher Breslin: 443-512-0330, FAX 443-512-0331 • **UK/EUROPE/ASIA** Michelle Field: +44 (0) 1223-326-524, FAX +44 (0) 1223-325-532 **JAPAN** Mashu Yoshikawa: +81 (0) 33235 5961, FAX +81 (0) 33235 5852; **SENIOR TRAFFIC ASSOCIATE** Deandra Simms

COMMERCIAL EDITOR Sean Sanders: 202-326-6430

CLASSIFIED (advertise@sciencecareers.org); **U.S.: RECRUITMENT SALES MANAGER** Ian King: 202-326-6528, FAX 202-289-6742; **INSIDE SALES MANAGER: MIDWEST/CANADA** Daryl Anderson: 202-326-6543; **NORTHEAST:** Allison Millar: 202-326-6572; **SOUTHEAST:** Tina Burks: 202-326-6577; **WEST:** Nicholas Hintibidze: 202-326-6533; **SALES COORDINATORS** Erika Bryant, Rohan Edmonson, Leonard Marshall, Shirley Young; **INTERNATIONAL SALES MANAGER** Tracy Holmes: +44 (0) 1223 326525, FAX +44 (0) 1223 326532; **SALES** Christina Harrison, Alex Palmer; **SALES ASSISTANT** Louise Moore; **JAPAN:** Jason Hannaford: +81 (0) 52 757 5360, FAX +81 (0) 52 757 5361; **ADVERTISING PRODUCTION OPERATIONS MANAGER** Deborah Tompkins; **SENIOR PRODUCTION SPECIALISTS** Robert Buck, Amy Hardcastle; **SENIOR TRAFFIC ASSOCIATE** Christine Hall; **PUBLICATIONS ASSISTANT** Mary Lagnaoui

AAAS BOARD OF DIRECTORS **RETIRING PRESIDENT, CHAIR** John P. Holdren; **PRESIDENT** David Baltimore; **PRESIDENT-ELECT** James J. McCarthy; **TREASURER** David E. Shaw; **CHIEF EXECUTIVE OFFICER** Alan I. Leshner; **BOARD** John E. Dowling, Lynn W. Enquist, Susan M. Fitzpatrick, Alice Gast, Linda P. B. Katchell, Cherry A. Murray, Thomas D. Pollard, Kathryn D. Sullivan



ADVANCING SCIENCE. SERVING SOCIETY

SENIOR EDITORIAL BOARD

John I. Brauman, Chair, Stanford Univ.
Richard Losick, Harvard Univ.
Robert May, Univ. of Oxford
Marcia McNutt, Monterey Bay Aquarium Research Inst.
Linda Partridge, Univ. College London
Vera C. Rubin, Carnegie Institution of Washington
Christopher R. Somerville, Carnegie Institution
George M. Whitesides, Harvard University

BOARD OF REVIEWING EDITORS

Joanna Aizenberg, Bell Labs/Lucent
R. McNeill Alexander, Leeds Univ.
David Altshuler, Broad Institute
Arturo Alvarez-Buylla, Univ. of California, San Francisco
Richard Amasino, Univ. of Wisconsin, Madison
Weinrat O. Andreadis, Max Planck Inst., Mainz
Kristi S. Anseth, Univ. of Colorado
John A. Bargh, Yale Univ.
Cornelia I. Bargmann, Rockefeller Univ.
Marisa Bartolomei, Univ. of Penn. School of Med.
Brenda Bass, Univ. of Utah
Ray H. Baughman, Univ. of Texas, Dallas
Stephen J. Benkovic, Pennsylvania St. Univ.
Michael J. Bevan, Univ. of Washington
Ton Bisseling, Wageningen Univ.
Mina Bissell, Lawrence Berkeley National Lab
Peer Bork, EMBL
Dianna Bowles, Univ. of York
Robert W. Boyd, Univ. of Rochester
Paul M. Brakefield, Leiden Univ.
Dennis Bray, Univ. of Cambridge
Stephen Buratowski, Harvard Medical School
William M. Burdak, Univ. of Alberta
Joseph A. Burns, Cornell Univ.
William P. Butz, Population Reference Bureau
Peter Carmeliet, Univ. of Leuven, VIB
Gerbrand Cocq, MIT
Mildred Cho, Stanford Univ.
David Clapham, Children's Hospital, Boston
David Clary, Oxford University

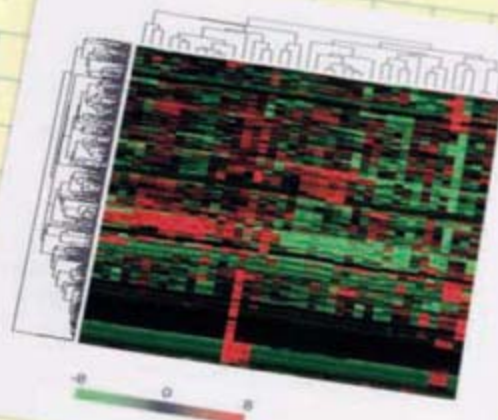
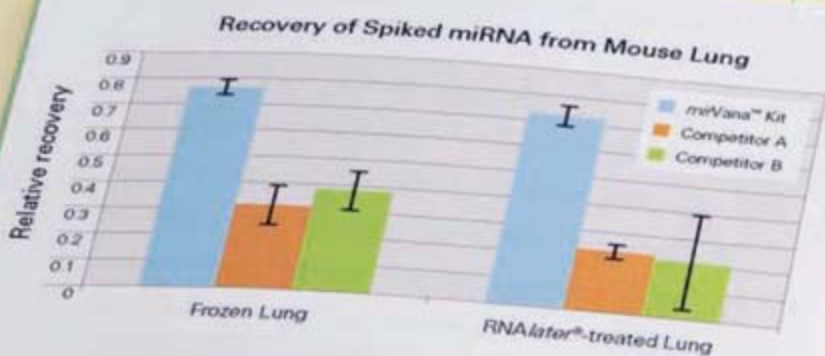
J. M. Claverie, CNRS, Marseille
Jonathan D. Cohen, Princeton Univ.
Stephen M. Cohen, EMBL
Robert H. Crabtree, Yale Univ.
F. Fleming Crim, Univ. of Wisconsin
William Cumberland, UCLA
George Q. Daley, Children's Hospital, Boston
Edward DeLong, MIT
Emmanouil T. Dermitzakis, Wellcome Trust Sanger Inst.
Robert Desimone, MIT
Dennis Discher, Univ. of Pennsylvania
Scott C. Doney, Woods Hole Oceanographic Inst.
W. Ford Doolittle, Dalhousie Univ.
Jennifer A. Doudna, Univ. of California, Berkeley
Julian Downard, Cancer Research UK
Denis Duboule, Univ. of Geneva/EPFL Lausanne
Christopher Dye, WHO
Richard Ellis, Cal Tech
Gerhard Ertl, Fritz-Haber-Institut, Berlin
Douglas H. Erwin, Smithsonian Institution
Barry Everitt, Univ. of Cambridge
Paul G. Falkowski, Rutgers Univ.
Ernst Feher, Univ. of Zurich
Tom Fenchel, Univ. of Copenhagen
Alain Fischer, INSERM
Jeffrey S. Flier, Harvard Medical School
Chris D. Frith, Univ. College London
Wolfram Gerstner, Swiss Fed. Inst. of Technology
Charles Godfrey, Univ. of Oxford
Jennifer M. Graves, Australian National Univ.
Christian Haass, Ludwig Maximilians Univ.
Dennis L. Hartmann, Univ. of Washington
Chris Hawkesworth, Univ. of Bristol
Martin Heimann, Max Planck Inst., Jena
James A. Hendler, Univ. of Maryland
Ray Hilborn, Univ. of Washington
Ove Hoegh-Guldberg, Univ. of Queensland
Ave A. Hoffmann, LaTrobe Univ.
Ronald R. Hoy, Cornell Univ.
Evelyn L. Hu, Univ. of California, Santa Barbara
Olli Ikkala, Helsinki Univ. of Technology
Meyer B. Jackson, Univ. of Wisconsin Med. School
Stephen Jackson, Univ. of Cambridge

Steven Jacobsen, Univ. of California, Los Angeles
Peter Jonas, Universität Freiburg
Daniel Kahne, Harvard Univ.
Bernhard Keimer, Max Planck Inst., Stuttgart
Elizabeth A. Kellog, Univ. of Missouri, St. Louis
Alan B. Krueger, Princeton Univ.
Lee Kump, Penn State
Mitchell A. Lazar, Univ. of Pennsylvania
Virginia Lee, Univ. of Pennsylvania
Anthony J. Leggett, Univ. of Illinois, Urbana-Champaign
Michael J. Lenardo, NIAID, NIH
Norman L. Letvin, Beth Israel Deaconess Medical Center
Olle Lindvall, Univ. Hospital, Lund
Richard Losick, Harvard Univ.
Ke Lu, Chinese Acad. of Sciences
Andrew P. MacKenzie, Univ. of St. Andrews
Raul Madariaga, Ecole Normale Supérieure, Paris
Anne Magurran, Univ. of St. Andrews
Michael Malim, King's College, London
Virginia Miller, Washington Univ.
Yasushi Miyashita, Univ. of Tokyo
Richard Morris, Univ. of Edinburgh
Edward Moser, Norwegian Univ. of Science and Technology
Andrew Murray, Harvard Univ.
Naoto Nagaosa, Univ. of Tokyo
James Nelson, Stanford Univ. School of Med.
Roeland Nolte, Univ. of Nijmegen
Helga Nowotny, European Research Advisory Board
Eric N. Olson, Univ. of Texas, SW
Erin O'Shea, Harvard Univ.
Elinor Ostrom, Indiana Univ.
Jonathan T. Overpeck, Univ. of Arizona
John Pendry, Imperial College
Philippe Poulin, CNRS
Mary Power, Univ. of California, Berkeley
Molly Przeworski, Univ. of Chicago
David J. Read, Univ. of Sheffield
Liz Real, Emory Univ.
Colin Renfrew, Univ. of Cambridge
Trewor Robbins, Univ. of Cambridge
Barbara A. Romanowicz, Univ. of California, Berkeley
Nancy Ross, Virginia Tech
Edward M. Rubin, Lawrence Berkeley National Lab
J. Roy Sambles, Univ. of Exeter

Jürgen Sandkühler, Medical Univ. of Vienna
David S. Schimel, National Center for Atmospheric Research
Georg Schulz, Albert-Ludwigs-Universität
Paul Schulze-Lepert, Max Planck Inst., Cologne
Terrence J. Sejnowski, The Salk Institute
David Sibley, Washington Univ.
Montgomery Slatkin, Univ. of California, Berkeley
George Somero, Stanford Univ.
Joan Steitz, Yale Univ.
Elisbeth Stern, ETH Zürich
Thomas Stocker, Univ. of Bern
Jerome Strauss, Virginia Commonwealth Univ.
Marc Tatar, Brown Univ.
Glenn Telling, Univ. of Kentucky
Marc Tessier-Lavigne, Genentech
Michiel van der Klis, Astronomical Inst. of Amsterdam
Derek van der Kooy, Univ. of Toronto
Bert Vogelstein, Johns Hopkins
Christopher A. Walsh, Harvard Medical School
Graham Warren, Yale Univ. School of Med.
Colin Watts, Univ. of Dundee
Julia R. Weertman, Northwestern Univ.
Jonathan Weissman, Univ. of California, San Francisco
Ellen D. Williams, Univ. of Maryland
R. Sanders Williams, Duke University
Ian A. Wilson, The Scripps Res. Inst.
Jerry Workman, Stowers Inst. for Medical Research
John R. Yates III, The Scripps Res. Inst.
Martin Zatz, NIMH, NIH
Huda Zoghbi, Baylor College of Medicine
Maria Zuber, MIT

BOOK REVIEW BOARD

John Aldrich, Duke Univ.
David Bloom, Harvard Univ.
Angela Creager, Princeton Univ.
Richard Swedner, Univ. of Chicago
Ed Wasserman, DuPont
Lewis Wolpert, Univ. College, London



The mirVana miRNA Isolation Kit recovered the most miRNA compared to two other kits

TaqMan MicroRNA Assay based profiling elucidates miRNA expression patterns across tissues and disease states

**mirVana™ microRNA Isolation.
TaqMan® Assay Quantitation.
All in Real Time.**

miRNA Expression Analysis Made Simple.

Due to their small size, microRNAs can be difficult to isolate and detect, creating a unique challenge to quantitate their expression levels. Applied Biosystems, now including Ambion, offers the only complete suite of reagents, instruments and protocols dedicated to the investigation of miRNAs using Real-Time PCR. Our optimized Ambion *mirVana™* miRNA Isolation Kit, efficient TaqMan™ MicroRNA RT Kit, sensitive and specific TaqMan MicroRNA Assays, proven Applied Biosystems Real-Time PCR Systems, and the protocols provided with them—provide a reliable and ready-to-use approach for quantitation of miRNA expression levels from a variety of sample types. The result? Lower barrier to get started, reduced experimental variability, and access to world-class technical support across your entire experiment—providing you the freedom to focus on making critical biological discoveries.

To start exploring right away, see our simple step-by-step guide to miRNA expression analysis experiment design at www.ambion.com/ABsynergy/miRNA

Ambion®

Proven Performance. Proven Together.

AB Applied Biosystems

From physics to nutrition

For careers in science,
turn to *Science*



If you want your career to bear fruit, don't leave it to chance. At ScienceCareers.org we know science. We are committed to helping you find the right job, and to delivering the useful advice you need. Our knowledge is

firmly founded on the expertise of *Science*, the premier scientific journal, and the long experience of AAAS in advancing science around the world. ScienceCareers.org is the natural selection. www.sciencecareers.org

Features include:

- Thousands of job postings
- Career tools from Next Wave
- Grant information
- Resume/CV Database
- Career Forum

ScienceCareers.org

We know science





Humidity cracked this medieval wooden altarpiece.

Forecasting Global Warming's Monumental Impact

If you plan to see the Coliseum, Notre Dame, and other European landmarks, the new Vulnerability Atlas might help you decide which ones to visit first—before climate change ruins them. Aimed at policymakers and preservationists, the atlas roughly maps how climate change caused by global warming could harm the continent's historical monuments, statues, and buildings over the next century. Produced by Noah's Ark, a 3-year, €1.2 million project sponsored by the European Commission, the atlas marries climate modeling with research on how wood, stone, glass, and other materials are damaged by climate-influenced factors. For example, it shows where in Europe attacks by wood-destroying fungi may increase because of warmer, wetter weather.

Cristina Sabbioni, a physicist at the Institute for Sciences of the Atmosphere and Climate in Bologna, Italy, who coordinated the project, says it's a "shame" that more attention has been paid to the impact of climate change on the skiing industry than on Europe's historical treasures. But attitudes may be changing. Later this month, UNESCO will call for research on how climate change endangers cultural heritage globally, notes May Cassar of University College London's Centre for Sustainable Heritage. "Noah's Ark just scratched the surface," she says.

Something in the Air

Trace amounts of cocaine are wafting through the air in some cities, according to a study released last month. Conducted by the Institute for Atmospheric Pollution of the Italian National

Research Council, the probe examined three cities: Rome, Taranto in southern Italy, and Algiers in Africa. Algiers was "clean" and Taranto had little cocaine in its air, says Ivo Allegri, director of the institute. But in Rome, which is home to more than 10,000 cocaine users, levels reached 0.1 nano-

grams per cubic meter in spots. In some locations, the concentration of cocaine was more than 10 times higher than that of dioxin, a ubiquitous pollutant, notes Angelo Cecinato, coordinator of the work.

Levels are likely similar in other major cities, Allegri says. And although media reports have jumped on the fact that the highest concentrations of cocaine were found near a university, Allegri stresses that "we have not suggested any cause-relation." Caution is warranted, says Norbert Frost of the European Monitoring Centre for Drugs and

Drug Addiction in Lisbon. "Air is a volatile medium, and I do not believe air analyses could be a good way of tracking drug addiction," he says. "Analyses on wastewaters are surely a more reliable survey tool."

Higgs Sighting du Jour

Particle physicists' most coveted prize, the Higgs boson, has been spotted again—according to Internet gossip. In January, bloggers reported that physicists working with CDF, one of two particle detectors fed by the Tevatron collider at Fermi National Accelerator Laboratory (Fermilab) in Batavia, Illinois, had seen signs of the particle. Now, researchers

with Fermilab's D0 detector supposedly see stronger evidence, albeit at a different mass. Terry Wyatt, a physicist at Manchester University in the U.K. and D0 co-spokesperson, says only that "it's not science until it's been approved" for official release.

With the brawnier Large Hadron Collider starting up next year in Switzerland and the Tevatron facing obsolescence, such rumors will likely proliferate, says Tommaso Dorigo, a CDF member from the University of Padua in Italy. "Rumors cannot be controlled because high-energy physics is a small world, and people have friends and like to talk about their work," he says. Dorigo should know: He reported both rumors on his blog.

BOTANY'S WAYBACK MACHINE

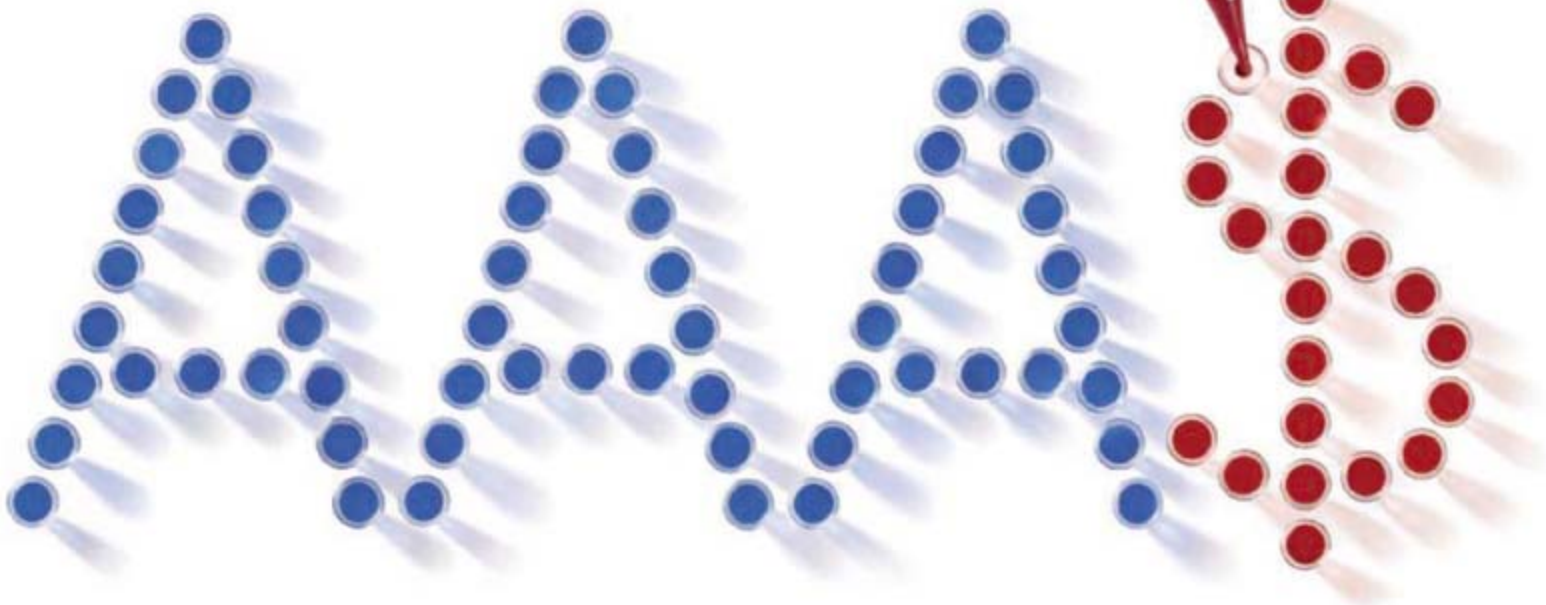
The classic literature in botany dates back to the early days of the printing press. Check out some of these hoary texts at *Botanicus*, an online library run by the Missouri Botanical Garden in St. Louis. The site features digitized versions of almost 200 titles published between 1480 and 1935 on plant systematics. You'll find works by German explorer Alexander von Humboldt, Harvard botanist Asa Gray, and Joseph Hooker, Darwin's confidant and defender. Many texts feature lavish illustrations, such as this painting of the water lemon (*Passiflora laurifolia*), which comes from a 19th century series that catalogs exotic plants in British gardens. >>

www.botanicus.org



Q

Who's working
to increase support
for science?



Top quality research depends on comprehensive support. AAAS is present at every stage of the process – from advising on funding policy initiatives to tracking the US Federal R&D budgeting process. As the experts, we brief Congressional staffers and representatives from

governments around the world. And only AAAS Funding Updates – sent out monthly – provide continual coverage of R&D appropriations. By actively working to increase support for research, AAAS advances science. To see how, go to www.aaas.org/support



ADVANCING SCIENCE. SERVING SOCIETY



IN THE COURTS

A FRIEND AT NIH. Former White House aide I. Lewis "Scooter" Libby Jr. may have earned national scorn for lying about his role in the disclosure of a CIA agent's identity. But he remains in the good graces of many political bigwigs—and at least one prominent science administrator: Anthony Fauci, head of NIH's National Institute of Allergy and Infectious Diseases.

Along with Donald Rumsfeld, Paul Wolfowitz, and Henry Kissinger, Fauci wrote a "presentencing" letter to the judge who presided over Libby's trial, vouching for Libby's "integrity, honesty, unselfishness, and tireless efforts in helping to safeguard our nation." District Judge Reggie Walton released the letters on 5 June—the same day he sentenced Libby to 30 months in prison and a \$250,000 fine for perjury and obstruction of justice during a federal investigation into how agent Valerie Plame's cover was blown.

Fauci says Libby contacted him after being convicted: "He said, 'We don't want you to offer any opinion about whether I'm guilty; it's just a plea for mercy.'" Fauci's two-page letter, written on official NIH letterhead (which federal rules allow), explains how he worked closely with Libby during the past 5 years on biodefense issues, including the drafting of the Project BioShield legislation.



Anthony Fauci

IN THE NEWS

MUM'S THE WORD. Two cancer researchers who made skeptical comments about a proposed anticancer drug have now gone silent after receiving phone and e-mail threats. Howard Scher of the Memorial Sloan-Kettering Cancer Center in New York City and Maha Hussain of the University of Michigan, Ann Arbor, expressed doubts about the adequacy of data from the Dendreon Corp. in Seattle, Washington, supporting a proposed "vaccine" for prostate cancer in private letters to the U.S. Food and Drug Administration (FDA) while serving on an advisory panel reviewing the application. According to a Memorial Sloan-Kettering spokesperson, Scher began to receive extremely hostile, anonymous messages after his comments became public. Scher was given special security protection at last week's meeting of the American Society of

Clinical Oncology in Chicago, Illinois. (Meanwhile, activist patients who want the Dendreon product approved staged a protest at the Capitol in Washington, D.C.) Hussain received similar threats, according to a 4 June story in *The New York Times*. Both scientists are withholding comment on the incident.



Novo Nordisk Foundation. The center, based at the University of Copenhagen, will study

MOVERS

MORE STRUCTURE. Structural biologist Michael Sundström has been named director of a new protein research center being launched with a \$108 million gift from Denmark's

the role of proteins in biological systems, disease, and therapy in order to speed up drug discovery.

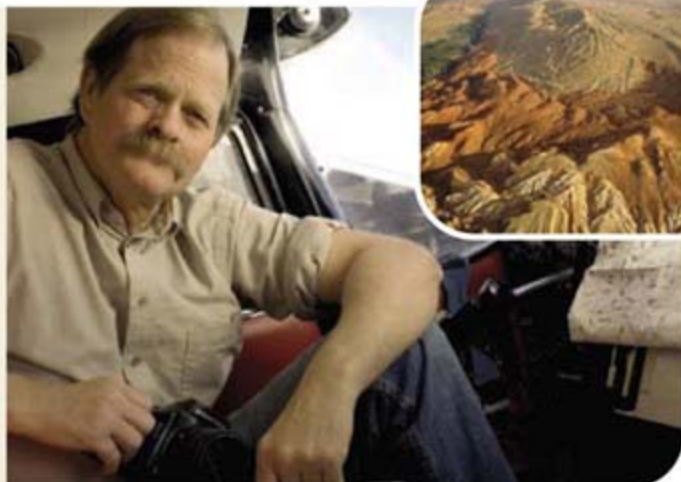
The 43-year-old Sundström, who has worked for the drug industry and is currently chief scientist at Oxford University's Structural Genomics Consortium, plans to build a staff of 100 young researchers to work on five specialty areas. He hopes that finding common themes, such as the pathways involved in tumor growth, will allow the research to be carried out "in a more coordinated fashion than in a normal academic environment." Ulla Wewer, dean of health sciences, says the gift will sustain the center for the first 5 years, after which researchers will seek outside grant support to extend their work in cancer, Alzheimer's disease, obesity, and other fields.

Sundström starts in September, and the center will formally open in fall 2008.

Two Cultures >>

BIRD'S-EYE VIEW. While most geologists stay on the ground, Michael Collier takes to the sky. An avid pilot and photographer, Collier has spent 3 decades illuminating the geological stories behind landscapes. In April, his 13th book was published—a glossy collection of photographs called *Over the Mountains: An Aerial View of Geology*. Several of the photos went on display last week at a solo show in the Washington, D.C., headquarters of AAAS (which publishes *Science*).

Collier, 56, majored in geology, then spent a few years as a boatman on the Grand Canyon. He earned a master's degree in structural geology, then a medical degree. When not photographing landscapes, he's a part-time family physician in Williams, Arizona. He has logged some 4000 hours in his 50-year-old Cessna 180, which he has nicknamed "Buzzard." "When I'm cutting and curling at 1000 feet, the stories begin to pop out in three dimensions," he says. (Inset shows folded rocks at Sheep Mountain, Wyoming.) His next book is about rivers.



Boost for
HIV/AIDS funding

1552

The genome in
a new light

1556

DRUG SAFETY

Heart Attack Risk Overshadows A Popular Diabetes Therapy

Regulators and physicians are once again on the defensive, nervously struggling to interpret revelations about a popular drug. This time the worry focuses on a treatment for diabetes that two separate analyses have linked to heart attacks. The drug, Avandia, has been on the market for 8 years and has been taken by millions of diabetes patients worldwide. In the 3 weeks since a physician at the Cleveland Clinic in Ohio warned about a heart attack hazard, the furor has prompted congressional hearings, patient anxiety, and demands that the U.S. Food and Drug Administration (FDA) explain why potentially severe problems with an approved drug have gone undetected until now.

The Avandia case shares eerie parallels with that of the anti-inflammatory drug Vioxx—except that Vioxx was clearly linked to heart attacks in a single, massive clinical trial and was quickly pulled off the market in 2004 by its maker, Merck. The Avandia case is murkier. Steven Nissen, chair of cardiovascular medicine at the Cleveland Clinic, found an alarming signal in a meta-analysis of 42 Avandia trials, and experts are still debating its implications. Nissen began investigating after noting an increase in heart attacks in two trials published last year. There, the differences were not statistically significant, but “I sat up and took notice,” says Nissen, who also spoke out against Vioxx.

To bring together a much broader swath of Avandia studies, Nissen used data released under a legal settlement by Avandia’s maker, GlaxoSmithKline. Sued in 2004 by New York Attorney General Eliot Spitzer on charges of concealing data on the antidepressant Paxil, the company had agreed to post online trial results. During a frenetic week in late April, Nissen and Cleveland Clinic statistician Kathy Wolski melded data from dozens of Avandia trials, including results of 27 still unpublished. They found that patients on Avandia were 43% more likely to have heart attacks than those in a comparison group.

After Nissen and Wolski’s results appeared online on 21 May in the *New England Journal*

of Medicine (*NEJM*), Glaxo and FDA revealed that Glaxo had performed a similar meta-analysis last year and found an increased heart attack risk of 31%. Glaxo had given the information to FDA and posted it quietly on its Web site—so quietly that Nissen didn’t discover it until 2 days before submitting his own meta-analysis for publication.

But what, exactly, have the new data revealed? Even Nissen agrees that meta-analyses, including his



Metadata moment. The Cleveland Clinic’s Steven Nissen testified before Congress about potential links between heart attacks and use of the diabetes drug Avandia.

and Wolski’s, have drawbacks. The number of heart attacks identified in more than 27,000 people was small: 86 in the Avandia group and 72 in the comparison group, in trials that lasted at least 24 weeks. And because the individual studies were not looking for heart attacks, they did not use a uniform definition.

Furthermore, meta-analyses combine trials that are different lengths and based on different types of comparisons. Because of the statistical challenges, a meta-analysis is often “an absolutely imprecise measure of risk,” says Darren McGuire, a cardiologist at the University of Texas Southwestern Medical Center in Dallas. But in the case of Avandia, “it’s the best

we have,” says McGuire, and “that’s the problem. It’s uncertain, ... but you can’t sweep it under the carpet.”

Researchers note that Nissen’s work is strengthened by Glaxo’s own meta-analysis. The company, however, is playing down the results. Meta-analyses are “ways of asking questions,” not answering them, says Anne Phillips, Glaxo’s clinical vice president for the cardiovascular and metabolic medicines development center. The company followed up with

an observational study of 33,000 patients in a health insurer’s database and found no increase in heart attack risk for those on Avandia, in a report published last week in *Pharmacoepidemiology and Drug Safety*.

Outside Glaxo, McGuire and many others are concerned enough to be asking how Avandia might cause heart attacks. The drug belongs to a class called thiazolidinediones; it reduces blood sugar mainly by making many of the body’s tissues more sensitive to insulin. This allows those tissues to better respond to the hormone and keeps glucose levels healthy.

Thiazolidinediones, however, have broad effects, turning off or on dozens of genes. The class has a troubled history. One member, the diabetes drug Rezulin, was yanked off the market in 2000 after being linked to liver failure. Thiazolidinediones, including the two currently on the market, are known to increase the risk of fluid

buildup and heart failure and carry warnings to that effect. Yet the heart attack signal has come as a surprise to many, in part because a study published in 2005 suggested that the other available thiazolidinedione—a drug called Actos from Takeda Pharmaceuticals and Eli Lilly—protects against heart attacks.

The heart attack risk, if confirmed, may be specific to Avandia, and some observers suspect that the cause may be the drug’s effect on lipids. A study published in 2005, led by Ronald Goldberg of the University of Miami, reported that whereas Actos lowers triglycerides, Avandia raises them. Avandia also raises LDL, or “bad” cholesterol, more so ▶





than Actos, and it raises HDL, or "good" cholesterol, less. David Nathan, director of the diabetes center at Massachusetts General Hospital in Boston, says this difference has made him reluctant to prescribe Avandia. On the other hand, says Jorge Plutzky, a preventive cardiologist at Harvard Medical School in Boston, the fluid buildup associated with both Actos and Avandia may increase heart attack risk.

Many researchers were banking on a

definitive answer from a large clinical trial run in Europe, Australia, and New Zealand called RECORD and funded by Glaxo, examining the cardiovascular effects of Avandia. In an interim analysis in *NEJM* last week (the trial is to end in late 2008), the study leaders found no heart attack signal associated with Avandia; they could not rule out the risk, either. But because the study reported a much lower rate of heart prob-

lems than predicted, some are concerned that it may not be powerful enough to answer this question.

"The sin of it is that we're still not sure" what's going on, says Nathan. Observers hope to learn more from an FDA advisory committee meeting slated for 30 July. For now, doctors and their patients are left to sift through data that's far from complete.

—JENNIFER COUZIN

PARTICLE PHYSICS

Delay in Europe Could Mean Extra Year for U.S. Collider

Physicists were hardly surprised when officials at the European lab CERN announced last week that the world's new highest-energy atom smasher, the Large Hadron Collider (LHC), will not start up in November as planned. Assembly of the \$3.8 billion accelerator near Geneva, Switzerland, was more than a month behind, leaving no time for a scheduled month-long "engineering run" before power becomes prohibitively expensive in the winter (*Science*, 6 April, p. 31).

But with the LHC's start-up delayed until April 2008, physicists in the United States are mulling another possibility: At a meeting last week at Fermilab National Accelerator Laboratory (Fermilab) in Batavia, Illinois, they began discussing whether to run the lab's venerable Tevatron collider for another year, through 2010.

Just a year ago, Fermilab physicists worried that the Tevatron would shut down before 2009 (*Science*, 2 June 2006, p. 1302). The 2009 run now seems likely, and researchers are speculating about running longer. "I would not want to see anything done that would preclude running in 2010," says Terry Wyatt of Manchester University in the U.K., who is co-spokesperson for the team working with D0, one of two particle detectors fed by the Tevatron. "Signing contracts to start dismantling the machine in October 2009 would be crazy."

The decision will begin with deliberations by the Particle Physics Project Prioritization Panel (P5), which advises

the U.S. Department of Energy (DOE) and the National Science Foundation. At the meeting, P5 heard updates from researchers working with D0 and the rival CDF detector. The panel will make its official recommendation for 2009 next month. Because the Tevatron is cranking out copious data while the LHC is delayed, "one can anticipate that we will recommend running in 2009," says P5 chair Abraham Seiden of the University of California, Santa Cruz.

Making the call for 2010 will be tougher. "It would take some unusual circumstances to justify running beyond 2009," Seiden says. The Tevatron might get a further lease on life if experimenters see signs of the long-sought Higgs boson or other particles, or if the LHC comes on slowly.

The timing will be tricky. To help DOE set its 2010 science budget, P5 must weigh in by the end of next summer. But the LHC won't

start smashing particles until next July. "The problem is that by next summer the LHC is barely turning on, so we won't know how things are going to go," says Pier Oddone, director of Fermilab.

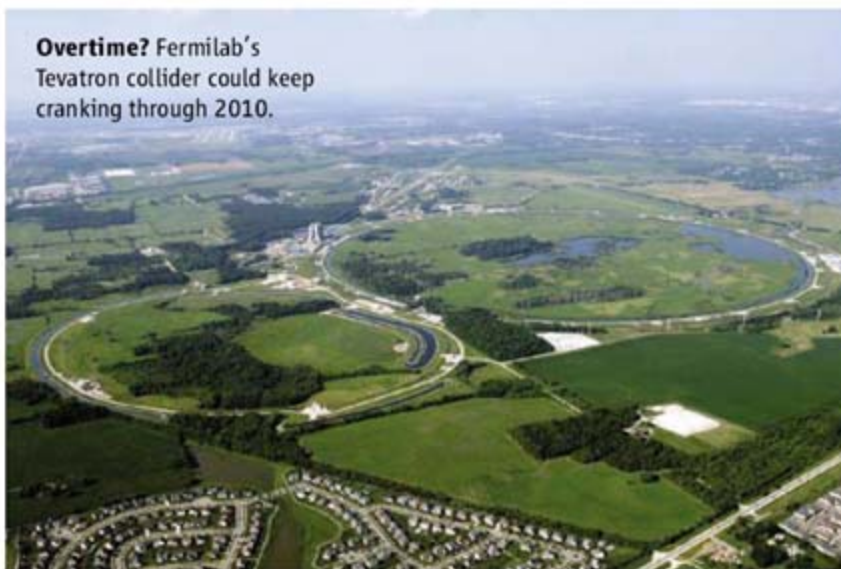
Fermilab officials must also determine whether enough people will stick around to keep the Tevatron going. Researchers are flocking to the LHC, and neither D0 nor CDF has a formal agreement to continue beyond 2009. However, Fermilab's Robert Roser, co-spokesperson for CDF, says that if researchers see solid evidence of the Higgs or something else, many will stay to cinch the discovery: "That would more or less guarantee we'll have enough people."

Running the Tevatron another year would cost about \$30 million, Oddone says. He hopes DOE could squeeze that amount from its \$750 million particle-physics budget without affecting Fermilab's neutrino experiments, work on the proposed International Linear Collider, and other projects.

No one expects the Tevatron to run beyond 2010. To make progress, experimenters must continually improve the collider to double and redouble the size of their data set. By running through 2010, the Tevatron should double the data it will have produced by the end of next year. But with no upgrades in the works, doubling it again would take 4 more years. By then, the LHC should have long since buried the Tevatron.

—ADRIAN CHO

Overtime? Fermilab's Tevatron collider could keep cranking through 2010.



GLOBAL HEALTH

Bush Boosts AIDS Relief: Cause for Applause and Pause

When President George W. Bush announced on 30 May that he wants to double the budget for the AIDS program he initiated to help financially strapped countries battle their epidemics, Democrats and Republicans alike applauded the move. Reflecting the sentiment on both sides of the aisle, Representative Tom Lantos (D-CA), who chairs the House Committee on Foreign Affairs that first authorized the President's Emergency Plan for AIDS Relief (PEPFAR) in 2003, said it was "music to my ears, and I will do all I can to ensure harmonious support for it." Many AIDS researchers immediately started to think about how PEPFAR II, as some are calling it, could reach more people with its prevention, care, and treatment efforts.

But HIV/AIDS advocates who closely track PEPFAR's every move had a less charitable reaction to the proposed \$30 billion plan, asserting that it's misleading to call it a doubling. Congress, they note, has steadily appropriated more money to PEPFAR, with the fiscal year 2008 payout totaling \$5.4 billion—close to the \$6 billion a year Bush wants for PEPFAR II. "To call the \$30 billion a doubling is really disingenuous," contends Asia Russell, who heads international advocacy for the Health Global Access Project in New York City. "Bush really announced a maintenance spending level for the next 5 years." Even Anthony Fauci, head of the National Institute of Allergy and Infectious Diseases in Bethesda, Maryland, and an architect of the original PEPFAR, says \$30 billion represents a "slight to modest increase."

On top of these monetary concerns, advocates and scientists alike want Congress to remove constraints on how PEPFAR money can be spent. When Bush first proposed PEPFAR as a 5-year, \$15 billion program, he insisted on specific provisions in the legislation, the most controversial of which requires that one-third of the money spent on prevention must go toward promoting abstinence before marriage. A March Institute of Medicine (IOM) report strongly urged Congress to remove these earmarks.

Several scientists who were involved with the IOM evaluation, although praising Bush's leadership and ongoing commitment, see ample room for improvement. One of those, James Curran, former HIV/AIDS chief at the Centers for Disease Control and Prevention in Atlanta, Georgia, and now dean of the Rollins School of Public Health at Emory University, also in Atlanta, says that earmarking funds for abstinence programs often pits PEPFAR against other donors and country plans. A study done by the Government Accountability Office reported in April 2006 that "meeting the spending requirement can undermine the integration of prevention programs" by, for example, forcing countries to cut funds for thwarting mother-to-child transmission or for education campaigns that target groups at high risk of becoming infected.

PEPFAR, which is authorized to run through 2008, to date has supported the anti-HIV treatment of more than 1.1 million people in 12 sub-Saharan African countries, Haiti, Guyana, and Vietnam. (Support can include anything from providing drugs to training health-care workers, funding labs, or helping these 15 "focus" countries develop policy.) By the end of September 2006, PEPFAR officials say it had supplied anti-HIV drugs to more than 500,000 infected pregnant women to pre-

vent transmission of the virus to their babies and provided care to 2 million AIDS orphans. Another 18.7 million people received HIV tests and counseling. "Lots of people's lives are being saved," says Mark Dybul, the Global AIDS Coordinator who heads PEPFAR.

Bush's latest proposal is "unquestionably a doubling of resources," says Dybul. He says PEPFAR's critics highlight "relatively minor issues" such as the size of the increase and the earmarks, ignoring the fact that many other developed countries contribute relatively little to the global HIV/AIDS efforts. "If I were an activist, I wouldn't be focusing on the \$30 billion but asking where's the rest of the world so that we can expand service?" (The Group of Eight industrialized nations, which includes the United States, last week announced that it would spend \$60 billion on HIV/AIDS "over the coming years," half of which would come from PEPFAR II.)

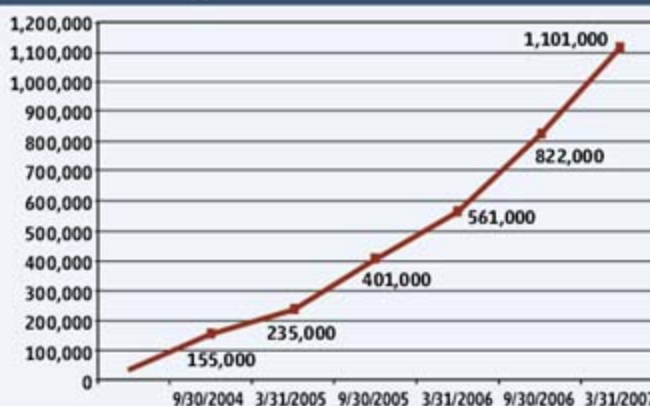
In March, Representative Barbara Lee (D-CA) introduced a bill that would strike the abstinence-only earmark from the original PEPFAR authorization; the bill is currently under consideration. Barry Bloom, dean of Harvard School of Public Health in Boston, says he hopes Congress excises all of the earmarks when it writes the legislation reauthorizing PEPFAR, probably in early 2008. "That kind of blanket micromanagement ends up wasting the public's money," says Bloom.

Other critical issues are how many people PEPFAR will treat and whether it will expand into more countries. Dybul says PEPFAR will hit its target of having 2 million on treatment next year. PEPFAR II calls for supporting the treatment of another half-million people, bringing the total to 2.5 million. The relatively small increase reflects the fact that PEPFAR has slowly ramped up whereas PEPFAR II will start off with at least 2 million on the treatment rolls and millions more in prevention programs. And rather than adding more focus countries, PEPFAR II calls for establishing "partnership compacts" that would require new countries to increase their own spending on HIV/AIDS and health-care systems in order to receive PEPFAR funds.

Michael Merson, who heads the Duke Global Health Institute in Durham, North Carolina, and once ran the Global AIDS Program for the World Health Organization, says he'd be "delighted" if Congress supported the president's request: "Whether it's enough or not enough, it's a lot more than we're doing for other global health needs." —JON COHEN



Number of Individuals Receiving Antiretroviral Treatment With PEPFAR Support



Making the grade. If PEPFAR stays on track, it will support the treatment of 2 million HIV-infected people in poor countries by the end of 2008.

MEDICINE

Initiative Aims to Merge Animal and Human Health Science to Benefit Both

Medical and veterinary science are like siblings who have grown apart. But now, there's a flurry of efforts to reunite them. Proponents of this idea, called "one medicine" or "one health," say that breaking down the walls between the two fields will help fight diseases that jump from animals to humans, such as SARS and avian influenza, and advance both human and animal health.

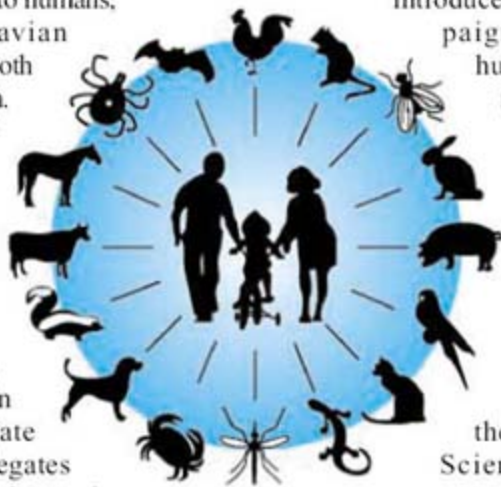
In April, the American Veterinary Medical Association (AVMA) decided to establish a 12-member task force to recommend ways in which vets can collaborate with colleagues in human medicine. In late June, the house of delegates of the American Medical Association (AMA) will vote on a resolution in support of strengthened ties between schools of medicine and veterinary science, increased collaboration in surveillance and the development of diagnostics, drugs, and vaccines across species barriers, and a "dialogue" with AVMA. The theme is also on the program at infectious-disease meetings in Europe and the United States this year.

Although still closely connected in the 19th century, human and animal medicine became increasingly disconnected in the 20th. Recent health emergencies have occasionally driven them back into each other's arms. The global outbreak of the H5N1 avian influenza strain, for instance, has led to closer ties between the human and animal health agencies at the global and country levels.

But such collaborations are the exception when they should be the norm, especially now, with dangerous new zoonoses popping up, says Laura Kahn, an internist at Princeton University. During the 1999 West Nile outbreak in the United States, vets saw birds dying while doctors noticed an uptick in patients with neurological symptoms, but it took a while before someone made the connection. Concrete plans still need to be fleshed out, Kahn says, and obstacles abound: For instance, educational collaborations could be tough in the United States, where there are only 28 vet schools, often in

rural areas, versus more than 140, mostly urban-based, schools of medicine.

The benefits of collaboration could go beyond zoonoses, says Jakob Zinsstag of the Swiss Tropical Institute in Basel. For instance, in Chad, Zinsstag has helped introduce joint vaccination campaigns for livestock and humans, which has helped raise vaccination rates of hard-to-reach nomadic populations. In the United Kingdom, **It's all connected.** Human and animal medicine should grow closer together, One Health supporters say.



the Comparative Clinical Science Foundation has announced plans to fund cross-species studies in areas as diverse as cancer, aging, and genetic disorders—which will yield different insights than the use of animals as models for human disease, Kahn says.

The term "one medicine" was coined in 1960s by Calvin Schwabe, a veterinary scientist and epidemiologist at the University of California, Davis, who died last year. The push to put his ideas into practice originates from a fairly small number of people. Kahn, who became a convert from studying emerging diseases and bioterrorism, got the ball rolling with an article in *Emerging Infectious Diseases* last year. She also wrote a "vision statement"—together with Florida veterinarian Bruce Kaplan and former government virologist and biotech executive Thomas Monath, now at the investment firm Kleiner Perkins Caufield & Byers in Menlo Park, California—supported by dozens of prominent researchers. They found an enthusiastic champion in AVMA President Roger Mahr.

In a way, the movement is also a struggle by veterinarians for a place at the table in public health, says Joan Hendricks, dean of the University of Pennsylvania's vet school. "We have been knocking politely at the door for a while," she says, but human medicine has been slow to respond. But if the AMA resolution gets passed next week, she adds, "it would be a phenomenal support."

—MARTIN ENSERINK

Hubble Due for Fall 2008 Makeover

It's official: In 15 months, NASA will send a space shuttle to service the aging Hubble Space Telescope. Plans to return to Hubble were put on hold 4 years ago after Columbia disintegrated. NASA chief Michael Griffin pledged last year to reverse his predecessor's decision to let Hubble die, but the space agency waited until Atlantis lifted off from its Florida launch pad last week to put the 10 September 2008 servicing flight on the busy shuttle schedule.

If the maintenance mission—its fifth—is successful, Hubble will sport two new instruments. The Cosmic Origins Spectrograph and Wide Field Camera 3 will, respectively, measure the structure and composition of matter and examine the universe in multiple wavelengths. By replacing gyroscopes and filling the fuel tank, the mission is also expected to extend the life of the telescope, first launched in 1990, to 2013. That's also when NASA intends to launch its James Webb Space Telescope, Hubble's follow-on.

—ANDREW LAWLER

Peer Review Peered At, Reviewed

Two new panels will try to figure out how to tweak the vaunted peer-review process at the National Institutes of Health (NIH) to cope with soaring numbers of applications and other pressures on the agency.

NIH has created two working groups—one external, one internal—to examine the "content, criteria, and culture of peer review" in light of flat budgets, a rising number of grant applications, shrinking success rates, and a dearth of experienced reviewers (*Science*, 20 April, p. 358). The external committee is co-chaired by cell biologist Keith Yamamoto of the University of California, San Francisco, a member of the last review panel 8 years ago. Yamamoto expects the new panel to probe the current emphasis on preliminary results and weigh the proper balance between the bona fides of the investigator and the value of the project itself. The internal group, co-chaired by Jeremy Berg, director of the National Institute of General Medical Sciences, will examine the same issues. Both panels are to gather input and report back in December.

Meanwhile, a House spending panel last week voted to add \$750 million next year to the agency's current \$29 billion budget, a 2.6% raise that lags biomedical inflation. The increase drops to 1.9% if \$200 million tagged for the global AIDS fund is removed.

—JOCELYN KAISER AND ELIOT MARSHALL



HIV/AIDS

AIDSTruth.org Web Site Takes Aim at 'Denialists'

For 20 years, a small but vocal group of AIDS "dissenters" has attracted international attention by questioning whether HIV causes the disease. Many AIDS researchers from the outset thought it best to ignore these challenges. But last year, another small and equally vocal group decided to counter the dissenters—whom they call "denialists"—with a feisty Web site, AIDSTruth.org. It has started to attract international attention itself. "It's great," says Mark Wainberg, head of the McGill AIDS Centre in Montreal, Canada. "We really need to get more people to understand that HIV denialism does serious harm. And we were in denial about denialism for a long time."

Launched by AIDS researchers, clinicians, and activists from several countries, AIDSTruth.org offers more than 100 links to scientific reports to "debunk denialist myths" and "expose the denialist propaganda campaign for what it is ... to prevent further harm being done to individual and public health." The site also has a section that names denialists and unsparingly critiques their writings, variously accusing them of homophobia, "scientific ignorance of truly staggering proportions," conspiracy theories, "the dogmatic repetition of the misunderstanding, misrepresentation, or mischaracterization of certain scientific studies," and flat-out lies. "There was a perceived need to take these people on in cyberspace, because that's where they operate mostly, and that's where the most vulnerable people go for their information,"

says immunologist John Moore, an AIDS researcher at the Weill Medical College of Cornell University in New York City.

Peter Duesberg, a prominent cancer researcher at the University of California, Berkeley, whom colleagues have pilloried ever since he first questioned the link between HIV and AIDS in 1987, remains unswayed by the Web site, which he derides in an e-mail interview as a "scientifically worthless mix of ad hominem, opinions, intolerance, and religious energy—instead of a theory and facts." Duesberg maintains that "many essential questions" about what he calls the "HIV-AIDS hypothesis" remain unanswered.

Two factors led Moore and like-minded thinkers (who now number 11) to take off the gloves and hit back with AIDSTruth.org, which went online in March 2006. One was an article in that month's issue of *Harper's* magazine, "Out of Control, AIDS and the Corruption of Medical Science," which chronicled Duesberg's travails for challenging dogma and also questioned the safety and effectiveness of an anti-HIV drug that's widely used to prevent transmission from an infected mother to her baby. Moore and other Web site co-founders wrote a 35-page critique of the article. The second trigger was the situation in South Africa. "Many people who had fought denialism in the early 1990s had lost interest in the subject, but in South Africa, it was at its peak," explains another founder of the Web site, Nathan Geffen of South Africa's

Truth be told. Protesters around the world assailed South Africa's health minister for questioning the worth of anti-HIV drugs.

Treatment Action Campaign. Geffen and others worried that his government might use the *Harper's* article to justify further inaction. "South Africa has more people living with HIV than any other country, and it's also been a place where AIDS denialism has had political support with terrible results."

The no-frills Web site receives no funding, doesn't pay contributors, and features no ads. It refuses to debate whether HIV causes AIDS, which it says "is as certain as the descent of humans from apes and the falling of dropped objects to the ground." It has also posted articles by authors of peer-reviewed publications who believe their findings have been distorted by people trying to prove that HIV/AIDS is a ruse. "The denialists tend to be grotesquely inaccurate," says Richard Jefferys, an activist with the Treatment Action Group in New York City who also helped start the site. "It's almost like the more outrageously inaccurate the claim is, the more they repeat it."

To the delight of Jefferys and others, a Supreme Court judge in Australia in April cited a debunking article on AIDSTruth.org in a closely followed case that involved a man convicted of endangering life for not revealing he was infected with HIV to sexual partners. The man appealed, claiming that no studies prove HIV causes AIDS. His defense consisted of two "expert" witnesses, one of whom was extensively questioned about allegations that she had misused a researcher's results on sexual transmission of HIV. The questions were inspired by an editorial posted on AIDSTruth.org. The judge concluded that neither defense witness—both of whom are branded as denialists on AIDSTruth.org—was qualified to express opinions on these questions. "There's a constant concern that by rebutting these things, you're giving them more credence—there's a thin line between slaying the monster and feeding it," says Jefferys. "The judge's decision made the Web site seem really worthwhile."

AIDSTruth.org has seen its popularity rise from about 60 unique visits a day to 150. But as Moore notes, "we're certainly not high up in the Google rankings." Then again, he argues, any effective rebuke to the "anti-scientific" opinions that attract so much attention is worth the effort. "If you ignore the denialists, they're not going to disappear," says Moore. "And they don't like the fact that we can get in their faces. They're used to being unchallenged."

—JON COHEN

CREDIT: ALEX WONG/GETTY IMAGES

HYDROLOGY

River-Level Forecasting Shows No Detectable Progress in 2 Decades

And you thought weather forecasters had it tough. Hydrologists looking to forecast the next flood or dangerously low river flow must start with what weather forecasters give them—predictions of rain and snow, heat and cold—and fold that into myriad predictive models. Then those models must in turn forecast how rain and any melted snow will flow from rivulet to river while liable to loss to evaporation, groundwater, reservoirs, and farmers' fields. During their century in the forecasting business, hydrologists have developed a modicum of skill, but a newly published study fails to find any improvement during the past 20 years in forecasting river levels out to 3 days.

"It's a pretty shocking result," says hydrologist Thomas Pagano of the U.S. Department of Agriculture's Natural Resources Conservation Service in Portland, Oregon, who was not involved in the study. If the new results are widely applicable, "we're treading water in terms of skill." The answer, Pagano and others say, is for hydrologic forecasters to evaluate their past performance much more rigorously.

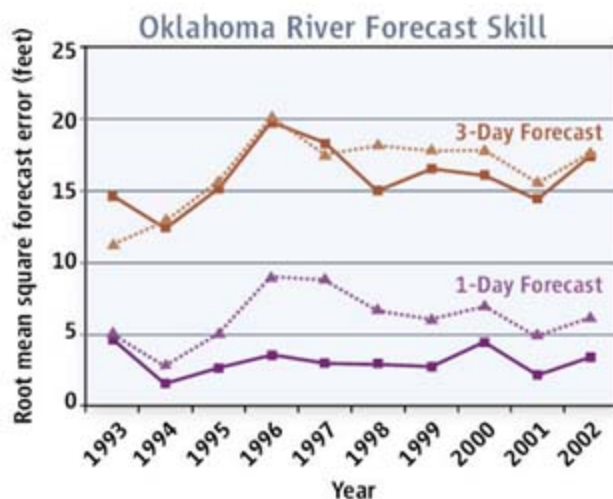
Grading past forecasts has long been standard practice in weather forecasting. Such forecast verification has shown that the introduction of Doppler radar in the early to mid-1990s really did lengthen warning times of tornadoes. Weather forecasters also compare proposed improvements in forecasting procedures against past performance before adopting them. Yet "little verification of hydrologic forecasts has been conducted to date," says hydrologist Edwin Welles of the National Weather Service (NWS) in Silver Spring, Maryland.

So Welles—who has worked at NWS since 1994—tackled hydrologic verification in his 2005 dissertation for the University of Arizona. He considered NWS forecasts and observations of river levels during 10 years at four locations in Oklahoma and during 20 years at 11 locations along the mainstem of the Missouri River. On the Missouri, a forecast location had 500 to 1000 upstream basins feeding water to it. Each basin required its own set of calibrated predictive models, each predicting a different step in water flow, such as

how much water was added by melting snow versus how much soaked into the ground.

In the April *Bulletin of the American Meteorological Society (BAMS)*, Welles and colleagues report mixed results. Forecasters showed real skill in predicting river levels 1 and 2 days in advance compared with assuming that river levels would not change. But despite new models, more-powerful computers, better ways of displaying data and results, and even improved precipitation forecasts from NWS, the 1- and 2-day predictions didn't become more accurate over the 1 or 2 decades of the verification study, at least in the two areas studied.

Troubleshooting hydrologic forecasting to understand why it's been resisting improvement will take "objective study and well-structured verification," says Welles, "not expert opinion or ad hoc experience." *BAMS*



Flat-lining. Although errors in river-level forecasts (solid lines) can be smaller than a simple assumption of no change (dotted lines), errors have not declined with changes in forecasting procedures.

Editor-in-Chief Jeff Rosenfeld agrees. Writing in an accompanying editorial, he finds that the Welles paper makes the point that "forecasting must include verification if it is to be scientific. Every forecast is like a hypothesis, and in science every hypothesis must ultimately be tested."

NWS is taking Welles's research seriously. It began verifying river forecasts at all 4000 of its locations last year. And last fall, an NWS team produced a plan based on Welles's research that should lead to a single hydrologic verification system by 2011. By then, forecasters should be stroking against the current toward better forecasts. —RICHARD A. KERR

War on TB

The World Health Organization (WHO) has jumped on the news wave following the Atlanta lawyer who flew commercially to several countries with a dangerous form of tuberculosis. WHO's Stop TB Partnership will issue new guidance this month for countries battling drug-resistant forms of the disease. Although TB is curable, drugs fail in one-third of people with multidrug-resistant strains and in more than two-thirds of those with extensively drug-resistant forms.

WHO's Paul Nunn says strengthening labs in the developing world is key. "South Africa has more laboratories capable of doing culture and drug-susceptibility testing than the rest of the continent put together," he says. The plan also calls for expanding surveillance and implementing infection-control measures in hospitals. The plan's estimated yearly cost is \$1 billion, but Nunn predicts it would save 1.2 million lives by 2015. —JON COHEN

Trial for Vaccines

Parents who blame vaccines for their children's autism finally have their day in court. Congress shielded vaccine manufacturers from liability in 1986, requiring that claims be filed with the U.S. Court of Federal Claims in Washington, D.C., before a federal compensation fund pay damages. More than 4800 parents have filed claims since 1999, and the court began hearing evidence this week in a representative test case.

The main focus is on a mercury-based preservative called thimerosal. Epidemiologists have found no link between autism and this ingredient, which has been phased out of almost all childhood vaccines (*Science*, 12 September 2003, p. 1454). "This sort of palaver has the potential to inhibit vaccination," rues William Schaffner of Vanderbilt University in Nashville, Tennessee. A ruling could take as long as a year. —ERIK STOKSTAD

Get Back to the Lab

Asian research funding could soon eclipse European public and private spending on research and development (R&D), says a new report released by the European Union (E.U.). China could overtake the E.U. by 2009 in terms of R&D spending as a percentage of gross domestic product, the report says. It notes that European industry contributes less to research: only 55% of total R&D spending, compared to 64% (U.S.), 67% (China), and 75% (both Japan and South Korea).

—DANIEL CLERY

GENOMICS

DNA Study Forces Rethink of What It Means to Be a Gene

Genes, move over. Ever since the early 1900s, biologists have thought about heredity primarily in terms of genes. Today, they often view genes as compact, information-laden gems hidden among billions of bases of junk DNA. But genes, it turns out, are neither compact nor uniquely important. According to a painstaking new analysis of 1% of the human genome, genes can be sprawling, with far-flung protein-coding and regulatory regions that overlap with other genes.

As part of the Encyclopedia of DNA

says Francis Collins, director of the National Human Genome Research Institute (NHGRI) in Bethesda, Maryland, “we’re beginning to understand the ground rules by which the genome functions.”

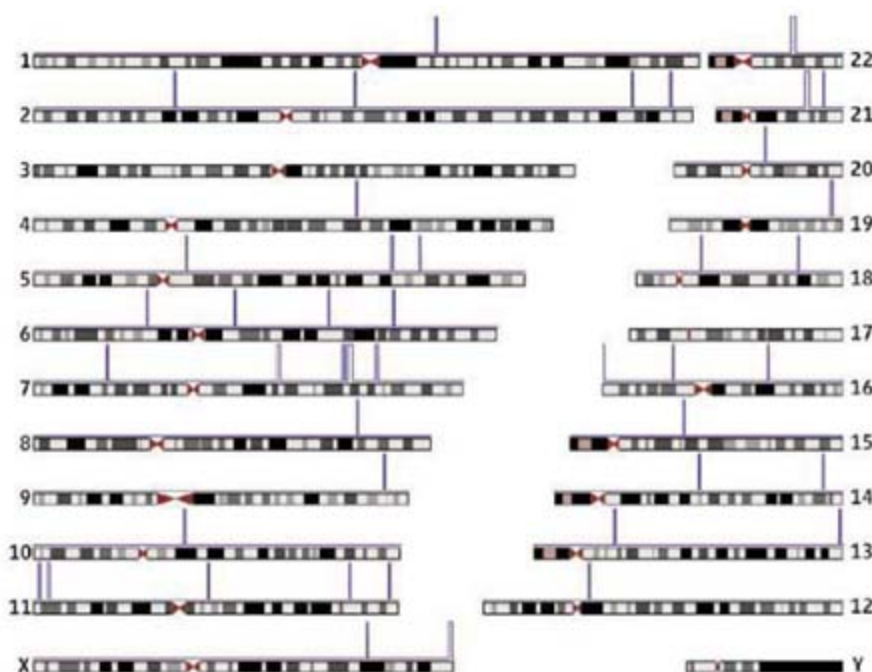
Once the human genome sequence was in hand by 2003, NHGRI set up ENCODE to learn what those 3 billion or so bases were all about. The initial 4-year, \$42 million effort, which tackled 1% of the human genome, brought new and existing experimental and computational approaches to bear, mapping

chains of amino acids by ribosomes. For other types of “genes,” RNA is the end product: Ribosomal RNAs become the backbone of the ribosome, for example.

Researchers used to think very little RNA was produced beyond mRNA and a smattering of RNA end products. But about half the transcripts that molecular biologist Thomas Gingeras of Affymetrix Inc. in Santa Clara, California, discovered in his RNA survey 2 years ago didn’t fit into these categories (*Science*, 20 May 2005, p. 1149), a finding ENCODE has now substantiated. The ENCODE researchers knew going in that the DNA they were studying produced about eight non-protein-coding RNAs, and they have now discovered thousands more. “A lot more of the DNA [is] turning up in RNA than most people



DNA work. For Ewan Birney, coordinating 300 authors to analyze 1% of the human genome (graphic, blue bars) was a rewarding challenge.



Elements (ENCODE) project, 35 research teams have analyzed 44 regions of the human genome covering 30 million bases and figured out how each base contributes to overall genome function. The results, compiled in a paper in the 14 June issue of *Nature* and 28 papers in the June issue of *Genome Research*, provide a litany of new insights and drive home how complex our genetic code really is. For example, protein-coding DNA makes up barely 2% of the overall genome, yet 80% of the bases studied showed signs of being expressed, says Ewan Birney of the European Molecular Biology Laboratory’s European Bioinformatics Institute in Hinxton, U.K., who led the ENCODE analysis.

Given the traditional gene-centric perspective, that finding “is going to be very disturbing to some people,” says John Greally, a molecular biologist at Albert Einstein College of Medicine in New York City. On the other hand,

not just genes but also regulatory DNA and other important features such as gene start sites. NHGRI now plans to spend about \$23 million annually over the next 4 years to perform a similar analysis of the whole genome, expecting that the lessons learned from the pilot ENCODE and new sequencing technologies will greatly reduce the costs of this extended project (*Science*, 25 May, p. 1120). “The goal is to measure all the different kinds of features across the human genome and ask which features go together to understand the whole package,” says George Weinstock, a geneticist at Baylor College of Medicine in Houston, Texas.

A key component of the pilot ENCODE is an analysis of the “transcriptome,” the repertoire of RNA molecules that cells create by transcribing DNA. For protein-coding genes, most of their RNA transcripts—the messenger RNA (mRNA)—get translated into

would have predicted,” says Collins.

ENCODE has produced few clues as to what these RNAs do—leaving some to wonder whether experimental artifacts inflated the percentage of DNA transcribed. Greally is satisfied that ENCODE used enough different techniques to show that the RNA transcripts are real, but he’s not sure they’re biologically important. “It’s possible some of these transcripts are just the polymerase [enzyme] chugging along like an Energizer bunny” and transcribing extra DNA, he suggests.

But in the 8 June issue of *Science* (p. 1484), Gingeras and his colleagues reported that many of the mysterious RNA transcripts found as part of ENCODE harbor short sequences, conserved across mice and humans, that are likely important in gene regulation. That these transcripts are “so diverse and prevalent across the genome just opens up the complexity of this whole system,” says Gingeras. ▶

The mRNA produced from protein-coding genes also held surprises. When Alexandre Reymond, a medical geneticist at the University of Lausanne, Switzerland, and his colleagues took a close look at the 400 protein-coding genes contained in ENCODE's target DNA, they found additional exons—the regions that code for amino acids—for more than 80%. Many of these newfound exons were located thousands of bases away from the gene's previously known exons, sometimes hidden in another gene. Moreover, some mRNAs were derived from exons belonging to two genes, a finding, says Reymond, that

“underscores that we have still not truly answered the question, ‘What is a gene?’” In addition, further extending and blurring gene boundaries, ENCODE uncovered a slew of novel “start sites” for genes—the DNA sequences where transcription begins—many located hundreds of thousands of bases away from the known start sites.

Before ENCODE started, researchers knew of about 532 promoters, regulatory DNA that helps jump-start gene activity, in the human DNA chosen for analysis. Now they have 775 in hand, with more awaiting verification. Unexpectedly, about one-quarter of the pro-

motors discovered were at the ends of the genes instead of at the beginning.

The distributions of exons, promoters, gene start sites, and other DNA features and the existence of widespread transcription suggest that a multidimensional network regulates gene expression. Gingeras contends that because of this complexity, researchers should look at RNA transcripts and not genes as the fundamental functional units of genomes. But Collins is more circumspect. The gene “is a concept that’s not going out of fashion,” he predicts. “It’s just that we have to be more thoughtful about it.”

—ELIZABETH PENNISI

SYNTHETIC BIOLOGY

Attempt to Patent Artificial Organism Draws a Protest

An activist group's concern about maverick genome sequencer J. Craig Venter's intention to patent an entirely synthetic free-living organism has thrown a spotlight on the emerging intellectual-property landscape in this hot new field. The protesters claim that Venter wants his company to become the Microsoft of synthetic biology, dominating the industry.

Venter hopes to use the artificial life form, which he says does not yet exist, as a carrier for genes that would enable the bug to crank out hydrogen or ethanol to produce cheap energy. Duke University law professor Arti Rai says the patent, if awarded, “could be problematic” only if Venter's product became the standard in the field. But Venter says this application is just the start: He plans to patent methods that would cover more than the single microbe described in the application. “We'd certainly like the freedom to operate on all synthetic organisms” that could serve as a chassis for swapping out genes, says Venter, whose research team is at the nonprofit J. Craig Venter Institute in Rockville, Maryland, but who recently started a company to commercialize the work.

Filed last October and published by the U.S. Patent and Trademark Office on 31 May, the application describes “a minimal set of protein-coding genes which provides the information required for replication of a free-living organism in a rich bacterial culture medium.” The application cites work by Hamilton Smith and others on Venter's team on a simple bacterium called *Mycoplasma genitalium* that they are using to determine the minimum number of genes for life. They want to synthesize this “minimal genome” from scratch, get it working inside a cell, then add genes to produce cheap fuels (*Science*, 14 February 2003, p. 1006).

In a press release, the ETC Group, a technology watchdog in Ottawa, Canada, called Venter's “monopoly claims ... the start of a high-stakes commercial race to synthesize and privatize synthetic life forms.” ETC calls for the U.S. and international patent offices to reject the patent so that societal implications can be considered. ETC also cited a recent *Newsweek* interview in which the scientist says he wants to create “the first billion- or trillion-dollar organism.”

Venter says this is just one of several patent applications that would give his company, Synthetic Genomics Inc., exclusive rights to methods for making synthetic organisms. The artificial *Mycoplasma* “may or may not be” the one used to generate hydrogen or ethanol,

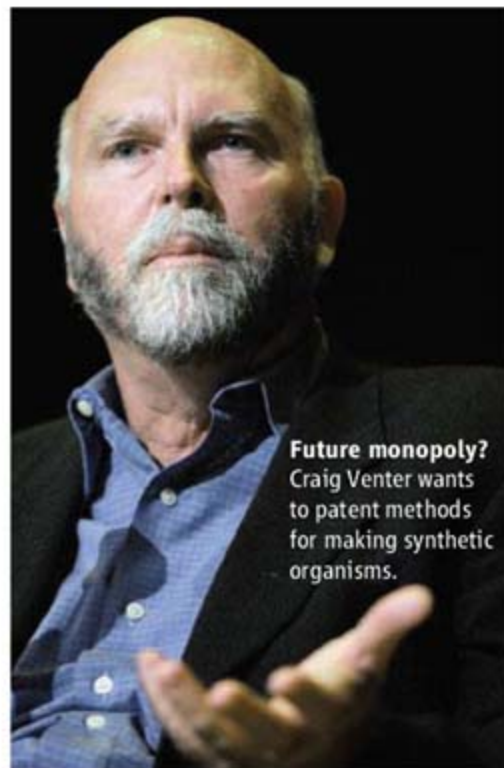
he says; his team is working on several species. “We haven't given any thought to” the licensing conditions, but in any case, they would not impede work in academic labs, says Venter, adding, “This is a problem that we hope will have hundreds of solutions.”

Rai says the notion that Venter's *Mycoplasma* strain will dominate the way Microsoft's Windows did is tenuous because “about 10 things would have to happen,” among them that Venter would create the organism, get the patent, and others would adopt his technology as the standard. Even if that happened, Venter “could do well [financially] and do good,” she says, by licensing the technology at low cost as a research tool, as happened with the original patents on recombinant DNA technology.

Other synthetic biologists don't seem fazed. “He's shooting an arrow in the general direction that things are going,” says Frederick Blattner of the University of Wisconsin, Madison, who has patented a stripped-down *Escherichia coli* and founded a company called Scarab Genomics that is commercializing the technology while disbursing it to academic researchers for a small cost. The more pertinent question, says Harvard's George Church, is whether the inventors' claims to have devised something useful will hold up, as there's no obvious reason why a completely synthetic *Mycoplasma* is needed rather than, say, modified *E. coli* to make hydrogen.

Massachusetts Institute of Technology synthetic biologist Tom Knight, who has pointed out that anyone could get around the patent simply by adding more than the 450 genes stipulated, says his complaint is that the application doesn't explain how to build the artificial cell. “I think it's rather tasteless,” Knight says.

—JOCELYN KAISER



Future monopoly?
Craig Venter wants to patent methods for making synthetic organisms.

CREDIT: MICHAEL NAGLE/GETTY IMAGES

Food for Thought

Did the first cooked meals help fuel the dramatic evolutionary expansion of the human brain?

RICHARD WRANGHAM WAS LYING beside a fire at home on a cold winter night in Boston 10 years ago when his mind wandered to the first hominids to cook food. He imagined a small group of *Homo erectus* huddled around a campfire in Africa, roasting a leg of wildebeest and sharing a morsel of singed potato or manioc.

As a Harvard University primatologist who studies wild chimpanzees in Africa, Wrangham knew that cooking is one of the relatively few uniquely human abilities. He also knew that our habit of predigesting our food by heating it allows us to spend less energy on digestion. And he suddenly realized that cooking is not merely the basis of culinary culture. It would have given our ancestors a big evolutionary advantage. "With cooking, we should see major adaptive changes," says Wrangham. He argues that cooking paved the way for the dramatic expansion of the human brain and eventually fueled cerebral accomplishments such as cave painting, writing symphonies, and inventing the Internet. In

fact, Wrangham presents cooking as one of the answers to a long-standing riddle in human evolution: Where did humans get the extra energy to support their large brains?

Expanding the brain demands a new supply of energy, because human brains are voracious. The brain consumes 60% of the energy expended by a resting newborn baby. And a resting adult's brain uses 25% of its energy, as opposed to 8% used on average by ape brains. But humans consume about the same amount of calories as smaller-brained mammals of similar body size—for example, small women have the same basal metabolic rate as large chimpanzees.

One classic explanation for this phenomenon is that humans saved energy by shrinking their gastrointestinal organs, effectively trading brains for guts as they shifted to a higher quality diet of more meat. That theory is now gathering additional support (see sidebar, p. 1560).

Wrangham thinks that in addition, our ancestors got cooking, giving them the same number of calories for less effort. He floated

Joy of cooking. Cooked food provides easy calories, but did *H. erectus* have campfires?

his hypothesis back in the late 1990s (*Science*, 26 March 1999, p. 2004), but now he's championing it with a slew of new data, some of which he presented at a recent symposium.* "Even small differences in diet can have big effects on survival and reproductive success," he says.

Other researchers are enthusiastic about the new results. They show "the fundamental importance of energy budgets in human evolution," says paleoanthropologist Robert Foley of Cambridge University in the U.K. But many aren't convinced by Wrangham's arguments that the first cooked meal was prepared 1.9 million to 1.6 million years ago, when the brain began to expand dramatically in *H. erectus*. They think that although saving energy by shrinking the gut may have been important at this time, the culi-

nary explosion came later, perhaps during the evolution of our own species less than half a million years ago. "What all these adaptations are about is increasing the bang for the buck nutritionally," says William R. Leonard, a biological anthropologist at Northwestern University in Evanston, Illinois. "The challenge ultimately is to work out the exact timing of what led to what."

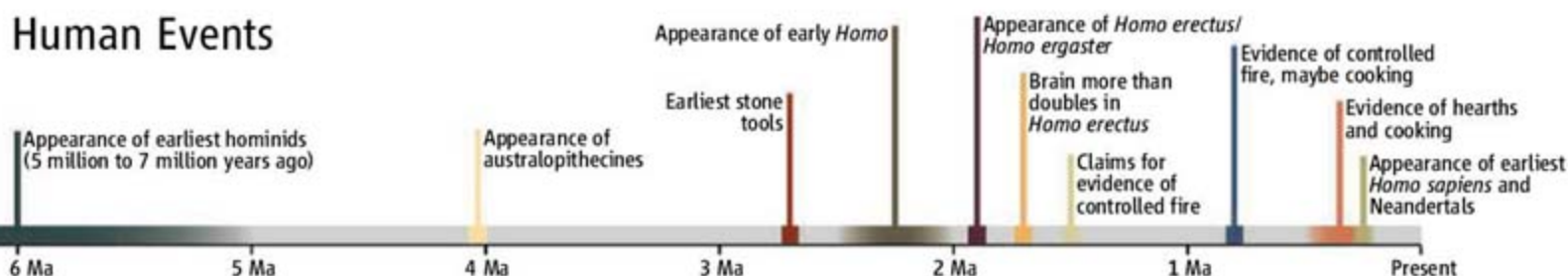
Boosting brainpower

Even those unsure about the role of cooking in human evolution agree that something crucial must have happened to our ancestors' energy budget. Line up the skulls of early hominids and you'll see why: From 1.9 million to 200,000 years ago, our ancestors tripled their brain size.

The earliest members of the human family, including the australopithecines that lived from 4 million to 1.2 million years ago (see timeline, p. 1559), had brains about the size

* "Primateology Meets Paleoanthropology Conference," 17–19 April, University of Cambridge, United Kingdom.

Human Events



of chimpanzees. The brain didn't expand dramatically until just after *H. erectus* appeared in Africa about 1.9 million years ago (where it is also known as *H. ergaster*), with a brain that eventually averaged 1000 cubic centimeters (cc), or about twice the size of a chimpanzee's. The next leap in brain capacity came 500,000 to 200,000 years ago with the evolution of our own species, whose brains average 1300 cc, and of Neandertals (1500 cc).

What spurred this dramatic growth in the *H. erectus* skull? Meat, according to a long-standing body of evidence. The first stone tools appear at Gona in Ethiopia about 2.7 million years ago, along with evidence that hominids were using them to butcher scavenged carcasses and extract marrow from bones. But big changes don't appear in human anatomy until more than 1 million years later, when a 1.6-million-year-old skull of *H. erectus* shows it was twice the size of an australopithecine's skull, says paleoanthropologist Alan Walker of Pennsylvania State University in State College. At about that time, archaeological sites show that *H. erectus* was moving carcasses to campsites for further butchering and sharing; its teeth, jaws, and guts all got smaller. The traditional explanation is that *H. erectus* was a better hunter and scavenger and ate more raw meat than its small-brained ancestors.

But a diet of wildebeest tartare and antelope sashimi alone isn't enough to account for these dramatic changes, says Wrangham. He notes that *H. erectus* had small teeth—smaller than those of its ancestors—unlike other carnivores that adapted to eating raw meat by increasing tooth size. He argues that whereas earlier ancestors ate raw meat, *H. erectus* must have been roasting it, with root vegetables on the side or as a fallback when hunters didn't bring home the bacon. "Cooking produces soft, energy-rich foods," he says.

To find support for his ideas, Wrangham went to the lab to quantify the nutritional impact of cooking. He found almost nothing in food science literature and began to collaborate with physiologist Stephen Secor of the University of Alabama, Tuscaloosa, who studies digestive physiology and metabolism in amphibians and reptiles. Secor's team fed 24 Burmese pythons one of four diets consisting of the same number

of calories of beef: cooked ground beef, cooked intact beef, raw ground beef, or raw intact beef. Then they estimated the energy the snakes consumed before, during, and after they digested the meat, by measuring the declining oxygen content in their metabolic chambers. Pythons fed cooked beef spent 12.7% less energy digesting it and 23.4% less energy if the meat was both cooked and ground. "By eating cooked meat, less energy is expended on digestion; therefore, more energy can be used for other activities and growth," says Secor.

Secor also helped Wrangham and graduate student Rachel Carmody design a pilot study in which they found that mice raised on cooked meat gained 29% more weight than mice fed raw meat over 5 weeks. The mice eating cooked food were also 4% longer on average, according to preliminary results. Mice that ate raw chow weighed less even though they consumed more calories than those fed cooked food. "The energetic consequences of eating cooked meat are very high," says Wrangham.

The heat from cooking gelatinizes the matrix of collagen in animal flesh and opens up tightly woven carbohydrate molecules in plants to make them easier to absorb. This translates into less time spent chewing: Chimpanzees spend 5 hours on average chewing their food whereas hunter-gatherers who cook spend 1 hour chewing per day. In fact, Western food is now so highly processed and easy to digest that Wrangham thinks food labels may underestimate net calorie counts and may be another cause of obesity.

The immediate changes in body sizes in the mice also suggest that our ancestors would have been able to get rapid benefits out of cooking, says Wrangham. That's why he thinks there would be little lag time between learning to cook and seeing anatomical changes in humans—and why he thinks early *H. erectus* must have been cooking. Less chewing and gnawing would lead to smaller jaws and teeth, as well as to a reduction in gut and rib cage size—all changes seen in *H. erectus*. Those

changes would be favored by selection: Dominant chimpanzees that nab the biggest fruit in a tree, for example, have more offspring, says Wrangham. "It seems to me that groups that cook would have much higher reproductive fitness," he says.

Under fire

Wrangham's synthesis of nutritional, archaeological, and primatological data adds up to a provocative hypothesis that hot cuisine fueled the brain. "It's such a nice explanation," says paleoanthropologist Leslie Aiello, president of the Wenner-Gren Foundation in New York City. She says the smaller teeth in *H. erectus* indicate to her that it wasn't chewing much tough raw food: "Something must be going on. If only there were evidence for fire."

And that's the stumbling block to Wrangham's theories: Cooking requires fire. Irrefutable evidence of habitual cooking requires stone hearths or even clay cooking vessels. Solid evidence for hearths, with stones or bones encircling patches of dark ground or ash, has been found no earlier than 250,000 years ago in several sites in southern Europe. Charred bones, stones, ash, and charcoal 300,000 to 500,000 years ago at sites in Hungary, Germany, and France have also been assigned to hearths. And burned flints, seeds, and wood found in a hearthlike pattern have been cited as signs of controlled fire 790,000 years ago in Israel (*Science*, 30 April 2004, p. 725).

But even the earliest of those dates are long after the dramatic anatomical changes seen in *H. erectus*, says Wrangham. He notes that evidence for fire is often ambiguous and argues that humans were roasting meat and tubers around the campfire as early as 1.9 million years ago.

Indeed, there are a dozen claims for campfires almost that ancient. At the same meeting, paleoanthropologist Jack Harris of Rutgers University in New Brunswick, New Jersey, presented evidence of burned stone

"Even small differences in diet can have big effects on survival and reproductive success."

—Richard Wrangham, Harvard University

Swapping Guts for Brains

Cooking is the latest theory to explain how humans can feed their voracious brains enough calories to survive (see main text), but there's another, classic explanation: As our ancestors began to eat more meat, they took in enough calories at each meal to permit their guts to shrink, saving energy from digestion that in turn helped fuel the brain. Called the expensive tissue hypothesis, this theory was proposed back in 1995 when paleoanthropologist Leslie Aiello, then of University College, London, and physiologist Peter Wheeler of Liverpool John Moores University discovered the tradeoff in guts and brains in 18 species of primates. They found that our gastrointestinal tract is only 60% of the size expected for a primate of similar size (*Science*, 29 May 1998, p. 1345).

Now, after a decade of stasis, the idea is getting new support from studies of birds, fish, and primates. Researchers are also expanding the theory by showing that these energetic tradeoffs only happen in animals that grow up slowly, suggesting that a slowdown in juvenile development set the stage for a large brain. "I'm extremely happy that people are taking this up," says Aiello. "Now we're going to get somewhere with it."

Aiello's hypothesis languished in the late 1990s, after researchers sought an energetic tradeoff in other animals—and didn't find it. Small-brained birds such as chickens don't have big guts, for example. And pigs have small brains and small guts.

But more nuanced animal studies are now shoring up the theory. Last year, Carel van Schaik and Karin Isler of the University of Zurich clarified the situation in birds. Most birds, streamlined for long flights, already possess relatively small guts, they explained in the *Journal of Human Evolution*. So the energetic tradeoff happens instead between brains and pectoral or breast muscles: Bigger birds such as turkeys need bigger pectoral muscles to get airborne, and they have smaller brains—these are "the dumb ones we like to eat," says van Schaik. Those with bigger brains have smaller pecks.

The hypothesis also "holds up very well" in six other species of primates, based on preliminary data on wild

monkeys and apes, says van Schaik. Brainy capuchin monkeys, for example, eat a high-quality diet of insects and bird eggs and have tiny guts. Howler monkeys have tiny brains and big guts to digest bulky leaves and fruit. "The new data beautifully show the tradeoff, gram for gram, between the brain and gut," says neurobiologist John Allman of the California Institute of Technology in Pasadena.

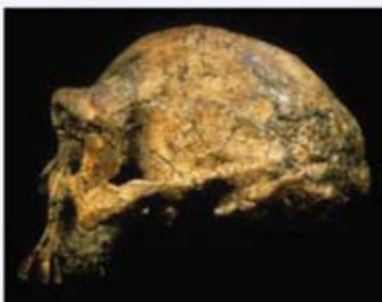
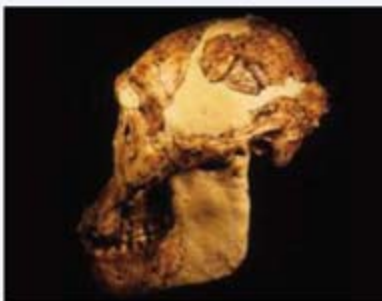
In another paper in press in the *Journal of Human Evolution*, van Schaik and Duke University graduate student Nancy Barrickman confirm earlier reports that primates can grow a big brain only if they adopt a particular life history strategy. Van Schaik's team shows that 28 species of pri-

mates, from tiny mouse lemurs to great apes, have slowed their metabolic rates, thus prolonging their juvenile years, postponing the age at which their first offspring are born, and living longer. This kind of life history is thought to be an adaptation for decreasing infant mortality and boosting maternal health in animals in which the adults have good chances for survival, says paleoanthropologist Jay Kelley of the University of Illinois, Chicago. It also allows primate brains time to grow larger and more complex before adulthood. "Once they slowed down life history, the big brain was inevitable," says Kelley.

Preliminary evidence from the eruption of molars in three *Homo erectus* juveniles, including the Nariokotome skeleton from Kenya, fits with this idea: The teeth suggest that this species had just begun a particularly dramatic developmental slowdown during childhood, a slowdown that reached an extreme in modern humans, says Christopher Dean of University College London.

In this scenario, our ancestors slowed down their development even more as their brains got larger, which required additional energy from a smaller gut and better diet. Thus, the expensive-tissue hypothesis works in primates and other mammals whose young grow up slowly, but not in animals that grow up fast and die young, such as pigs. The energetic tradeoff with the brain can only happen if brains have enough time during development to grow big. "It turns out Leslie [Aiello] was exactly right—with a footnote," says van Schaik.

—A.G.,



Big, bigger, biggest. The brain of *Australopithecus* (top) is half the size of *Homo erectus* (middle) and one-third the size of *H. sapiens* (bottom).

tools 1.5 million years ago at Olduvai Gorge in Tanzania and at Koobi Fora in Kenya, along with burned clay. *H. erectus* has been found at both sites. Claims by other researchers include animal bones burned at high temperatures 1.5 million years ago at Swartkrans, South Africa, and clay burnt at high temperatures 1.4 million years ago in the Baringo basin of Kenya.

But where there is smoke there isn't necessarily cooking fire: None of these teams can rule out beyond a doubt that the charring comes from natural fires, although Harris argues that cooking fires burn hot at 600° to 800°C and leave a trail different from that of bush fires, which often burn as low as 100°C.

All the same, those most familiar with *H. erectus* aren't convinced they were chefs.

Walker says that if the species was cooking with fire, he and others should have found a trail of campfires associated with its bones and stone tools. Others agree: "I think Wrangham's timing is wrong; cooking is associated with the rapid expansion of the brain in Neandertals and modern humans in the past half-million years," says neurobiologist John Allman of the California Institute of Technology in Pasadena. Paleoanthropologist C. Loring Brace of the University of Michigan, Ann Arbor, agrees. He notes that less than 200,000 years ago, the lower faces of Neandertals and modern humans became smaller, and this is about the same time evidence appears for earth-oven cookery: "While fire has been under control back near 800,000 years, its use in the systematic preparation of food has only

been over the last 100,000-plus years."

Others, such as Carel van Schaik of the University of Zurich, think that cooking may have played an important role early on, along with other adaptations to expand human brainpower. As Aiello observes, the big brain was apparently the lucky accident of several converging factors that accentuate each other in a feedback loop. Critical sources of energy to fuel the brain came from several sources—more meat, reduced guts, cooking, and perhaps more efficient upright walking and running. The order in which our ancestors adopted these energy-saving adaptations is under hot debate, with the timing for cooking hardest to test. Regardless, "it's all beginning to come together," says Aiello.

—ANN GIBBONS

MARINE BIOLOGY

Florida Red Tide Brews Up Drug Lead for Cystic Fibrosis

Among the nasty compounds produced by the organism responsible for Florida's red tides is one with some surprising properties

Karenia brevis packs a powerful punch for a tiny organism. The culprit behind Florida's notorious red tides, the dinoflagellate produces a dozen toxins. And when a red tide coincides with an onshore breeze, emergency rooms brace for an influx of patients: The organism's airborne poisons, collectively known as brevetoxins, constrict bronchioles and send asthmatics and others with breathing difficulties scrambling for treatment. So the last thing you might expect from this nasty organism is a compound that alleviates wheezing and shortness of breath and helps clear mucus from the lungs. Yet one oddball in *K. brevis*'s armamentarium, a compound called brevenal, does just that, at least in sheep. It's being evaluated as a potential treatment for the debilitating lung disorder cystic fibrosis (CF), which afflicts 30,000 people in the United States, and researchers are poised to test it on Florida's endangered manatees next time some of the mammals are poisoned by a red tide.

Brevenal's surprising properties have been under investigation since the compound was first discovered in 2004 at the Center for Marine Science (CMS) at the University of North Carolina, Wilmington. New findings reported at the Society of Toxicology meeting in Charlotte, North Carolina, in late March indicate that the compound binds to a novel receptor in the lung, and that a synthetic version seems to work as well as the natural compound in laboratory and animal tests. Yet to be determined, however, is just why *K. brevis* produces a compound that counteracts some of the effects of its own fearsome suite of toxins. But then again, it's not clear why it produces those toxins either, notes CMS Director Daniel Baden.

From beach to bedside?

The oceans have long been touted as a potential source of new drug candidates, and researchers have systematically scoured sponges, corals, and marine microorganisms for likely compounds. Brevenal wasn't found that way: A shortage of guppies for

routine toxicology screening led to its serendipitous discovery.

CMS pharmacologist Andrea Bourdelais was measuring the lethality of extracts isolated from brevetoxins by adding a tiny bit of test material to a beaker containing water and a guppy. If the fraction is toxic, the fish dies. Toxicologists usually retire fish that survive such tests to prevent subsequent chemical interactions, but the laboratory's supply of guppies was running low, so Bourdelais reused the survivors. When she added a known toxic fraction to beakers with leftover guppies, to her surprise, they did not die. "I had a spontaneous gut feeling—a gee-whiz moment—that the

William Abraham, research director at Mount Sinai Medical Center in Miami Beach, Florida, who had determined that all brevetoxins set off bronchoconstriction in a sheep model of asthma. Brevenal, he discovered, suppresses this effect.

Defective sodium transport is a hallmark of CF; it draws water away from airway surfaces, making mucus drier and stickier. Sodium channels are therefore a primary target for CF drugs, so Abraham compared brevenal to the CF drug amiloride in the sheep model. In the January 2005 *American Journal of Respiratory and Critical Care Medicine*, he reported that brevenal not only blocks bronchoconstriction, but it also increases mucus clearance—and it does so at concentrations 1 million-fold lower than amiloride. "We were excited that brevenal may have potential as a CF drug," says Abraham, based on its apparent potency compared to amiloride, which has a mediocre track record in the clinic. Also intrigued was AAI Pharma Inc., a company headquartered in Wilmington, North



Split personality. *Karenia brevis* (inset), which causes Florida's red tides (above), produces an antidote to its own bronchoconstricting toxins.

first material was an antidote to the second one," Bourdelais recalls.

Bourdelais subsequently showed that the mysterious extract (later named brevenal) protects guppies from death by brevetoxins in a dose-dependent fashion. The lab already had discovered that brevetoxins act on sodium channels, so Bourdelais used a standard lab test to check whether brevenal prevents the toxins from binding to the sodium channel receptor. It did. Bourdelais then sent the mysterious compound to

Carolina. It negotiated an exclusive license in 2004 to explore brevenal's potential as a treatment for CF.

Since then, Baden, Bourdelais, Abraham, and their colleagues have continued to probe brevenal's modus operandi. At the toxicology meeting, they reported that it acts on a new drug target: It binds a novel receptor in lung tissue associated with voltage-gated sodium channels; amiloride binds a related receptor, the epithelial sodium channel receptor. Baden also

reported that chemists in the laboratory of Makoto Sasaki at Tohoku University in Sendai, Japan, have synthesized brevenal from cheap starting materials. Dubbed ME-1, the synthetic agent performs as well as natural brevenal in receptor-binding assays and in preventing bronchoconstriction and clearing lung mucus in sheep, Baden reported.

Promises of new therapies for CF surface regularly, but many fizzle out. And in spite of its early promise, brevenal still has a long way to go. Steve Fontana, vice president of legal affairs at AAI Pharma, says the company's scientists are evaluating brevenal and its derivatives for safety and biological activity. Once they find the best drug candidate, the company will file an Investigational New Drug application with the U.S. Food and

Drug Administration (FDA), but clinical trials are several years out.

In fact, humans may not be the first test subjects for brevenal's therapeutic potential. That honor may go to Florida's endangered manatees.

"A red tide event spreads like a wildfire and poisons birds, fish, sea turtles, manatees, and dolphins," says Andrew Stamper, a veterinarian at Disney's Animal Programs in Lake Buena Vista, Florida. In March and April of this year, about 30 manatees died following a red tide spike, and 150 died in 1996 from red tide poisoning. Only 3000 of the mammals are estimated to live along Florida's coast.

In February, Stamper received a "compassionate use" permit from FDA to evalu-

ate the safety and effectiveness of brevenal in manatees. Stamper's colleague, veterinarian David Murphy of Lowry Park Zoo in Tampa, Florida, will test brevenal on rescued manatees brought to the zoo's rehabilitation center. When poisoned by brevetoxins, manatees become paralyzed and drown because they cannot hold their head above water to breathe. Murphy straps lifejackets underneath rescued manatees and supports their half-ton bodies in shallow tanks. Normal breathing resumes in a few days, but full recovery takes months. Brevenal "will add a new weapon in our arsenal," Murphy says. The next time a red tide hits, "we'll be ready to go," says Stamper.

—CAROL POTERA

Carol Potera is a science writer in Great Falls, Montana.

GEOPHYSICS

Stalking a Volcanic Torrent

The setting of the climax of the *Lord of the Rings*, New Zealand's Mount Ruapehu is earning a second reputation as a laboratory for understanding killer mudslides

MOUNT RUAPEHU, NEW ZEALAND—From a helicopter, the steaming lake nestled in the snowy crater below looks inviting, like a giant Jacuzzi for Maori gods. But taking a dip would be a bad idea: Mount Ruapehu's rocky chalice burbles with scalding sulfuric acid. The otherworldly volcano was used for scenes of the hobbit Frodo ascending perilous Mount Doom in the *Lord of the Rings*. But the real Mount Doom is a killer, too. Cradling a deep lake between its 2500-meter peaks, Ruapehu is prone to lahar flows, one of the most dangerous—and least understood—volcanic hazards. In 1953, a lahar (an Indonesian word meaning mudslide) here knocked out a train bridge; 5 minutes later, a passenger train plummeted into a gorge, killing 151 people.

Earlier this year, Ruapehu's acidic lake was unleashed again. Noxious waters blasted down the slopes, picking up rocks as big as cars along the way. But this time, not a single person was hurt.

Not only was the lahar predicted by an early warning system, but the event also generated "orders of magnitude more data than for any other lahar event anywhere in the world," says Vernon Manville, a volcanologist at the Institute of Geological and

Nuclear Sciences (GNS) in Taupo, New Zealand. "This has been a 10-year experiment in the making." The information mother lode should help scientists better protect the millions of people who live in the path of lahar-generating volcanoes around the world.

Wiring up Mount Doom

In 1995, Ruapehu's roughly 50-year cycle of eruptions kicked in again. Gobs of lava burped up from the bottom of the crater, adding 7 meters of loose ash and stones, called tephra, to the rim. The deepened crater soon filled with snowmelt from above and sulfuric acid and other material from



Bracing for the big one. Ready for a world first: recording data from a volcanic lahar in action.

fumaroles below. One of Ruapehu's grumbles late last year triggered an earthquake that whipped the lake into a frenzy, slamming the crater walls with 6-meter waves. "It was clear that it was only a matter of time" before the tephra rim failed and caused a lahar, says Manville.

But exactly when the big one would strike was unknown. The inherent unpredictability of lahars is what makes them so dangerous, says Cynthia Gardner, a geologist at the Cascades Volcano Observatory in Vancouver, Washington. Most eruptions are preceded by a telltale increase in underground vibrations, swelling of the slopes, and changes in the composition of vented gases. But a lahar "can occur without warning," Gardner says. Besides eruptions and earthquakes, even a heavy rain can be enough to loosen unstable material at the top of many steep volcanoes. Gravity does the rest.

Another deadly aspect of lahars is the great distances they can travel down river valleys, sometimes hundreds of kilometers from a volcano. "Imagine," says Gardner, "a rushing surge of water coming toward you that's tens of meters thick" and carrying boulders, trees, and even houses. The best chance of survival is to get out of the way—only lahars are too fast to outrun. The deadliest lahar in recent history occurred in 1985, when an eruption of the Nevado del Ruiz volcano in Columbia triggered mudslides 50 meters thick that buried a town 70 kilometers away, killing 23,000 people.

To warn of an impending lahar at Ruapehu, a team led by Harry Keys, an engineer at the New Zealand Department of Conservation, wired up the mountain. His group installed underground microphones, called geophones, at the lake's rim to record



Mount Doom, brooding. Data from Ruapehu's lahar flow will help better protect millions of people living near other volcanoes.

vibrations. A buried wire was set to trip if the tephra dam broke, and a depth meter was deployed in the lake to record sudden drops. Geophones on the slopes listened for approaching flows. When any signal leaped above the background noise, an alarm message was sent automatically to scientists, police, and the highway authorities.

Scientists thought this would give a good idea of when a Ruapehu lahar would strike; where was another question. "What we're learning is that lahars evolve," says Sarah Fagents, a geophysicist at the University of Hawaii, Manoa. Although a lahar may start as a liquid with the low viscosity of water, it quickly becomes as thick as wet concrete as it picks up fine sediment, then morphs back into a less-viscous flow as it sheds particulates down the slope. As if that weren't already hard enough to simulate on a computer, as a lahar rips up material here and dumps it there, the changing terrain steers the flow.

"A whole lot of footwork" was required to record how Ruapehu's slopes looked before a lahar struck, says Alison Graettinger, a graduate student at the University of Waikato in nearby Hamilton. The grunt work included taking samples and Global Positioning System measurements to map out the composition and distribution of material on the slopes. The researchers also used light detection and ranging (LIDAR) technology to build three-dimensional models of land features by firing laser pulses and measuring the delay of the reflection.

By early 2007, all that remained on the scientists' to-do list was to install the last lahar-weighing sensor and a camera. Before the team could finish, nature intervened.

Chronicling its wrath

At 11:21 a.m. on 18 March, a 20-meter-wide section of the tephra dam crumbled.

The breach trebled in size in 10 minutes. At its peak, the lake discharged the equivalent of an Olympic swimming pool of water every 4 seconds. By the time the flow ended a couple of hours later, 1.3 million cubic meters had drained.

For the first time ever, researchers knew a lahar was on the way and watched the event unfold.

The ultimate cause of the dam's failure was 5 days of heavy rain that nudged up the water level inside the crater by a half-meter. However, signs of trouble had begun appearing months earlier. In January, the team found that the dam was becoming more electrically conductive—an indicator that water was infiltrating the dam's porous matrix—and that tephra sediment was trickling down its outer surface. The major collapse was preceded by several smaller ones starting more than an hour before—all captured on camera. These early tremors were also picked up by the geophones and set off the alarm system.

It was clear this was no false alarm when a "landslide-type failure" cut the trip wire. Layers began sloughing from the dam's outer surface inward until erosion reached "a critical point" and rapidly accelerated about 15 minutes later, says Chris Massey, a GNS geological engineer in Wellington. The lahar traveled 155 kilometers along river paths until it reached the ocean at 3 a.m. the next morning. The damage was minor—a small bridge, a block of toilets, and a farmer's pump shed were destroyed—and the alarm system allowed authorities to close highways well in advance to clear the way.

Since that day, a team led by Manville and Shane Cronin, a volcanologist at Massey University, has worked nonstop to gather data from Ruapehu before wind and rain erase the evidence. The techniques used

to establish the "before" picture—such as LIDAR scans and field sampling—are being repeated to get the "after." Data analysis is just beginning, but it is already providing "a unique insight into how natural dams fail," Massey says. For example, he says, it is clear that the dam's stability "was highly sensitive to relatively minor changes in lake water level."

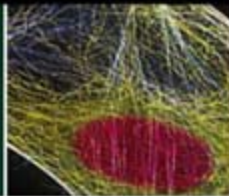
Down the mountain, other data revealed that as the lahar surged along a riverbed, it may have created a soliton, a standing wave that can propagate over great distances without losing energy or changing shape. Photographs of the lahar's leading edge seem to show such a wave, and analysis of water samples indicates that the lahar was pushing a huge swell of fresh river water ahead of it. Solitons have been observed in canals, says GNS geophysicist Desmond Darby, but this is the first evidence of one generated by a volcano. Although the soliton didn't make the lahar any more vicious, it's "an interesting phenomenon," Manville says. The Ruapehu researchers will present findings next month at a meeting of the International Union of Geodesy and Geophysics in Perugia, Italy.

The ongoing scrutiny of Ruapehu's latest lahar could save lives elsewhere. Probably the biggest threat is in Ecuador, where some 100,000 people live in the direct path of potential lahars from Mount Cotopaxi, says Patricia Mothes, a volcanologist at the Geophysical Institute in Quito. The data coming out of New Zealand get at "some of the questions that I always have" about how to assess lahar risk, she says, such as which conditions are more likely to spawn sediment-laden lahars capable of "transporting huge boulders very long distances."

Someday, Mount Doom may become more famous for saving lives than for menacing hobbits. —JOHN BOHANNON

Celol cultures

1568



Multifunctional agriculture systems

1570



LETTERS | BOOKS | POLICY FORUM | EDUCATION FORUM | PERSPECTIVES

LETTERS

edited by Etta Kavanagh

Culture, Conflict, and... Climate?

DESPITE THE HISTORICAL MILITARY ROLE OF ANTHROPOLOGY IN UNDERSTANDING LOCAL peoples during the Colonial period (1), defense policy-makers and academic researchers rarely play well together in the proverbial sandbox. A general Cold War-era preoccupation with technological superiority, combined with the negative aftereffects of poor cultural understanding of opposing forces in the Vietnam War, left the U.S. Department of Defense (DOD) unprepared to integrate cultural knowledge into a comprehensive intellectual infrastructure. In the current "Global War on Terror" or "Long War" era, it needs such tradecraft now more than ever.

The article "Pentagon asks academics for help in understanding its enemies" (Y. Bhattacharjee, *News Focus*, 27 Apr., p. 534) outlines a new DOD initiative, called Human Social Culture Behavior (HSCB) Modeling, designed to begin and encourage advanced anthropological analyses of cultures that the U.S. military might encounter during overseas operations. This relatively inexpensive defense transformation—largely a shift in thinking—could have benefits beyond active counterinsurgency warfare and counterterrorism. This is increasingly important, given the recent DOD emphasis on stability operations throughout the world—proactively preventing failed states and discouraging formation of terrorist havens.

HSCB models may have further applications to one of the most pressing environmental problems of our time—global climate change. Reputable and reasonable projections suggest that future changes in climate will increase the frequency and severity of food and water shortages, heat-related illnesses, and infectious disease epidemics (2). These outcomes may exacerbate local tensions, act as a "threat multiplier" in some unstable regions, and significantly increase the risk of state failure in regions of strategic importance (3). If HSCB models can be expanded to incorporate environmental knowledge, they might be used effectively to prevent or mitigate environmentally induced conflict. Conversely, climate change will also have local positive effects, and knowledge of the environmental terrain will have benefits in those situations as well. Ultimately, in a climate of change, cultural and environmental knowledge could be integrated into a global early warning system, detecting the sorts of changes that might signal instability and a need for intervention. Earlier this year, the House accepted provisions, inserted into the FY08 intelligence authorization bill, that explicitly direct the U.S. intelligence community to consider climate impacts when preparing future National Intelligence Estimates. At the time of writing, similar provisions are being considered by the Senate.

"[C]ultural and environmental knowledge could be integrated into a global early warning system..."

—Drapeau and Mignone

MARK D. DRAPEAU^{1*} AND BRYAN K. MIGNONE^{2*}

¹AAAS Science & Technology Policy Fellow, Center for Technology and National Security Policy, National Defense University, Fort Lesley J. McNair, Washington, DC 20319, USA. E-mail: DrapeauM@ndu.edu. ²Science & Technology Fellow, Foreign Policy Studies Program, The Brookings Institution, 1775 Massachusetts Avenue, NW, Washington, DC 20036, USA. E-mail: bmignone@brookings.edu

*These views are those of the authors and not the official views of the National Defense University, the U.S. Defense Department, or the U.S. Government.

References

1. M. McFate, *Mil. Rev.* **85**, 24 (March–April 2005).

2. Intergovernmental Panel on Climate Change, *Climate Change 2007: Impacts, Adaptation and Vulnerability*, available at www.ipcc.ch/ (2007).
3. The CNA Corporation, *National Security and the Threat of Climate Change*, available at <http://SecurityAndClimate.cna.org/> (2007).

Better Use of Existing Knowledge

IT IS ENCOURAGING TO SEE THE FOCUS ON cross-cultural research by the U.S. Department of Defense ("Pentagon asks academics for help in understanding its enemies," Y. Bhattacharjee, *News Focus*, 27 Apr., p. 534). However, the same information is effectively gathered by interviewing local experts and having representatives of the United States "on the ground" to sort through the data. Our State Department does a good job with this and understood the problems with invading Iraq quite well. However, this advice was ignored. Perhaps it would be more productive to study our institutions and see how we can better make use of the good knowledge that we have, rather than generating redundant data, which have a high probability of also being ignored. It has been said that the most effective way to deflect accountability in government is to study the problem for long enough for the next election to take place (and memories to fade).

A related concern is how to address solutions once the problem is obvious. This "riding the tiger" problem ("if you get off, it will eat you") needs a focus on amnesty for error, but not for intransigence. During delays in correction, much damage is done that could and should be avoided.

CHRISTOPHER BATICH

College of Engineering, University of Florida, Gainesville, FL 32611, USA.

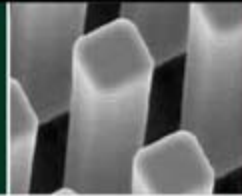
Grazing and "Degradation"

IT IS HARD TO SEE, GIVEN PREVIOUS ANALYSIS (1), the point of redefining "nonequilibrium" systems as "all systems that are not at equilibrium," as L. Gillson and M. T. Hoffman do in their Perspective "Rangeland ecology in a changing world" (*Perspectives*, 5 Jan., p. 53). This would apply almost everywhere and



Brain circuits
and cognition

1578



Food safety

1579

would be inconsistent with many publications. Few ecologists use “equilibrium” to mean that species track their resources precisely; they emphasize constrained variation in abundance, despite stochasticity (2). Correlations between regional and temporal variation in rainfall and herbivore abundance confirm equilibrium consumer-resource dependence when viewed at sufficient spatial and temporal scales (3–5). The real challenge is to distinguish the subset of resources in the system that limit large herbivore numbers from those that do not, and to understand how species of plant and animal in each subset respond to herbivory (6, 7). Crucially, a nonequilibrium area for one species may be a key resource for another.

Gillson and Hoffman ask how “degradation” can be defined in naturally variable systems. This problem and its solution are not

unique to grasslands. Relatively natural protected areas are used as “biodiversity benchmarks,” and their state in a particular season is compared with management treatments in the same region and season (8–10). There is substantial literature on the effects of grazing, and taxa vary in their responses. “Degradation” to one person can be “improvement” to another—as with controversies over traditional grazing to prevent natural succession in semi-natural habitats (8). Societies must decide subjectively and explicitly which changes in wildlife are acceptable.

CLIVE HAMBLER,¹ SUSAN M. CANNEY,¹
MALCOLM J. COE,¹ PETER A. HENDERSON,¹
ANDREW W. ILLIUS²

¹Department of Zoology, University of Oxford, South Parks Road, Oxford OX1 3PS, UK. ²Institute of Evolutionary Biology, School of Biological Sciences, University of Edinburgh, Edinburgh EH9 3JR, UK.

References

1. A. W. Illius, T. G. O'Connor, *Ecol. Appl.* **9**, 798 (1999).
2. D. L. Lack, *The Natural Regulation of Animal Numbers* (Clarendon Press, Oxford, 1954).
3. M. J. Coe *et al.*, *Oecologia* **22**, 341 (1976).
4. C. W. D. Gibson, J. Hamilton, *Oecologia* **61**, 230 (1984).
5. C. Hambler *et al.*, *Science* **307**, 673 (2005).
6. A. W. Illius, T. G. O'Connor, *Oikos* **89**, 283 (2000).
7. A. W. Illius, *Science* **307**, 674 (2005).
8. C. Hambler, *Conservation* (Cambridge Univ. Press, Cambridge, 2004).
9. S. M. Canney, *Satellite Mapping of Vegetation Change: Human Impact in an East African Semi-arid Savanna* (Pisces Conservation Ltd., Lymington, UK, 2001).
10. A. R. E. Sinclair *et al.*, *Proc. R. Soc. London Ser. B* **269**, 2401 (2002).

Response

DEFINITIONS OF DISEQUILIBRIUM AND NON-equilibrium have been discussed previously in the literature (1, 2). The term “disequilibrium” was originally used to define systems that were stochastically driven and not affected by density-dependent effects (3, 4). Illius and O'Connor (5) subsequently redefined the term by applying it to key resource areas, affected by density-dependent competition. The term “disequilibrium” has thus been used in two distinct ways in the literature. It was our aim to make this distinction clear and to focus on how density dependence and stochasticity

CELL BIOLOGY

Thousands of Products. Hundreds of Techniques. Infinite Possibilities.

One Book.



The combination of Upstate®, Chemicon® and Millipore brings together all the leading tools for cell biology—including the most advanced stem cell products. All in one book. To see for yourself, request a copy of our new Cell Biology Application Guide today.

www.millipore.com/OneBook

upstate | CHEMICON
now part of Millipore

interact in nonequilibrium systems (where a nonequilibrium system is defined as a system that tracks a changing environment and therefore doesn't reach equilibrium). We apply the term "disequilibrium" in its original sense only to that subset of systems that are dominated by stochasticity, but agree with Illius and O'Connor that competition may be important at key resource areas.

The lack of clarity over the usage of the terms "disequilibrium" and "nonequilibrium" has obscured the fact that there is general agreement that complex ecological systems are affected by both density dependence and environmental stochasticity. Our Perspective presented a view based on complex systems theory that shows how density dependence and stochasticity interact, and how density dependence can occur at different population sizes, depending on rainfall and therefore forage availability and quality. This synthesis is supported by empirical work demonstrating interactions between rainfall variability, nutrient cycling, and grazing (6, 7).

Our Perspective raised the possibility that nonequilibrium systems may lose resilience if heavily grazed, because of an increased dominance of annual and unpalatable plants.

Annual-dominated systems are more sensitive to drought than perennial-dominated systems, and this potential or actual loss of resilience—in terms of the ability of the system to absorb disturbance without changing to a new domain of attraction—has implications for rural livelihoods. In many rangelands, traditional practices and institutional responses to environmental variability (e.g., mobility, herd-splitting, more restrictions on grazing) have already been eroded because of the loss of grazing lands, the imposition of fixed stocking rates, and the desire of many national governments to settle mobile pastoralists. The management options available are therefore limited, and high variability in annual-dominated, disequilibrium systems may increase the vulnerability of farmers to environmental fluctuations and drive livelihood diversification, particularly where long-distance seasonal migration of people and livestock is no longer an option. There is thus a need for a greater integration of micro-economic research to understand how farmers have adapted and diversified their management responses and livelihood strategies in response to restricted access to grazing and water (8–10).

We agree with Hamblin *et al.* that defining degradation in variable ecosystems is a chal-

lenge not unique to rangelands. Our point was that ecosystem variability tends to occur within upper and lower bounds, and once ecological or environmental thresholds are exceeded, the system will then vary within new limits. Knowledge of when and why these transitions occur is an essential underpinning of the scientific aspects of range management. As we also pointed out in our Perspective, however, an understanding of the effects of different management options on plant communities still leaves policy-makers with the challenge of deciding what is an acceptable outcome in terms of plant diversity and ecosystem resilience, while also considering the effects on rural livelihoods.

LINDSEY GILLSON AND M. T. HOFFMAN

Institute for Plant Conservation, Botany Department, University of Cape Town, Private Bag X3, Rondebosch 7701, South Africa. E-mail: Lindsey.Gillson@uct.ac.za

References

1. F. D. Richardson, B. D. Hahn, M. T. Hoffman, *Ecol. Model.* **187**, 491 (2005).
2. D. D. Briske, S. D. Fuhlendorf, F. E. Smeins, *J. Appl. Ecol.* **40**, 601 (2003).
3. J. E. Ellis, D. M. Swift, *J. Range Manage.* **41**, 450 (1988).
4. R. Behnke, H. I. Scoones, C. Kerven, Eds., *Range Ecology at Disequilibrium: New Models of Natural Variability and Pastoral Adaptation in Africa Savannas* (Overseas Development Institute, London, 1993).

Congratulations
to the

Robert J. and Claire Pasarow Foundation
2006 Medical Research Award
Recipients

Cancer Research Award

Tony Hunter, PhD
The Salk Institute

Cardiovascular Research Award

Daniel Steinberg, MD, PhD
University of California, San Diego

Neuropsychiatry Research Award

Huda Zoghbi, MD
Baylor College of Medicine

Board of Directors

Jack D. Barchas, M.D., Claire Pasarow, Anthony Pasarow,
Susan Pasarow, Ronald Evans, Ph.D., Brian Henderson,
M.D., Judith Swain, M.D., Joseph Van der Meulen, M.D.,
Alexander Varshavsky, Ph.D.

For more information, please contact
Jack D. Barchas at (212) 746-3770

A request for Nominations for the 2007 Pasarow Foundation
Awards will be advertised in an early December issue
of *Science*.

FREE
with registration

Science Alerts in Your Inbox

Get daily and weekly E-alerts on the latest news and research! Sign up for our e-alert services and you can know when the latest issue of *Science* or *Science Express* has been posted, peruse the latest table of contents for *Science* or *Science's* Signal Transduction Knowledge Environment, and read summaries of the journal's research, news content, or Editors' Choice column, all from your e-mail inbox. To start receiving e-mail updates, go to: <http://www.sciencemag.org/ema>

Science Posting Notification
Alert when weekly issue is posted

ScienceNOW Weekly Alert
Weekly headline summary

Science News This Week
Brief summaries of the
journal's news content

ScienceNOW Daily Alert
Daily headline summary

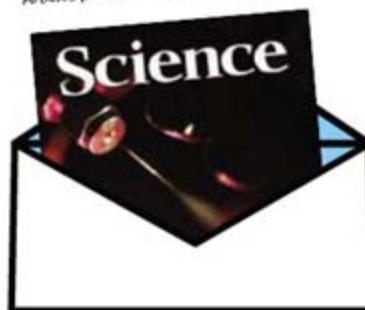
Science Magazine TOC
Weekly table of contents

Science Express Notification
Articles published in advance of print

STKE TOC
Weekly table
of contents

Editors' Choice
Highlights of the recent
literature

This Week in Science
Summaries of research
content



5. A. W. Illius, T. G. O'Connor, *Ecol. Appl.* **9**, 798 (1999).
6. D. J. Augustine, S. J. McNaughton, *Ecosystems* **9**, 1242 (2006).
7. D. Ward, *Science* **22**, 101 (2005).
8. B. M. Campbell *et al.*, *Ecol. Econ.* **60**, 75 (2006).
9. M. A. Janssen, J. M. Anderies, B. H. Walker, *J. Environ. Econ. Manage.* **47**, 140 (2004).
10. M. Quaas *et al.*, *Ecol. Econ.* **62**, 251 (2007).

A Brief History of the FFAG Accelerator

THE NEWS FOCUS ARTICLE "A HALF-CENTURY late, alternative accelerator takes off" by E. Cartlidge (16 Feb., p. 933) notes the recent revival of the fixed-field alternating-gradient synchrotron (FFAG) accelerator concept, but does not give the history of FFAG. Tihro Ohkawa in Japan, Keith Symon in the United States, and Andrei Kolomensky in Russia independently invented the FFAG concept. The U.S. group, the Midwest Universities Research Association (MURA), had been formed to develop plans for a high-energy research accelerator program in the Midwest in the early 1950s, and it was within this group that Symon conceived of FFAG and that the three different FFAG electron accelerators were built and operated, studying many aspects of accelerator

physics. After MURA learned of Ohkawa's independent invention of FFAG, he was invited to visit the MURA group for the summer of 1955 and then, in 1956, came to the United States to work within MURA for a few years.

LAWRENCE W. JONES,¹ ANDREW M. SESSLER,² KEITH R. SYMON³

¹Department of Physics, University of Michigan, Ann Arbor, MI 48109-1040, USA. ²Lawrence Berkeley National Laboratory, Berkeley, CA 94720, USA. ³Department of Physics, University of Wisconsin, Madison, WI 53706, USA.

TECHNICAL COMMENT ABSTRACTS

COMMENT ON "Carbon-Negative Biofuels from Low-Input High-Diversity Grassland Biomass"

Michael P. Russelle, R. Vance Morey, John M. Baker, Paul M. Porter, Hans-Joachim G. Jung

Tilman *et al.* (Reports, 8 December 2006, p. 1598) argued that low-input high-diversity grasslands can provide a substantial proportion of global energy needs. We contend that their conclusions are not substantiated by their experimental protocol. The authors understated the management inputs required to establish prairies, extrapolated globally from site-specific results, and presented potentially misleading energy accounting.

Full text at www.sciencemag.org/cgi/content/full/316/5831/1567b

RESPONSE TO COMMENT ON "Carbon-Negative Biofuels from Low-Input High-Diversity Grassland Biomass"

David Tilman, Jason Hill, Clarence Lehman

We discovered that biofuels from low-input high-diversity mixtures of native perennial prairie plants grown on degraded soil can provide similar bioenergy gains and greater greenhouse gas benefits than current corn ethanol produced from crops grown in monoculture on fertile soil with high inputs. Russelle *et al.*'s technical concerns are refuted by a substantial body of research on prairie ecosystems and managed perennial grasslands.

Full text at www.sciencemag.org/cgi/content/full/316/5831/1567c

Letters to the Editor

Letters (~300 words) discuss material published in *Science* in the previous 3 months or issues of general interest. They can be submitted through the Web (www.submit2science.org) or by regular mail (1200 New York Ave., NW, Washington, DC 20005, USA). Letters are not acknowledged upon receipt, nor are authors generally consulted before publication. Whether published in full or in part, letters are subject to editing for clarity and space.

IMMUNODETECTION

Thousands of Biotoools. Decades of Experience. Countless Options.

One Book.



The combination of Upstate®, Chemicon® and Millipore brings together all the leading tools for immunodetection—including the latest antibodies for life science research. All in one book. To see for yourself, request a copy of our new Immunodetection Application Guide today.

www.millipore.com/OneBook

upstate | CHEMICON
now part of Millipore

CELL BIOLOGY

The Culture of Cell Culture

M. Susan Lindee

Culturing *Life*, Hannah Landecker's history of cell culture, is a sly commentary on our mixed-up, topsy-turvy biological world, circa 2007. Mouse-human hybrids, immortal cells, cloned puppies, genetically modified crops, and dinosaur proteins

Culturing Life

How Cells Became Technologies

by Hannah Landecker

Harvard University Press, Cambridge, MA, 2007. 288 pp. \$35, £22.95, €32.30. ISBN 9780674023284.

found in fossilized bone all suggest that organisms are plastic, unstable, and not even the masters of their own cells, which can live outside them, perhaps "forever." Landecker's work tracks the practices and technologies implicated in this unsettling state

of affairs over the last century.

Drawing primarily on the methods sections of published scientific papers, a nontraditional historical resource, Landecker (an anthropologist at Rice University) explores techniques for handling cells outside the body. She proposes that the emergence of new methods of cell manipulation produced a scientific and social climate in which living matter is assumed to be material that can be started or stopped at will. Time and place are her underlying subjects: She asks how cells became "autonomous" and how they became "immortal."

Cell culture techniques were first developed in the 1880s, but Landecker begins her story with the work of Ross Harrison, who in 1907 demonstrated that tissue fragments could live in vitro for weeks at a time. Their survival for so long under controlled laboratory conditions was greeted by scientific observers with disbelief and excitement: A cell with a life of its own was a truly novel object.

In early 1912, the eccentric and controversial Alexis Carrel, a physiologist at the Rockefeller Institute, drew on Harrison's methods to culture a pulsating chicken heart. Carrel (the Nobel laureate in physiology that year) fused philosophical and biological imperatives in his work, choosing to grow heart muscle tissue because of its dramatic appeal to students, other scientists, and the public. Carrel wanted to suggest the possibili-

ties of immortality, and public interpretation followed this line of reasoning in spectacular news stories promoting his work.

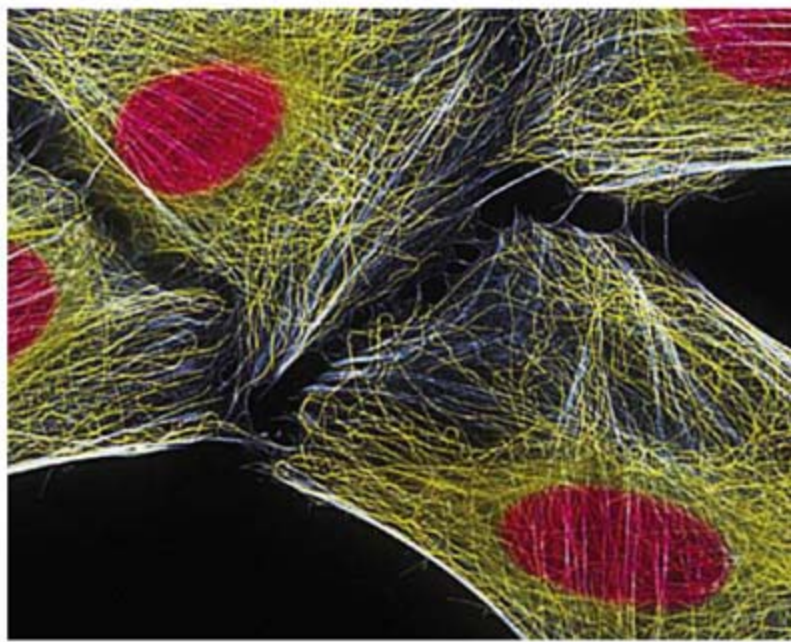
The most famous immortal cell, of course, is HeLa, cultured by George and Margaret Gey at Johns Hopkins University in 1951 and still an extremely important laboratory technology. After George Gey showed that polio could infect the cultures, the need to test the Salk vaccine led to the first effort to grow HeLa cells in large quantities. In 1953, the National Foundation for Infantile Paralysis established a central production laboratory at the Tuskegee Institute. It shipped 600,000 cultures of HeLa over the next two years, in the process developing the methods and shipping practices that facilitated the widespread use of the cell line in many other contexts. Without the sense of national urgency that characterized the polio vaccine program, this rapid standardization and dissemination of HeLa would have been unlikely. Gey's policy of traveling with a few tubes of HeLa, tucked into his shirt pocket next to his chest to keep them warm, could never have had the same impact. Later the line became too successful, an overaggressive contaminant, and a major quality control problem, potentially invalidating many scientific studies.

The story of the African-American patient Henrietta Lacks and her cancerous cervical cells has fascinated people for more than 50 years. Landecker considers the many popular stories written about HeLa and proposes that they help us to understand an emerging transition in ideas about technological and human life. HeLa, she shows, has been repeatedly construed by scientists, journalists, and others in terms that conflate the person who died of cancer and the cell line, with calculations of their "combined age" and cumulative weight ("what she would weigh now"). Spectral images of Lacks wandering "somewhere, with freshly painted toenails and curlers in her hair" and images of the patient as saint or martyr illuminate the characteristics of a scientifically mediated, disembodied immortality. These narratives, Landecker suggests, reflect ten-

sions around a new possibility for everyone: that a tissue sample taken from one's body could go on to have an independent, enduring, and highly distributed life as a subject of biomedical attention and interest.

The technical potential of cell culture began to reshape genetics in the 1950s and 1960s, when techniques for hybridizing cells seemed to provide a way around the inconvenience of sexual breeding. The fact that cells from different species could be fused also suggested that, at least at the cellular level, there were no mechanisms for recognizing incompatibility between species. Somatic cell hybridization was astonishing, almost unbelievable, to early scientific observers. But it quickly became the basis of sophisticated research programs in multiple domains.

Boris Ephrussi proposed with some trepidation in 1972 that it had become possible to make almost any kind of hybrid cell, from across all of biology, for any kind of purpose. And Lewis Thomas observed that the "labora-



Focus of many narratives. HeLa cells.

tory trick" of cell fusion was the "most unbiologic of all phenomena, violating the most fundamental myths of the last century" (1).

Fundamental myths, as Landecker reminds us, are a part of scientific history. Her account of the development of cell culture techniques delineates the shifting meaning of the whole organism, as it has come to be seen as a biological stage through which cellular materials cycle in time. By juxtaposing the practical details of deep freezers, record-keeping practices, and nutrient media with changing public and scientific discourses of life and death, she provides critical historical and anthropological insight into the meanings of hybridity, autonomy, plasticity, and immortality of cellular life.

The reviewer is at the Department of History and Sociology of Science, 365 Logan Hall, University of Pennsylvania, 249 South 36th Street, Philadelphia, PA 19104-6304, USA. E-mail: mlindee@sas.upenn.edu

Her work also provides a thoughtful perspective on the contemporary public and scientific spectacle of “Stuart Little” mice, stem cell legislation, pharmaceuticals, and other chimeras. Cell culture, she suggests, has changed what it means to be biological.

Reference

1. L. Thomas, *The Lives of a Cell: Notes of a Biology Watcher* (Viking, New York, 1974).

10.1126/science.1142574

ARCHAEOLOGY

Folsom Points

Dennis Stanford

The results of excavations during the 1920s at the Folsom, New Mexico, site demonstrated to most scientists' satisfaction that prehistoric people hunted ice age bison in North America. These finds also dispelled decades of acrimonious debate regarding the timing of human arrival in the Western Hemisphere. Scientific publications and presentations resulting from this ground-breaking research discussed the age of the bone bed, bison taxonomy, and possible strategies used to trap and kill these members of the Pleistocene megafauna. The unique fluted projectile points found among the bone became the index fossils for the Folsom technological horizon. Even with the landmark site's important role in the development of American archaeology, David Meltzer's *Folsom: New Archaeological Investigations of a Classic Paleoindian Bison Kill* is the first comprehensive report published on it.

Near the 75th anniversary of the Folsom discovery, Meltzer (an anthropologist at Southern Methodist University) embarked on an interdisciplinary program to reinvestigate the site. Using methods unknown in the 1920s, the project aimed to refine our understanding of the ecological context of this bison kill and the cultural and taphonomic events that shaped its archaeological record. For instance, it was unclear whether the bone bed represented a single killing event, what hunting strategies were employed, and whether a campsite was established near the kill.

The strength of the reinvestigation resides in the results obtained by modern paleoenvironmental and geological collaborative studies; these are presented in detail along with



In situ. The Folsom point found in August 1927 between two ribs of the extinct bison.

fresh archaeological discoveries. Throughout the book, Meltzer weaves a historical thread from the notes, letters, and communications of previous investigators. His in-depth summaries present their thoughts, worries, criticisms, disagreements, and headline-shaping hypotheses. Placing the early conclusions within the context of the new investigations, Meltzer compares, contrasts, and interprets them. When one considers the methodological advancements and expansion of archaeological knowledge over the past 75 years, it is striking how well many of the original interpretations hold up.

The latest research provides new insights about the paleotopographic setting of the kill area. Subsurface contours of the underlying bedrock (mapped by correlating core and auger hole data) suggest that two short northeast-trending gullies or “paleotributaries” with relatively steep sides coalesced roughly 60 m before they emptied into a larger southeast-flowing drainage. This topographic situation would have provided several 90-degree turns and steep banks for casting spears or darts down on the bison. These landscape features offer the best clues for a method used to kill the bison, but exactly how that task was accomplished at Folsom still remains a matter of conjecture.

Studies of pollen samples collected from Bellisle Lake (located on nearby Johnson Mesa) and from the bone bed itself, along with information gained from the study of land snails and carbon and nitrogen stable isotopes derived from the bison bone, suggest that climatic conditions during the Folsom

period were cooler and drier than at present, with scattered wet places on the landscape. These environmental conditions are broadly consistent with late glacial records elsewhere in the region.

Even though researchers from the many disciplines involved in the project “helped throughout the fieldwork, analysis, and writing, going above and beyond the call of co-author obligations,” they were recognized only by an authorship status of “with”—thereby making Meltzer the sole author rather than editor, as is normal in interdisciplinary works. This approach appears to be unfair to his collaborators, especially graduate students and younger professionals establishing careers. In addition, important data can be missed when a nonspecialist, no matter how talented, rewrites a technical research report. For example, although long, the discussion of the geology fails to present stratigraphic cross sections that clearly illustrate the sedimentary units and identify locations of samples referred to in numerous figures and tables. The single labeled figure of the stratigraphy (figure 5.1)—a 1928 photograph taken of a profile in the North Bank of the arroyo, not seen by the modern investigators—does not satisfy an enquiring mind. If Vance Holliday had been the lead author of the geologic section, perhaps he would have provided these important diagrams. What might be missing from other chapters?

The book includes boiler-plate questions concerning artifacts, technological organization, and mobility. But few are answered, either because their resolution is beyond the reach of current archaeological methods or because of the site's small sample size. The

reinvestigation confirms that one fall in an arroyo, late-ice age hunters killed more than 30 bison cows and calves. For insight into the technological, logistical, and social decisions made by these sophisticated big game hunters, the data gleaned from the stones and bones at Folsom are insufficient. Those complex issues are best approached through

considerations of other Folsom sites where processing and camping areas have been found with larger and more diverse artifact assemblages.

I was excited about doing this review: Folsom archaeology is one of my favorite topics, and I have always considered Meltzer an excellent wordsmith. However, in *Folsom* he veers away from his usual engaging style to produce a too-dense study.

10.1126/science.1129537

Folsom

New Archaeological Investigations of a Classic Paleoindian Bison Kill

by David J. Meltzer

University of California Press, Berkeley, 2006.
388 pp. \$55, £35.95.
ISBN 9780520246447.

ENVIRONMENT

Sustainable Development of the Agricultural Bio-Economy

N. Jordan,^{1*} G. Boody,² W. Broussard,³ J. D. Glover,⁴ D. Keeney,⁵ B. H. McCown,⁶ G. McIsaac,⁷ M. Muller,⁵ H. Murray,⁸ J. Neal,⁹ C. Pansing,¹⁰ R. E. Turner,¹¹ K. Warner,¹² D. Wyse¹

A “bio-economy” based on agricultural biomass is emerging in the United States that offers an avenue toward energy independence and a more “green” economy (1). Models for biomass production range from monocultures of annual and perennial crops to seminatural plant communities (2, 3). Monocultures are simpler to implement, but will likely perpetuate problems that have arisen from current monocultures of annual crops (mainly corn, soybean, wheat, and cotton). Recently, market-based agricultural policies have resulted in large payments to farmers and landowners to make up the difference between low commodity prices and costs of production (4); from 1997 to 2006, producers received 30% of their net farm income in direct government payments (5). Environmental problems are frequently associated with cultivation of the annual crops that are eligible for subsidy payments, including degradation of water quality with sediment, nutrients, and pesticides; hydrologic modifications contributing to flooding and groundwater depletion; disruption of terrestrial and aquatic wildlife habitats; emission of greenhouse gases; and degradation of air quality with odors, pesticides, and particulates (6).

Farm size has increased, and few people are able to enter farming, harming rural communities socially and economically (7). In the Corn Belt states such as Iowa, over half the

land is owned by absentee landowners (8), which makes implementation of conservation practices more difficult. Now, excess corn and soybean stocks are being converted to biofuels, and demand for corn has skyrocketed, resulting in a considerable expansion of corn production and concomitant environmental impacts (9).

Despite troubling implications of these current trends, research and development (R&D) and policy have focused on maximizing biomass production and optimizing its use

A U.S. farm policy shift to joint production of commodities and ecological services will advance sustainable agriculture.

Multifunctional Production Systems

Agricultural multifunctionality is defined as the joint production of standard commodities (e.g., food or fiber) and “ecological services.” Examples of the latter include increased recreational opportunities in agricultural landscapes and protection of biodiversity and water quality (13). Biomass-production systems such as mixtures of multiple species (3), tree cropping on farmland (14), and managed wetlands (15) use perennial plant species as the basis of joint production.



Multifunctional landscape in Iowa, USA.

(1), with far less emphasis on evaluation of environmental, social, and economic performance (9). This imbalance may provoke many interest groups to oppose growth of such an agricultural bio-economy (10).

Current federal programs and policy on environmental quality in agricultural landscapes mainly subsidize retirement of land from active production. This has produced substantial environmental benefits (11), but serious problems remain. Major additional gains may result from a “working landscape” approach that improves environmental performance of active farmland by rewarding farmers for delivering environmental benefits, as well as food and biomass (12). Our proposals aim to promote working landscapes by capitalizing on the potential of “multifunctional” agriculture.

There is mounting evidence that these systems can produce certain ecological services more efficiently and effectively than agroecosystems based on annual crops. Examples include (i) soil and nitrogen loss rates from perennial crops are less than 5% of those in annual crops (16); (ii) perennial cropping systems have greater capacity to sequester greenhouse gases than annual-based systems (17); (iii) in certain scenarios, some perennial crops appear more resilient to climate change than annuals, e.g., increases of 3° to 8°C are predicted to increase North American yields of the perennial crop switchgrass (*Panicum virgatum*) (18); and, (iv) among species of concern for conservation, 48% increased in abundance when on-farm perennial land cover was increased in European Union incentive programs (19).

¹Agronomy and Plant Genetics Department, University of Minnesota, St. Paul, MN 55018; ²Land Stewardship Project, White Bear Lake, MN 55110; ³Department of Oceanography and Coastal Sciences, Louisiana State University, Baton Rouge, LA 70803; ⁴The Land Institute, Salina, KS 67401; ⁵Institute for Agriculture and Trade Policy, Minneapolis, MN 55404; ⁶Center for Integrated Agricultural Systems, University of Wisconsin-Madison, Madison, WI 53706; ⁷Department of Natural Resources and Environmental Sciences, University of Illinois, Urbana, IL 61801; ⁸Minnesota Institute for Sustainable Agriculture, University of Minnesota, St. Paul, MN 55108; ⁹Leopold Center for Sustainable Agriculture, Iowa State University, Ames, IA 50011; ¹⁰Mississippi River Basin Alliance, Minneapolis, MN; ¹¹Coastal Ecology Institute, Louisiana State University, Baton Rouge, LA 70803; ¹²Environmental Studies Institute, Santa Clara University, Santa Clara, CA 94053, USA.

*Author for correspondence. E-mail: jorda020@umn.edu

Multifunctional production systems can be highly valuable. The 34-million-acre Conservation Reserve Program (CRP) has been estimated to produce \$500 million/year in benefits from reduced erosion and \$737 million/year in wildlife viewing and hunting benefits at a cost of ~\$1.8 billion (11). If benefits such as carbon sequestration are added, CRP likely produces a net gain in many areas, if not for the entire nation.

Diversified grassland agroecosystems on degraded agricultural land can increase both carbon storage and net energy gain in biofuel production (3). This could provide 15% of electricity demand and eliminate 15% of CO₂ emissions if implemented globally.

Restored wetlands on flood-prone farmland can provide biomass, increase wildlife abundance, and improve water quality by processes such as denitrification (15). Denitrification in managed wetlands is estimated to reduce costs of biological nutrient removal in municipal water treatment by about 15%.

An assessment of the potential economic, social, and environmental performance of multifunctional systems is provided by a simulation study performed for two representative agricultural watersheds in the upper Midwest United States [subbasins of Wells Creek (16,264 ha) and the Chippewa River (17,994 ha) in Minnesota] (13). Results indicated that benefits could be attained by increased cultivation of perennial crops without increasing public costs. Environmental benefits included improved water quality, increased fish abundance, increased carbon sequestration, and decreased greenhouse gas emissions. Economic benefits included social capital formation, greater farm profitability, and avoided costs associated with specific environmental damages. The most extensive land-use change scenario (7 to 14% conversion to perennials) was projected to produce the greatest reductions in sediment and nutrient loading to waterways; sediment loading was reduced by as much as 80%. Total government payments were projected to decline by 13%. These projections offer a widely applicable model for agroecosystems in the Midwest United States.

Testing the Model

Multifunctional systems have been tested only at relatively small scales. We propose creation of a network of research and demonstration projects to establish and evaluate economic enterprises based on multifunctional production systems. This program will also help test and refine federal farm-bill policy

to support biomass production.

State, federal, and private agencies should pool their resources to support this network. These projects must be sufficiently scaled to address the complexity inherent in landscape-scale multifunctionality and in the feedback loops connecting natural, human, and social resources. They should be established in medium-sized watersheds (~5000 km²) and should be managed by groups that encompass multiple stakeholders and levels of government. Such an effort is under way in a larger subbasin of the Chippewa River in Minnesota (13), focused on development of grasslands for biofuel and meat and dairy food production.

Financial and policy support should be given to the multi-stakeholder processes of learning, deliberation, negotiation, and experimentation that are needed to establish and evaluate research and demonstration projects. Such processes might help, for example, to simplify complex funding landscapes of subsidy policy like the one that appears to be hindering biofuel development in the United Kingdom (20). Stirrings of the necessary approach are evident in recent strategic alliances among regional and national groups concerned with the environment, renewable energy development, and agriculture [e.g., see (21, 22)].

Research must be focused on the trade-offs that arise, e.g., between wildlife habitat and biomass production. Models indicated that the form of the trade-off determined whether wildlife-friendly farming was more cost-effective than an alternative policy, the retirement of "marginal" farmland to increase wildlife habitat (23). More broadly, modeling has indicated that many trade-off problems might be overcome if a sufficient range of ecological services (e.g., water-quality protection, as well as wildlife conservation) was provided (13). Empirical research is urgently needed in the context of specific enterprises, such as biofuel production.

Conclusions

Two key policy instruments to achieve the goals we have described are the omnibus farm bill and the existing agricultural R&D infrastructure. Agricultural subsidies in 2005 exceeded \$24 billion, and the 2007 farm bill deliberations should highlight how these federal dollars could better achieve national priorities. In particular, the new farm bill should provide the agricultural R&D infrastructure with incentives to evaluate multifunctional production as a basis for a sustainable agricultural bio-economy. We judge that this can be done with very

modest public investments (~\$20 million annually). A variety of strong political constituencies now expects a very different set of outputs from agriculture, and the U.S. farm sector could meet many of these expectations by harnessing the capacities of multifunctional landscapes.

References

1. A. Eaglesham, Ed., *Summary Proceedings: Third Annual World Congress on Industrial Biotechnology and Bioprocessing*, Toronto, 11 to 14 July 2006; nabc.cals.cornell.edu/pubs/WCIBB2006_proc.pdf.
2. L. Reijnders, *Energy Policy* **34**, 863 (2006).
3. D. Tilman, J. Hill, C. Lehman, *Science* **314**, 1598 (2006).
4. Economic Research Service (ERS), U.S. Department of Agriculture (USDA), *A History of American Agriculture, 1607–2000* (ERS Post 12, Washington, DC, September 2000); www.agclassroom.org/gan/timeline/index.htm.
5. ERS, *Farm Income: Data Files* (ERS, Washington, DC, 2007); www.ers.usda.gov/data/FarmIncome/finfidmu.htm.
6. R. N. Lubowski et al., *Environmental Effects of Agricultural Land-Use Change: The Role of Economics and Policy* (Economic Research Report no. 25, ERS, Washington, DC, 2006); www.ers.usda.gov/Publications/err25/.
7. C. W. Stofferhan, *Industrialized Farming and Its Relationship to Community Well-Being: An Update of a 2000 Report by Linda Lobao* (prepared for the Attorney General, State of North Dakota, 2006); www.und.nodak.edu/misc/ndrural/Lobao%2008%20Stofferahn.pdf.
8. M. Duffy, *AgDM Newsl.* (October 2004), www.extension.iastate.edu/agdm/articles/duffy/DuffyOct04.htm.
9. D. Kennedy, *Science* **316**, 515 (2007).
10. Institute for Agriculture and Trade Policy (IATP), "Assessing the bioeconomy" [survey] (IATP, Minneapolis, MN, 2006); www.agobservatory.org/issue_bioeconomy.cfm.
11. P. Sullivan et al., *The Conservation Reserve Program: Economic Implications for Rural America* (Agricultural Economic Report no. 834, ERS, Washington, DC, 2004); www.ers.usda.gov/Publications/AER834.
12. D. R. Keeney, L. Kemp, in *The Role of Biodiversity Conservation in the Transition to Rural Sustainability: Proceedings of North Atlantic Treaty Organization Advanced Research Workshop on Biodiversity Conservation and Rural Sustainability*, S. Light, Ed., Krakow, Poland, November 2002 (IOS Press, Amsterdam, 2004), pp. 29–47.
13. G. Boody et al., *BioScience* **55**, 27 (2005).
14. U. Jørgensen, T. Dalgaard, E. S. Kristensen, *Biomass Bioenergy* **28**, 237 (2005).
15. D. L. Hey, L. S. Urban, J. A. Kostel, *Ecol. Eng.* **24**, 279 (2005).
16. C. J. Gantzer, S. H. Anderson, A. L. Thompson, J. R. Brown, *J. Soil Water Conserv.* **45**, 641 (1990).
17. G. P. Robertson, E. A. Paul, R. R. Harwood, *Science* **289**, 1922 (2000).
18. R. Brown, N. Rosenberg, C. Hays, W. Easterling, L. Mearns, *Agric. Ecosyst. Environ.* **78**, 31 (2000).
19. D. Kleijn et al., *Ecol. Lett.* **9**, 243 (2006).
20. P. Thornley, *Energy Policy* **34**, 2087 (2006).
21. Green Lands Blue Water Initiative, www.greenlandsbluewater.org.
22. RiverMap, www.rivermap.org.
23. R. E. Green, S. J. Cornell, J. P. W. Scharlemann, A. Balmford, *Science* **307**, 550 (2005).
24. We thank participants in the Green Lands Blue Water Initiative, as well as C. Dybas, W. Jackson, S. Morse, and S. Pimm. Funding was obtained primarily through the Coastal Ocean Program, National Oceanic and Atmospheric Administration, and a grant from the Kellogg Foundation.

APPLIED PHYSICS

Recent Progress and Continuing Puzzles in Electrostatics

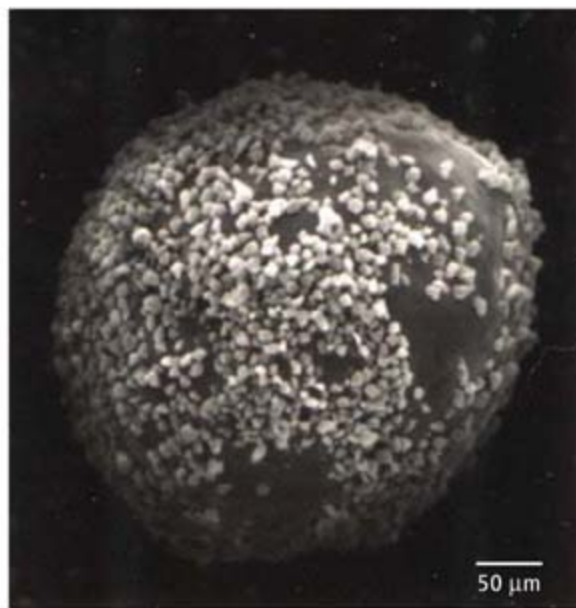
L. B. Schein

Electrostatic effects are all around us. Children rub balloons that then stick on walls. Copy machines and laser printers rely on the charging of small, colored, insulating toner particles to form images. And we have all been jolted after walking across a rug in dry weather and touching a doorknob. Electrostatic charging also causes lightning, damage to semiconductor devices, and super-tanker explosions.

To control these effects, we need to know how charging occurs and how electrostatic forces behave. Surprisingly, although electrostatic charging is well known, it remains among the most poorly understood areas of solid-state physics. Several recent studies have improved our insights into electrostatic charging and adhesion, which in turn may foster advances in the near future that could influence multibillion-dollar industries.

Charging between metals is well understood and is directly related to the difference in work function (the energy required to remove an electron) between the metals (1, 2). But when insulators are involved, which is almost always the case in the examples above, our understanding is rudimentary. Most researchers believe that insulator charging is a surface phenomenon. However, when the surfaces of two materials are brought together and separated, the actual contact area is difficult to determine. In addition, the precise nature of the surfaces is usually not well defined: Dust particles, surface contaminants, and even ultrathin water layers may constitute the outer surface. The number of surface molecules involved in the charging process is extremely small, on the order of one molecule in 10^4 or 10^5 . The determination of the nature of the charging sites by surface science tools remains an unsolved solid-state physics problem. As one can imagine, creating a reproducible surface and obtaining experimental reproducibility among laboratories has been a challenge.

The need for reproducible toner charge in electrophotography (2, 3) (the copier and laser-printer technology) has led to materials ideal for controlled insulator charging experi-



Extreme closeup. A scanning electron micrograph of 10- μm toner particles on a 200- μm carrier particle used in electrophotography. Detailed understanding of how these particles become electrostatically charged and the resultant adhesive force have improved the imaging technology.

ments. The figure shows a scanning electron micrograph of a mixture of insulating powders. Both the small powder (polymeric toner particles) and the large powder (polymer-coated magnetic particles called carrier particles) are insulators.

When these powders are mixed, electrostatic charge exchange occurs. The mixture is net neutral, with one sign of the charge on the toner particles and the other sign on the carrier particle. By virtue of the charge on the powders, they adhere to each other. This micrograph, therefore, shows the two fundamental issues associated with insulator charging: charge exchange and adhesion. This mixture of insulating powders is used in copy machines and laser printers because magnetic forces can move the large particles, which in turn move the smaller, hard-to-control toner particles that are attached.

Experiments with these powders have helped researchers settle some questions about charging mechanisms. Two theories that describe how insulator charging is limited by surface properties have been suggested. One theory assumes that there are electronic surface states on the insulating particles and that charge is exchanged to equi-

brating the “surface work functions” (4). (Quotation marks are used because it is unclear whether the concept of work function is useful in insulators—excess electronic charges cannot move or lose energy to establish thermodynamic equilibrium.) The second theory assumes that insulators charge until an electric field, called the effective electric field, is created at the interface between the particles (5, 6).

Using mixtures of powders similar to those shown in the figure, my colleagues and I have found that only the electric field model is consistent with the data (7, 8). The effective electric field is easily calculated from the data: It depends on the material and is on the order of $10\text{ V}/\mu\text{m}$. Unfortunately, it is difficult to account for this value of the effective electric field with any simple model. For example, if the field is associated with a solid-state energy change (1 eV) divided by the distance at which

electron transfer by tunneling ceases (1 nm, which is used successfully in the theory of metal-metal charging), the predicted field is $1000\text{ V}/\mu\text{m}$, two orders of magnitude larger than observed.

Despite this discrepancy, the electric field model is a step forward, allowing a test of suggested models of insulator charging. For example, models that invoke bulk properties almost surely will not be valid. Any suggested surface model needs to account for this effective electric field. Through the years many “models” or correlations have been suggested for insulator charging (1, 2). These include correlations with dielectric constant, the basic and acidic nature of the materials, polymer “work function,” and surface chemistry determined by measuring the residence time of probe molecules using inverse gas chromatography (9, 10). However, no reasonable explanation of the effective electric field has yet emerged.

Charged insulators adhere to surfaces, which is important in electrophotography where electric fields are used to move charged toner particles to form images after overcoming their adhesion. Particle adhesion has generally been thought to be due to the simple

The author is an independent consultant in San Jose, CA, USA. E-mail: schein@prodigy.net

electrostatic attraction of the charges on the particle to induced charges in the adhering surface. However, experiments have shown (11) that the adhesion is at least one order of magnitude larger than predicted by a model in which the charged object is represented by putting the total charge in the center of the object. Even with modifications to include nonuniform charge distributions (11) and nonelectrostatic forces of adhesion (12), these models cannot explain the observations.

Instead, the enhanced adhesion seems to be caused by the discreteness of charge, which is the way nature provides us with charge (i.e., one electron has exactly 1.6×10^{-19} Coulomb of charge) (13). Discrete charges near the contact points produce strong electrostatic forces approximately equal to the force of the total charge in the center of the particle. The physical picture that appears to describe the data is that there is electrostatic adhesion at every contact point (due to discrete charges). To minimize adhesion, the number of contact points needs to be minimized.

This idea has practical implications in electrophotography (14, 15). The number of contact points was minimized by coating the toner particles with about a monolayer of 10-nm-diameter silica nanoparticles. A toner particle with uniform small protrusions around

the surface will, when placed on a flat surface, make contact only at a minimum number of protrusions, minimizing both electrostatic and van der Waals adhesion. This new toner has adhesive forces lower by a factor of at least 10 than those of commercially available toner, which has resulted in the implementation of a new electrophotographic development system. The result is a true desktop color laser printer that is presently under development, which is much smaller—about the same volume as a black-and-white laser printer—and much less expensive than is currently commercially available (16, 17).

Our understanding of the charging mechanisms in insulating particles is still rudimentary, although a specific model, the electric field model, appears to have been experimentally verified. If the effective electric field could be associated with material properties of insulators, a rational approach to the design of the charging properties of insulators will be possible, changing the multibillion dollar industry of toner manufacture in electrophotography. The new understanding of charged particle adhesion has led to the design of low adhesion toner, which will dramatically change the color electrophotographic printing industry. Perhaps the concept of reducing adhesion by coating particles with a mono-

layer of nanometer-diameter silica will be useful in other technologies.

References and Notes

1. J. Lowell, A. C. Rose-Innes, *Adv. Physics* **29**, 947 (1980).
2. L. B. Schein, *Electrophotography and Development Physics* (Laplacian Press, Morgan Hill, CA, 1996).
3. C. B. Duke, J. Noolandi, T. Thieret, *Surf. Sci.* **500**, 1005 (2002).
4. L.-H. Lee, *Photogr. Sci. Engin.* **22**, 228 (1978).
5. A. Kondo, *Denshi Syasin Gakkai* **43**, 26 (1979).
6. A. Kondo, *Proceedings of the Reprographics Conference* (The Technical Association for the World Wide Pulp, Paper, and Converting Industry, Atlanta, GA, 1980), p. 153.
7. L. B. Schein, M. LaHa, D. Novotny, *Phys. Lett. A* **167**, 79 (1992).
8. G. S. P. Castle, L. B. Schein, *J. Electrostatics* **36**, 165 (1995).
9. R. P. N. Veregin *et al.*, *J. Imaging Sci. Technol.* **50**, 282 (2006).
10. R. P. N. Veregin *et al.*, *J. Imaging Sci. Technol.* **50**, 288 (2006).
11. D. A. Hays, *J. Adhesion* **51**, 41 (1995).
12. B. Gady, D. J. Quesnal, D. S. Rimai, S. Leone, P. Alexandrovich, *J. Imaging Sci. Technol.* **43**, 288 (1999).
13. W. S. Czarnecki, L. B. Schein, *J. Electrostatics* **61**, 107 (2004).
14. L. B. Schein, W. S. Czarnecki, *J. Imaging Sci. Technol.* **48**, 412 (2004).
15. L. B. Schein, W. S. Czarnecki, B. Christensen, T. Mu, G. Galliford, *J. Imaging Sci. Technol.* **48**, 417 (2004).
16. B. Wang, E. Shih, T. Mu, D. Tsai, L. B. Schein, *J. Imaging Sci. Technol.* **50**, 368 (2006).
17. This system is under development at Aetas Systems (Taiwan), which has employed the author as a consultant.

10.1126/science.1142325

ASTRONOMY

Waves in the Sun's Core

Frank Hill

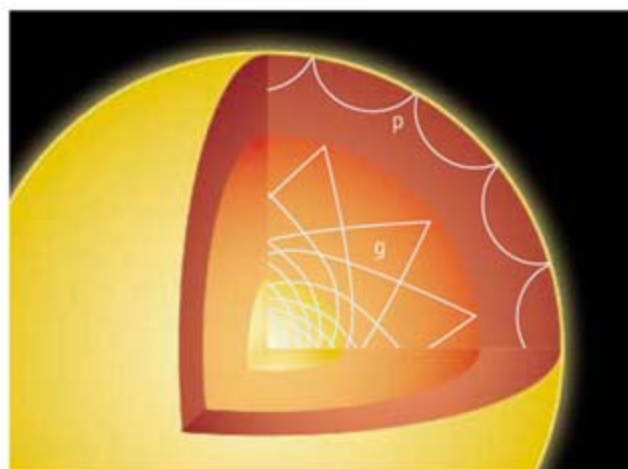
Although we cannot use light waves to see inside the Sun and other stars, we can learn about their interiors from mechanical waves generated deep within. These waves, similar in some ways to seismic waves on Earth, come in two main types: gravity waves or "g modes" that are driven by buoyancy, and pressure waves or "p modes," which are ordinary sound waves. Helioseismologists seek to understand what is happening inside the Sun by observing the oscillations produced on the solar surface by these modes. Such studies have produced many solar surprises, including a bizarre pattern of internal rotation (1); twisting flows below sunspots that produce strong flares (2); and evidence that the neutrinos generated by the fusion in the core change their nature as they

travel through the solar plasma (3). However, until now we have not been able to probe the deepest part of the Sun, where fusion reactions create the energy that sustains life on Earth. On page 1591 of this issue, García *et al.* report their work on g modes, which offers the most promising hope we

Waves deep within the Sun may help astronomers see the normally hidden core where energy-producing fusion reactions occur.

have so far of examining the Sun's core (4).

The p modes are trapped in the Sun's outer layers, and only a very few penetrate below a fractional radius of 0.2 into the core of the Sun. The g modes, on the other hand, are trapped in the core as well as in the radiative zone, as shown in the figure. This makes them extremely valuable for reporting the temperature, pressure, and motions at the solar center. Because they are trapped so deeply, however, they produce an effect at the solar surface that is, at



Good vibrations. A cross section of the solar interior showing examples of the ray paths of different waves. Whereas the p modes are mainly confined to the outer layers, the g modes propagate near the center and can provide information about the core. García *et al.* may have observed g mode signatures in the oscillations of the Sun's surface.

The author is at the National Solar Observatory, National Optical Astronomy Observatories, Tucson, AZ 85726, USA. E-mail: fhill@nso.edu

CREDIT: ADAPTED BY P. HUEY/SCIENCE

best, about three orders of magnitude smaller than what can be detected with current or foreseeable systems (5–7) such as the SOHO (Solar and Heliospheric Observatory) and SDO (Solar Dynamics Observatory) spacecraft, or the ground-based GONG (Global Oscillation Network Group) program.

Yet solar *g* modes do have one characteristic that makes their detection a bit more feasible: They are predicted to maintain phase coherence for years. Phase coherence means that all the waves stay in sync, so that many waves could work together to produce a distinct and useful signal. This possibility motivated García *et al.* to study a 10-year sequence of observations now available from the GOLF (Global Oscillation at Low Frequency) instrument on SOHO.

García *et al.* also exploited another characteristic of *g* modes: Their periods are evenly spaced, unlike *p* modes, which have evenly spaced frequencies. By building a model that explored the range of likely periods, along with the possible effects of rotation on the *g* modes, García *et al.* were able to identify a structure in the period spectrum of the GOLF data. The characteristics of this observed structure are strikingly similar to the theoretical spectrum that they constructed, making this the best indication yet that the *g* modes do indeed exist and are not cousins of Lewis Carroll's precisely described and long-sought but mythical snark.

In addition to adding weight to the evidence for the existence of solar *g* modes, García *et al.* also provide a rough estimate of the rotation rate of the core. This question has been debated for at least two decades in the helioseismology community, and there are a few bottles of vintage wine waiting to be awarded to the winner of some friendly bets on whether the core rotates faster or slower than the surface. García *et al.* are squarely in the "faster than surface" camp with these results. However, a more accurate answer must await computation of joint inversions of both the *p*-mode and *g*-mode frequencies into values of rotation rate.

Even though this is an exciting result for helioseismology, stellar structure, and solar physics, a crucial step remains before it can be truly accepted. As in all of science, confirmation is vitally important and especially so when the phenomenon has been sought for a long time, as the *g* modes have been. It is essential that the same analysis be performed on other data sets, and that an independent analysis be devised that can reveal the same feature in the original data set. Helioseismology is a subtle business, and several helioseismic results that would have been very exciting if true have fallen by the wayside when they could not be confirmed. However, confirmation requires the existence of an independent data set,

and this may not be the case in the near future for helioseismology.

There are only two major imaging helioseismology systems in the world—the GONG program and the SOHO spacecraft. SOHO is reaching the end of its lifetime and will be replaced by the SDO mission, which is scheduled for launch in 2008. However, the Astronomy Division of the National Science Foundation, which funds the GONG program, recently conducted a high-level review to identify funds for operating future facilities. One of the recommendations of this review (8) is to close GONG 1 year after the successful launch of SDO, unless outside funds for GONG operations can be identified. If this happens, helioseismology will be unable to confirm its most exciting results and may die completely as a science, which would be a pity.

References

1. M. J. Thompson, J. Christensen-Dalsgaard, M. S. Miesch, J. Toomre, *Annu. Rev. Astron. Astrophys.* **41**, 599 (2003).
2. D. Mason *et al.*, *Astrophys. J.* **645**, 1543 (2006).
3. J. N. Bahcall, M. H. Pinsonneault, S. Basu, *Astrophys. J.* **555**, 990 (2002).
4. R. A. García *et al.*, *Science* **316**, 1591 (2007); published online 3 May 2007 (10.1126/science.1140598).
5. V. Domingo, B. Fleck, A. I. Poland, *Solar Phys.* **162**, 1 (1995).
6. <http://sdo.gsfc.nasa.gov/>
7. J. W. Harvey *et al.*, *Science* **272**, 1284 (1996).
8. www.nsf.gov/mps/ast/ast_senior_review.jsp

10.1126/science.1144337

IMMUNOLOGY

The Shape of Things to Come

Katherine A. Fitzgerald and Douglas T. Golenbock

A successful vaccine is usually a combination of two agents. One is an antigen, the foreign substance that triggers an immune response—namely, the production of antibodies that recognize the antigen and lead to the destruction of pathogens that bear it. The other component is an adjuvant, which boosts this immune response by enhancing the activation of immune cells (T cells and antibody-producing B cells). Adjuvants that hold considerable promise in vaccine development are ligands for certain members of the Toll-like receptor (TLR) family that are expressed on the surface of immune cells. But to harness

these ligands therapeutically, a detailed mechanistic understanding of their adjuvant effects is needed. Two reports in this issue, by Mata-Haro *et al.* on page 1628 (1) and by Ohto *et al.* on page 1632 (2), provide new insights into the manner by which Toll-like receptor 4 (TLR4) becomes activated by adjuvants, and reveal molecular mechanisms by which recognition of different ligands by the same receptor shapes the immune response in different ways.

Among the ligands that activate TLRs are deoxycytidylate-phosphate-deoxyguanylate (CpG) DNA, which activates TLR9, and monophosphoryl lipid A, derived from the active moiety (lipid A) of bacterial endotoxin (lipopolysaccharide), which activates TLR4. Recognition of lipid A and related molecules by TLR4 requires MD-2. MD-2 lacks a transmembrane domain and binds to the extra-

Mechanistic understanding of how ligands can fine-tune the immune response may lead to better vaccine adjuvants.

cellular domain of TLR4 (3). Activating the TLR4–MD-2 receptor complex is thought to involve reorganization of the cytoplasmic Toll–interleukin-1 receptor (TIR) domain of TLR4, enabling the recruitment of four adapter molecules: MyD88, Mal (also called TIRAP), TRIF (also called TICAM1), and TRAM (also called TICAM2) (4). These adapters, in turn, initiate signal transduction pathways that lead to the production and secretion of molecules that regulate immune cells, called cytokines, as well as increased expression of molecules on the surface of specialized immune cells (dendritic cells) that enhance T cell activation.

Ohto *et al.* report the crystal structure of MD-2, both in its native state and bound to lipid IVa. Lipid IVa is similar in structure to lipid A but inhibits bacterial lipopolysaccharide. Lipid IVa also lacks two of the six fatty

The authors are in the Division of Infectious Diseases and Immunology, University of Massachusetts Medical School, Worcester, MA 01605, USA. E-mail: kate.fitzgerald@umassmed.edu; douglas.golenbock@umassmed.edu

acids present on lipid A that is found in the lipopolysaccharide of *Escherichia coli* or *Salmonella typhimurium*.

Mata-Haro *et al.* report that monophosphoryl lipid A somehow engages the TLR4–MD-2 complex differently from lipopolysaccharide, thereby selectively activating only the TRIF-TRAM signaling pathway. These events result in T cell activation (see the figure). The concomitant failure of monophosphoryl lipid A to engage the MyD88-Mal pathway (which controls the expression of certain proinflammatory cytokines) appears to account for the lack of harmful endotoxic effects normally associated with activating TLR4–MD-2. These observations provide an empirical basis to support the safe use of monophosphoryl lipid A as an adjuvant, because they show that it is not simply a weak endotoxin: Equivalent adjuvant activity was obtained in animals that were treated with monophosphoryl lipid A and lipopolysaccharide, yet monophosphoryl lipid A exhibited minimal toxicity.

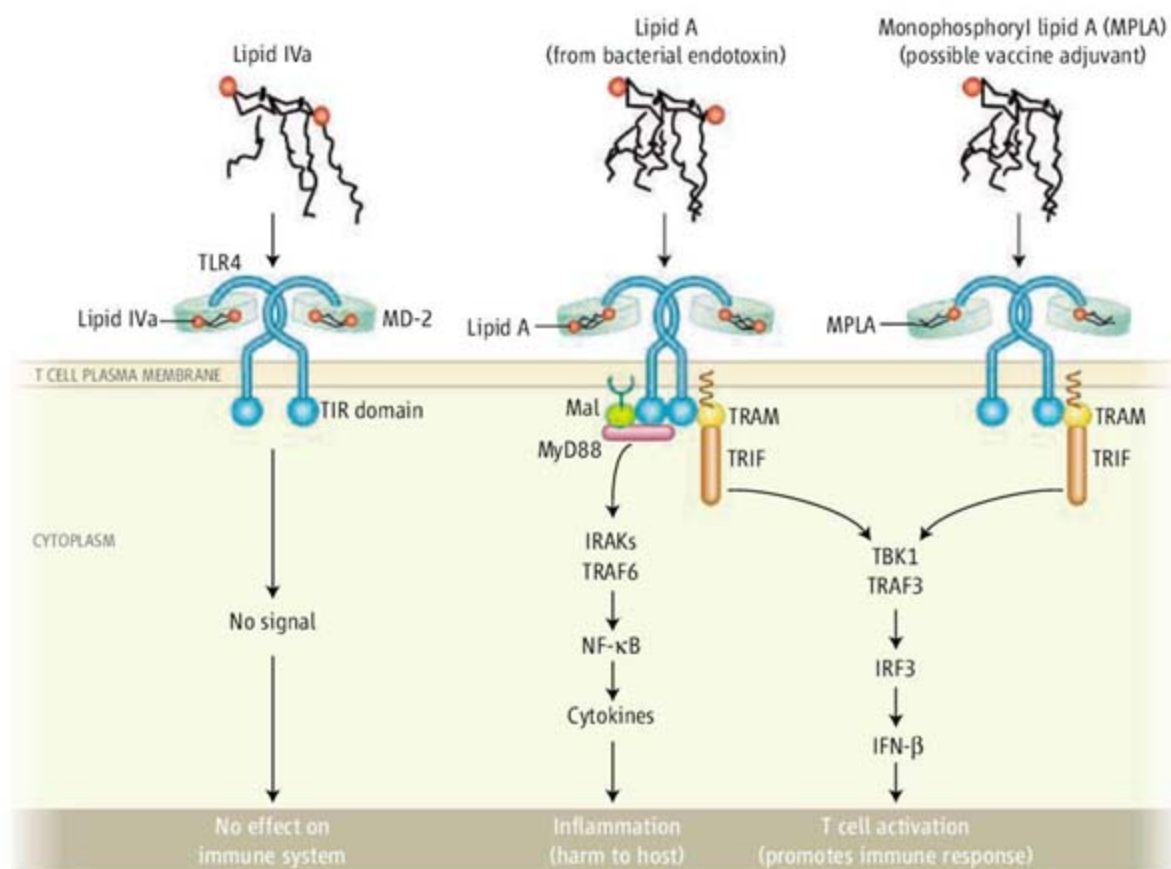
Although TLR4 has long been considered to be the lipopolysaccharide receptor, there has been no direct evidence that its lipid A moiety actually binds to the receptor. By contrast, there is substantial evidence that lipid A and several of its analogs, such as lipid IVa and monophosphoryl lipid A, bind MD-2 (5). Thus, the most widely held theories in the TLR field suggest that the true ligand for TLR4 is not lipopolysaccharide, but a conformationally active form of MD-2. It is of great interest, therefore, that Ohto *et al.*'s resolved structure of MD-2 shows an oval-shaped, highly ordered molecule with a hydrophobic cavity sufficient in size to fit the four fatty acyl residues of lipid IVa. It is not clear how MD-2 can fit additional acyl residues present on lipid A, but endotoxicity is likely related to a conformational change in MD-2 that allows this to occur.

It may be overly optimistic to conclude that we now know the shape of MD-2 in the absence of ligand, because the structure of MD-2 was resolved with contaminating myristic acid within the hydrophobic core. Nonetheless, the overall similarity, if not

identity, of MD-2 and MD-2 bound to lipid IVa suggests that we now know the conformation of MD-2 in its inactive state. We regrettably must still speculate about how the shape of MD-2 might change when bound to a stimulatory ligand such as lipid A or monophosphoryl lipid A.

Our best understanding of TLR4–MD-2 signaling comes from studies using highly purified lipopolysaccharide or synthetic

different cell types and/or in response to different ligands: one involving all four adapters (4), another involving only the MyD88-Mal pair (6), and another that selectively triggers a TRAM-dependent response that is independent of MyD88 and Mal and mostly independent of TRIF (7). Mata-Haro *et al.* add yet another level of complexity and demonstrate that monophosphoryl lipid A, presumably when bound to MD-2,



Rules of engagement. The TLR4–MD-2 complex is expressed as dimers on the surface of immune cells (T and B cells, phagocytes). Lipid A and two of its analogs, lipid IVa and monophosphoryl lipid A, bind to MD-2. There is no direct evidence that these lipids bind TLR4. The specific engagement of each lipid may cause structural changes in MD-2 and TLR4, resulting in new protein binding sites in the cytoplasmic domain of TLR4. The resulting recruitment of specific adapter proteins activates distinct signaling pathways and associated cellular responses.

forms of lipid A. Until recently, it was thought that upon TLR4 activation by any cognate ligand, all four adapter proteins were recruited to the same receptor homodimer, triggering the simultaneous activation of two signaling pathways—that which promotes the expression of proinflammatory cytokines via the transcription factor NF-κB (the MyD88-Mal pathway), and the signaling cascade that triggers expression of the cytokine type I interferon via the transcription factor IRF3 (the TRIF-TRAM pathway) (4). Evidence is mounting that this may not be the case but instead, different “flavors” of these responses are activated depending on the nature of the ligand engaging MD-2. Indeed, several modes of signaling by TLR4 have been reported in

selectively triggers the TRIF-TRAM signaling pathway only to elicit adjuvant activity. The authors suggest that the failure to engage the MyD88-Mal pathway may occur because phosphatidylinositol 3-kinase is activated. This enzyme, which hydrolyzes phosphatidylinositol 4,5-bisphosphate in the plasma membrane, could block Mal function. Mal contains a binding domain for phosphatidylinositol 4,5-bisphosphate, an interaction that facilitates its recruitment to domains in the plasma membrane containing TLR4 (8). This would preclude the recruitment of MyD88 and activation of NF-κB-driven inflammation.

One plausible explanation for different modes of TLR4 signaling is that the nature of ligand-bound MD-2 may differentially acti-

vate TLR4, resulting in different arrangements of the TIR domain in the cytoplasmic region of TLR4. The structure of MD-2 provides clues as to how this might come about. For example, one of the true surprises of the MD-2 structure is that neither of the two lysine residues that flank its hydrophobic pocket (Lys¹²⁸ and Lys¹³²) bind the 1- or the 4-phosphate of lipid IVa, contrary to previous predictions (9). It may be that the same phosphates on lipid A are free to interact with TLR4 and thereby influence how the receptor undergoes conformational changes or, alternatively, forms dimers or higher-order receptor aggregates. Highly toxic forms of lipid A, which have six to eight acyl chains, must sit differently in the hydrophobic pocket of MD-2, perhaps enabling the lipid to bind more effi-

ciently to TLR4. Depending on how many phosphates bind to TLR4, if any at all, or how tight the binding might be, the TLR4–MD-2 complex might form distinct types of signaling platforms in the cytoplasmic domains of TLR4 dimers and hence selectively recruit adapter molecules. Such speculations make it imperative that a high-resolution structure of MD-2 bound to a proinflammatory endotoxin ligand such as lipid A, as well as of MD-2 bound to the extracellular domain of TLR4, be resolved. Additional studies should focus on the selective recruitment of adapter molecules by different TLR4–MD-2 ligands. Better integrating the studies of function and structure will enable the design of new adjuvants and other drugs for the myriad of human inflammatory disorders associated with TLRs,

including systemic lupus erythematosus, sepsis, and asthma.

References and Notes

1. V. Mata-Haro *et al.*, *Science* **316**, 1628 (2007).
2. U. Ohto, K. Fukase, K. Miyake, Y. Satow, *Science* **316**, 1632 (2007).
3. C. Nishitani *et al.*, *J. Biol. Chem.* **281**, 38322 (2006).
4. L. A. J. O'Neill, A. G. Bowie, *Nat. Rev. Immunol.* **7**, 353 (2007).
5. A. Visintin, K. A. Halmen, E. Latz, B. G. Monks, D. T. Golenbock, *J. Immunol.* **175**, 6465 (2005).
6. Z. Jiang *et al.*, *Nat. Immunol.* **6**, 565 (2005).
7. P. Georgel *et al.*, *Virology* **362**, 304 (2007).
8. J. C. Kagan, R. Medzhitov, *Cell* **125**, 943 (2006).
9. A. Visintin, E. Latz, B. G. Monks, T. Espevik, D. T. Golenbock, *J. Biol. Chem.* **278**, 48313 (2003).
10. We thank J. Meng for helpful discussions and design of the figure.

10.1126/science.1144483

ATMOSPHERE

How Will the Stratosphere Affect Climate Change?

Mark P. Baldwin, Martin Dameris, Theodore G. Shepherd

The recent projections of climate change considered by the Intergovernmental Panel on Climate Change (IPCC) (1), which focus on the troposphere (up to 10-km altitude), are based on climate models that largely neglect the effects of the stratosphere on climate change. Yet, the stratosphere (at altitudes of 10 to 50 km) contains Earth's protective ozone layer, which affects the energy balance of the lower atmosphere. Furthermore, circulation changes in the lower stratosphere (up to 20-km altitude) affect tropospheric weather and climate, especially at high latitudes (2). Why is it so difficult to include stratospheric effects in IPCC projections?

In the past ~25 years, the composition of the stratosphere has changed substantially. Abundances of anthropogenic greenhouse gases (3) and ozone-depleting substances (4) have risen, while the ozone layer has thinned (see the figure). Following the successful implementation of the Montreal Protocol, which regulates production of ozone-depleting substances, the concentrations of these substances in the stratosphere have stabilized,

and the severity of the ozone hole is expected to decrease over the coming decades. However, concentrations of most greenhouse gases will continue to rise.

The temperature of the stratosphere is determined by small quantities of gases that interact with the incoming solar and outgoing infrared radiation. Ozone heats the stratosphere by absorbing solar ultraviolet radiation. Greenhouse gases (including ozone and ozone-depleting substances) both absorb and emit infrared radiation and can thus either heat or cool the atmosphere, depending on the balance between absorption and emission; for each gas, this balance depends on altitude and temperature (2). In the case of carbon dioxide, increased abundances cause a net warming of the troposphere and a net cooling of the stratosphere.

Satellite observations confirm that the stratosphere has cooled since 1979, in response to a combination of increasing carbon dioxide and ozone depletion (5). In the lower stratosphere, the global-mean cooling appears to be primarily attributable to ozone depletion (5). However, the radiative changes in the lower stratosphere depend strongly on latitude: Ozone depletion has led to cooling outside of the tropics, especially in polar regions (6), whereas the direct radiative effects of ozone-depleting substances have had a substantial warming effect in the tropics (7).

Changes in stratospheric chemistry and circulation associated with ozone recovery may affect the patterns of future climate change.

This latitudinal dependence implies that the north-south temperature gradient and the wind structure of the lower stratosphere must also have changed. The altered winds modify the propagation of atmospheric Rossby waves (which are responsible for large-scale modulations of the jet stream) from the troposphere into the stratosphere. Such changes in stratospheric winds in turn affect weather and climate at Earth's surface.

For example, the ozone hole in the Southern Hemisphere spring has affected Antarctic surface climate (8). In the Northern Hemisphere, a natural oscillation of equatorial stratospheric winds with a period of roughly 2 years affects midwinter surface wind patterns over northern Europe (9). During winter, wind shifts in the lower stratosphere precede similar wind shifts at the surface (10), with substantial changes to both weather and the likelihood of extreme weather events (11). The mechanisms by which stratospheric circulation changes are communicated to the surface are not well understood (12), but any long-term changes to stratospheric winds and temperatures are likely to affect surface climate and climate variability.

The changes to temperature and circulation in the lower stratosphere over the past ~25 years seem to have been driven primarily by changes in ozone-depleting substances and ozone depletion. They can thus be ex-

M. P. Baldwin is at Northwest Research Associates, Bellevue, WA 98009, USA. E-mail: mark@nwra.com. M. Dameris is at the Institut für Physik der Atmosphäre, Oberpfaffenhofen, 82234 Weßling, Germany. E-mail: martin.dameris@dlr.de. T. G. Shepherd is in the Department of Physics, University of Toronto, Toronto, M5S 1A7 Canada. E-mail: tgs@atmos.physics.utoronto.ca



pected to reverse as the ozone layer recovers. This reversal may obscure, or even alter, the climate-change signal from other greenhouse gases. Therefore, studies attempting to explain and predict climate change must account for the combined effects of climate change and ozone recovery.

The coupled atmosphere-ocean climate models that are used to understand past and future climate change generally do not have substantial interactive chemistry or even well-represented stratospheres. These models often include the radiative effects of ozone-depleting substances and of ozone depletion, but they are not designed to predict changes to the ozone layer or the dynamics of stratosphere/troposphere coupling. Many of the models considered in the recent IPCC report (1) held stratospheric ozone forcing constant during the 21st century. In any case, without a well-represented stratosphere, it is unlikely that the dynamical response to stratospheric radiative changes can be captured.

Coupled chemistry-climate models, such as those used in (5), include good representations of the stratosphere and interactive ozone chemistry and can therefore simulate changes to the ozone layer and their coupling to climate change. According to these models, ozone recovery will not be a simple reversal of ozone depletion. Rather, the stratospheric cooling from increasing greenhouse gases will accelerate the recovery of the ozone

layer, so that pre-1980 ozone abundances are expected to be reached in the middle of this century. The main reason for this acceleration is that most ozone-destroying chemical reactions will be slowed as the stratosphere cools. Beyond 2050, the ozone layer is predicted to become thicker than observed at any time in the last century as the stratosphere continues to cool.

Nearly all climate models with well-represented stratospheres indicate that the large-scale equator-to-pole overturning circulation, called the Brewer-Dobson circulation (13), will accelerate under climate change (14). This would lead to weaker westerly winds and higher temperatures in the extratropics during winter and spring. Such circulation changes would be expected to couple downward to affect surface weather, especially over the Arctic and Europe. However, stratospheric models have so far used prescribed ocean-surface temperatures, which strongly damp any tropospheric response to stratospheric changes.

Inclusion of stratospheric ozone-climate effects in coupled atmosphere-ocean climate models will not significantly alter the overall estimates of globally averaged surface warming. However, because of the possibility of dynamical responses to the stratospheric changes, projections of the evolution of polar climate could be substantially different, especially in the winter and spring in the Northern

Ozone and climate. Chemical reactions on polar stratospheric clouds, such as those shown here (taken over Sweden from the NASA DC-8 on 14 January 2003), lead to stratospheric ozone depletion. Models predict that the ozone hole will recover over the course of this century, affecting climate patterns in the stratosphere and at Earth's surface.

Hemisphere and spring and summer in the Southern Hemisphere. Estimates of the future evolution of rainfall and storms in northern mid-latitudes could also change.

Predicting the future effects of stratospheric change on surface climate is a substantial task. Doing so will require models that combine the coupled oceans of the current climate-prediction models with the detailed stratospheric radiation and chemistry of chemistry-climate models. This modeling was impractical for the 2007 IPCC report. It is an impending challenge for modelers to include a full representation of

stratospheric circulation and chemistry in the climate simulations for the next IPCC report.

References and Notes

1. *Contribution of Working Group I to the Fourth Assessment Report of the Intergovernmental Panel on Climate Change* (2007), www.ipcc.ch.
2. *IPCC Special Report on Safeguarding the Ozone Layer and the Global Climate System* (2005), www.ipcc.ch/activity/sroc/index.htm.
3. The main anthropogenic greenhouse gases are carbon dioxide, methane, nitrous oxide, and some fluorinated gases. Water vapor, the most important greenhouse gas, is not affected directly by human activities.
4. The main ozone-depleting substances are chlorofluorocarbons and bromofluorocarbons.
5. *WMO/UNEP Scientific Assessment of Ozone Depletion* (2007), ozone.unep.org/Assessment_Panels/SAP/Scientific_Assessment_2006/index.shtml.
6. K. P. Shine *et al.*, *Q. J. R. Meteorol. Soc.* **129**, 1565 (2003).
7. P. M. Forster, M. Joshi, *Clim. Change* **71**, 249 (2005).
8. N. P. Gillett, D. W. J. Thompson, *Science* **302**, 273 (2003).
9. D. W. J. Thompson, M. P. Baldwin, J. M. Wallace, *J. Clim.* **15**, 1421 (2002).
10. M. P. Baldwin, T. J. Dunkerton, *Science* **294**, 581 (2001).
11. D. W. J. Thompson, J. M. Wallace, *Science* **293**, 85 (2001).
12. D. W. J. Thompson, J. C. Furtado, T. G. Shepherd, *J. Atmos. Sci.* **63**, 2616 (2006).
13. J. R. Holton *et al.*, *Rev. Geophys.* **33**, 403 (1995).
14. N. Butchart *et al.*, *Clim. Dyn.* **27**, 727 (2006).
15. We thank P. Forster, B. J. Hoskins, M. Ponater, K. Trenberth, and F. Zwiers for discussions. M.P.B. is supported by NSF under the U.S. Climate Variability and Predictability Program, NSF-Office of Polar Programs, NOAA-Office of Global Programs, and NASA. T.G.S. is supported by the Natural Sciences and Engineering Research Council of Canada, Canadian Foundation for Climate and Atmospheric Sciences, and Canadian Space Agency.

10.1126/science.1144303

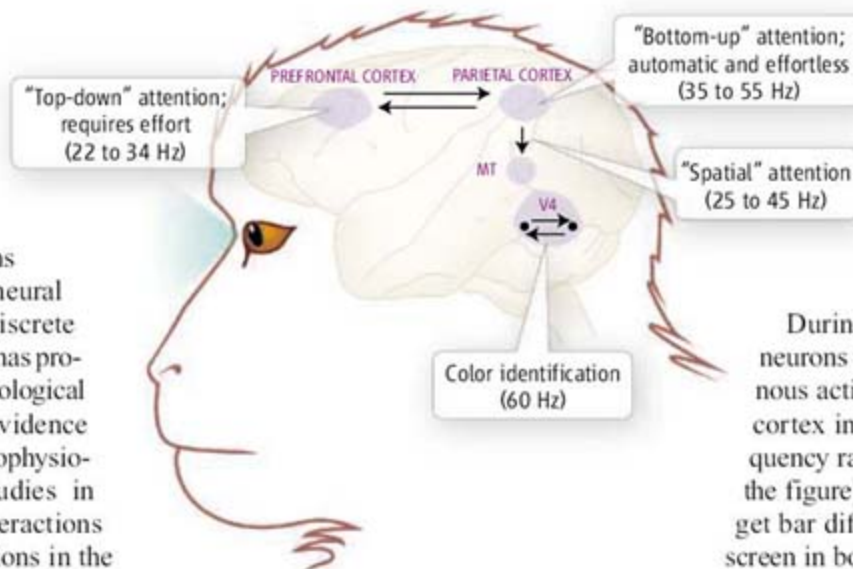
NEUROSCIENCE

Neural Networks Debunk Phrenology

Robert T. Knight

Systems neuroscience aims to understand how billions of neurons in the mammalian brain support goal-directed behavior, such as decision making. Deciphering how individual neurons respond to sensory inputs or motor decisions has focused on delineating the neural basis of these processes in discrete regions of the brain's cortex, and has provided key insights into the physiological basis of behavior. However, evidence from neuropsychological, electrophysiological, and neuroimaging studies in humans has revealed that interactions between widespread neural regions in the brain underlie fluid, organized behavior. Two papers in this issue, by Womelsdorf *et al.* on page 1609 (1) and Saalmann *et al.* on page 1612 (2), and a recent paper in *Science* by Buschman and Miller (3), unravel the details of these interactions by assessing the simultaneous activity of neurons in multiple sites of the mammalian brain. The studies show that network interactions among anatomically discrete brain regions underlie cognitive processing and dispel any phrenological notion that a given innate mental faculty is based solely in just one part of the brain.

Buschman and Miller used a classic experimental approach of manipulating "top-down" and "bottom-up" attention in monkeys. Top-down searching—for example, searching for the infamous Waldo character in a children's book illustration—typically requires effort. By contrast, bottom-up searching is predominantly an automatic behavior, such as finding a red balloon in a sea of blue balloons—the red balloon literally "pops out" of the visual scene. Buschman and Miller recorded neuronal activity from multiple sites in the prefrontal and parietal cortical areas of the monkey brain (the cortex is largely responsible for high-level cognitive processes such as attention, memory, and decision-making).



Communicating at a distance. Oscillatory neuronal (electrical) activity in defined frequency ranges supports synchronous interactions between anatomically distinct regions of the mammalian brain (illustration of rhesus macaque shown) during cognitive tasks that require deliberate or automatic attention, memory, or visual processing.

These regions are several centimeters apart, but are connected by extensive bundles of axons (neuronal extensions that form the circuitry of the brain), suggesting that they might communicate with each other while the animal performs behavioral tasks. In classic single-neuron recording studies, different brain areas are examined by different investigators, who observe different tasks in different animals. The advantage of recording from multiple sites in the brain simultaneously is that these factors are held constant, thus allowing precise analysis of the relative timing of neural activity in the same animal.

Buschman and Miller determined both the electrical activity of individual neurons (called single-unit activity) and the net ensemble activity of many neurons (called the local field potential) in the monkey brain. Repetitive activity of these neuronal ensembles is manifested as oscillatory activity in different frequency bands, which can be readily extracted from the ongoing electrical activity of the brain. During a top-down serial visual search, the monkeys had to detect a colored

Intracortical recordings reveal that distinct regions of the mammalian brain must synchronize their activity to support certain behaviors.

bar (the target) that shared color and line-orientation properties with other bars on a computer screen. Because the target bar was similar to other bars on the screen, the monkey had to search to pick out the salient target, a task requiring deliberate effort.

During this task, prefrontal cortical neurons were activated first, and synchronous activity with neurons in the parietal cortex increased in the 22 to 34 Hz frequency range in the prefrontal cortex (see the figure). For the bottom-up task, the target bar differed from all other bars on the screen in both color and orientation, leading to rapid and effortless identification. In response to this scheme, parietal neurons were activated first, and synchronous activity with the prefrontal cortex was observed at a frequency range of 35 to 55 Hz in the parietal cortex. The findings highlight two-way interaction between these distinct regions of the mammalian cortex, with communication pathways tuned to different frequencies.

The work by Saalmann and colleagues extends these observations, using single-unit and local field potential recordings focused on the effect of the parietal cortex on the area that perceives motion (MT area) of the monkey brain. The MT is connected to many different cortical regions of the brain and plays a major role in perceiving movement. Because the posterior parietal cortex is involved in spatial processing, Saalmann *et al.* reasoned that it might communicate with the MT. For these experiments, a monkey has to judge whether two sets of stacked bars, presented half a second apart from each other, match in both the spatial location of the bars and their orientation in space. As in the Buschman and Miller study, neuronal activity was recorded simultaneously in the parietal and MT sites of the brain. The authors detected single-unit activity in the posterior parietal cortex before that in the MT, and synchrony between these two regions at a 25 to 45 Hz frequency range in the MT. A phase delay in synchronous activity between these two regions is indicative of a top-down effect of the posterior parietal

The author is in the Department of Psychology, Helen Wills Neuroscience Institute, University of California, Berkeley, Berkeley, CA 94720-3190, USA. E-mail: rtnknight@berkeley.edu

cortex on the MT during this matching task.

Using a similar experimental logic, Womelsdorf *et al.* analyzed three single-unit activity and local field potential data sets obtained from cats and monkeys. These activities were recorded from areas in the brain (called 18 and 21a in the cat and V1 and V4 in the monkey) involved in vision, including color, object, and stereoscopic processing. The authors observed that the phase delay (in milliseconds) of oscillations in the local field potential between nearby sites (from 1 mm to 1 cm apart) determined the efficacy of synchronized neuronal activity between the sites. It has been shown previously in animals that local field potential in the frequency range of 4 to 7 Hz predicts both single-unit activity and higher frequency (30 to 200 Hz range) oscillatory activity (4). This local mechanism, involving coupling of a brain rhythm and single-unit activity, has been proposed to synchronize neural activity between regions, enabling effective communication between brain areas (5).

Taken together, the three papers indicate that top-down signals between brain regions regulate the flow of information and that distributed neural networks that use oscillatory dynamics support a broad spectrum of neural processing and behavior. The results in cats and monkeys also nicely parallel findings in humans. For instance, brain lesion, electrophysiological, and neuroimaging research in humans (6, 7) has shown that top-down signals from prefrontal and parietal cortices regulate attention and working-memory capacity. The findings in animals that oscillatory dynamics support network activity and enhance the efficacy of synchronized activity between distributed neural regions has also been observed in humans. Intracranial data from subdural electrodes in the human cortex have shown that oscillations in the 4 to 7 Hz frequency range are coupled to high-frequency oscillations in the 30 to 150 Hz range in areas similar to those studied in the monkey brain by Buschman and Miller and by Saalmann *et al.* Further, this particular coupling mechanism is used to delineate task-specific network activity (8, 9). A recent human intracranial study reports that single-unit activity in the human brain is synchronized to local field potentials in the 4 to 7 Hz and 1 to 3 Hz frequency ranges in the hippocampus (10), further supporting the observations initially reported in animals.

It is now widely agreed that defining network interactions is key to understanding normal cognition. There are also numerous psychiatric disorders, such as depression, seasonal affective disorder, mania, and even

some cases of psychosis, that are episodic and are not associated with defined neuroanatomical damage. Might it be that some of the periodic symptoms are caused by intermittent network dysfunction, caused by disturbed oscillatory dynamics? If so, then the work by Buschman and Miller, Womelsdorf *et al.*, and Saalmann *et al.* may have a great impact on our understanding of these disorders.

One mystery remains: How is information in oscillatory activity encoded? The individual spike train rate (the number of times a neuron fires each second) or spiking frequency (the rhythm at which a neuron fires) is not sufficient for coding the vast array of processes that underlie perception,

memory, or decision making. Nevertheless, the three groups have laid the groundwork for deciphering this neural code.

References

1. T. Womelsdorf *et al.*, *Science* **316**, 1609 (2007).
2. Y. B. Saalmann, I. N. Pigarev, T. R. Vidyasagar, *Science* **316**, 1612 (2007).
3. T. J. Buschman, E. K. Miller, *Science* **315**, 1860 (2007).
4. G. Buzsaki, A. Draguhn, *Science* **304**, 1926 (2004).
5. P. Fries, *Trends Cogn. Sci.* **291**, 1560 (2005).
6. F. S. Barcelo, S. Suwazono, R. T. Knight, *Nat. Neurosci.* **3**, 399 (2000).
7. A. Raz, J. J. Buhle, *Nat. Rev. Neurosci.* **7**, 367 (2006).
8. J. E. Lisman, M. A. Idiart, *Science* **267**, 1512 (1995).
9. R. Canolty *et al.*, *Science* **313**, 1626 (2006).
10. J. Jacobs, M. J. Kahana, A. D. Ekstrom, I. Fried, *J. Neurosci.* **27**, 3839 (2007).

10.1126/science.1144677

MATERIALS SCIENCE

Food Pathogen Detection

Carl A. Batt

New methods for detecting food pathogens can quickly identify single microbes, but major hurdles must be overcome before they can be introduced to practical use.

The detection of food pathogens is crucial for food safety; detection methods must be fast, sensitive, and accurate. Yet, almost all techniques used today to identify specific pathogens in foods take at least 48 hours, and some take as long as a week. Further confounding the challenge is the need to address “zero tolerance,” a standard that mandates that no viable pathogens are allowed in certain foods. To meet zero-tolerance levels, detection methods need to be sensitive down to a single pathogen in a prescribed sample. Current methods require several days to achieve this standard, because they rely on culturing the pathogen to increase its numbers to detectable levels.

In contrast, modern detection systems currently under development analyze food based on the detection of a specific spectroscopic, immunological, or genetic signature (see the figure). These methods are potentially faster than currently used methods by virtue of their enhanced sensitivity, with a detection limit of a single cell, in some cases in real time. However, the methods have not yet been introduced to practical use, because they are difficult to integrate with sample preparation and handling practices (1). Sample preparation is

tedious because the target pathogens cannot be extracted and concentrated by simple physical means. In addition, sample preparation typically depends on the nature of the sample. Thus, extracting pathogens from water is different than extracting the same pathogens from milk, let alone ground beef.

Furthermore, it is often difficult to assess the efficacy of the new methods as compared to the classic means of detection, because the former are rarely tested on real food samples and do not necessarily yield results that can be translated into commonly accepted units of measure (such as colony-forming units). Finally, methods that are rapid and sensitive must also be field-portable. A method that requires the sample to be shipped to a central laboratory for analysis with sophisticated equipment introduces a delay in the overall time to complete the analysis.

Not even the question “what do we want to know?” has a simple answer. The symptoms induced by a food pathogen are obvious, especially to the victim, but biochemical and metabolic differences between virulent and nonvirulent strains may not be as dramatic. The genome of *Escherichia coli* O157:H7 differs vastly from that of its cousin *E. coli* K-12 (2), but from a biochemical perspective, they are very similar. The fundamental question is thus whether a food contains a pathogen that causes a person to become ill

The author is in the Department of Food Science, Cornell University, Ithaca, NY 14853, USA. E-mail: cab10@cornell.edu

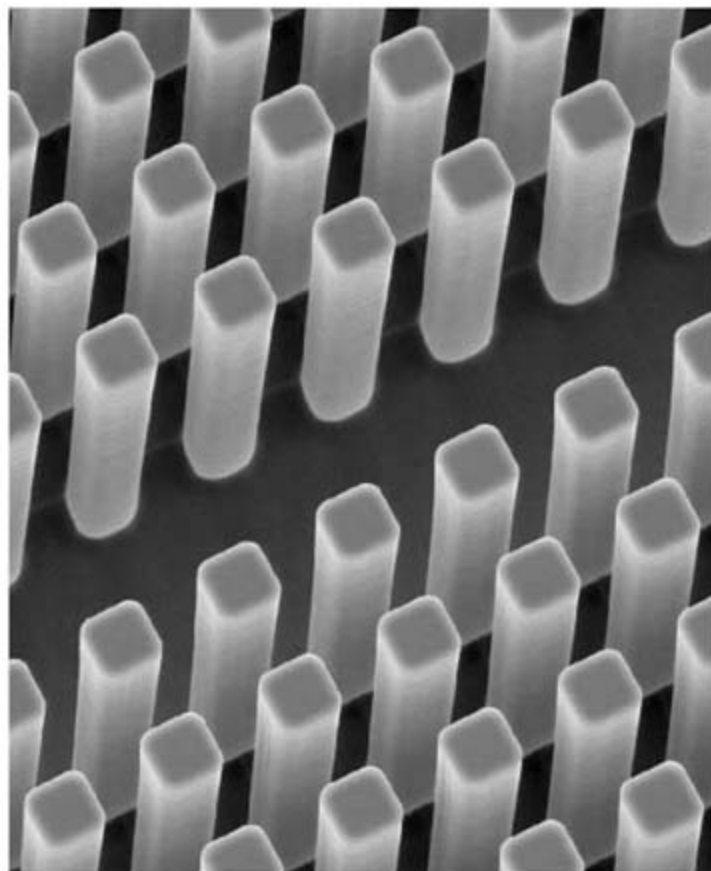
when he or she ingests it.

This outcome-based analysis is counter to any current or anticipated technologies that simply identify the presence of a particular target organism. One potentially interesting assay is based on the physiological response of cells isolated from the fish *Betta splendens* (3). The pigmentation pattern of these cells changes when they are exposed to toxigenic strains of *Bacillus cereus*, and this change can be monitored by microscopy. This system is unique in that its readout does not depend on a microbiological or biochemical definition of a particular strain, but rather is related to the toxigenicity of the pathogen.

The main challenge in food pathogen detection technology is familiar to anyone who has worked with any analytical instrument: detecting the signal against background noise. Various identifying signals can be used to detect a particular organism. Attempts to harness spectroscopic signatures have been reported (4). Direct physical signals of this kind are intriguing because they circumvent challenges with reagents that complicate the assay merely by the need to add them or by compromising specificity. Biochemical, immunological, and more recently genetic-based methods have enhanced specificity, but typically then require some signal transducer to provide a readout that indicates the presence of the pathogen.

The challenge for spectroscopic measurements is that they rely on an indirect signature that is difficult to correlate to a particular pathogen. Furthermore, there is a lot of noise in biological samples. These methods work well when the organism is examined in isolation (and even better in a vacuum), but are challenged when that organism is surrounded by the biological matrix that makes up food. The low signal-to-noise ratio is confounded by the desired, if not legislated, mandate of zero tolerance (5). In the spectroscopic noise that food presents, detecting the spectroscopic signal of a single bacterium is virtually impossible.

The signal-to-noise problem can be overcome by introducing a mechanism to deliver



Fast and sensitive. Scanning electron micrograph of silicon pillars that are part of an integrated "lab on a chip" for the purification and detection of nucleic acids (1). The pillars are 10 μm by 10 μm by 50 μm and capture DNA through electrostatic binding to their surface.

the target bacterium to a highly sensitive sensor, away from the food. Detection can be very simple. For example, a single *E. coli* bacterium can be detected by measurement of its mass while it is perched on the tip of a cantilever. The cantilever is modified with microfabrication to pattern a gold pad at the end, upon which *E. coli*-specific antibodies are attached (6). When a bacterium is captured by this antibody, the sensors measure the change in mass (7).

Mass-based methods such as this are intrinsically nonspecific; it is the antibody that introduces specificity, shifting the detection paradigm from a classic identification to an immunological signature. The challenges are twofold. First, antibodies need to be reasonably close to their target antigen to bind. Diffusion is not an option, especially given the viscosity of a medium like food. Second, they are not absolutely specific and may therefore lead to false-positives.

To bring the target analyte in close proximity to the detector, a microfluidic interface is required that can sample a large volume of liquid and pass it within a few hundred nanometers of the sensor (1). However, most food samples are particulate and prone to clogging of micrometer- and submicrometer-sized channels. These problems may potentially be

overcome by using sample preparation methods in which both captured biomolecules (that is, antibodies) and target analytes can diffuse freely (8). However, in most existing methods, one or more components tend to be fixed onto a solid surface.

One of the most promising approaches to detecting a single bacterium was realized almost 20 years ago with the invention of the polymerase chain reaction (PCR). This method can detect a single copy of a target DNA sequence, and can thus in theory detect a single pathogenic bacterium in food. It is promising because it detects the organism by amplifying the target rather than the signal, and is therefore less prone to producing false-positives. A target DNA can be amplified 1-million-fold in less than an hour, with sensitivities in theory down to a single target pathogen. However, before PCR can find widespread application in food pathogen detection, sample preparation and delivery of the target nucleic acid sequence to the PCR-detection component must be simplified.

Even if these practical hurdles can be overcome, other obstacles will remain. The new methods focus on characteristics that are different from traditional microbiological analyses, yet most food regulations are based on pathogen identity as defined by classic methods and traditional nomenclature. For example, *E. coli* O157:H7 is defined by reactivity with a set of antisera, whereas *Salmonella* DT104 is defined by sensitivity to a particular bacteriophage. Any deviation that includes genetic, spectroscopic, or other signatures must account for this traditional definition of the organism.

Advances in methods for the detection of pathogens will need to be accompanied by an equivalent effort in the area of sample preparation. Detection systems alone will not eliminate pathogens from the food supply, nor is it reasonable to expect that the food supply can be made "sterile." Ensuring food safety is a complex issue that requires advances in technology as well as education of food suppliers and the general public.

References

1. N. C. Cady, S. Stelick, M. V. Kunnakkam, C. A. Batt, *Sens. Actuators B* **107**, 332 (2005).
2. N. T. Perna *et al.*, *Nature* **409**, 529 (2001).
3. K. P. Dierksen *et al.*, *J. Appl. Toxicol.* **24**, 363 (2004).
4. C. Yu, A. Ganjoo, H. Jain, C. G. Pantano, J. Irudayaraj, *Anal. Chem.* **78**, 2500 (2006).
5. *Fed. Regist.* **60**, 49553 (1995).
6. B. Ilic *et al.*, *J. Vac. Sci. Technol. B* **19**, 2825 (2001).
7. D. Ramos, J. Tamayo, J. Mertens, M. Calleja, A. Zaballos, *J. Appl. Phys.* **100**, 106105 (2006).
8. M. L. Ochoa, P. B. Harrington, *Anal. Chem.* **77**, 5258 (2005).

The Macroecological Contribution to Global Change Solutions

Jeremy T. Kerr,^{1*} Heather M. Kharouba,¹ David J. Currie²

Anthropogenic global changes threaten species and the ecosystem services upon which society depends. Effective solutions to this multifaceted crisis need scientific responses spanning disciplines and spatial scales. Macroecology develops broad-scale predictions of species' distributions and abundances, complementing the frequently local focus of global change biology. Macroecological discoveries rely particularly on correlative methods but have still proven effective in predicting global change impacts on species. However, global changes create pseudo-experimental opportunities to build stronger, mechanistic theories in macroecology that successfully predict multiple phenomena across spatial scales. Such macroecological perspectives will help address the biotic consequences of global change.

By changing global climate, expanding and intensifying land uses, polluting, introducing exotic species, and overharvesting biological resources (1), human activities have accelerated extinction rates massively (2). The biotic consequences of these factors, collectively the study of global change biology, are apparent in progressive degradation of ecosystem services upon which humans rely (3), climate change-induced shifts in species' distributions toward the poles (4) and higher elevations (5), and in rapidly changing phenologies (6). The policy responses necessary to overcome such enormous challenges must draw on many scientific disciplines and apply to the full range of spatial scales over which global changes exert their effects.

Even though many of these effects will occur over broad spatial scales [e.g., (7)], most global change biology studies concentrate on smaller, often experimental, areas (Fig. 1). The local processes discovered by such studies are essential to predict how global changes might proceed and can scale up in surprising ways to illuminate broader-scale trends. For example, experimental warming of alpine meadows caused unexpected changes in species composition toward woody shrubs that led to substantial release of stored soil carbon (8). This biological feed-forward mechanism has global implications because, if it is representative of other areas, it implies the existence of a tipping point beyond which climate change could accelerate rapidly. The controlled, experimental approach frequently used in global change research also makes for

strong inference: It is virtually certain that the treatment (in this case, warming) caused the effect (biotic community transition leading to soil carbon release). In many global change studies, however, strong inference within highly controlled experimental settings is purchased at the cost of clear broad-scale applicability. For instance, biotic interactions among three fruit fly

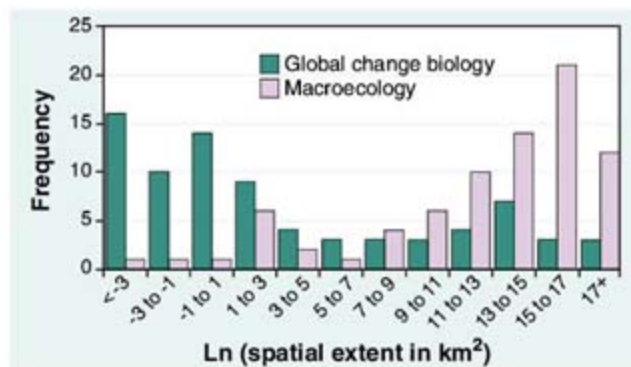


Fig. 1. The contrast in characteristic spatial scales of macroecology and global change biology is evident from this survey of recent publications in the two journals that address these disciplines most consistently: *Global Ecology and Biogeography* (GEB, which presents itself as the journal of macroecology) and *Global Change Biology* (GCB). We started with the most recent issue (December 2006 for GCB and January 2007 for GEB) and worked back until equal sample sizes of 79 studies for each journal were reached. Studies without an interpretable spatial extent (e.g., some meta-analyses) were omitted, but for all others, the spatial extents were recorded. Green bars represent results for global change biology and purple bars, for macroecology.

species and their parasitoid predator determined their distributions and abundances within an experimental microcosm (9). Widespread though such interactions may be, little evidence yet suggests they are similarly dominant at the regional extents over which predictions for species range shifts are most widely needed (10).

Macroecology is a recent research program that aims to develop quantitative predictions of the abundance and distribution of species, usual-

ly over broad areas (landscapes to continents) (Fig. 1) or for large numbers of species. These research aims are ideal to address key global change issues at immediately relevant spatial scales (11). There is no shortage of problems needing solutions. The impacts of broad-scale climate and land-use change on geographical patterns of species richness can be predicted with macroecological methods, potentially helping direct conservation resources to regions where need is greatest. Similarly, studies of patterns and impacts of biological invasions across islands suggest strategies that could reduce future losses. Such macroecological patterns are supported by increasingly mechanistic hypotheses with clear global change applications. Here, we review a range of macroecological concepts of particular and immediate relevance to global change research, as well as obstacles hindering their more widespread use. Broad-scale research methods have already proven valuable for global change research, but new developments in macroecology greatly enhance its potential contribution.

Potential and Problems for Macroecology in Global Change Research

Brown's seminal book in macroecology begins with an example—the effect of climate change on species living on mountaintops—that clearly demonstrates the discipline's relevance to global change (12). As with most macroecological studies, this one used observational data within a correlative framework, a common approach when focusing on regional phenomena at their native spatial scales.

Macroecological approaches to critical global change phenomena have since proliferated considerably. For instance, predatory mammal species have been introduced widely on oceanic islands. The number of recent extinctions among island birds, particularly endemics, depends strongly on numbers of exotic predatory mammals that have been introduced to those islands. Preventing further introductions of exotic predators is a critical part of conservation strategies for islands (13). This study's reliance on correlative models weakens its grip on cause and effect slightly: Habitat losses might have contributed to the observed effects (14, 15). However, it is difficult to think of a small-scale, experimental approach that would

have been as broadly applicable and, as a result, immediately useful. Similarly, effects of land-use change on species conservation have also been ascertained with spatial correlations of broad-scale data sets. Endemic and threatened species are heavily concentrated in tropical mountain ranges in sub-Saharan Africa, coincident with high human population densities. Combined with the observation that the bushmeat trade contributes strongly to mammal decline, this corre-

¹Department of Biology, Canadian Facility for Ecoinformatics Research (CFER), University of Ottawa, Ottawa, ON K1N 6N5 Canada. ²Department of Biology, University of Ottawa, Ottawa, ON K1N 6N5 Canada.

*To whom correspondence should be addressed. E-mail: jkerr@uottawa.ca

lation suggests a course for conservation that accommodates the agricultural land uses of local peoples while improving regional protected area networks (16).

Macroecology's signature statistical approach has also provided the foundation for some of ecology's strongest theories. Island biogeography is perhaps the most widely influential ecological theory, and it is built on observations that species numbers on islands increase with island area but decrease with isolation (Fig. 2A) (17). This theory has also proven extraordinarily valuable for global change research. As climate warms, woodlands in the mountainous southwestern United States will shift to higher elevations. The ensuing reduction in their area is expected to eliminate 9 to 62% of small-mammal species currently inhabiting these habitats (12). The relationship between habitat area and species richness has been further refined to reflect the reality that species in human-altered landscapes use natural and modified habitats to varying degrees. This countryside species-area relationship predicts the conservation status of terrestrial mammals in Central America and also yields more optimistic (and accurate) assessments of extinction rates (18).

Despite their frequent reliance on correlation, macroecological relationships are built on solid biological foundations. For instance, the specific thermal tolerances of bird species differ considerably—the golden-crowned kinglet (*Regulus satrapa*) is absent from parts of North America where winter temperatures consistently drop below about -18°C , while prairie warblers (*Dendroica discolor*) inhabit only warmer areas above 7°C (19). By considering large species assemblages simultaneously, strong macroecological relationships can emerge from species-specific patterns (20) that help predict biotic responses to global change. For instance, climate predicts global patterns of bird species richness (21). Within Europe, the spatial relationship between bird community composition and climate successfully predicts the trajectory of those communities as climate has changed (22). Although derived from a purely spatial analysis, this macroecological relationship also explains how climate change has altered bird community composition through time.

Converting macroecological discoveries into predictions about global change biology is often difficult and always risky. Obtaining suitable data is frequently a formidable challenge. Beyond this, however, several additional problems must be overcome. First, macroecological studies often depend on post hoc curve-fitting, capable of producing very strong statistical relationships (23). Unfortunately, competing, mechanistically dissimilar hypotheses can each predict the same pattern, and macroecologists rarely have recourse to experimentation to ascertain cause and effect (12). Instead, differences in support among hypotheses are taken to mean differences in their likelihood of being true, a conclusion that

sophisticated statistical arguments can strengthen but not prove. The latitudinal gradient of diversity is a classic example: Latitude predicts global species diversity quite well for most taxa (24). It relates to diversity, however, exclusively because it is a surrogate for collinear environmental variables, like temperature. Second, predicting the biological impacts of global change involves extrapolation, sometimes beyond any combination of environmental conditions that have been recorded. There are currently no modern analogs for some vegetation assemblages that existed in the late glacial period in eastern North America, which likely arose from combinations of climate variables that also lack contemporary analogs (25). Strong theoretical and empirical evidence for a specific prediction can reduce, not eliminate, such extrapolative uncertainties. Finally, unique or stochastic phenomena create irreducible noise in macroecological relationships, as the flora and fauna of the Krakatau islands testify (26). It should be noted that such rare events provide opportunities for pseudo-experimental tests of new and existing hypotheses, as shown by subsequent studies of colonization and succession on Krakatau.

Strengthening Macroecological Contributions to Global Change Biology

If macroecological research is to make effective, reliable contributions to global change biology, it must improve its capacity to demonstrate cause and effect. Experimental tests of hypotheses—the usual scientific method to distinguish cause from correlation—are normally impractical, unethical, or both at broad spatial scales (12). Instead, frontier macroecological studies begin by testing for links between some biological phenomenon (B) and environmental predictors (E) using statistical tools. Such relationships are usually based on observations of some spatial pattern. However, if E truly causes B, then those spatial relationships should be consistent as conditions change, the essence of experimentation (27).

In other words, spatial relationships should be consistent temporally if they are true. Spatial variation in bird species richness in North America relates strongly to gradients of primary productivity. However, seasonal variation in bird species richness also tracks the annual cycle of primary production: Birds track resource availability over the course of the year (28). In this case, natural environmental changes lead to the same biological response observed from a purely spatial relationship. It is ironic that global change also provides pseudo-experimental opportunities to test macroecological relationships. Biology-environment relationships for native species, for instance, can be compared to those for exotic species to generate an independent test of the consistency of macroecological relationships (29).

Research based on historical data, with its temporal perspective on natural and anthropogenic change, is invaluable when predicting biotic outcomes of global change (30). Climate

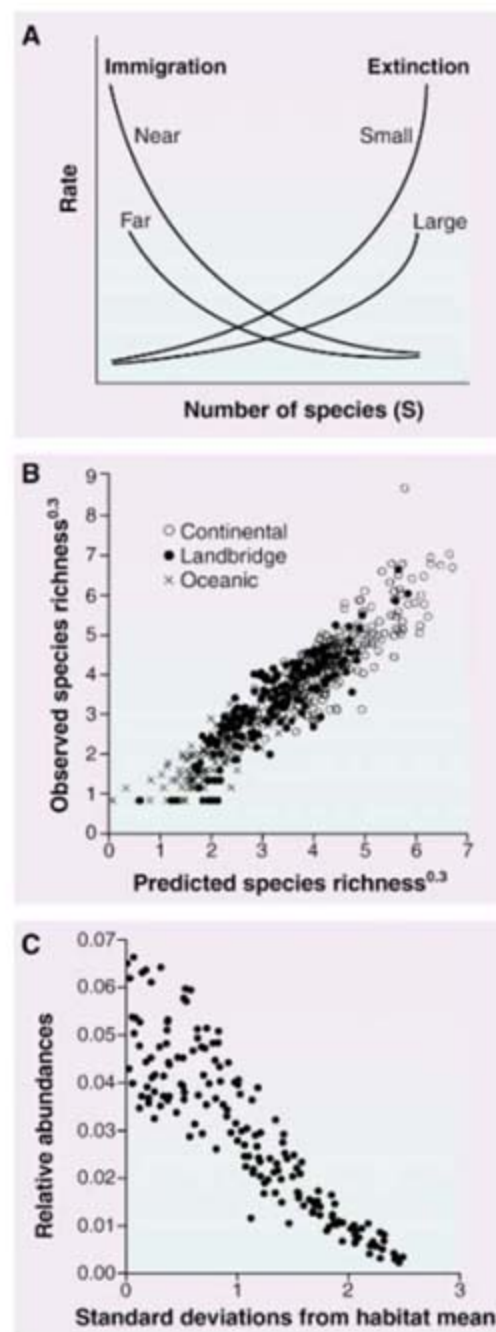


Fig. 2. (A) The classic model of island biogeography (17) proposes that the statistical effects of area and isolation result from two underlying processes: the rate of colonization by new species and the rate of extinction of established species. These two rates depend upon the number of species on the island, island area, and island isolation. (B) A combination of area, isolation, and climate predicts bird species richness in defined areas on continents and on oceanic islands anywhere in the world (35). (C) The mechanism underlying climatic effects on species richness is more controversial. Stochastic niche theory (40) provides a possibility: the relative abundances of species, and therefore their persistence in an assemblage in a defined area, may vary as a function of the number of standard deviations separating the actual environmental condition within a habitat from the species' climatic optimum. The greater this separation, the less abundant the species is predicted to be. These data are derived from simulations in which habitat temperature and species' optimum temperatures have Gaussian distributions.

partly determines where species-range boundaries occur (31), so climate change causes boundaries to shift, a fact with well-known paleoecological precedents. But past range shifts, such as those following glacial retreat, occurred across landscapes with little or no human influence. By contrast, human activities now affect most terrestrial areas (32), which are likely to inhibit the capacity of species to keep up with shifting climatic conditions. In Canada, climate and land-use changes during the 20th century were considerable in many areas. Butterfly species richness tracked changing growing-season temperatures over this time period, as predicted from the purely spatial relationship between temperature and richness (33). That this spatial relationship remains consistent through time improves confidence that temperature actually does partially cause the pattern of butterfly richness and is another example where global change offers macroecologists a pseudo-experiment. Human population density is also a positive spatial predictor of butterfly richness, a result also observed among British birds (34). However, in areas of Canada where human population density increased over the 20th century, butterfly richness declined (33). No model will necessarily hold under new or unforeseen environmental circumstances.

One can assess the robustness of macroecological relationships by testing them under independent conditions. This can most easily be done through space: Do relationships developed in one part of the world accurately predict pat-

terns in geographically independent areas? For example, the spatial relationship between bird species richness and a combination of climate, area, and isolation of islands predicts richness among continental localities and vice versa (35) (Fig. 2B). Similarly, plant family richness in any given biome or phytogeographic province of the world can be predicted from the richness-climate relationship derived based on the rest of the world (36). Collectively, such tests demonstrate the robustness of the underlying species richness-energy hypothesis addressed by these studies and the increasingly important role occupied by training and testing data in macroecology.

Process-based models of natural systems provide more detailed, mechanistic predictions. A classic example again is MacArthur and Wilson's theory of island biogeography (Fig. 2A). This mechanistic theory builds on simple, macroecological observations to include processes of immigration by new species and extinction of species already present to generate a dynamic equilibrium of species richness on islands. This simple hypothesis explains the initial macroecological observation (i.e., richness-area), but also successfully predicts a suite of new phenomena: compositional turnover at equilibrium, effects of factors that enhance immigration (corridors or "stepping stones"), faunal collapse, and so forth. Adding climatic effects to this model greatly expands its reach, enabling it to predict diversity on mainlands and islands alike (35). Such models are particularly powerful because they predict several different phenomena, not just the first

pattern of interest. Their greater mechanistic detail suggests many tests (alleviating criticisms that macroecological hypotheses are merely the result of post hoc curve-fitting) (23) and they potentially predict the behavior of systems under a wider range of conditions.

More recent theories expand the number of natural biological patterns that can be reduced to a small number of basic, underlying processes. For example, the metabolic theory of ecology begins by noting that many aspects of organisms' biology, like population abundance (37) and evolutionary rates (38), depend upon individual body size and ambient temperature. Similarly, neutral theory proposes that stochastic dispersal and speciation-extinction events can predict the relative abundances of species, which are treated as being functionally indistinguishable, within biotic communities (39). Stochastic niche theory (40) combines characteristics of neutral theory with environmentally dependent resource competition to further improve predictions of relative abundances of species. This approach recognizes niche-based differences among species, such as the optimal, within-habitat temperatures for the growth of their propagules (Fig. 2C). Where temperature is a major determinant of species' niche boundaries, for instance, stochastic niche theory may help predict the consequences of climate change. The theory is strengthened further by its potential to predict independent phenomena, like the unexpected pattern of increased invasion success in biologically diverse communities (41).

Yet, in process-based models, there is an inescapable tension between capturing mechanistic detail and retaining the capacity to predict natural variation (42, 43). The most practical models for predicting natural patterns will not require large numbers of parameters, especially if they are difficult to measure. Instead, such models will inevitably make inexact assumptions to simplify systems that might otherwise be unmanageably complex (44, 45). Decisions about which approach to take depend largely on whether the predictive capacity of complex models justifies the effort necessary to parameterize them. If including species-by-species environmental tolerances and competitiveness for particular limiting resources improves or expands predictions of macroecological and global change trends (40) (Fig. 2C), adding complexity would have practical benefits. A related macroecological example illustrates this point. Climate is generally acknowledged as the best overall predictor of species richness, but new analyses based on South American birds suggest that climate predicts species richness only for broadly distributed species (46). Patterns of richness among species with smaller ranges relate more strongly to historical processes or habitat heterogeneity (47). In this case, subdividing species by the extent of their geographic ranges adds detail necessary to establish useful global change predictions from macroecological observations.

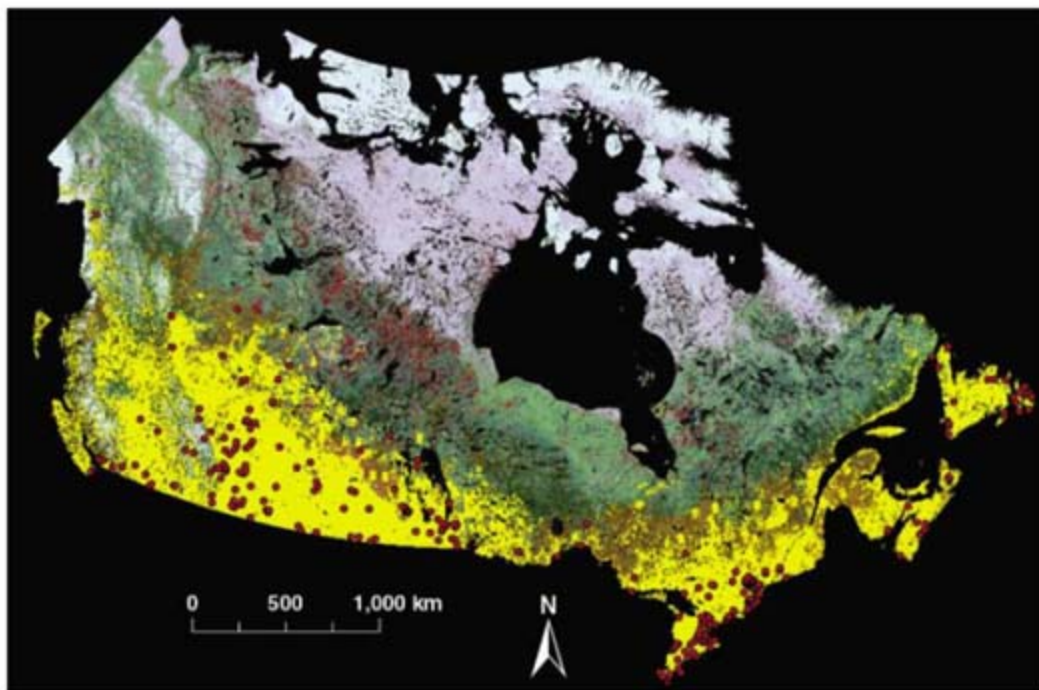


Fig. 3. Biological observations, if available, often include only a species name and a location where it was observed. Observation points across Canada for *Vanessa atalanta* (red admiral) are shown in red, derived from the Canadian National Collection (59). These are overlaid on a niche model (yellow) of its range derived with Maximum Entropy (60). Environmental data, such as the satellite-based land-use map (61) beneath the niche model, are capable of far greater spatial consistency than biological data, although they almost never achieve equally high local detail. Remote sensing is particularly useful for detecting rapid changes, as shown here, where recent forest fires beyond the northern frontiers of this butterfly species' range are in dark red.

As Einstein famously noted, models should be as simple as possible, but no simpler.

Detecting Macroecological and Global Change Signals

Before even the most elegant macroecological hypothesis can be applied to global change, reliable data must be found. On the environmental side, satellite and aerial remote sensing now provide spatially continuous measurements of an array of environmental characteristics over large areas, allowing near real-time detection of human-induced and natural changes (48, 49) (Fig. 3). Biological data are far more localized (e.g., plant censuses in 0.1-ha plots; amphibians or birds heard or seen at a particular site). Environmental measurements with correspondingly high local detail are, at best, on the edge of what remote sensing can accomplish, although that edge is advancing (50).

The well-known mismatch between sparse biological observations and spatially continuous remote-sensing data (Fig. 3) hinders the development of biological theory that scales successfully from localities to regions and continents (48, 51). Biological databases require "boots on the ground" and cannot keep up with frequent, even daily, updates provided by remote-sensing sources. Many biological data are stored inaccessible in museums or by individual researchers. The Global Biodiversity Information Facility (www.gbif.org) and related initiatives, like the nascent Global Earth Observation System of Systems for Biodiversity, will improve this situation considerably and lower one of the simplest barriers to building effective responses to global change: knowing what species are present in an affected area. These ongoing monitoring activities are essential to detecting and modeling biotic responses to global change and can be effective without comprehensive data (52).

Species niche models can help reduce the mismatch between sparse biological observations and spatially continuous environmental data (53). These models use detailed environmental data to describe, in spatial terms, species' niche boundaries, transforming a small number of presence-only observations (although some data sets include presence and absence data) across a region into a spatially continuous prediction of its entire range (54, 55) (Fig. 3). The results yielded by these models can be surprisingly powerful. In Madagascar, satellite data were used to develop range models for chameleon species (56). These models consistently predicted the presence of chameleon species in unsurveyed areas beyond the chameleons' known ranges. Several sister species to those being modeled were then discovered in these areas. Despite their great promise, niche models must be used with caution. Different modeling techniques predict vastly divergent climate-change impacts on the ranges of four South African Proteaceae species, from a range expansion of >300% to a loss of >90% (57). Integrating predictions from several modeling methods—ensemble forecasting—may

reduce such wild uncertainties (58). However, projecting niche models through time requires a space-for-time substitution that is demonstrably unreliable (33). Niche models will continue to play a role in macroecological and global change research but cannot replace biological monitoring programs that collect primary data.

Conclusions

Although macroecology still needs correlative approaches to explore its rapidly expanding frontiers, stronger methods reveal mechanisms more readily and reduce confounding effects intrinsic to broad-scale, nonexperimental research. These methods include a critical and expanding role for remote sensing and perhaps niche modeling in the measurement of relevant biological and environmental characteristics. More important, however, global change furnishes macroecology with pseudo-experimental opportunities that improve macroecology's predictions and global change relevance. Warming climates in the 20th century, for instance, allow for temporal tests of the species richness-energy hypothesis, which might improve quantitative predictions of how spatial patterns of diversity will change in the coming decades.

Models that specify mechanisms or that predict many phenomena at once, like stochastic niche theory or metabolic theory, play an increasing role in theoretical macroecology. The versatility of these models staves off criticisms that macroecology cannot reach past its historically correlative framework to grapple effectively with causation. As the reliability of these models is tested and improved, especially by ensuring that they are consistent temporally as well as spatially, their potential to provide specific solutions to global change problems will also increase. Concern about global change is justifiably intense because of its expanding biological consequences and effects on the sustainability of the human enterprise. Macroecology is built on strong biological foundations and offers important, broad-scale theories that will help address these urgent global change issues.

References and Notes

1. Millennium Ecosystem Assessment (World Resources Institute, Washington, DC, 2005).
2. R. May, J. Lawton, N. Stork, in *Extinction Rates*, J. Lawton, R. May, Eds. (Oxford Univ. Press, Oxford, 1995), pp. 1–24.
3. D. Schröter et al., *Science* **310**, 1333 (2005).
4. C. Parmesan, *Annu. Rev. Ecol. Syst.* **37**, 637 (2006).
5. R. J. Wilson et al., *Ecol. Lett.* **8**, 1138 (2005).
6. T. L. Root, L. Hughes, in *Present and Future Phenological Changes in Wild Plants and Animals*, T. E. Lovejoy, L. Hannah, Eds. (Yale Univ. Press, New Haven, CT, 2005), pp. 61–74.
7. J. A. Foley et al., *Science* **309**, 570 (2005).
8. J. Harte, S. Saleska, T. Shih, *Environ. Res. Lett.* **1**, 014001 (2006).
9. A. J. Davis et al., *Nature* **391**, 783 (1998).
10. A. Guisan, W. Thuiller, *Ecol. Lett.* **8**, 993 (2005).
11. T. H. Blackburn, K. J. Gaston, *Glob. Ecol. Biogeogr.* **15**, 537 (2006).
12. J. H. Brown, *Macroecology* (Univ. of Chicago Press, Chicago, 1995).
13. T. M. Blackburn et al., *Science* **305**, 1955 (2004).
14. R. K. Didham et al., *Science* **307**, 1412a (2005).

15. T. M. Blackburn et al., *Science* **307**, 1412b (2005).
16. N. D. Burgess et al., *Biol. Conserv.* **134**, 164 (2007).
17. R. H. MacArthur, E. O. Wilson, *The Theory of Island Biogeography* (Princeton Univ. Press, Princeton, NJ, 1967).
18. H. M. Pereira, G. C. Daily, *Ecology* **87**, 1877 (2006).
19. T. Root, *Ecology* **69**, 330 (1988).
20. T. Rangel, J. A. F. Diniz-Filho, *Ecography* **28**, 253 (2005).
21. D. Storch et al., *Ecol. Lett.* **9**, 1308 (2006).
22. N. Lemoine, H. C. Schaefer, K. Bohning-Gaese, *Glob. Ecol. Biogeogr.* **16**, 55 (2007).
23. B. J. McGill, *Oikos* **102**, 679 (2003).
24. B. A. Hawkins, J. A. F. Diniz-Filho, *Ecography* **27**, 268 (2004).
25. S. T. Jackson, J. W. Williams, *Annu. Rev. Earth Planet. Sci.* **32**, 495 (2004).
26. R. J. Whittaker, J. M. Fernandez-Palacios, *Island Biogeography: Ecology, Evolution, and Conservation* (Oxford Univ. Press, Oxford, New York, 2007).
27. D. J. Currie et al., *Ecol. Lett.* **7**, 1121 (2004).
28. D. H-Acevedo, D. J. Currie, *Glob. Ecol. Biogeogr.* **12**, 461 (2003).
29. G. F. Thuiller, M. Rouget, R. M. Cowling, *Ecography* **29**, 733 (2006).
30. K. J. Willis, H. J. B. Birks, *Science* **314**, 1261 (2006).
31. C. Parmesan et al., *Oikos* **108**, 58 (2005).
32. E. Sanderson et al., *Bioscience* **52**, 891 (2002).
33. P. J. White, J. T. Kerr, *Ecography* **29**, 908 (2006).
34. K. L. Evans, K. J. Gaston, *Glob. Ecol. Biogeogr.* **14**, 187 (2005).
35. A. Kalmar, D. J. Currie, *Ecology* **88**, 1309 (2007).
36. A. P. Francis, D. J. Currie, *Am. Nat.* **161**, 523 (2003).
37. J. H. Brown, J. F. Gillooly, A. P. Allen, V. M. Savage, G. B. West, *Ecology* **85**, 1771 (2004).
38. A. P. Allen, J. F. Gillooly, V. M. Savage, J. H. Brown, *Proc. Natl. Acad. Sci. U.S.A.* **103**, 9130 (2006).
39. S. P. Hubbell, *The Unified Neutral Theory of Biodiversity and Biogeography* (Princeton Univ. Press, Princeton, NJ, 2001).
40. D. Tilman, *Proc. Natl. Acad. Sci. U.S.A.* **101**, 10854 (2004).
41. D. F. Sax, S. D. Gaines, J. H. Brown, *Am. Nat.* **160**, 766 (2002).
42. R. Levins, *Am. Sci.* **54**, 421 (1966).
43. A. Guisan, N. E. Zimmermann, *Ecol. Model.* **135**, 147 (2000).
44. B. J. McGill, B. A. Maurer, M. D. Weiser, *Ecology* **87**, 1411 (2006).
45. A. C. Algar, J. T. Kerr, D. J. Currie, *Glob. Ecol. Biogeogr.* **16**, 170 (2007).
46. W. Jetz, C. Rahbek, *Science* **297**, 1548 (2002).
47. C. Rahbek et al., *Proc. R. Soc. London B Biol. Sci.* **274**, 165 (2007).
48. J. T. Kerr, M. Ostrovsky, *Trends Ecol. Evol.* **18**, 299 (2003).
49. H. M. Pereira, H. David Cooper, *Trends Ecol. Evol.* **21**, 123 (2006).
50. W. Turner et al., *Trends Ecol. Evol.* **18**, 306 (2003).
51. K. J. Willis, R. J. Whittaker, *Science* **295**, 1245 (2002).
52. R. J. Scholes, R. Biggs, *Nature* **434**, 45 (2005).
53. C. H. Graham et al., *Trends Ecol. Evol.* **19**, 497 (2004).
54. J. Elith et al., *Ecography* **29**, 129 (2006).
55. D. B. Botkin et al., *Bioscience* **57**, 227 (2007).
56. C. J. Raxworthy et al., *Nature* **426**, 837 (2003).
57. R. G. Pearson et al., *J. Biogeogr.* **33**, 1704 (2006).
58. M. B. Araujo, M. New, *Trends Ecol. Evol.* **22**, 42 (2007).
59. R. A. Layberry et al., *The Butterflies of Canada* (Univ. of Toronto Press, Toronto, 1998).
60. S. J. Phillips et al., *Ecol. Model.* **190**, 231 (2006).
61. J. T. Kerr, J. Cihlar, *Glob. Ecol. Biogeogr.* **12**, 161 (2003).
62. J.T.K. led the writing and major conceptual development for this review. J.T.K., H.M.K., and D.J.C. acknowledge funding from the Natural Sciences and Engineering Research Council of Canada (NSERC). Infrastructure funds from the Canadian Foundation for Innovation and Ontario Ministry of Research and Innovation (to J.T.K.) are also gratefully acknowledged. Discussions with R. May, D. Tilman, and others at the Royal Society Symposium on Theoretical Ecology in Oxford, and helpful comments from three anonymous reviewers, improved this manuscript. We are grateful to D. Tilman for providing original data for Fig. 2C.

10.1126/science.1133267

The Mass of Dwarf Planet Eris

Michael E. Brown* and Emily L. Schaller

The discovery of Kuiper belt object (KBO) 2003 UB313 (1), now officially named Eris, prompted the recent reevaluation of Pluto's status as a planet and the creation of a new category called "dwarf planets": objects in orbit around the Sun that are large enough to be in hydrostatic equilibrium but have insufficient mass to gravitationally dominate their region of the solar system. Eris is larger than Pluto (2, 3) and thus the largest currently known member of dwarf planets.

The subsequent discovery of Dysnomia (4), a satellite of Eris, presented the opportunity to directly measure the mass of Eris by determining the Keplerian orbit of the satellite. Observations of Eris and Dysnomia were obtained on 20, 21, 30, and 31 August 2006 (UT) with the Keck Observatory laser guide star adaptive optics (LGS AO) system (5, 6). Observations from the Hubble Space Telescope (HST) were taken on 3 December 2005 and 30 August 2006. From measurements of the relative positions of Dysnomia on these six nights (Fig. 1 and table S1) plus the position from the discovery on 10 September 2005, we determined the orbit of Dysnomia by using a Powell χ^2 minimization scheme to find the optimal orbital parameters. We first attempted to fit a purely circular orbit in which the five free parameters are semimajor axis, orbital period, inclination, longitude of the ascending node, and mean anomaly. The best fit orbit has a χ^2 value of 6.5 or a reduced χ for nine degrees of freedom (14 x, y coordinates minus 5 orbital parameters) of 0.7, indicating an excellent fit to the model. Expanding the model to allow an eccentric orbit gives a best-fit eccentricity of ~ 0.007 and only a marginally lower reduced χ^2 of 0.6, suggesting that the current observations contain no statistical evidence for a noncircular orbit. Derived orbital elements along with uncertainties from Monte Carlo analysis appear in table S2.

From the 30 August 2006 HST image at a wavelength of $0.6 \mu\text{m}$, we measured a relative brightness ratio between the two objects of only 0.21 ± 0.01 ($1-\sigma$)%. The small relative brightness of Dysnomia is inconsistent with the dynamical-friction-aided capture mechanism proposed for the majority of KBO satellites (7), but detailed simulations show that such small satellites can be formed from the debris after a giant impact (8). A collisionally produced satellite of the size of Dysnomia that tidally evolved outward from an initial location near the Roche limit would be predicted to have a roughly 15-day circular orbit [Supporting Online Material (SOM) text], consistent with the derived orbit of Dysnomia. Owing to the low mass of Dysnomia, this outward orbital

expansion would have slowed the spin period of Eris by only a part in $\sim 10^{-5}$.

Whereas the other two KBO systems that appear to be products of giant impacts, Pluto and 2003 EL61, contain multiple satellites, satellites almost an order of magnitude fainter than Dysnomia can be ruled out beyond the orbit of Dysnomia from deep HST observations (SOM text). For a purely tidally evolved system, any satellite beyond the orbit of Dysnomia must be larger than Dysnomia, and thus such a system can be ruled out. Interior to ~ 0.4 arc sec, however, the expected fractional brightness of a

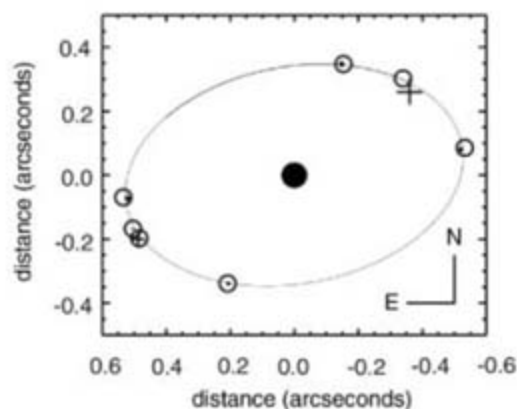


Fig. 1. The projected orbit of Dysnomia around Eris. Observations are shown as crosses of the size of the $1-\sigma$ uncertainty. The predicted positions at the time of observations are shown by open circles. The solid circle in the center is 10 times the actual angular size of Eris.

tidally evolved satellite is ~ 0.0007 , which is beyond our detection ability (SOM text). Any additional purely tidally evolved satellites of Eris would be expected to be closer and fainter than these limits. Although such additional small faint satellites cannot be ruled out, the current limits and the apparently circular orbit of Dysnomia suggest that Eris might indeed be a single-satellite system.

From the period and semimajor axis of the orbit of Dysnomia, we can use Kepler's laws to calculate a mass for the Eris-Dysnomia system of $1.66 \times 10^{22} \pm 0.02 \times 10^{22}$ kg or 1.27 ± 0.02 of the mass of Pluto. With any plausible assumptions of albedo and density, Dysnomia's mass in the system is negligible. In addition to being the largest, Eris is also the most massive known dwarf planet.

From this mass measurement and the previous size measurements, we can calculate the

density of Eris. The initial indirect IRAM radiometric measurement suggested a diameter of 3000 ± 400 km (2), whereas the later HST direct measurement found a smaller diameter of 2400 ± 100 km (3). By using the more direct measurement with the smaller uncertainty, we obtain a density of $2.3 \pm 0.3 \text{ g cm}^{-3}$. This density is consistent with the moderately high 2.03 ± 0.06 , 2.06 ± 0.01 , and $\sim 2.6 \text{ g cm}^{-3}$ densities known for Pluto, Triton, and the large KBO 2003 EL61, respectively (9–11). Using the earlier indirect IRAM diameter measurement would give a density of only $1.2 \pm 0.6 \text{ g cm}^{-3}$, which is significantly lower than other objects of comparable size in the outer solar system, giving confidence, although not confirmation, in the more direct HST diameter measurement with the smaller uncertainty.

Recent direct and indirect measurements of the densities of smaller KBOs (12, 13) suggested lower-than-expected densities for objects in the outer solar system and thus a deficit of rocky material or a surplus of pore space. The similarly high densities of Eris, Pluto, Triton, and 2003 EL61, in contrast, all require rock fractions of $\sim 70\%$ or higher (14), as anticipated from expected cosmochemical abundances in the protosolar neighborhood.

References and Notes

- M. E. Brown, C. A. Trujillo, D. L. Rabinowitz, *Astrophys. J.* **635**, L97 (2005).
- F. Bertoldi, W. Altenhoff, A. Weiss, K. M. Menten, C. Thum, *Nature* **439**, 563 (2006).
- M. E. Brown, E. L. Schaller, H. G. Roe, D. L. Rabinowitz, C. A. Trujillo, *Astrophys. J.* **643**, L61 (2006).
- M. E. Brown et al., *Astrophys. J.* **639**, L43 (2006).
- P. L. Wizinowich et al., *Pub. Astron. Soc. Pacific* **118**, 297 (2006).
- Materials and methods are available on Science Online.
- P. Goldreich, Y. Lithwick, R. Sari, *Nature* **420**, 643 (2002).
- R. M. Canup, *Science* **307**, 546 (2005).
- M. W. Buie, W. M. Grundy, E. F. Young, L. A. Young, S. A. Stern, *Astron. J.* **132**, 290 (2006).
- B. A. Smith et al., *Science* **246**, 1422 (1989).
- D. L. Rabinowitz et al., *Astrophys. J.* **639**, L238 (2006).
- D. C. Jewitt, S. S. Sheppard, *Astron. J.* **123**, 2110 (2002).
- J. A. Stansberry et al., *Astrophys. J.* **643**, 556 (2006).
- W. B. McKinnon, J. I. Lunine, D. Banfield, in *Neptune and Triton*, D. P. Cruikshank, Ed. (Univ. Arizona Press, Tucson, 1995), pp. 807–878.
- This research is supported by a Presidential Early Career Award to M.E.B. In addition, E.L.S. is supported by a NASA graduate student research fellowship. We thank J. Aycock, R. Campbell, A. Conrad, K. Grace, J. Lyke, C. Melcher, C. Sorenson, M. van Dam, and C. Wilburn at Keck Observatory, without whom these complicated LGS AO observations would not have been possible.

Supporting Online Material

www.sciencemag.org/cgi/content/full/316/5831/1585/DC1

Materials and Methods

SOM Text

Tables S1 and S1

29 December 2006; accepted 14 March 2007

10.1126/science.1139415

Division of Geological and Planetary Sciences, California Institute of Technology, Pasadena, CA 91125, USA.

*To whom correspondence should be addressed. E-mail: mbrown@caltech.edu

The Release 5.1 Annotation of *Drosophila melanogaster* Heterochromatin

Christopher D. Smith,^{1,2} ShengQiang Shu,³ Christopher J. Mungall,³ Gary H. Karpen^{2,4*}

The repetitive DNA that constitutes most of the heterochromatic regions of metazoan genomes has hindered the comprehensive analysis of gene content and other functions. We have generated a detailed computational and manual annotation of 24 megabases of heterochromatic sequence in the Release 5 *Drosophila melanogaster* genome sequence. The heterochromatin contains a minimum of 230 to 254 protein-coding genes, which are conserved in other Drosophilids and more diverged species, as well as 32 pseudogenes and 13 noncoding RNAs. Improved methods revealed that more than 77% of this heterochromatin sequence, including introns and intergenic regions, is composed of fragmented and nested transposable elements and other repeated DNAs. *Drosophila* heterochromatin contains "islands" of highly conserved genes embedded in these "oceans" of complex repeats, which may require special expression and splicing mechanisms.

The goal of genome annotation is to identify sequence features that have a biological role in the organism, but a telomere-to-telomere DNA sequence is not yet available for complex metazoans, including humans. The missing genomic "dark matter" is the heterochromatin, which is generally defined as repeat-rich regions concentrated in the centric and telomeric regions of chromosomes. Centric heterochromatin makes up at least 20% of human and 30% of fly genomes, respectively; thus, even for well-studied organisms such as *Drosophila melanogaster*, fundamental questions about gene number and global genome structure remain unanswered.

Once considered "junk" DNA, it is now clear that heterochromatin contains essential genes and also contributes to genome stability and chromosome segregation (1–3). In addition, heterochromatin participates in RNA interference mechanisms that epigenetically repress gene and transposable element (TE) expression, which may "immunize" genomes against the invasion and expansion of selfish DNA elements (4, 5). Despite differences in heterochromatin sequence composition between genomes, commonalities in the structures, chromatin modifications, and presence of genes suggest that *D. melanogaster* heterochromatin is an excellent model for studying repeat-rich genomic DNA in other species, including the 40% repetitive human euchromatin (6, 7).

Annotation overview. The *Drosophila* Heterochromatin Genome Project has generated 16

megabases (Mb) of finished or near-finished heterochromatin sequence from *D. melanogaster*, as well as 8 Mb of draft whole genome shotgun (WGS) heterochromatic assemblies (8, 9). We performed computational and manual curation to produce the Release 5.1 annotation of this 24 Mb of heterochromatin sequence, which excludes degenerate sequence reads not incorporated into the final sequence assembly (AnnUextra) (10, 11). Several repeat-finding programs were implemented, including RepeatRunner (12) and Tandem Repeats Finder (TRF) (13). New data from the research community were incorporated, including GenBank third-party annotations and Heidelberg gene predictions (14). Lastly, the conservation of *D. melanogaster* heterochromatin genes was assessed by identifying putative gene orthologs in more than 16 species [supporting online material (SOM) text and data].

The annotations include protein-coding genes, non-protein-coding RNAs (ncRNAs), repetitive sequences, and other functional elements. The majority of nonrepeat annotations (64%) mapped to a chromosome arm, including regions contiguous with the euchromatic arms (chromosome arm h; e.g., 2Rh) and internal scaffolds that have been cytologically localized to an arm (chromosome arm Het; e.g., 2RHet) (8, 9). The remaining annotations are not mapped to a chromosome arm (36%) and reside on Arm U (Unmapped). Although the highly repetitive simple sequence component of *D. melanogaster* heterochromatin remains unassembled (8, 9), few unique genes have been identified in these regions, and thus the current annotation is likely to include the majority of heterochromatic genes.

Protein-coding genes and comparative analysis. Previous studies indicated that at least 32 essential genetic loci are present in the heterochromatin (1). Using clone-based evidence [expressed sequence tag (EST) and cDNA] and predicted orthology, we annotated 613 protein-coding genes and gene fragments in the 24 Mb

of Release 5 heterochromatin (Table 1, SOM text, and data) (11). Currently, 41% of these genes have supporting clone-based evidence, including 137 annotations with full-length cDNAs generated by the Berkeley *Drosophila* Genome Project (BDGP) (15). The incorporation of new EST sequences from Exelixis (16), which were generated with random primers, was instrumental for finding new internal splice sites and missed exons and was used to refine at least 43 gene models (Fig. 1) (11). New evidence resulted in 16 cases of Release 3.2b genes that were merged into seven larger Release 5.1 genes (e.g., CG41520 in Fig. 1) and two genes from Release 3.2b that were split into four smaller genes in Release 5.1.

A subset of the annotations represents single-exon fragments of coding sequences present in small scaffolds, and these fragments should not yet be considered as complete genes. We classified gene annotations as either single-exon genes (186) or multi-exon genes (427) in order to more conservatively estimate higher-quality complete gene models without losing information about potentially incomplete genes (Fig. 2). Heterochromatin single-exon genes are currently less supported by clone-based evidence; roughly 50% of heterochromatic multi-exon genes and 61% of euchromatic single-exon genes had EST or cDNA support, compared to only 20% of single-exon genes.

Because many genes lacked EST or cDNA support, the translated basic local alignment sequence tool (TBLASTN) was used to identify putative orthologs for heterochromatin genes in 16 other insect genomes and more distantly related vertebrate species (17) (Fig. 3A). We defined orthologs as unique, top-scoring TBLASTN-identified sequences, although no evidence currently exists to support conserved function. Overall, more than 99% of the annotations had an ortholog identified in at least one species (Fig. 3A). Orthologs were identified for 86 to 98% of heterochromatin protein-coding genes in the four species (*D. simulans*, *D. erecta*, *D. sechellia*, and *D. yakuba*) most closely related to *D. melanogaster*, and 55 to 70% of genes are conserved in the more distantly related Drosophilids. In addition, 22 to 46% of genes are conserved in distantly related insects (such as the silkworm, mosquito, honeybee, wasp, and beetle), and 13% of all protein-coding genes had significant alignments to proteins in even more diverged species (Fig. 3A). We conclude that the majority of *D. melanogaster* heterochromatic genes are highly conserved in insect lineages that span 300 million years of evolution and that a surprising number share significant similarity with proteins from vertebrate species that diverged more than 900 million years ago (18).

The conservation patterns were bimodal, such that nearly 20% of protein-coding genes were conserved in fewer than 4 species, whereas more than 30% were conserved in all 16 insect species (Fig. 3B). This trend suggests the existence of

¹Department of Biology, San Francisco State University, San Francisco, CA 94132, USA. ²*Drosophila* Heterochromatin Genome Project, Department of Genome and Computational Biology, Lawrence Berkeley National Laboratory, Berkeley, CA 94720, USA. ³National Center for Biomedical Ontology, Lawrence Berkeley National Laboratory, Berkeley, CA 94720, USA. ⁴Department of Molecular and Cell Biology, University of California at Berkeley, Berkeley, CA 94720, USA.

*To whom correspondence should be addressed. E-mail: karpen@fruitfly.org

distinct groups of *Drosophila* lineage-specific genes and another subset of ultraconserved insect genes. Closer examination of the 163 genes with orthologs in four or fewer species revealed that 93% had orthologs only in the four species most closely related to *D. melanogaster* (Fig. 3B, SOM text, and data). Conservation in only the

Drosophilid lineage or melanogaster subgroup may identify more recently evolved genes (SOM text). Indeed, some open reading frames (ORFs), such as odorant-binding proteins or receptors, tend to evolve faster than do other genes and are often found in only a single species (19, 20). More in-depth study will be required to determine whether

the lineage-specific Drosophilid genes are conserved because of function or because there has been insufficient time for ORFs to diverge.

Analysis of orthology data, gene prediction, and cDNA and EST clone evidence shows that 96% of heterochromatin multi-exon genes and 89% of single-exon genes are supported by two or more types of evidence (Fig. 2, A and B). These results demonstrate that single-exon genes probably represent parts of bona fide, full-length genes that will be merged into more complete genes as the sequence assemblies and cDNA resources are improved, as observed for fragmented annotations in prior releases (e.g., CG41520 in Fig. 1). Comparative genomic support for small single-exon genes also suggests that there may be many more conserved exons in other parts of less well assembled Drosophilid genomes (21).

We inferred 1030 conserved introns between well-conserved exons of the orthologs identified in the 16 insect genomes. Heterochromatin gene introns are, on average, five times longer than introns in euchromatic genes [4949 versus 1149 base pairs (bp)], and may be as long as 1 Mb (22). The longest contiguous intron we have identified is 224,977 bp in the *Snap25* gene (11). Intron lengths are highly conserved among euchromatin gene orthologs (Fig. 3C), whereas heterochromatin intron lengths were correlated in species closely related to *D. melanogaster* but were poor-

Table 1. Annotation summary. ND, not done.

Data type	Release 2 (2000)	Release 3.1 (2002)	Release 3.2b (2004)	Release 5.1 (2006)
Annotated sequence (Mb)	3.8	12.1	14.2	24
Sequence length of repeats (Mb/%)	ND	6.3/52	6.3/75	18/77
Sequence length of exons (Mb/%)	0.15/4	0.33/2.7	0.43/3.0	1.33/5.5
Repeat nest fragments (number/Mb)	ND	ND	ND	10084/10
Full-length TEs	ND	ND	ND	202
Total annotations	130	447	556	11038
Protein-coding genes	130	297	472	613
Single-exon genes	43	58	195	187
Genes with finished cDNAs	48	58	92	137
Protein-coding genes with any EST/cDNA clone evidence	ND	80	142	250
Pseudogenes	0	1	7	32
ncRNAs	0	3	14	13
Recursive splice sites	ND	ND	ND	16
Miscellaneous annotations	ND	ND	ND	9
Unassembled ribosomal DNA fragments	0	6	52	67

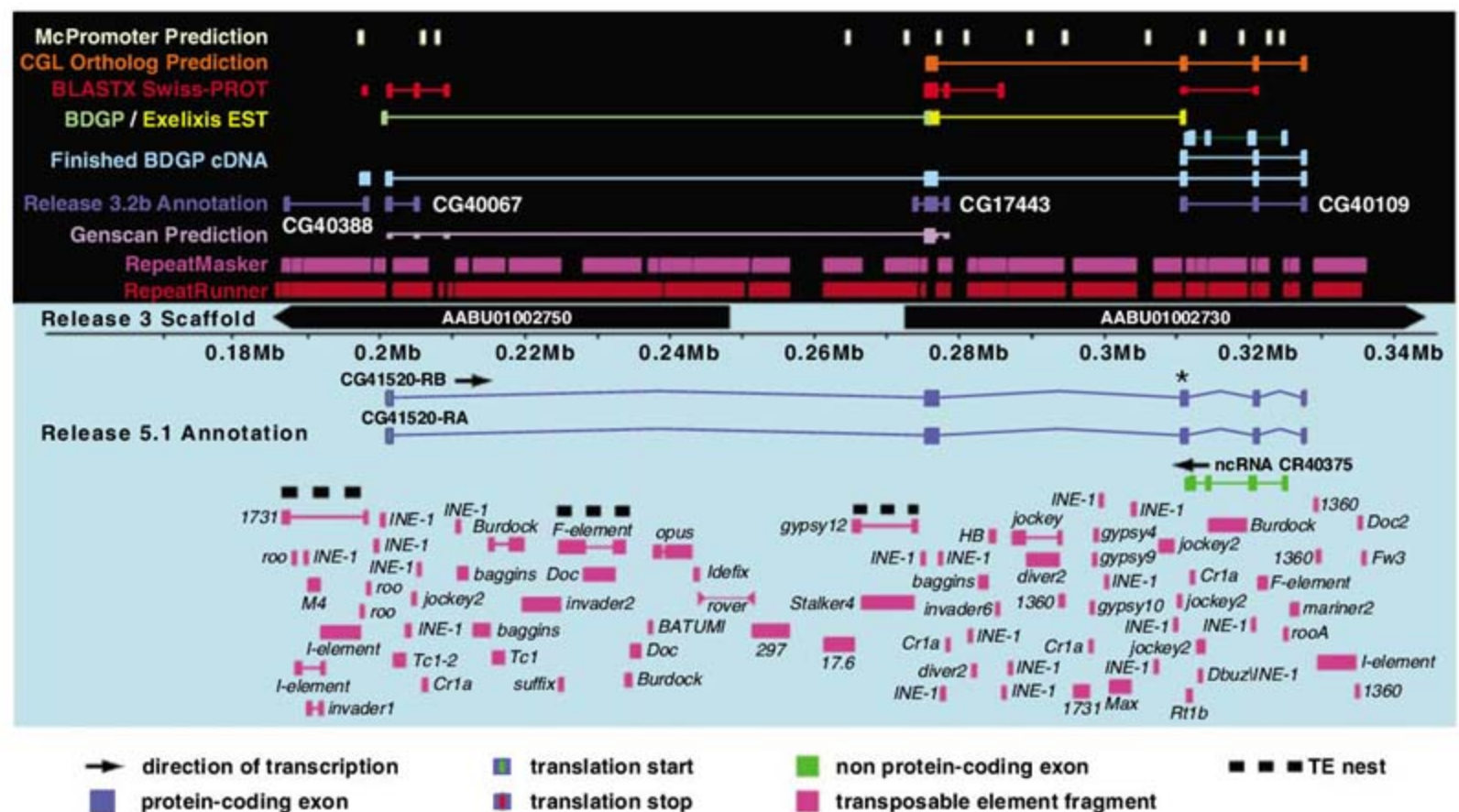


Fig. 1. Computational pipeline results used for the Release 5.1 annotation. An *Apollo* (36) screenshot of the evidence (black region) and Release 5.1 annotations (light blue region) for scaffold CP000218, which was produced by merging, extending, and finishing the Release 3 WGS scaffolds (AABU01002750 and AABU010027230) (9). New cDNA evidence was used to merge the Release 3.2b

annotations CG40067, CG17443, and CG40109 into one Release 5.1 gene (CG41520) and to identify an alternative exon for CG41520-RB (asterisk). ncRNA CG40375 is shown on the opposite strand to illustrate that it is nested within CG41520. CG40388 represents a Release 3.2b gene that is now annotated as a TE fragment. Complete annotation and evidence are shown in (11).

ly correlated for more distantly related species. For example, intron lengths for *D. erecta* orthologs were correlated in both euchromatin [correlation coefficient (r) = 0.48] and heterochromatin (r =

0.58), whereas *D. virilis* gene intron lengths were correlated in euchromatin (r = 0.37) but not in heterochromatin (r = 0.14) (Fig. 3C). A list of conserved introns, their average lengths, and the

percent conservation of flanking coding exons is provided (SOM text and data).

One of the features of heterochromatic genes is that introns and intergenic regions are com-

Fig. 2. Evidence of *D. melanogaster* heterochromatin protein-coding gene annotations. Venn diagrams show the percentage of protein-coding genes supported by gene prediction (pink), EST or cDNA (yellow), and/or BLASTX/TBLASTN comparative genomic evidence (blue). (A) Multi-exon genes are likely to be complete, whereas (B) single-exon genes are likely to represent genes that are fragmented across multiple scaffolds. The number of genes measured for each class are indicated, as well as the number and percent of genes with putative orthologs in melanogaster group species, nonmelanogaster group Drosophilids, or other insect species.

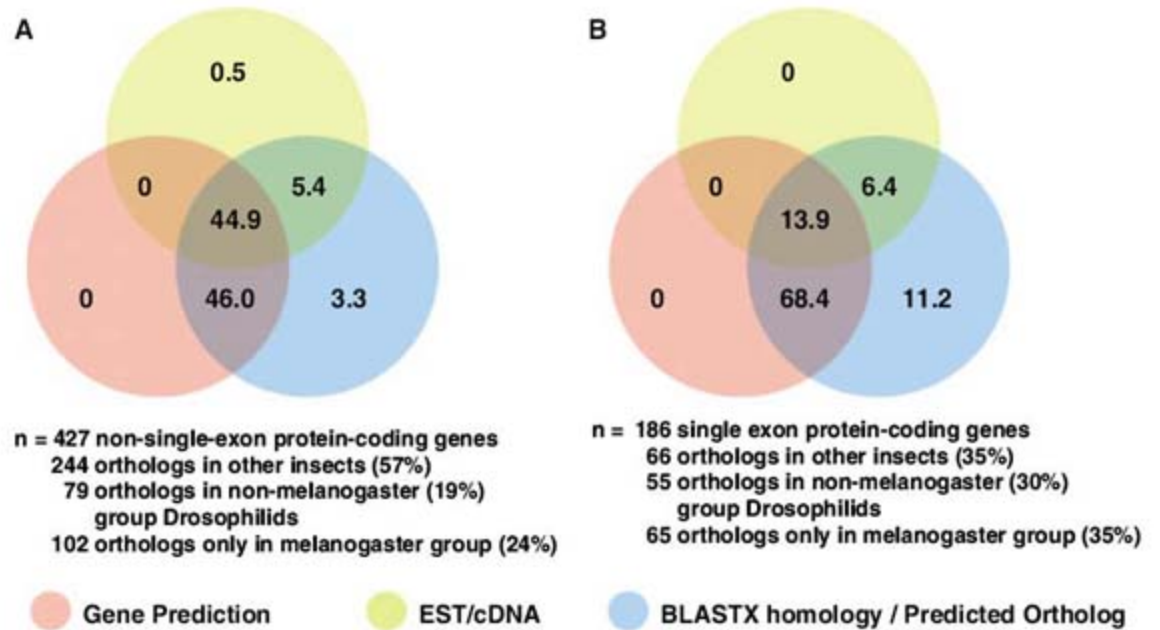
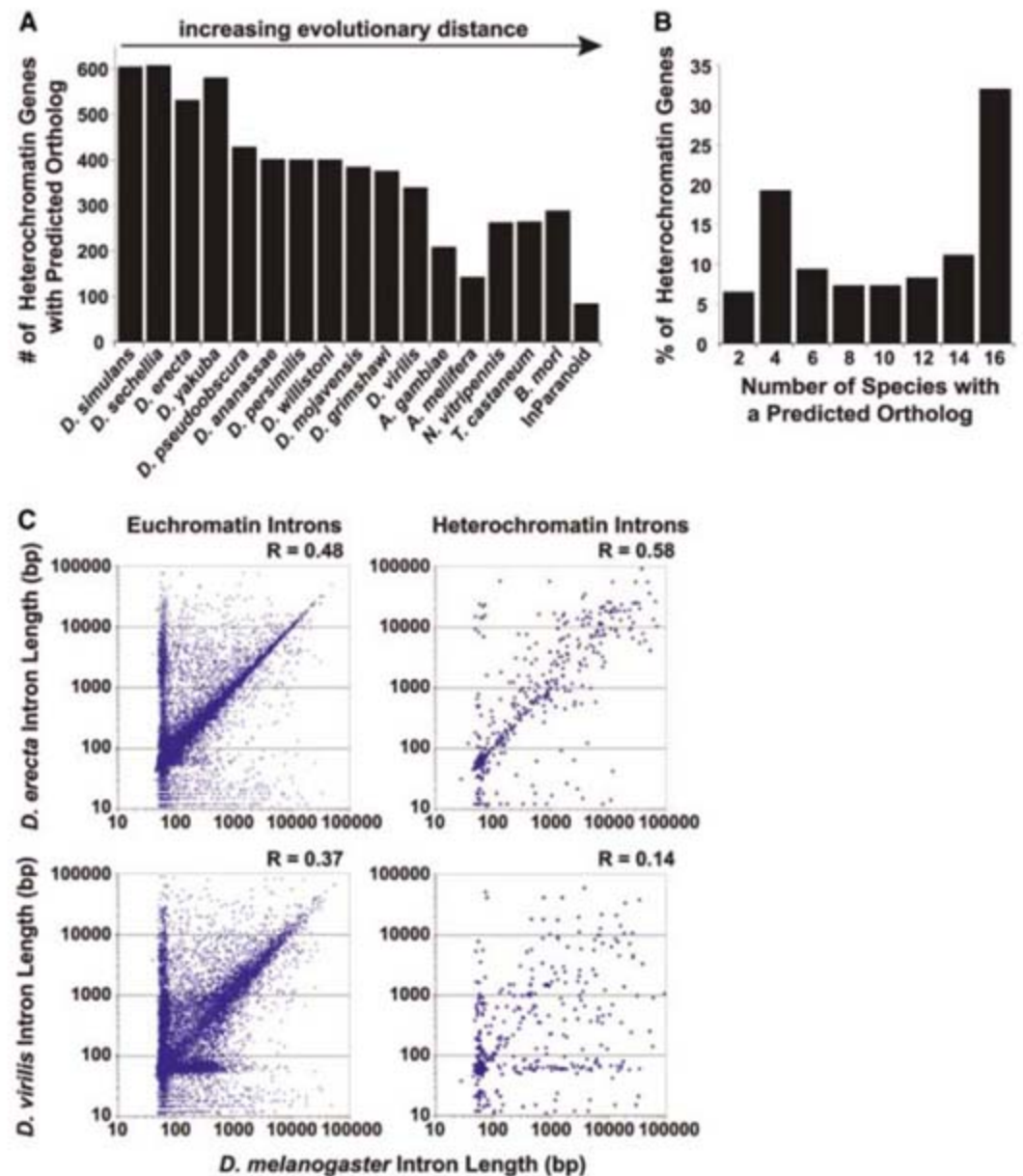


Fig. 3. Comparative analysis summary for *D. melanogaster* heterochromatin genes. (A) Number of heterochromatin protein-coding genes with a predicted ortholog in a given species, ordered (left to right) by increasing evolutionary distance from *D. melanogaster*. (B) Frequency histograms showing the percentage of heterochromatin protein-coding genes with a predicted ortholog in the 16 insect species tested. (C) Scatter plots of intron lengths (bp) for euchromatin and heterochromatin protein-coding gene introns conserved in either *D. erecta* or *D. virilis*. Each data point refers to a single conserved intron. Correlation coefficients (r) for intron lengths are indicated.



posed almost entirely of repeated sequences, predominantly fragmented TEs (Fig. 1). There was no appreciable difference in the average repeat density or composition of intronic (56%) versus intergenic sequences (63%) (11). Changes in intron length are most often due to TE insertions and excisions and simple repeat expansions. The high repeat content of introns and regulatory regions suggests that regulation of heterochromatic gene expression may differ from euchromatic genes. We identified 16 recursive splice sites (RSSs) shown to aid in the splicing of long introns (23), including 8 RSSs located in long heterochromatin gene introns ranging from 11 to 166 kilobases (kb). Of particular interest are three RSSs predicted in the 23.6-kb intron of CG40120, only one of which was previously predicted because of gaps in the sequence assembly (23). Fifty-six percent of the RSS motifs were embedded within retrotransposons, suggesting that cis TE sequences may be used to splice out TEs that invade heterochromatin genes.

Non-protein-coding genes. We identified 13 putative non-protein-coding genes in the heterochromatin (Table 1), defined as single-copy genes with EST or cDNA support that contained protein-coding ORFs that were substantially shorter than the length of the transcript. Spliced ESTs and cDNAs were identified for 11 of the ncRNA annotations, excluding the possibility of false positives generated by the priming of polymerase chain reaction products from adenine (A)-rich regions. Analysis of the two unspliced ncRNAs suggested that the clones were not primed from genomic A-rich regions. 5 out of 13 ncRNAs contain

~100 bp of the 600-bp *INE-1* TE consensus in the 3' end of the transcript, which is insufficient for autonomous transposition but may represent a conserved motif. The ncRNA gene CR40375 is nested in the intron of the protein-coding gene CG41520 (Fig. 1). Recent reports (24) suggest that thousands of transcribed regions are coregulated with genes and may represent missing coregulated genes or novel 5' untranslated region (UTR) exons. We found the converse case; new cDNA evidence suggests that the 5' UTR exon of the Release 3.2b gene CG40084 represents a ncRNA (CR41594) (11). Further analysis will be required to determine whether these ncRNA annotations represent functional genes.

Pseudogenes. Protein-coding genes that are near-perfect but truncated copies of genes found elsewhere in the genome were annotated as pseudogenes. The *D. melanogaster* genome has far fewer identified pseudogenes than do other metazoan genomes (25). For example, the three-gigabase human genome is estimated to contain ~20,000 pseudogenes of various types (26), whereas the 120-Mb *D. melanogaster* R4.3 euchromatin has only 51 annotated pseudogenes (27). We identified 32 putative pseudogenes in the *D. melanogaster* heterochromatin sequence, representing a threefold increase in pseudogene density in heterochromatin versus euchromatin (1.3 versus 0.425 pseudogenes per Mb) (Table 1 and SOM text). The enrichment of repetitive sequences in both fly heterochromatin and human euchromatin, relative to *D. melanogaster* euchromatin, may facilitate the formation of pseudogenes by increasing the probability of large- or small-scale duplications.

Repeats and transposable elements. Repeats were defined by significant alignment to known RepBase repetitive sequences identified by RepeatMasker (28), BLASTX homology to TE proteins, or TRF (29) results (10). The application of these improved methods demonstrated that 18 Mb (77%) of the annotated heterochromatin could be classified as repetitive or transposable elements, a 4-Mb (20%) increase compared with the previous annotation (1). About 50 previously identified protein-coding genes have been reannotated as repetitive features. For example, CG40388 was annotated as a protein-coding gene in Release 3.2b but annotated as a 1731 repeat in Release 5.1 (Fig. 1). The euchromatin sequence was previously reported to consist of 3.86 to 6% of repetitive sequence (30, 31). Our methods provide better recognition of TE fragments, small tandem repeats, and short ORFs from degenerate TEs, and they identified 7% of the Release 5 euchromatin as repetitive (Fig. 4), similar to other estimates (32). The sequenced *D. melanogaster* heterochromatin has an overall repeat and TE content more than 10 times that of fly euchromatin and is more similar to the repeat density in human euchromatin (40%) (6, 7).

We measured the repeat content and gene distribution across the heterochromatin sequence in 100-kb sections and calculated the average density for each region (Fig. 4). Lower overall repeat content was observed for regions more distal from the centromere, especially for the heterochromatic regions on chromosome arm 3Rh (Fig. 4). In addition, the unmapped scaffolds had a higher repeat content than the heterochromatin regions that have been mapped to the chromosome arms (Fig. 4). In general, there was a strong inverse correlation between the repeat and gene content of a region ($r = -0.89$) (Fig. 4). Euchromatin had an average gene density of 12.6 genes per 100 kb, whereas heterochromatin contained 1.8 to 4.4 genes per 100 kb (2.9 genes per 100 kb overall). Exceptions include Xh and XHet, with 9.2 and 6.4 genes per 100 kb. Chromosome arm 3Rh had an average gene content even higher than that of typical euchromatin (19 genes per 100 kb) and a 20% average repeat content, which is significantly lower than the rest of the heterochromatin (Fig. 4).

We further categorized the average percentage of retrotransposons, DNA transposons, and other repeats (Fig. 4). Roughly two-thirds (16 Mb, 66%) of the heterochromatin is composed of retrotransposon sequences [33% long terminal repeats (LTRs) and 33% long interspersed nuclear elements (LINEs)]. DNA transposons are overrepresented on the relatively repeat-rich euchromatin regions of the fourth chromosome of *D. melanogaster* (33) but constitute only 15% of the Release 5 heterochromatin, which does not include the fourth chromosome heterochromatin (8, 9). TRF-identified tandem repeats and satellite repeats make up ~10% of the available heterochromatin sequence, which is significantly higher than in the euchromatin sequence (~3%), espe-

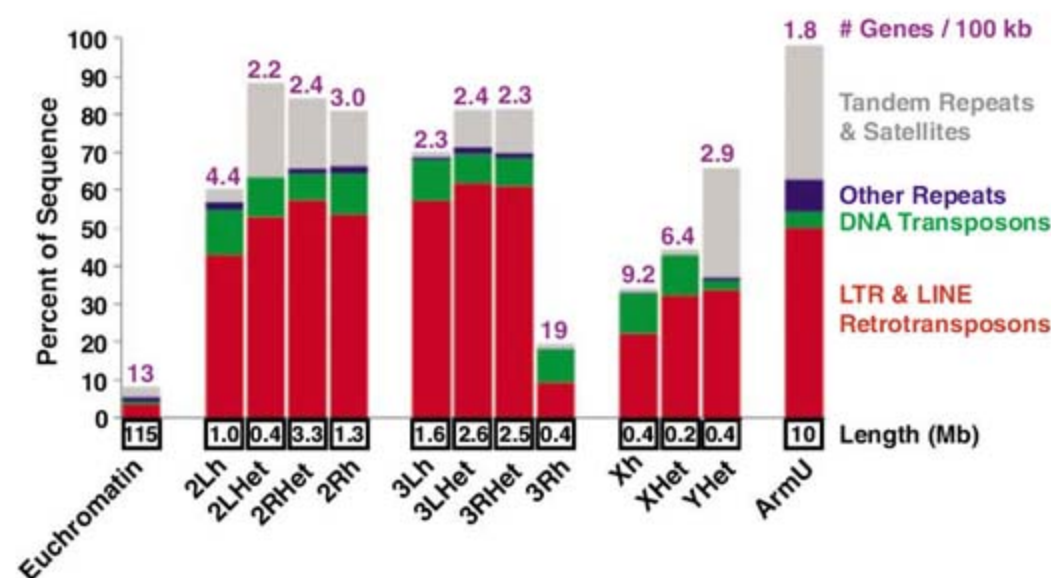


Fig. 4. Density of repeat and gene features across the heterochromatin. The average percentages of indicated annotation types are shown for each chromosome region (total length in boxes below the x axis). Euchromatin is an average of the noncentric regions of arms 2, 3, and X only. 2Lh, 2Rh, 3Lh, 3Rh, and Xh describe heterochromatic regions that are contiguous with the chromosome arms, whereas the Het regions are mapped to arms and ordered, but not necessarily in the correct orientation (8, 9). The average percentages of sequences for LTR- and LINE-like retrotransposons (red), DNA transposons (green), other and unknown repeats (blue), and TRF tandem repeats and satellite sequences (gray) are indicated. The average number of genes per 100 kb is shown above each histogram.

cially in the proximal centric regions of chromosomes 2 and 3 and the Y chromosome (Fig. 4). Calculations of tandem-repeat content are likely to be an underestimate, because WGS3 sequence underrepresents the difficult-to-clone satellite DNA and tandem-repeat regions. Unlike the Y chromosome and autosomal heterochromatin, the available X chromosome sequence is not enriched for tandemly repeated sequences. Our repeat analysis indicates that nearly all of the ArmU and ArmUExtra (10) sequence is composed of repetitive sequences, further suggesting that we have identified most of the unique sequence available in the *D. melanogaster* heterochromatin.

The majority of repetitive TE-like sequences in heterochromatin is not intact. We found 202 full-length TEs in the heterochromatin (2% of heterochromatic TEs), compared with 361 full-length TEs reported for the nonpericentromeric euchromatin (20.6% of euchromatic TEs). The most recent annotation of the Release 4 euchromatin identified nests of TEs that were fragmented, interdigitated, and transposed into one another (32). Our manual curation identified 846 repeat nests in newly sequenced regions of the Release 5 heterochromatin, compared with 112 nested TEs in the euchromatin. We annotated 117 instances where there were two nested TEs (i.e., a TE jumped into a TE that itself had jumped into a TE) and 17 instances where four or more TEs were nested (Fig. 1).

Conclusions. The assembly of a more complete genome sequence (9) and an integrated annotation set for *D. melanogaster* provides a

reference set of genes and other features that will be useful for investigating the biological functions of heterochromatin in flies and other organisms. These results are now fully integrated, with information about the euchromatin, in FlyBase (34) and GenBank (35).

These results demonstrate that repetitive and TE sequences constitute at least 77% of the 24 Mb of heterochromatin sequence. Although there are more full-length TEs and TE nests in the centric heterochromatin relative to the euchromatin, it appears that most heterochromatic TEs are fragmented and not capable of autonomous transposition. As with the euchromatin, the repetitive sequences in heterochromatin are dominated by LTR- and LINE-like retrotransposons. We have identified a substantial amount of tandemly repeated sequences in the most proximal centric heterochromatin of the second, third, Y, and unmapped chromosomes, but not in the currently sequenced X chromosome. These carefully annotated repetitive regions provide opportunities for more in-depth analysis of their functions and evolution. For example, a recent study showed that at least 80% of *piwi*-associated small RNAs, which regulate transposon activity, map to the release 5 heterochromatin (4).

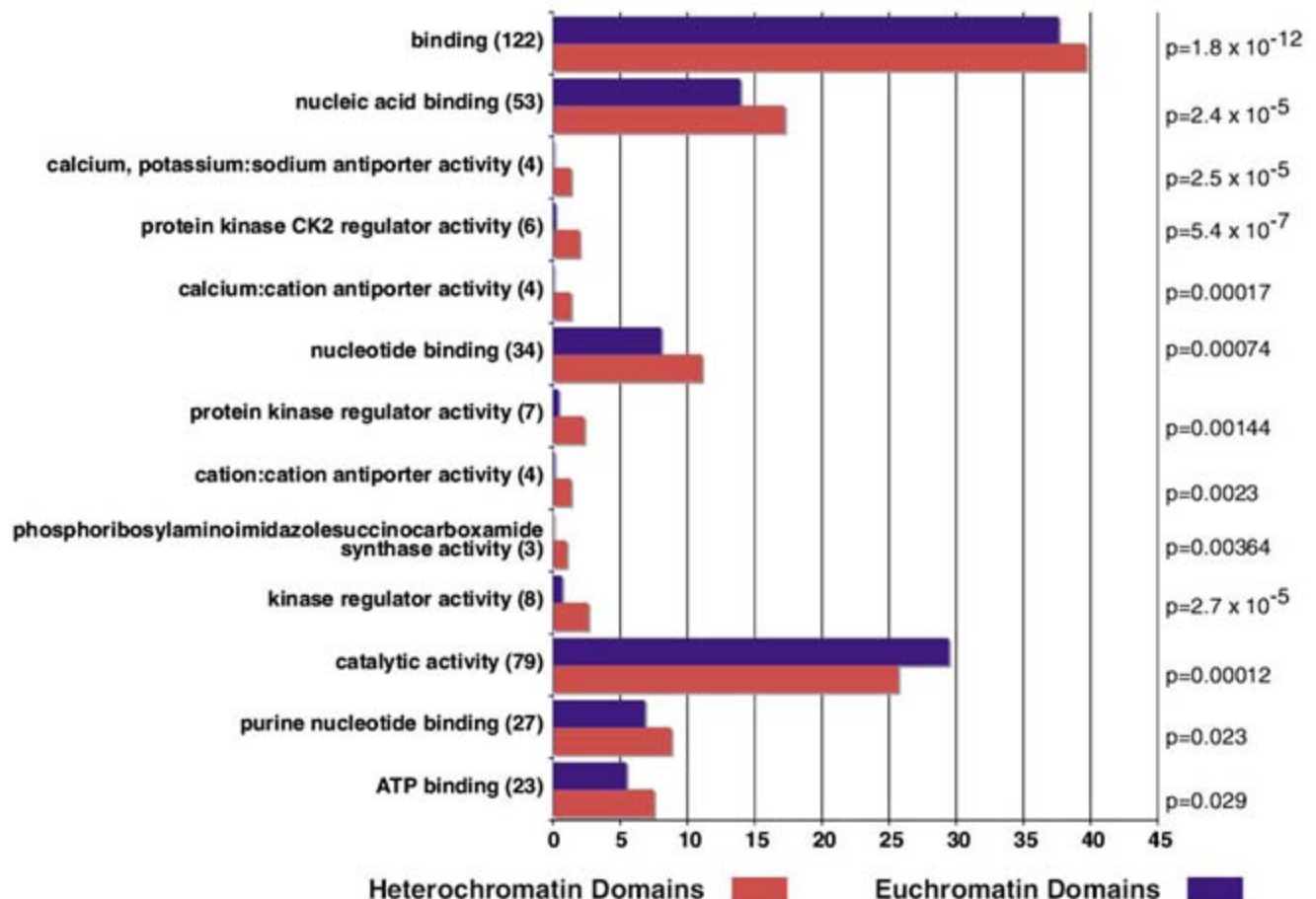
We found that more than 99% of the protein-coding genes and gene fragments are conserved in other insect species. A subset of the protein-coding genes (35%) appears to be present in only the *melanogaster* group of Drosophilids, suggesting recent evolution. Of the 613 protein-coding genes identified, 137 are considered complete by the criterion of having a full-length

cDNA. Another 115 protein-coding genes are only partially supported by clone evidence, with ~360 genes lacking EST or cDNA evidence. Thus, there are 475 annotated protein-coding genes that are likely to represent fragments from larger genes. Based on an average of ~four to five exons observed for complete euchromatin and heterochromatin genes, we estimate that these 475 fragments represent 95 to 119 full-length genes, and thus we approximate that there are 230 to 256 protein-coding genes in the currently sequenced heterochromatin.

The gene density in heterochromatin is substantially lower than it is in euchromatin and is inversely correlated with repeat content. Based on our RepeatRunner analysis, only 9% (2.2 out of 24 Mb) of the Release 5 heterochromatin is a unique sequence, of which 60% (1.3 Mb) is annotated as exons; thus, only 5.4% of the sequenced heterochromatin is exonic, compared with 25% of the euchromatin. The average protein-coding and ncRNA gene density for the annotated heterochromatin is 10 to 11 genes per Mb, compared with 127 genes per Mb in the euchromatin. We have identified 32 pseudogenes in the heterochromatin, including 8 in the poorly represented Y chromosome sequences, representing a density of pseudogenes that is at least three times that of euchromatin. The high repeat content of heterochromatin may provide recombination substrates that increase the frequency of tandem and segmental duplications.

Despite differences in gene density, there are many similarities between the basic structures and putative functions of euchromatic and het-

Fig. 5. Overrepresented GO terms in heterochromatin versus euchromatin genes. The percentages of GO molecular-function domains for genes in heterochromatin (red) and euchromatin (blue) are shown. Numbers in parentheses indicate the actual number of domains in heterochromatin. *P*-value significance scores are shown to the right. Complete GO analyses are presented in the SOM text.



erochromatic genes. Based on cDNA-supported genes, it appears that euchromatin and heterochromatin genes have, on average, a similar number of exons and transcript variants per gene. In general, heterochromatic and euchromatic genes appear to encode a similar spectrum of functions, based on gene ontology (GO) analysis (Fig. 5). Some classes of genes are overrepresented in the heterochromatin, relative to the euchromatin. For example, heterochromatin genes are enriched 35-fold for putative membrane cation transporters domains (4 out of 308 heterochromatin domains versus 5 out of 13,500 euchromatin domains). Heterochromatic genes are also enriched for domains involved in DNA (53 domains) or protein binding (122 domains) that may regulate chromatin structure or function, including histone variants and proteins (Fig. 5, SOM text, and data) (11). This raises the intriguing possibility that heterochromatin may encode genes involved in its own establishment or maintenance.

Heterochromatin genes can reside in regions that approach 90% repeat content. Heterochromatin gene introns are usually composed of fragmented TE sequences (Fig. 1), are on average five times longer than euchromatin gene introns, and display less length conservation in interspecies comparisons. We found nine recursive splice site motifs nested in the long introns of heterochromatin genes, which may regulate splicing in repeat-rich regions. The underlying mechanisms that allow essential genes to be expressed and regulated in otherwise silent chromatin remain unknown. Studying heterochromatin in other species promises to shed light

on whether there are cis sequences that define or regulate boundaries between euchromatin and heterochromatin and if there are genic and non-genic regions of heterochromatin in other repeat-rich regions, including human euchromatin.

References and Notes

1. R. A. Hoskins *et al.*, *Genome Biol.* **3**, RESEARCH0085 (2002).
2. The Arabidopsis Genome Initiative, *Nature* **408**, 796 (2000).
3. B. A. Sullivan, M. D. Blower, G. H. Karpen, *Nat. Rev. Genet.* **2**, 584 (2001).
4. J. Brennecke *et al.*, *Cell* **128**, 1089 (2007).
5. S. C. Elgin, S. I. Grewal, *Curr. Biol.* **13**, R895 (2003).
6. E. S. Lander *et al.*, *Nature* **409**, 860 (2001).
7. J. C. Venter *et al.*, *Science* **291**, 1304 (2001).
8. H. R. Carlson Jr., *et al.* (www.fruitfly.org/sequence/release5genomic.shtml) (2006).
9. R. Hoskins *et al.*, *Science* **316**, 1625 (2007).
10. Materials and methods are available as supporting material on Science Online.
11. Supplemental data can be downloaded from [ftp://ftp.dhgp.org/pub/DHGP/Science_2007_Supplemental_Data](http://ftp.dhgp.org/pub/DHGP/Science_2007_Supplemental_Data). Future updates will be released through www.flybase.net.
12. C. D. Smith *et al.*, *Gene* **389**, 1 (2007).
13. G. Benson, *Nucleic Acids Res.* **27**, 573 (1999).
14. M. Hild *et al.*, *Genome Biol.* **5**, R3 (2003).
15. Berkeley Drosophila Genome Project, www.fruitfly.org/.
16. C. Kopyzynski *et al.*, www.ncbi.nlm.nih.gov/entrez/viewer.fcgi?db=nucleotide&val=59874298.
17. K. P. O'Brien, M. Remm, E. L. Sonnhammer, *Nucleic Acids Res.* **33**, D476 (2005).
18. K. J. Peterson *et al.*, *Proc. Natl. Acad. Sci. U.S.A.* **101**, 6536 (2004).
19. S. Foret, R. Maleszka, *Genome Res.* **16**, 1404 (2006).
20. H. M. Robertson, K. W. Wanner, *Genome Res.* **16**, 1395 (2006).
21. Assembly, Alignment, and Annotation of Drosophilid Genomes, http://rana.lbl.gov/drosophila/wiki/index.php/Main_Page.
22. A. M. Reugels, R. Kurek, U. Lammermann, H. Bunemann, *Genetics* **154**, 759 (2000).

23. J. M. Burnette, E. Miyamoto-Sato, M. A. Schaub, J. Conklin, A. J. Lopez, *Genetics* **170**, 661 (2005).
24. J. R. Manak *et al.*, *Nat. Genet.* **38**, 1151 (2006).
25. P. M. Harrison, D. Milburn, Z. Zhang, P. Bertone, M. Gerstein, *Nucleic Acids Res.* **31**, 1033 (2003).
26. D. Torrents, M. Suyama, E. Zdobnov, P. Bork, *Genome Res.* **13**, 2559 (2003).
27. R. A. Drysdale, M. A. Crosby, *Nucleic Acids Res.* **33**, D390 (2005).
28. A. F. A. Smit, R. Hubley, P. Green, RepeatMasker Open-3.0, www.repeatmasker.org/.
29. G. Benson, *Nucleic Acids Res.* **27**, 573 (1999).
30. J. S. Kaminker *et al.*, *Genome Biol.* **3**, RESEARCH0084 (2002).
31. H. Quesneville *et al.*, *PLoS Comput. Biol.* **1**, e22 (2005).
32. C. M. Bergman, H. Quesneville, D. Anxolabehere, M. Ashburner, *Genome Biol.* **7**, R112 (2006).
33. E. E. Slawson *et al.*, *Genome Biol.* **7**, R15 (2006).
34. FlyBase, www.flybase.net/.
35. GenBank, www.ncbi.nlm.nih.gov/.
36. S. E. Lewis *et al.*, *Genome Biol.* **3**, RESEARCH0082 (2002).
37. We thank E. Frise for maintaining the hardware and software used in these studies; M. Yandell for providing the specialized comparative genomics library-based software used in our analyses; A. Dernburg, D. Acevedo, J. Carlson, S. Celniker, R. Hoskins, and C. Kennedy for their helpful comments on the manuscript and input on annotations; and the members of the BDGP for cDNA sequencing. This work was supported by the National Human Genome Research Institute grant R01-HG000747 to C.D.S. and G.H.K. and NIH grant U54 HG004028-01 to S.S. and C.J.M.

Supporting Online Material

www.sciencemag.org/cgi/content/full/316/5831/1586/DC1
Materials and Methods

SOM Text

SOM Tables (D to F, I, and J)

References

11 January 2007; accepted 7 May 2007
10.1126/science.1139815

REPORTS

Tracking Solar Gravity Modes: The Dynamics of the Solar Core

Rafael A. García,^{1,2*} Sylvaine Turck-Chièze,^{1,2} Sebastian J. Jiménez-Reyes,³ Jérôme Ballot,^{2,4} Pere L. Pallé,³ Antonio Eff-Darwich,^{3,5} Savita Mathur,^{1,2} Janine Provost⁶

Solar gravity modes have been actively sought because they directly probe the solar core (below 0.2 solar radius), but they have not been conclusively detected in the Sun because of their small surface amplitudes. Using data from the Global Oscillation at Low Frequency instrument, we detected a periodic structure in agreement with the period separation predicted by the theory for gravity dipole modes. When studied in relation to simulations including the best physics of the Sun determined through the acoustic modes, such a structure favors a faster rotation rate in the core than in the rest of the radiative zone.

Helioseismology reveals the solar interior through surface observations of oscillation modes propagating inside the Sun (1, 2). Pressure-driven modes (p modes) provide a very detailed picture of the solar interior (3). Measurements of the position of the base of the convective zone (4) and the helium abundance (5) are some examples of the results achieved by the study of such modes. The structural in-

versions of the precise p-mode frequencies provide the stratification of crucial variables, such as the sound speed down to 0.05 solar radius (R_{\odot}) (6, 7). However, p modes are less sensitive to other structural variables such as density. There is less agreement between this parameter and the models in the deepest layers of the radiative zone. Moreover, the dynamical properties (8) of the solar interior (more than 60% of the total mass,

below $0.3R_{\odot}$) are not well defined. For example, large uncertainties still remain in the solar rotation profile below $0.2R_{\odot}$ (Fig. 1) because of the lack of sensitivity and the poor spatial resolution of the modes toward the deep interior (9).

To progress at greater depths and down into the solar core requires the study of another type of waves—the gravity-driven modes (g modes), for which the driving force is buoyancy. These modes are trapped within the radiative region of the Sun and become evanescent in the convective zone, reaching the solar surface with amplitudes that could be very small (10). Even considering their low surface amplitudes, g modes remain

¹DSM/DAPNIA/Service d'Astrophysique, CEA Saclay, 91191 Gif-sur-Yvette Cedex, France. ²AIM—Unité Mixte de Recherche CEA—CNRS—Université Paris VII—UMR 7158, CEA Saclay, 91191 Gif-sur-Yvette Cedex, France. ³Instituto de Astrofísica de Canarias (IAC), 38205 La Laguna, Tenerife, Spain. ⁴Max-Planck-Institut für Astrophysik, Karl-Schwarzschild-Str. 1, Postfach 1317, 85741 Garching, Germany. ⁵Departamento de Edafología y Geología, Universidad de La Laguna, Tenerife, Spain. ⁶Département Cassiopée, UMR CNRS 6202, Observatoire de la Côte d'Azur, BP 4229, 06304 Nice Cedex 4, France.

*To whom correspondence should be addressed. E-mail: rafael.garcia@cea.fr

the best probes to provide information from the solar core up to the top of the radiative region.

Solar g modes have been actively sought since 1976, without success (11). Recently, an upper limit of $\sim 1 \text{ cm s}^{-1}$ has been obtained by looking for relevant spikes in the Fourier spectrum of the observed signal above a given statistical threshold (typically 90% confidence level) and in the frequency region above $150 \mu\text{Hz}$ (12–14). A more sophisticated search of multiplets (instead of individual spikes) reduces the detection level to a few millimeters per second, yielding some g-mode candidates with a confidence level between 90% (15) and 98% (16). However, some ambiguity still surrounds their identification (attributed to quadrupole, $\ell = 2$, modes). Some scenarios have been studied explaining the visible peaks, which could constrain the physics and dynamics of the solar core. Here, we looked instead for the almost constant predicted separation (ΔP_ℓ , Fig. 2) between the periods of gravity modes with the same degree ℓ and consecutive radial order n . These separations are related to the structure and dynamics of the solar core (17). Indeed, this method is extremely sensitive to the rotation rate of the inner solar layers (18).

We used almost 10 years of velocity observations (11 April 1996 to 21 October 2005) from the Global Oscillation at Low Frequency (GOLF) instrument aboard the ESA/NASA Solar and Heliospheric Observatory (SOHO) mission. SOHO is placed around the L_1 Lagrangian point, a region at 1.5 million km from Earth toward the Sun where the gravitational field between the Sun and the Earth-Moon system equilibrates the centrifugal force. This privileged position allows continuous and uninterrupted observations of the Sun, essential for helioseismology, and provides a very stable environment. The GOLF instrument is a resonant scattering spectrophotometer (19) designed to measure line-of-sight velocity displacements of the solar photosphere. The analysis of the temporal variation of the velocity (20) in Fourier space allows the determination of the solar oscillation parameters and the derivation of the properties of the solar interior (21).

From the velocity measurements, we computed the power spectral density (PSD) by means of a fast Fourier transform algorithm. To look for the periodic signature of the g modes in this PSD, we computed a second power spectrum of the PSD between 25 and $140 \mu\text{Hz}$ (22). A broad structure in the region centered at $\sim 24 \text{ min}$ appears in this power spectrum (Fig. 3). To characterize this feature, we first used two indicators: the maximum amplitude reached (6.5σ) and the average power (2.95 times the average power of the rest of the spectrum). This feature has a high signal-to-noise ratio and is a wide structure rather than a single spike. Using a Monte Carlo simulation of $N = 6 \times 10^5$ realizations (22), we estimated the probability (likelihood) of finding a similar structure, in terms of both indicators mentioned above, produced only by pure noise with the same statistical distribution as in the GOLF

data between 22 and 26 min. We found that the likelihood that this structure is not due to noise is 99.49%. Because of the finite number of realizations, there is an uncertainty of 0.13%.

The significant structure of the GOLF power spectrum reveals the existence of quasi-periodic features somewhere in the PSD. Excluding an instrumental origin or a relation with convection (22), we studied the consequences of assuming that it is produced by the asymptotic properties of the dipole ($\ell = 1$) g modes. If this is the case, the position of the periodic structure in the PSD should follow the predicted positions of the gravity modes. To check this hypothesis, we reconstructed the fitted waves in the PSD that produced the ΔP_1 peak structure found between 22 and 26 min in the power spectrum (22).

The most striking result of this work is that the reconstructed waves issued from the real GOLF data show a pattern with their maxima at positions

near those expected from solar models (Fig. 4 and fig. S7), which supports the conjecture that they are due to gravity modes. Using the previous Monte Carlo simulation, we were able to count the number of noise realizations that matched the characteristics of the structure in the GOLF power spectrum, and to show a reconstructed wave that behaves like the one expected from g modes. To do so, we correlated the reconstructed wave of a fixed solar model with the reconstructed wave of the real data as well as with the one from the Monte Carlo simulation. To be less dependent on the physics and dynamics of the model chosen, we used three different g-mode predictions from three different solar models: the seismic model (23), the standard model S (24), and the Nice standard solar model (25). We also used different scenarios for the dynamics inside the solar core. Thus, various solar core rotation rates placed at different depths in the solar core and with different rotation axis inclina-

Fig. 1. Inversion of the solar rotation rate (Ω) using modes $\ell \leq 25$ from long time series (2088 days) of GOLF (29) and Michelson Doppler Imager (MDI) (30). In the convective zone, the differential rotation rate at different colatitudes is plotted. In the radiative region, the rotation becomes rigid down to $\sim 0.3R_\odot$. The horizontal and vertical 1σ error bars progressively increase toward the core because the p modes are less and less sensitive and because fewer and fewer modes are available for the inversion at these depths. Below $0.2R_\odot$ the rotation profile is unknown.

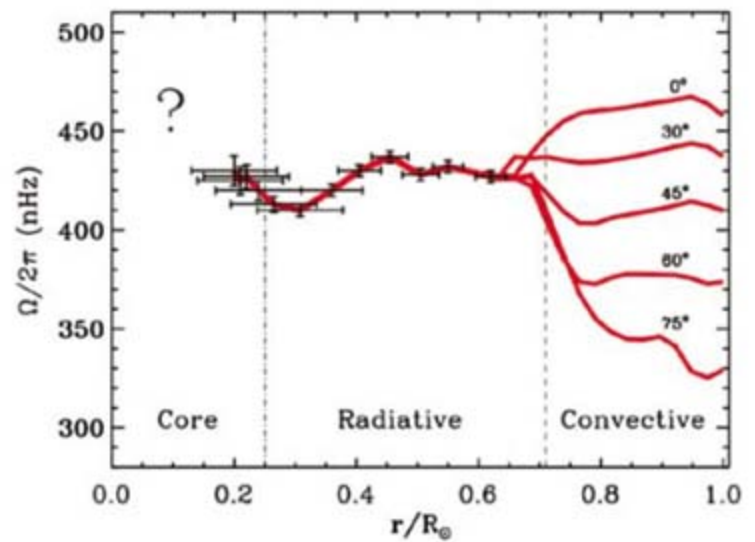
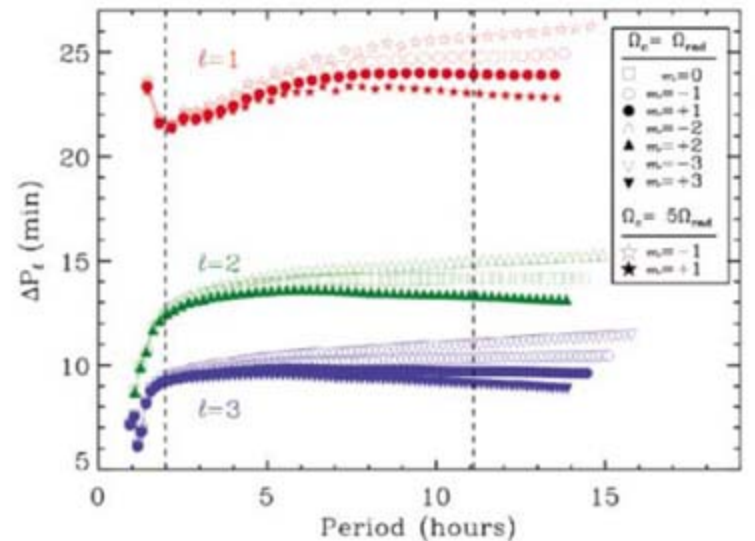


Fig. 2. Separations in period, ΔP_ℓ , between consecutive radial orders ($n, n + 1$) gravity modes for $\ell = 1, 2$, and 3 (red, green, and blue, respectively), using the theoretical frequencies from the seismic model. The constant periodicity is achieved at 6, 4, and 2 hours for the modes $\ell = 1, 2$, and 3, respectively. Ω_c is the angular velocity of the solar core, $\Omega_{\text{rad}} \approx 433 \text{ nHz}$ is the angular velocity of the remaining radiative zone, and m is azimuthal order. The star symbols show the effect, on the dipole ($\ell = 1$) modes, of an increased solar core rotation rate—up to 5 times that of the remaining radiative zone ($\Omega_c = 5\Omega_{\text{rad}}$)—below a core radius $R_c = 0.15R_\odot$. For the sake of clarity, we have not drawn the effect for higher-degree modes. Inside the zone limited by the two vertical dashed lines (from ~ 2 to ~ 14 hours, corresponding to 25 to $140 \mu\text{Hz}$), we expect periodicities between 22 and 26 min for the $\ell = 1$ mode, between 9 and 15 min for the $\ell = 2$ mode, and between 5 and 11 min for the $\ell = 3$ mode.



tions were used (22). The correlation of the reconstructed waves of these sets of models with that of the real GOLF data—in the region between 2 and 8.5 hours—always gave a correlation above 20%, with the highest values around 50%. The correlations with the Monte Carlo simulations were usually below 1%. Only 905 of the $N = 6 \times 10^5$ realizations reached 20% correlation, and only 43 of these realizations reached 50% correlation. Thus, the likelihood that this kind of periodic structure in the GOLF data is not produced by noise is at least 99.85% and can reach 99.99% in the best case (up to 4σ level of a normal distribution).

The set of parameters that characterizes the physics and dynamics inside the solar core is too large to be totally constrained by this first analysis. However, from all the sets of g-mode predictions used, we obtained better correlations with those having an inner rotation rate in the range three to five times the rest of the radiative region, this being independent of the inclination axis and the radius of the core used (better results

at $0.15R_{\odot}$). The correlation is higher with the model with a higher rotation rate in the core (Fig. 4). Unfortunately, the solar rotation profiles used in the simulations of the core are unrealistic (i.e., a constant rotation rate without differential rotation). On the other hand, the comparison with simulations including noise (fig. S10) tends to favor the hypothesis of a finite lifetime for the g modes, as recently suggested (26). In both cases, further studies will be necessary.

The analysis presented here shows the robust detection of a spectral feature compatible with the presence of a periodic pattern in the PSD with a confidence level above 99.49% (corresponding to more than 3σ of a normal distribution). The accurate study of this quasi-periodic pattern found in the GOLF data is compatible with the presence of gravity dipole modes with radial orders from $n = -4$ to -26 , with a confidence level above 99.85%. A detailed comparison with solar models tends to favor a faster core rotation than in the rest of the radiative zone, with a confidence level

Fig. 3. Power spectrum of the PSD, normalized to the standard deviation, for the real GOLF data (top) and a numerical simulation (bottom) of $\ell = 1, 2$, and 3 gravity modes computed using the seismic model, for a core rotating at 433 nHz and without noise. The shaded region corresponds to the zone where the ΔP_1 peak is expected. This pattern changes slightly (with maxima at $\sim 7.3\sigma$ or 6σ) when shorter frequency ranges in the PSD are used (fig. S2). The horizontal dashed line at 5.81σ corresponds to 99.7% confidence level for individual peaks (equivalent to 3σ level of a normal distribution). A full interpretation of the other highest peaks at low period is given in (22).

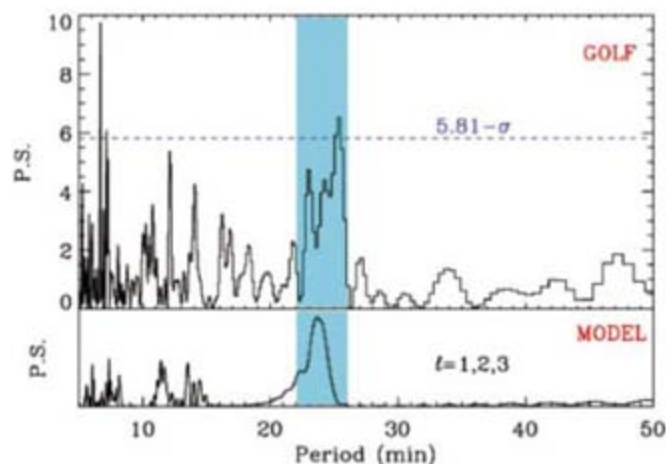
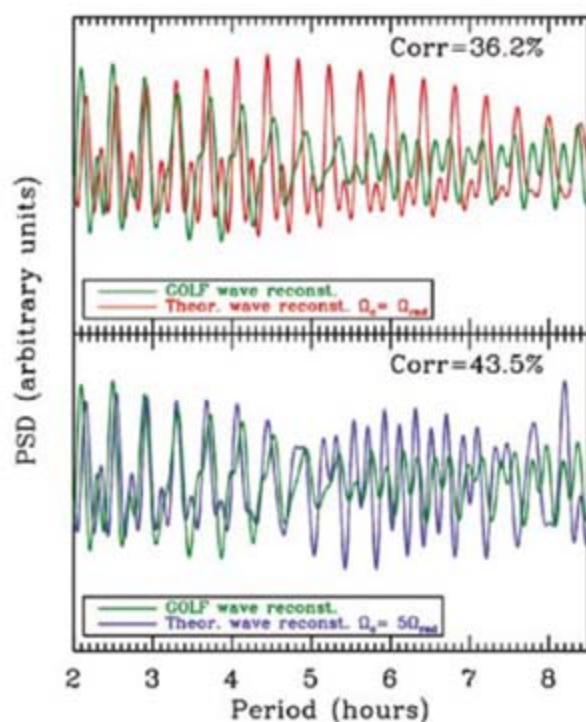


Fig. 4. Reconstructed waves in the PSD (arbitrary units) corresponding to the peak structure between 22 and 26 min in the power spectrum for the GOLF data. (Top) Comparing the theoretical reconstructed waves (red curve) with the one issued from GOLF (green curves), we first observe that the maxima match rather well the expected positions of the g modes at low periods. Moreover, the latter is wider and for periods greater than 4 hours it is divided into two waves, which suggests the presence of both m components of the $\ell = 1$ modes (higher splitting). The correlation between both reconstructed waves is 36.2%. (Bottom) The higher correlation, 43.5%, between the second model (a core rotating 5 times as fast as the radiative zone below $R_c = 0.15R_{\odot}$) and GOLF tends to favor a faster rotation rate in the core than in the rest of the radiative zone. As a comparison, the correlation with randomized data is below 1% (fig. S8).



above 99.99%. The detection of g-mode asymptotic properties opens the opportunity for further studies of the rotation and the magnetic field inside the deepest layers of the Sun and can stimulate further observational studies with SOHO, ground-based networks, and next-generation space missions such as Picard (27) and DynaMICS (28).

References and Notes

1. J. Christensen-Dalsgaard, *Rev. Mod. Phys.* **74**, 1073 (2002).
2. The oscillation modes are characterized by three quantum numbers: the radial order n , the angular degree ℓ , and the azimuthal order m ($-\ell \leq m \leq \ell$).
3. D. O. Gough *et al.*, *Science* **272**, 1296 (1996).
4. J. Christensen-Dalsgaard, D. O. Gough, J. Toomre, *Science* **229**, 923 (1985).
5. S. V. Vorontsov, V. A. Baturin, A. A. Pamiatnykh, *Nature* **349**, 49 (1991).
6. S. Basu *et al.*, *Mon. Not. R. Astron. Soc.* **292**, 243 (1997).
7. S. Turck-Chièze *et al.*, *Astrophys. J.* **555**, L69 (2001).
8. M. J. Thompson *et al.*, *Science* **272**, 1300 (1996).
9. M. J. Thompson, J. Christensen-Dalsgaard, M. S. Miesch, J. Toomre, *Annu. Rev. Astron. Astrophys.* **41**, 599 (2003).
10. P. Kumar, E. J. Quartaert, J. N. Bahcall, *Astrophys. J.* **458**, L83 (1996).
11. H. Hill, C. Fröhlich, M. Gabriel, V. Kotov, in *Solar Interior and Atmosphere*, A. N. Cox, W. C. Livingston, M. S. Matthews, Eds. (Univ. of Arizona Press, Tucson, AZ, 1991), p. 562.
12. T. Appourchaux *et al.*, *Astrophys. J.* **538**, 401 (2000).
13. A. H. Gabriel *et al.*, *Astron. Astrophys.* **390**, 1119 (2002).
14. W. J. Chaplin *et al.*, *Mon. Not. R. Astron. Soc.* **336**, 979 (2002).
15. S. Turck-Chièze *et al.*, *Astrophys. J.* **604**, 455 (2004).
16. S. Turck-Chièze *et al.*, in *Helio- and Astroseismology: Towards a Golden Future*, D. Danesy, Ed. (European Space Agency, Noordwijk, Netherlands, 2004), pp. 85–90.
17. S. Mathur, S. Turck-Chièze, S. Couvidat, R. A. García, in *Beyond the Spherical Sun: A New Era of Helio- and Astroseismology*, K. Fletcher, Ed. (European Space Agency, Noordwijk, Netherlands, 2006), pp. 95–98.
18. J. Provost, G. Berthomieu, *Astron. Astrophys.* **165**, 218 (1986).
19. A. H. Gabriel *et al.*, *Sol. Phys.* **162**, 61 (1995).
20. R. A. García *et al.*, *Astron. Astrophys.* **442**, 385 (2005).
21. S. Turck-Chièze *et al.*, *Solar Phys.* **175**, 247 (1997).
22. See supporting material on Science Online.
23. S. Couvidat, S. Turck-Chièze, A. G. Kosovichev, *Astrophys. J.* **599**, 1434 (2003).
24. J. Christensen-Dalsgaard *et al.*, *Science* **272**, 1286 (1996).
25. J. Provost, G. Berthomieu, P. Morel, *Astron. Astrophys.* **353**, 775 (2000).
26. B. Dintrans, A. Brandenburg, A. Nordlund, R. F. Stein, *Astron. Astrophys.* **438**, 365 (2005).
27. G. Thuillier, S. Dewitte, W. Schmutz, *Adv. Space Res.* **38**, 1792 (1991).
28. S. Turck-Chièze *et al.*, in *Trends in Space Science and Cosmic Vision 2020*, F. Favata, J. Sanz-Forcada, A. Giménez, B. Battrock, Eds. (European Space Agency, Noordwijk, Netherlands, 2005), pp. 193–203.
29. R. A. García *et al.*, *Sol. Phys.* **220**, 269 (2004).
30. S. G. Korzenik, *Astrophys. J.* **626**, 585 (2005).
31. The GOLF experiment is based on a consortium of institutes (Institut d'Astrophysique Spatiale, CEA/Saclay, Nice, and Bordeaux Observatories, France; IAC, Spain) involving a large number of scientists and engineers, as enumerated in (19). SOHO is a mission of international cooperation between ESA and NASA. This work is supported in part by Spanish MEC grant AYA2004-04462. We thank T. Appourchaux, W. J. Chaplin, and all the PHOEBUS group (12) for useful discussions and comments.

Supporting Online Material

www.sciencemag.org/cgi/content/full/1140598/DC1

Materials and Methods

Figs. S1 to S10

References

30 January 2007; accepted 19 April 2007

Published online 3 May 2007;

10.1126/science.1140598

Include this information when citing this paper.

Tuning the Quantum Stability and Superconductivity of Ultrathin Metal Alloys

Mustafa M. Özer,^{1*} Yu Jia,² Zhenyu Zhang,^{3,1} James R. Thompson,^{1,3} Hanno H. Weiering^{1,3,†}

Quantum confinement of itinerant electrons in atomically smooth ultrathin lead films produces strong oscillations in the thickness-dependent film energy. By adding extra electrons via bismuth alloying, we showed that both the structural stability and the superconducting properties of such films can be tuned. The phase boundary (upper critical field) between the superconducting vortex state and the normal state indicates an anomalous suppression of superconducting order just below the critical temperature, T_c . This suppression varies systematically with the film thickness and the bismuth content and can be parametrized in terms of a characteristic temperature, T_c^* (less than T_c), that is inversely proportional to the scattering mean free path. The results indicate that the isotropic nature of the superconductive pairing in bulk lead-bismuth alloys is altered in the quantum regime.

A variety of fundamentally important condensed matter phenomena has been discovered through “quantum engineering,” whereby new low-dimensional materials can be realized via control of the quantum mechanical boundary conditions. Examples include quantum Hall effects in semiconductor heterostructures (1) and giant magnetoresistance in magnetic superlattices (2). In these cases, the fabrication of the systems was achieved by classical growth methods, such as molecular beam epitaxy, yet the resulting systems exhibited collective quantum mechanical properties under proper conditions. More recently, it has been demonstrated that the quantization of kinetic energy of itinerant electrons within low-dimensional metal systems can be important even in the formation stages of the systems themselves, as manifested by the quantum stability of metallic thin films and nanostructures (3–9). Creation of such quantum structures via electronic growth offers unprecedented opportunities to explore various physical and chemical properties in the quantum regime (10–14).

For electronic growth, lead has served as an archetype system, partly because it is a soft metal, making electronic effects more pronounced than strain effects, and partly because the Fermi wavelength, λ_F , is nearly commensurate with the interatomic layer spacing, d , along the $\langle 111 \rangle$ direction, with $2.07d \cong 3\lambda_F/2$ (6). This near-commensurability between the electronic and crystallographic length scales leads to a reentrant bilayer-by-bilayer growth mode, characterized by stable growth of double atomic layers with

periodic interruptions of even-odd switching (6–8). Remarkably, the quantum stability of the lead films, derived from single or nearly free electron pictures, can also influence the collective properties of the electrons in the strongly correlated regime, such as the superconducting properties of the systems (12–15). In particular, it was shown that the superconducting transition temperature of ultrathin Pb(111) films oscillates as a function of the film thickness because of the quantum size effect (12, 13), suggesting the possibility that the supercurrents are supported by a set of weakly coupled two-dimensional (2D) quantum channels. Generally, quantum size effects should be observable only if the quantum-level spacing is substantially larger than the level broadening \hbar/τ due to carrier scattering (τ being the scattering lifetime of the

electrons) (16). This stringent requirement may be met via electronic growth of specularly smooth ultrathin films (14, 15).

We show that the quantum stability and the superconducting properties of ultrathin lead films can be tuned by adjusting the Fermi wavelength of the two-dimensional (2D) electron systems via controlled bismuth doping. For values of x from 0 to 20% Bi, the $\text{Pb}_{1-x}\text{Bi}_x$ phase diagram (17) constitutes a solid solution with face-centered-cubic structure and a constant lattice parameter, 4.95 Å, equal to that of bulk Pb. A competing hexagonal ϵ phase above 20% Bi tentatively sets the upper concentration limit of the alloying experiment. PbBi alloy films were deposited onto atomically clean Si(111) 7×7 surfaces in ultrahigh vacuum. Codeposition at ~ 120 K, followed by postannealing at 200 to 300 K, produced atomically flat single-crystalline alloy films as observed by scanning tunneling microscopy (STM) and low-energy electron diffraction. No segregation of Bi was evident from x-ray photoelectron spectroscopy.

A series of STM images for the $\text{Pb}_{89}\text{Bi}_{11}$ alloys of different thicknesses shows that, similar to the case of pure Pb, the alloy films exhibit a reentrant bilayer-by-bilayer growth mode (8) but with different quantum beating patterns (Fig. 1). The observed stable thickness sequence is 4-6*7-9-11-13-15-17-19*20...ML, where the asterisks indicate the locations of the even-odd crossover [throughout this paper, the thickness counts exclude the one-monolayer (ML)-thick wetting layer (8)]. At the higher concentration of $\text{Pb}_{80}\text{Bi}_{20}$, the alloys do not exhibit quantum growth but simply follow classical layer-by-layer growth throughout the entire thickness range, demonstrating that quantum coherence is suppressed by sufficiently strong disorder scattering.

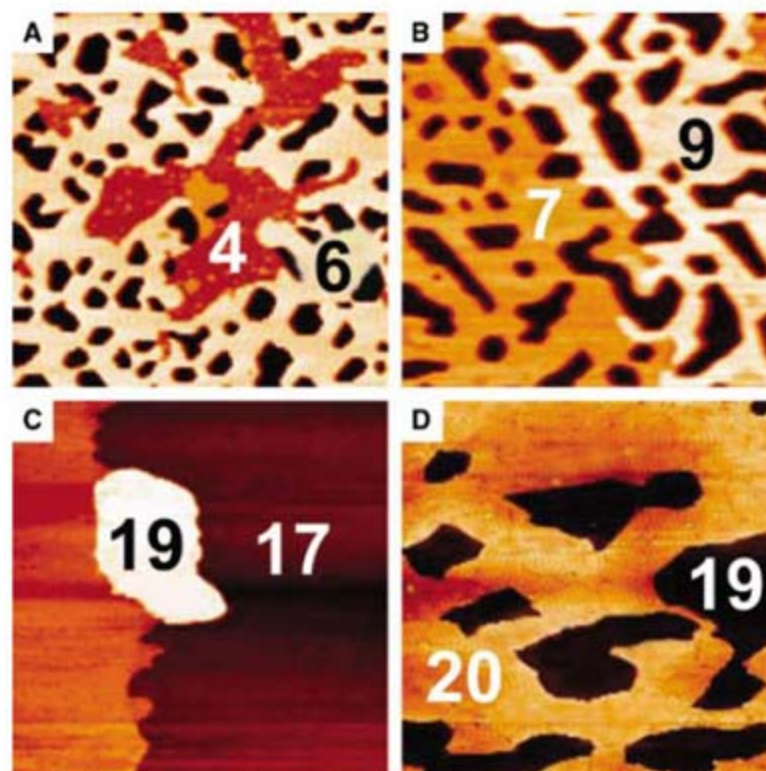


Fig. 1. STM images revealing the quantum growth mode of $\text{Pb}_{89}\text{Bi}_{11}$ alloy films, with bilayer growth (A) for 4- and 6-ML thicknesses and (B) for 7- and 9-ML thicknesses. The black pores in these high-resolution images are uncoated regions extending down to the wetting layer. Films used for superconductive studies were atomically smooth and completely covered the substrate, as verified at lower resolution. (C) Bilayer growth in a thicker film (also with a 1-ML terrace from the substrate). (D) Single-layer growth near a 19-20 odd-even crossover thickness. All image sizes are ~ 400 nm \times 400 nm.

¹Department of Physics and Astronomy, University of Tennessee, Knoxville, TN 37996, USA. ²School of Physics and Engineering, Zhengzhou University, Zhengzhou, Henan, 450052, China. ³Materials Science and Technology Division, Oak Ridge National Laboratory, Oak Ridge, TN 37831, USA.

*Present address: Department of Physics, University of Texas, Austin, TX 78712, USA.

†To whom correspondence should be addressed. E-mail: hanno@utk.edu

To understand how Bi doping affects the quantum stability of PbBi alloy films, we performed first-principles calculations of their energetics within density functional theory (DFT). Calculations utilized the Vienna Ab Initio Simulation Package code with ultrasoft pseudopotentials, plane wave basis sets (18, 19), and the generalized-gradient-approximation to describe exchange-correlation effects (20). The calculated surface energy for freestanding $\text{Pb}_{89}\text{Bi}_{11}$ alloy films versus thickness is shown in Fig. 2A. For $x = 11\%$ Bi and (111) growth orientation, we adopted a 3×3 supercell where one out of nine Pb atoms in each layer is replaced by a Bi atom. The two curves represent extreme

cases in the layer-to-layer Bi distribution: The black curve represents the surface energy of a $\text{Pb}_{89}\text{Bi}_{11}$ slab where the (111) layers are stacked to maximize the average Bi-Bi distance; the red curve corresponds to (111) stacking to minimize it. Importantly, these extreme cases have the same beating periodicity of 13 ML and the even-odd crossover occurs near the same location of 12 ML, showing that the precise spatial correlations of Bi dopants have only a marginal effect on the quantum stability of the alloys.

As further refinement, we considered the effect of the substrate, which shifts the phases of the electronic states and changes the precise location of the even-odd crossovers (9). Excel-

lent matching between the substrate and film lattices was accomplished by rotating the 3×3 $\text{Pb}_{89}\text{Bi}_{11}$ (111) unit cell over 19.1° and matching it onto a slightly expanded (by 2.7%) $\sqrt{7} \times \sqrt{7}$ substrate (effectively introducing an additive but constant strain energy in the substrate). The surface energy and its second derivative (inset) as a function of film thickness for $\text{Pb}_{89}\text{Bi}_{11}$ slabs on Si(111) are shown in Fig. 2B. The location of the first even-odd crossover has shifted to 6 ML, in precise quantitative agreement with the experiment. We also investigated quantum oscillations in the alloy energetics for higher Bi contents, namely $\text{Pb}_{0.86}\text{Bi}_{0.14}$ (with $\sqrt{7} \times \sqrt{7}$ supercells) and $\text{Pb}_{0.75}\text{Bi}_{0.25}$ (with 2×2

Fig. 2. (A) Calculated surface energy of a $\text{Pb}_{89}\text{Bi}_{11}$ free-standing alloy slab. The black curve (circles) and red curve (squares) represent the surface energy for maximum and minimum Bi-Bi separation in the film growth direction, respectively. (B) Surface energy of a $\text{Pb}_{89}\text{Bi}_{11}$ alloy on a Si(111) substrate; (inset) its second derivative versus film thickness.

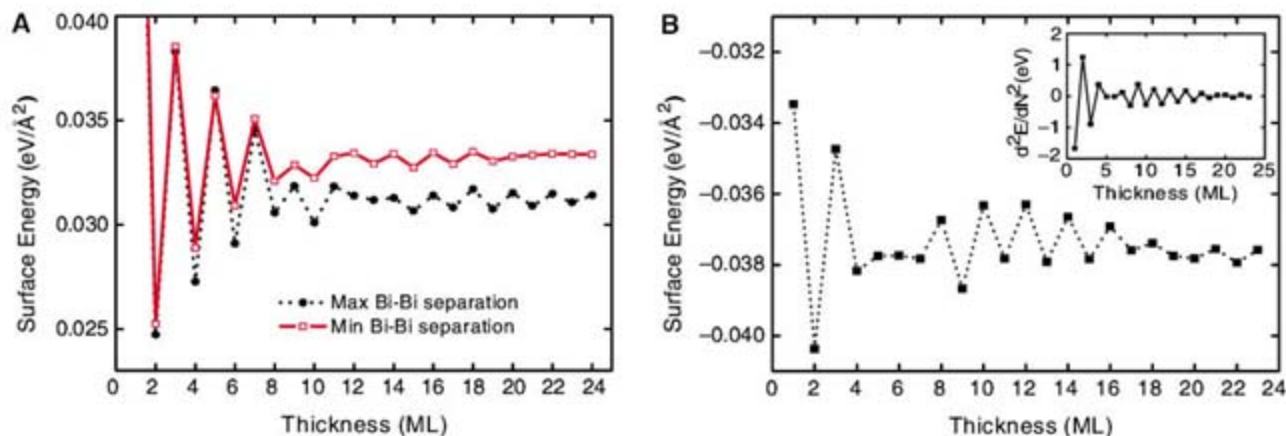


Fig. 3. Characteristic temperatures T_c and T_c^* versus $1/d$, the inverse film thickness: (A) for pure Pb, (B) for $\text{Pb}_{89}\text{Bi}_{11}$, and (C) for $\text{Pb}_{80}\text{Bi}_{20}$ quantum alloys. The T_c^* values were obtained by extrapolating the linear part of the upper critical field $H_{c2}(T)$ to zero dc field, as illustrated in Fig. 4. (D) The normalized offset $(T_{c0} - T_c^*)/T_{c0}$ as a function of the inverse mfp . Error bars indicate an estimated uncertainty of 3 standard deviations, due mostly to uncertainty in determining T_c^* .

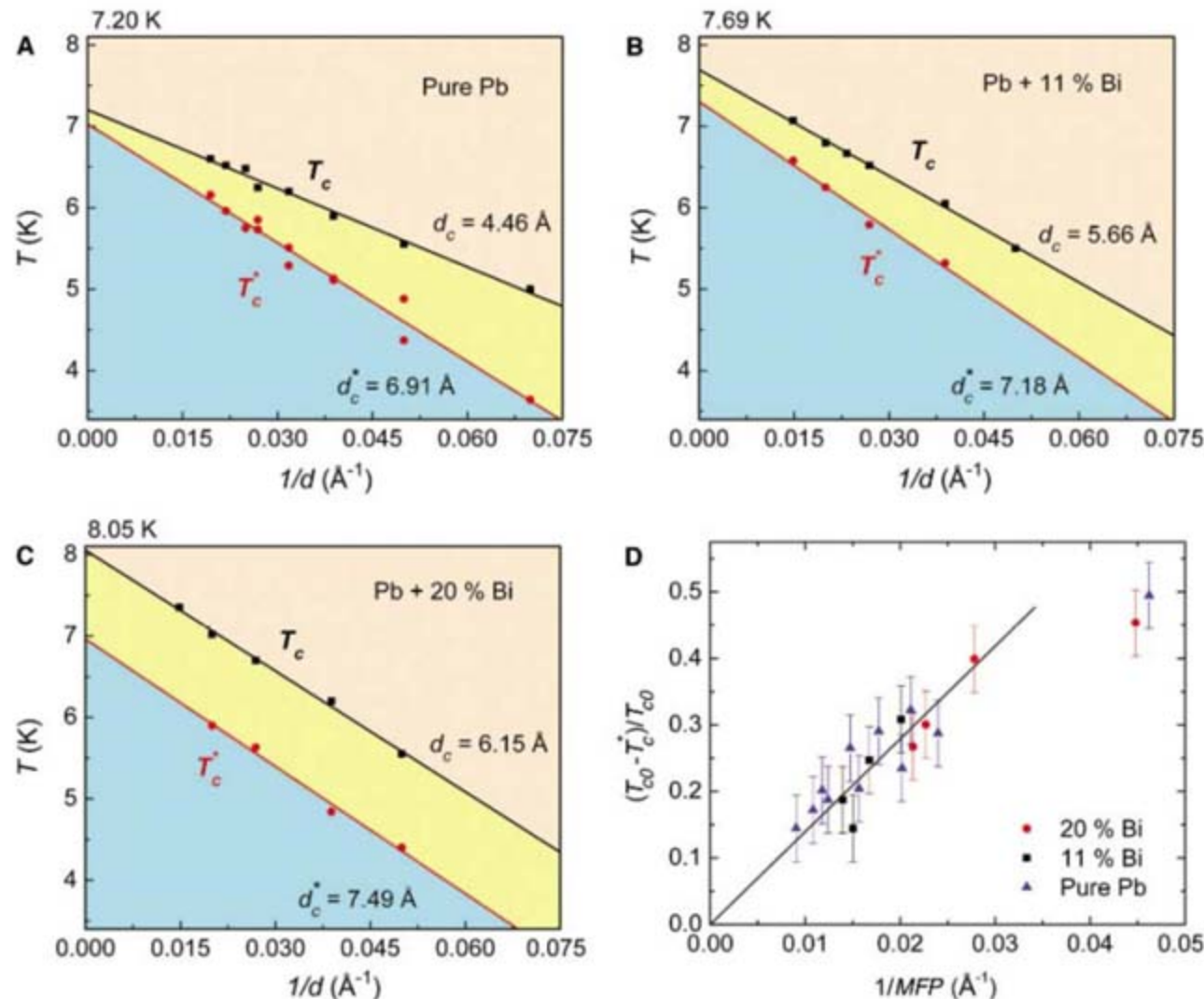
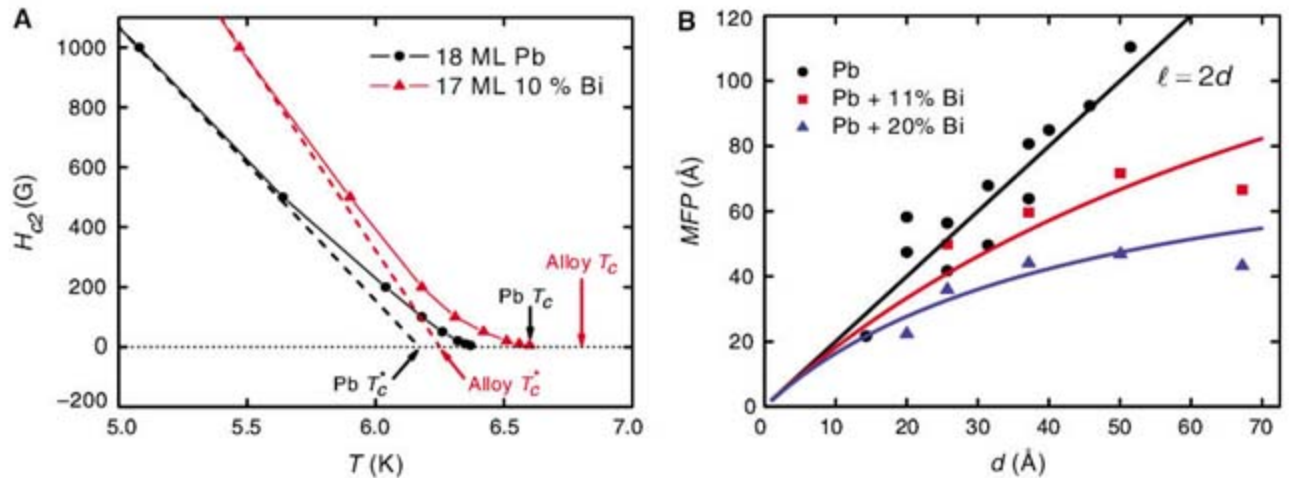


Fig. 4. (A) Temperature dependence of the upper critical field for pure Pb and 11% Bi alloy films of similar thicknesses, showing a more pronounced curvature for the alloy. The dashed lines defining T_c^* are extrapolations from the linear Ginzburg-Landau regime. **(B)** Electronic mean free path for pure Pb and Pb-Bi alloy films. The solid lines are a Matthiessen-rule modeling of combined boundary and impurity scattering.



supercells). The artificial rotation of the $\text{Pb}_{89}\text{Bi}_{11}$ (111) layers and the constant strain energy in the substrate do not alter the accuracy of the thickness-dependent stability (9, 21). The main conclusions are that the beating periodicity increases with increasing Bi content (i.e., to 15 ML and 17 ML, respectively), and that the magnitudes of the quantum oscillations become weaker. The latter finding is consistent with the observed absence of bilayer growth in the $\text{Pb}_{0.8}\text{Bi}_{0.2}$ alloy films, where classical layer-by-layer growth is found.

Having demonstrated experimentally and theoretically that electronic quantum confinement is a compelling enabler for synthesizing ultrathin metal alloy films with tunable composition, we then focused on their superconductive properties. In particular, the superconducting transition temperature, T_c , was determined inductively, with a superconducting quantum interfering device magnetometer (14), from the onset of the ac diamagnetic moment $m(T) = m' + im''$ induced by a 10-mOe ac field. The results are plotted versus the inverse film thickness, d (Fig. 3, A to C). As observed for pure Pb films (14, 15), we have $T_c(d) = T_{c0}(1 - d_c/d)$, where T_{c0} is the critical temperature of the corresponding bulk alloy and d_c is the extrapolated thickness threshold for the emergence of superconductivity. Such a linear variation with the inverse film thickness has usually been interpreted as a boundary effect, arising from the inclusion of a surface-energy term in the Ginzburg-Landau equations for the superconductive free energy (22). Extrapolation to infinite thickness ($1/d \rightarrow 0$) yields excellent agreement with the bulk T_{c0} values of 7.20, 7.69, and 8.05 K for Pb, $\text{Pb}_{89}\text{Bi}_{11}$, and $\text{Pb}_{80}\text{Bi}_{20}$ alloys, respectively (23).

Bulk Pb is a type I s-wave superconductor for which films with thicknesses below ~ 250 nm become type II, thereby possessing a mixed (or "vortex") state below an upper critical magnetic field, $H_{c2}(T)$ (24). We determined $H_{c2}(T)$ from the onset of the ac magnetic moment in the presence of a colinear dc field applied normal to the films. For a given film thickness and temperature, H_{c2} increases with increasing Bi concentration (Fig. 4A). According to the Ginzburg-Landau

formula (25), $H_{c2}(T) = \Phi_0/2\pi\xi_{\text{GL}}^2(T)$ ($\Phi_0 = h/2e = 2.07 \times 10^{-7}$ G cm² being the flux quantum), the observed elevation of H_{c2} indicates a reduced coherence length, ξ_{GL} , from the value for pure Pb, due to alloy scattering. The carrier mean free path (mfp), $l(d)$, is obtained from the Ginzburg-Landau relation $\xi_{\text{GL}}(d) = 0.739[\xi_0^{-2} + 0.882(\xi_0/l)^{-1}]^{-1/2}(1 - T/T_c)^{-1/2}$ (25), where $\xi_0 = 905$ Å is the Bardeen-Cooper-Schrieffer (BCS) coherence length of bulk Pb. Its value was renormalized for the alloy films to account for their higher T_{c0} .

For pure Pb films, l_{pb} varies linearly with the thickness, indicative of boundary scattering. In contrast, the mfp for each of the alloys appears to saturate, due to alloy scattering (Fig. 4B). The total mfp $l(d)$ can be fitted by using Matthiessen's rule, $l^{-1}(d) = l_{\text{pb}}^{-1} + l_{\text{imp}}^{-1}$, where $l_{\text{pb}} = 2d$ is the mfp due to boundary scattering and l_{imp} is the mfp due to impurity scattering. This yields l_{imp} values of 200 Å and 90 Å for the 11% and 20% alloys, respectively, in good agreement with mfp estimates obtained from the $\rho \times l$ product of the corresponding bulk alloys (23, 26).

In earlier studies for pure Pb films (14, 15), $H_{c2}(T)$ was observed to markedly flatten near T_c , resulting in a characteristic "hockey stick" profile that is particularly noticeable for the thinner films (Fig. 4A). The origin of the hockey stick shape can now be explored as it becomes systematically more pronounced with increasing doping concentration. The strong curvature near T_c marks a profound departure from anisotropic Ginzburg-Landau theory, which predicts that $H_{c2} \propto (1 - T/T_c)$ (25). The upper critical field resumes Ginzburg-Landau-like behavior below a characteristic temperature, T_c^* , as defined by extrapolating the linear part of the low-temperature H_{c2} curve to zero field (Fig. 4A). The resulting T_c^* values of the alloy films are included in Fig. 3.

Both T_c and T_c^* are found to vary systematically with the inverse nanoscale dimension $1/d$. Also, for a given thickness d , the separation between T_c and T_c^* increases with Bi content, caused largely by the expected T_c increase with Bi concentration (23); in contrast, T_c^* is only marginally affected. Interestingly, T_c^* does not extrapolate to the T_{c0} value of the corresponding

bulk alloy. The latter finding indicates that the thickness of the quantum alloys is only an indirect parameter in controlling T_c^* . A quantity better describing of this behavior is the scattering mfp , as demonstrated by plotting the normalized offset $(T_{c0} - T_c^*)/T_{c0}$ as a function of the inverse mfp in Fig. 3D. All the data for clean Pb and for the 11% and 20% PbBi alloys collapse onto a straight line passing through the origin, whereas no such collapse is possible when plotting this quantity as a function of $1/d$ (27). This strongly indicates that mfp is a key parameter determining T_c^* .

Similar crossover phenomena in the temperature dependence of the upper critical field of metallic thin films and superlattices have been attributed to compositional fluctuations, in conjunction with the appropriate boundary condition for the superconducting wave function or order parameter (28). This interpretation conflicts with our experimental observation of a T_c^* in pure Pb films; it is also questionable theoretically for the present case of ultrathin films on a nonmetallic substrate (28). Superconductivity between T_c and T_c^* is weak and suppressed by scattering, in apparent violation of Anderson's theorem for uniform order parameters, which states that T_c and the condensation energy should not be affected by potential scattering (25). Our observations indicate that the nature of the microscopic pairing in these conventional superconductors is altered in the confined geometry. The tunability of the electronic, structural, and superconducting properties of ultrathin metal alloys thus offers new possibilities for fundamental studies of these features in the quantum regime.

References and Notes

1. D. C. Tsui, H. L. Stormer, A. C. Gossard, *Phys. Rev. Lett.* **48**, 1559 (1982).
2. M. N. Baibich *et al.*, *Phys. Rev. Lett.* **61**, 2472 (1988).
3. A. R. Smith, K.-J. Chao, Q. Niu, C.-K. Shih, *Science* **273**, 226 (1996).
4. Z. Y. Zhang, Q. Niu, C.-K. Shih, *Phys. Rev. Lett.* **80**, 5381 (1998).
5. V. Yeh, L. Berbil-Bautista, C. Z. Wang, K. M. Ho, M. C. Tringides, *Phys. Rev. Lett.* **85**, 5158 (2000).
6. C. M. Wei, M. Y. Chou, *Phys. Rev. B* **66**, 233408 (2002).
7. M. H. Upton, C. M. Wei, M. Y. Chou, T. Miller, T.-C. Chiang, *Phys. Rev. Lett.* **93**, 026802 (2004).

8. M. M. Özer, Y. Jia, B. Wu, Z. Y. Zhang, H. H. Weiering, *Phys. Rev. B* **72**, 113409 (2005).
9. Y. Jia, B. Wu, H. H. Weiering, Z. Y. Zhang, *Phys. Rev. B* **74**, 035433 (2006).
10. L. Aballe, A. Barinov, A. Locatelli, S. Heun, M. Kiskinova, *Phys. Rev. Lett.* **93**, 196103 (2004).
11. A. G. Danese, F. G. Curti, R. A. Bartynski, *Phys. Rev. B* **70**, 165420 (2004).
12. Y. Guo *et al.*, *Science* **306**, 1915 (2004).
13. D. Eom, S. Qin, M. Y. Chou, C. K. Shih, *Phys. Rev. Lett.* **96**, 027005 (2006).
14. M. M. Özer, J. R. Thompson, H. H. Weiering, *Nat. Phys.* **2**, 173 (2006).
15. M. M. Özer, J. R. Thompson, H. H. Weiering, *Phys. Rev. B* **74**, 235427 (2006).
16. N. Trivedi, N. W. Ashcroft, *Phys. Rev. B* **38**, 12298 (1988).
17. R. Hultgren, P. D. Desai, D. T. Hawkins, M. Gleiser, K. K. Kelley, *Selected Values of the Thermodynamic Properties of Binary Alloys* (American Society for Metals, Metals Park, OH, 1973).
18. G. Kresse, J. Hafner, *Phys. Rev. B* **47**, 558 (1993).
19. G. Kresse, J. Furthmüller, *Comput. Mater. Sci.* **6**, 15 (1996); and references therein.
20. J. P. Perdew, Y. Wang, *Phys. Rev. B* **45**, 13244 (1992).
21. Z. G. Suo, Z. Y. Zhang, *Phys. Rev. B* **45**, 13244 (1998).
22. J. Simonin, *Phys. Rev. B* **33**, 7830 (1986).
23. R. C. Dynes, J. M. Rowell, *Phys. Rev. B* **11**, 1884 (1975).
24. G. J. Dolan, J. Silcox, *Phys. Rev. Lett.* **30**, 603 (1973).
25. M. Tinkham, *Introduction to Superconductivity* (Dover, Mineola, NY, 1996).
26. Klaus Schröder, *CRC Handbook of Electrical Resistivities of Binary Metallic Alloys*, (CRC, Boca Raton FL, 1983). The room temperature resistivity ρ of $Pb_{1-x}Bi_x$ alloys increases linearly, 1.0 microhm cm/atomic % Bi for $x < -0.2$. Assuming the phonon contribution does not change, the resistivity due to impurity scattering is 11 microhm cm for the 11% alloy, etc.
27. The only data points falling significantly below the straight line are for the 5-ML films, for which $H_{c2}(T)$ increases faster than linearly below T_c^* .
28. V. M. Gvozdkov, *Low Temp. Phys.* **25**, 936 (1999).
29. This work was funded by NSF under contracts DMR-0244570 (M.M.O. and H.H.W.) and DMR-0606485 (Z.Z.); by the Division of Materials Sciences and Engineering (H.H.W., J.R.T., and Z.Z.), Office of Basic Energy Sciences, U.S. Department of Energy under contract DE-AC05-00OR22725 with Oak Ridge National Laboratory, managed by UT-Battelle, Limited Liability Corporation; and by National Science Foundation of China (Y.J.); grant no. 10574113).

6 March 2007; accepted 3 May 2007
10.1126/science.1142159

Metal Chlorides in Ionic Liquid Solvents Convert Sugars to 5-Hydroxymethylfurfural

Haibo Zhao, Johnathan E. Holladay, Heather Brown, Z. Conrad Zhang*

Replacing petroleum feedstocks by biomass requires efficient methods to convert carbohydrates to a variety of chemical compounds. We report the catalytic conversion of sugars giving high yield to 5-hydroxymethylfurfural (HMF), a versatile intermediate. Metal halides in 1-alkyl-3-methylimidazolium chloride are catalysts, among which chromium (II) chloride is found to be uniquely effective, leading to the conversion of glucose to HMF with a yield near 70%. A wide range of metal halides is found to catalyze the conversion of fructose to HMF. Only a negligible amount of levulinic acid is formed in these reactions.

A sustainable future for the chemical industry requires feedstocks based on renewable rather than steadily depleting sources. Inability to effectively transform five- and six-carbon carbohydrate building blocks derived from nature is a major barrier toward this challenging goal. Glucose and fructose, two abundant six-carbon sugar molecules, are potential feedstocks for this purpose, and recent

efforts have focused on converting them to 5-hydroxymethylfurfural (HMF) (1), a versatile intermediate between biomass-based carbohydrate chemistry and petroleum-based industrial organic chemistry (2). HMF and its derivatives could potentially replace voluminously consumed petroleum-based building blocks (3), which are currently used to make plastics and fine chemicals. Recently, Dumesic and co-workers introduced the idea of using HMF as a key intermediate to produce liquid alkanes from renewable biomass resources (4). High production cost currently limits the availability and use of HMF industrially.

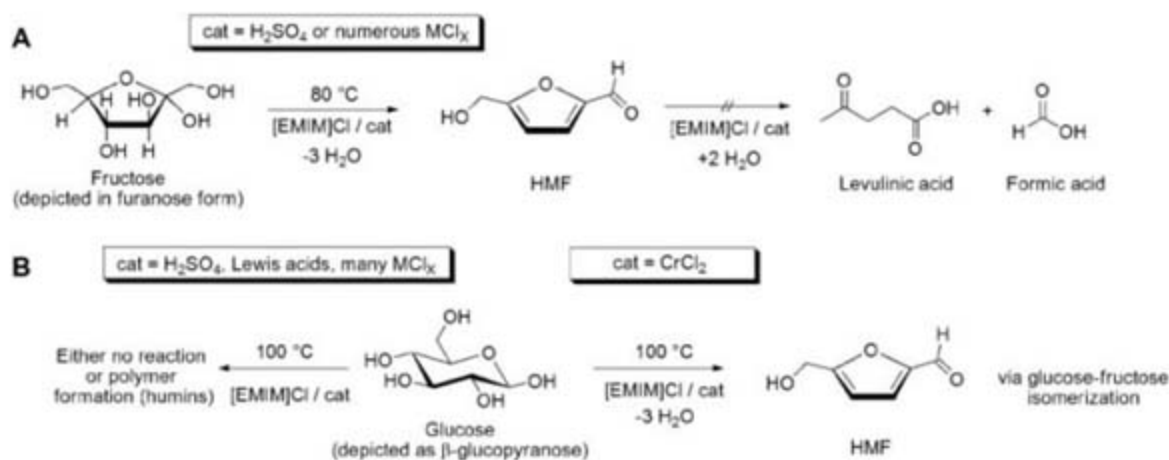
A process to produce pure HMF from abundant renewable carbohydrates in high yield at low energy cost must be developed before a biorefinery platform can be built on the basis of this substrate. Current processes to produce HMF involve the use of acid catalysts and are mainly limited to fructose as feed (5–7). A drawback with acid catalysts is that they cause various side reactions, significantly increasing the cost of product purification. For example, in water under acidic conditions, HMF decomposes to levulinic acid and formic acid. Levulinic acid is particularly difficult to separate from HMF. Substituting glucose as a feed substantially reduces HMF yields and produces additional by-products (8, 9).

A study by Antal and co-workers suggested that HMF is formed from dehydration of fructose in its furanose form (10) and occurs through a series of cyclic furan intermediates (11). Others have suggested HMF is formed through an acyclic mechanism proceeding through an enediol pathway (11–14). The enediol is proposed as an intermediate in the isomerization of glucose to fructose. Glucose has competing reaction pathways that lead to formation of by-products. In one pathway, dehydration forms nonfuran cyclic ethers; in another, C-C bond scission occurs through reverse aldol condensation (14). To obtain high HMF yields from glucose thus requires effective methods for selective in situ isomerization to fructose.

Institute for Interfacial Catalysis, Pacific Northwest National Laboratory, Post Office Box 999, Richland, WA 99352, USA.

*To whom correspondence should be addressed. E-mail: conrad.zhang@pnl.gov

Fig. 1. (A) Fructose conversion to HMF at 80°C for 3 hours. Catalytic amounts of H_2SO_4 or various metal halides promote the chemistry. Very little levulinic acid is formed. (B) Glucose conversion to HMF at 100°C for 3 hours. $CrCl_2$ resulted in a 70% yield of HMF, whereas other catalysts such as H_2SO_4 , Lewis acids, or other metal halides gave yields less than 10%.



HMF yield has been shown to increase significantly in systems that partition HMF from H₂O. Dumesic and co-workers, building on the work of several earlier researchers, demonstrated high yields from fructose by using strong polar organic solvents, such as dimethylsulfoxide (DMSO), in aqueous-organic reaction media (7). Other solvent systems have also shown promising results. HMF can be formed in high yields from fructose in 1-H-3-methylimidazolium chloride solvent, which also acts as an acidic catalyst (15, 16). In sugar-solubilizing 1-alkyl-3-methylimidazolium chloride solvents, water is not needed as part of the solvent system, and the actual amount of H₂O present is reduced to the water formed during dehydration. By minimizing HMF exposure to acidic aqueous solutions at elevated temperatures, HMF yield loss to levulinic acid is kept very low.

In our own work, we have built upon this concept by using sugar-solubilizing high-purity 1-alkyl-3-methylimidazolium chloride, [AMIM]Cl, as a solvent class. Our method is distinguished from previous reports in that we observe high yields of HMF from fructose without added acid. Even more importantly, one of these solvent-catalyst systems is able to produce HMF in high yields from glucose, the first step in our ultimate goal of developing a system to generate HMF from complex biomass such as cellulose.

We tested the reactivity of fructose in three [AMIM]Cl solvents, where A represents octyl, butyl, or ethyl (17). Because [EMIM]Cl (E is ethyl) was equivalent or better than the other two solvents, we report results in this system (Fig. 1). Figure 2 shows the results of simply heating fructose and glucose in high-purity (99.5%) [EMIM]Cl (18). At sufficiently high-temperatures, fructose was converted to HMF, but the yield dropped substantially between 120° and 80°C. In contrast, glucose did not produce any substantial amount of HMF even at 180°C. When water was added to the solvent ([EMIM]Cl:H₂O = 5:1), glucose was effectively inert.

We were able to catalyze the dehydration of fructose at 80°C by addition of a catalytic amount of a number of metal halides (Fig. 1A). For example, HMF yields ranging from 63 to 83% were achieved in 3 hours when using 6 mole percent (mol %) loading (based on sugar) of CrCl₂, CrCl₃, FeCl₂, FeCl₃, CuCl, CuCl₂, VCl₃, MoCl₃, PdCl₂, PtCl₂, PtCl₄, RuCl₃, or RhCl₃ (fig. S1). The product mixtures were very clean: Yields of levulinic acid and α -angelicalactone were less than 0.08%. Not all metal halides were effective; for example, the alkali chlorides, LaCl₃ and MnCl₂, did not work.

We also looked at mineral and Lewis acid catalysts. Mineral acids were effective as expected. An 80% HMF yield was achieved when 18 mol % H₂SO₄ (relative to fructose) was used. A lower acid loading (1.8 mol %) gave 75% yield. In contrast, the widely studied AlCl₃-Lewis acid was not effective at molar ratios between 0.5 and 2 (19).

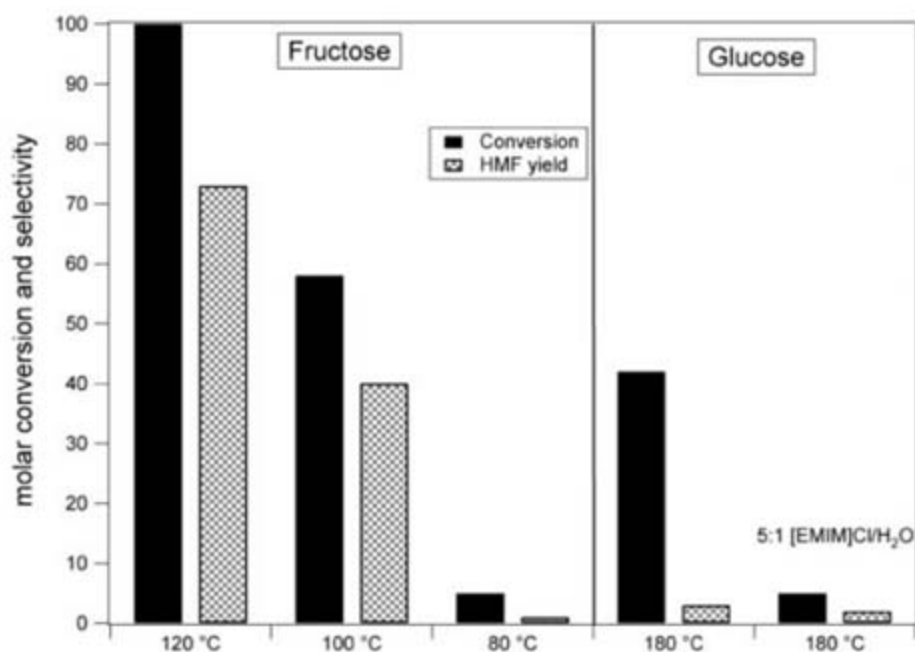


Fig. 2. Fructose and glucose conversion in [EMIM]Cl. Fifty mg of sugar was added to 500 mg of [EMIM]Cl and heated for 3 hours at the temperature indicated (no catalyst was added).

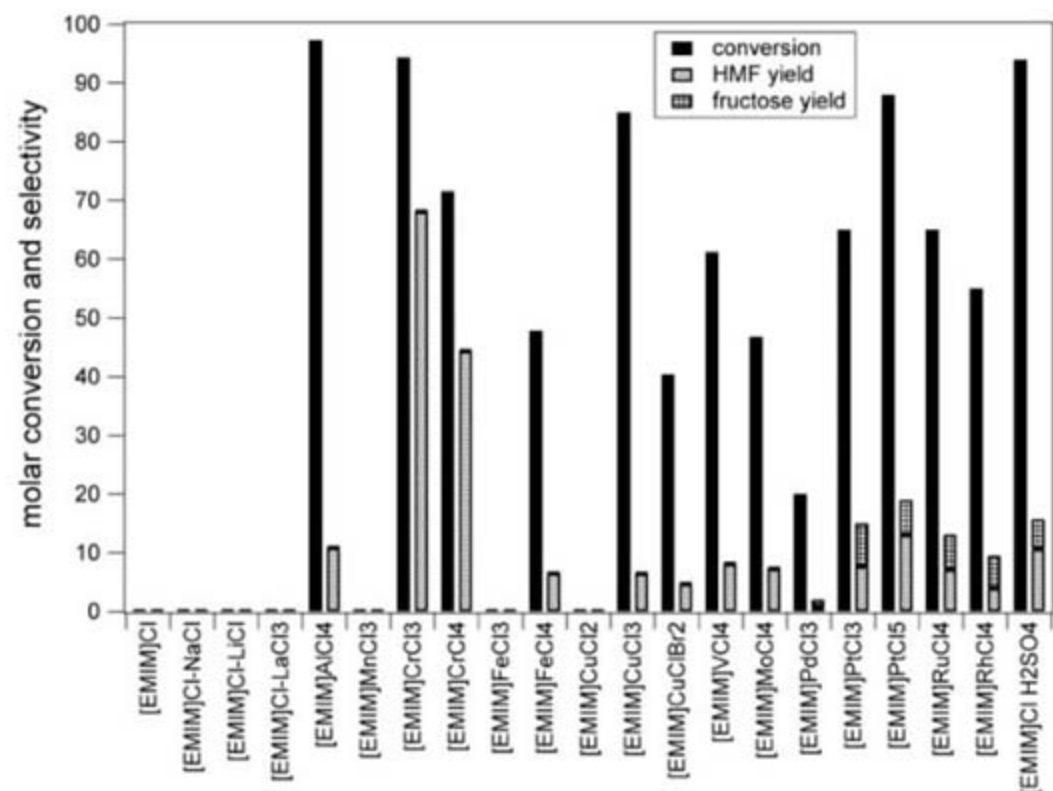


Fig. 3. Glucose conversion in [EMIM]Cl treated with numerous catalysts, most of which are effective for fructose dehydration. Only CrCl₂ leads to high HMF yield from glucose.

We repeated these studies with use of glucose as feed but raised the temperature to 100°C because of its lower reactivity (Fig. 1B). Twelve of the metal halides tested showed 40% conversion of glucose, but only one catalyst, CrCl₂, gave HMF in high yield (Fig. 3). HMF yield in [EMIM]Cl containing sulfuric acid or AlCl₃ was only 10%. The results were reproduced at least 20 times, and HMF yields for systems that did not contain CrCl_x were consistently 10% or less, whereas CrCl₂ afforded HMF yields of 68 to 70%, a previously elusive efficiency from glucose. The

products from the other catalysts included sugars such as mannose, dehydration products such as 1,6-anhydroglucose, and poorly characterized polymeric products [determined by ¹³C nuclear magnetic resonance (NMR) spectroscopy].

For many of the catalysts, glucose conversion was high even though HMF yields were low (Fig. 2). We did a number of control experiments to demonstrate that the low HMF yield in these instances was not the result of HMF instability under the reaction conditions. After heating pure HMF at 100°C for 3 hours in the presence of

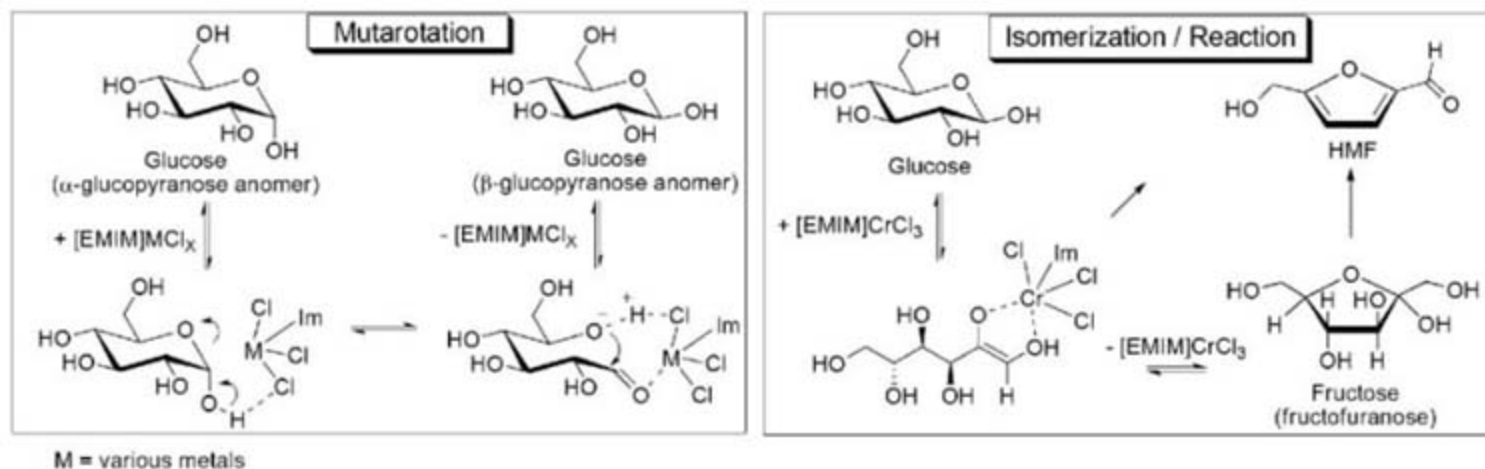


Fig. 4. Proposed metal halide interaction with glucose in [EMIM]Cl. CuCl_2 and CrCl_2 catalyze the mutarotation leading to interconversion of α - and β -glucopyranose anomers. CrCl_2 leads to the isomerization of glucopyranose to fructofuranose, followed by dehydration to HMF.

CrCl_2 , 98% was recovered. When CrCl_2 was not added to [EMIM]Cl, HMF recovery was only 28%. Similar studies were done with other metal halides (HMF recoveries noted in parentheses): CuCl_2 (85%), VCl_4 (86%), and H_2SO_4 (98%). Interestingly, catalytic amounts of certain metal chlorides appear to play a role in stabilizing HMF. Catalysts usually enhance reactions; the concept of a catalytic amount of a substance, in less than stoichiometric quantities, blocking or quenching a reaction is most unusual.

In a second study, we examined HMF stability in the presence of sugar and catalyst. In these tests, xylose, a five-carbon sugar that cannot form HMF, was used. Fifty mg of a 1:1 mixture of HMF and xylose were added to 500 mg of the appropriate [EMIM]Cl-catalyst system and heated to 100°C for 3 hours. HMF recovery was high (recoveries given in parentheses): CrCl_2 (83%), CuCl_2 (90%), and VCl_4 (83%). HMF once again was more stable in the presence of metal halide; HMF recovery in [EMIM]Cl-xylose without catalyst was 66%. The data show that the low HMF yield cannot be accounted for by product instability under reaction conditions. Instead metal halides, such as CuCl_2 and VCl_4 , catalyze undesired reaction pathways.

The singular effectiveness of catalytic amounts of CrCl_2 in [EMIM]Cl for the conversion of glucose to HMF was unanticipated. In an effort to understand the results, we turned to spectroscopy. Our NMR study showed that the glucose starting material, when dissolved in the [EMIM]Cl solvent, is predominantly an α -anomer. Solvation of sugars occurs through hydrogen bonding of chloride ions of the solvent with the carbohydrate hydroxy groups (20). However, this interaction is insufficient to cause mutarotation (that is, α - to β -anomer conversion; Fig. 4). Little interconversion of the α - and β -anomers occurred in [EMIM]Cl, even after several hours at 80°C. However, in the presence of a catalytic amount of CuCl_2 or CrCl_2 , mutarotation leading to an equilibrium mixture of anomers was rapid (figs. S2 and S3). In the ^1H NMR spectrum, the six $-\text{OH}$ resonances were sharp. In the presence of

catalytic amounts of CuCl_2 the $-\text{OH}$ resonances shifted upfield and were very broad, indicating exchange through interactions with the metal (21).

[AMIM]Cl structures are known to be weakly coordinating (22) and do not compete with sugar for the binding of the metal chlorides. Our hypothesis is that sugar-metal coordination is responsible for the catalysis. To characterize the prevailing coordination bonding motif, we examined the effect of adding stoichiometric glycerol or glyceraldehyde to glucose solutions. Glucose can be thought of as a glycerol molecule attached to a glyceraldehyde molecule. By using NMR spectroscopy, we confirmed that glyceraldehyde exists as a hemiacetal dimer in [EMIM]Cl, which makes it a very good mimic for glucopyranose. In the competition reactions, glycerol had no impact on the catalysis, and 70% yield of HMF was achieved from glucose. Glyceraldehyde, however, did affect the chemistry: Reaction inhibition was observed. HMF yield was reduced to less than 20%, and glucose conversion was reduced to $\sim 60\%$. In addition, we evaluated 2,2'-bipyridine as a strongly coordinating ligand (5:1 molar ratio to Cr). In the presence of the strongly coordinating ligand, the reaction essentially shut down: HMF yield was less than 2%, and glucose recovery was 90%. The results of the glycerol and glyceraldehyde competition studies show that the metal interacts with the hemiacetal portion of glucopyranose but that there is little interaction with the polyalcohol portion of the sugar.

Although we lack a clear picture of why CrCl_2 is a singularly effective catalyst in [EMIM]Cl solvent, we are able to offer some insights into the mechanism. We studied the kinetic behavior of CrCl_2 , CuCl_2 , and FeCl_2 , which show dramatic differences in their reaction pathways (fig. S4). The rate of glucose conversion was highest with CrCl_2 ; CuCl_2 was reactive, but mainly gave condensation products; and FeCl_2 showed no reaction. With CuCl_2 , multiple products were formed, including mannose, HMF, and 1,6-anhydroglucose. This diverse

product mix suggests that CuCl_2 coordination with the sugar is different from that of CrCl_2 .

To explain the results with CrCl_2 , we show a mechanism consistent with the data (Fig. 4). Because only 0.5% by weight of CrCl_2 was added to the solvents, the plausible formation of $[\text{EMIM}]^+\text{CrCl}_3^-$ would consume only an equimolar amount of [EMIM]Cl with respect to CrCl_2 , according to Eq. 1:



We propose that the CrCl_3^- anion plays a role in proton transfer, facilitating mutarotation of glucose in [EMIM]. A critical role of CrCl_3^- is to effect a formal hydride transfer, leading to isomerization of glucose to fructose. As discussed above, all other tested metal chlorides failed to convert glucose to fructose in the [EMIM]Cl solvent. A chromium enolate may be the key intermediate (23). Once fructose is formed, dehydration of fructofuranose is rapid in the presence of the catalyst in the solvent. Lowering the dielectric constant of the media by addition of organic solvents (10:1 glycerol to [EMIM]Cl) results in loss of catalytic activity. Other metal halides also bind to glucose. However, they promote alternative reaction paths that do not lead to the desired products.

References and Notes

1. T. A. Werpy et al., "Top value added chemicals from biomass" [U.S. Department of Energy (DOE) report number DOE/GO-102004-1992, Golden, CO, 2004; www.nrel.gov/docs/ty04osti/35523.pdf].
2. B. Kamm, M. Kamm, M. Schmidt, T. Hirth, M. Schulze, in *Biorefineries: Industrial Processes and Products*, B. Kamm, P. R. Gruber, M. Kamm, Eds. (Wiley, Weinheim, Germany, 2006), vol. 2, pp. 97-149.
3. M. Bicker, J. Hirth, H. Vogel, *Green Chem.* **5**, 280 (2003).
4. G. W. Huber, J. N. Chheda, C. J. Barrett, J. A. Dumesic, *Science* **308**, 1446 (2005).
5. F. S. Asghari, H. Yoshida, *Ind. Eng. Chem. Res.* **45**, 2163 (2006).
6. B. F. M. Kuster, *Starch Starke* **42**, 314 (1990).
7. Y. Róman-Leshkov, J. N. Chheda, J. A. Dumesic, *Science* **312**, 1933 (2006).
8. S. K. Tyrlik, D. Szerszen, M. Olejnik, W. Danikiewicz, *Carbohydr. Res.* **315**, 268 (1999).
9. M. Watanabe et al., *Carbohydr. Res.* **340**, 1925 (2005).

10. Sugars exist as cyclic structures in solution. In H₂O, fructose is about 68% fructopyranose and 32% fructofuranose, and glucose is about 99% glucopyranose and 1% glucofuranose (24). In this paper, we use the terms fructose and glucose in reference to the sugars in any of their conformers.
11. M. J. Antal, W. S. L. Mok, G. N. Richards, *Carbohydr. Res.* **199**, 91 (1990).
12. Z. Srokol *et al.*, *Carbohydr. Res.* **339**, 1717 (2004).
13. B. M. Kabyemela, T. Adschiri, R. M. Malaluan, K. Arai, *Ind. Eng. Chem. Res.* **38**, 2888 (1999).
14. B. M. Kabyemela, T. Adschiri, R. M. Malaluan, K. Arai, *Ind. Eng. Chem. Res.* **36**, 1552 (1997).
15. C. Lansalot-Matras, C. Moreau, *Catal. Commun.* **4**, 517 (2003).
16. C. Moreau, A. Finiels, L. Vanoye, *J. Mol. Catal. Chem.* **253**, 165 (2006).
17. Materials and methods can be found on Science Online.
18. The [EMIM]Cl in this study gave a pH of 7 when mixed with H₂O in a 1:1 ratio. The pH of less-pure ionic liquids ranged from neutral to acidic.
19. At a mole ratio of 2, the melt is a Lewis acid (25).
20. R. C. Remsing, R. P. Swatloski, R. D. Rogers, G. Moyna, *Chem. Commun.* 1271 (2006).
21. CuCl₂ was used to study sugar-metal interactions, because chromium is strongly paramagnetic and the line-broadened spectrum was uninformative.
22. Z. C. Zhang, *Adv. Catal.* **49**, 153 (2006).
23. L. Mønsted, O. Mønsted, *Inorg. Chem.* **44**, 1950 (2005).
24. S. J. Angyal, *Adv. Carbohydr. Chem. Biochem.* **42**, 63 (1984).
25. K. M. Dieter, C. J. Dymek Jr., N. E. Heimer, J. W. Rovang, J. S. Wilkes, *J. Am. Chem. Soc.* **110**, 2722 (1988).
26. This work was supported by the Laboratory Directed Research and Development Program at the Pacific Northwest National Laboratory (PNNL), a multiprogram national laboratory operated by Battelle for the U.S. DOE under contract no. DE-AC06-76RL01830. Part of the research described in this paper was performed at the Environmental Molecular Science Laboratory, a national scientific user facility located at PNNL. We thank A. Appel for running the NMR experiments.

Supporting Online Material

www.sciencemag.org/cgi/content/full/316/5831/1597/DC1

Materials and Methods

Figs. S1 to S4

12 February 2007; accepted 18 April 2007

10.1126/science.1141199

Extracellular Proteins Limit the Dispersal of Biogenic Nanoparticles

John W. Moreau,^{1*} Peter K. Weber,² Michael C. Martin,³ Benjamin Gilbert,⁴ Ian D. Hutcheon,² Jillian F. Banfield^{1,4,5}

High-spatial-resolution secondary ion microprobe spectrometry, synchrotron radiation-based Fourier-transform infrared spectroscopy, and polyacrylamide gel analysis demonstrated the intimate association of proteins with spheroidal aggregates of biogenic zinc sulfide nanocrystals, an example of extracellular biomineralization. Experiments involving synthetic zinc sulfide nanoparticles and representative amino acids indicated a driving role for cysteine in rapid nanoparticle aggregation. These findings suggest that microbially derived extracellular proteins can limit the dispersal of nanoparticulate metal-bearing phases, such as the mineral products of bioremediation, that may otherwise be transported away from their source by subsurface fluid flow.

Sulfate-reducing bacteria can lower the concentrations of metals in anoxic waters by sequestering metals into nanoparticles (1–3). However, these particles are potentially highly mobile because of their small size (4) and can redissolve quickly if conditions change (5). Sulfide nanoparticles may be <2 nm in diameter [comparable in size to aqueous molecular clusters (6)]; most have a diameter of 2 to 6 nm (2, 7). Aggregation can restrict nanoparticle transport by inducing settling (8, 9), and it can drive crystal growth, leading to decreased solubility (10, 11). Some organics can promote aggregation. Amine-bearing molecules, for example, have been shown to organize sulfide nanoparticles into semiconductor nanowires (12). We investigated the hypothesis that natural organic matter contributes to the formation of densely aggregated nanoparticulate ZnS spheroids and is preserved in nanometer-scale pores (7). We used micro-

analytical and direct isolation approaches to analyze nanoparticle aggregates formed in natural sulfate-reducing bacterial biofilms (7, 13). We also experimentally evaluated the potential for various amino acids to induce rapid aggregation of metal-sulfide nanoparticles.

We examined sulfate-reducing bacteria-dominated biofilms collected from the Piquette Pb and Zn Mine, a flooded system (pH ~7, ~8°C) in southwestern Wisconsin (13). Ultramicrotomed biofilm sections that contained spheroidal aggregates of biogenic ZnS nanoparticles (figs. S1 to S4) were imaged with transmission electron microscopy (TEM) before in situ elemental microanalysis with secondary ion mass spectrometry at a spatial resolution of ~50 nm (NanoSIMS) (14). N in the samples was detected by NanoSIMS as CN⁻, NO⁻, and NS⁻ secondary ions and was quantified by comparison to reference samples (14, 15).

A comparison of TEM images with NanoSIMS S distribution maps demonstrates that ZnS spheroids are the only structures within the biofilm that contain significant S concentrations (Fig. 1, A to C). The composite NanoSIMS data show the intimate association of N with biofilm ZnS (Fig. 1, A to C); N is present throughout these aggregates at significantly higher levels than in abiotic ZnS reference materials (Fig. 1, D and E). Pores in the ZnS spheroids appear as low-diffraction-contrast features in TEM images because of a lower concentration of sphalerite

nanoparticles (fig. S2). Porous regions are associated with the highest N concentrations (Fig. 1, B and C). N concentration measurements for individual spheroids varied by 14% (relative SD, $n = 134$ spheroids), as compared with an average measurement precision of 4%, for individual ZnS aggregates with an average diameter of 700 nm. We estimated an average N concentration for all analyzed biofilm ZnS spheroids of 1.6 weight % (wt %), with a 95% confidence interval of 0.8 to 3 wt % (14). By comparison, the average N concentration of synthetic ZnS aggregates was ~100 times lower than it was for biofilm ZnS spheroids.

The small nitrate concentration of mine water (~3 µg/g) was removed from the biofilm during sample processing and was therefore not expected to be the source of N in ZnS. To test this prediction, we analyzed the spheroids for NO⁻, relative to CN⁻ (14). The CN⁻/NO⁻ ratio for a reference sample of KNO₃ dissolved in graphite (14) ranged from <1 to 200, with a median ratio of ~6. The average CN⁻/NO⁻ ratio of bacterial spores, an organic N reference, was 2950 ± 520 (SD). The average CN⁻/NO⁻ ratio of the biofilm ZnS was 3300 ± 870 (SD). Measurement precision for CN⁻/NO⁻ in the biofilm ZnS was similar to sample variability because of low NO⁻ secondary-ion intensities. Based on these analyses, we concluded that N in the biofilm ZnS was present neither as nitrate nor nitrite and was therefore organic in nature (14). This conclusion was further supported by the presence of amide absorption features in the infrared spectra discussed below. From the average N content of ZnS estimated above and an average amino acid N concentration of ~11 wt %, the ZnS spheroids contained ~14 wt % amino acids.

Areas with cell-like morphologies enriched in N (Fig. 1) and P (fig. S8) are interpreted as being either whole or degraded microbial cells. These features are morphologically distinct from ZnS spheroids, arguing against spheroid formation by nanoparticle encrustation and infilling of cells. We inferred that the spheroids formed by the aggregation of biogenic ZnS nanoparticles (13) with extracellular polypeptides or proteins. This process may have involved the adsorption of amino acids or peptides onto nanoparticle surfaces (16) or the

¹Department of Earth and Planetary Science, University of California Berkeley, Berkeley, CA 94720, USA. ²Glenn T. Seaborg Institute, Lawrence Livermore National Laboratory (LLNL), Livermore, CA 94551, USA. ³Advanced Light Source, Lawrence Berkeley National Laboratory, Berkeley, CA 94720, USA. ⁴Earth Science Division, Lawrence Berkeley National Laboratory, Berkeley, CA 94720, USA. ⁵Department of Environmental Science, Policy, and Management, University of California Berkeley, Berkeley, CA 94720, USA.

*Present address: U. S. Geological Survey, Water Resources Division, 8505 Research Way, Middleton, WI 53562, USA. †To whom correspondence should be addressed. E-mail: jwmoreau@usgs.gov

coaggregation of protein molecules and nanoparticles. High N concentrations along the surfaces of some aggregates suggest protein-rich regions (Fig. 1, B and C).

Synchrotron radiation-based Fourier-transform infrared spectroscopy (SR-FTIR), with roughly 10 μm spatial resolution, was used to characterize organics associated with biofilm ZnS aggregates (14). SR-FTIR analysis revealed that absorptions at ~ 1580 and 1640 cm^{-1} were associated only with ZnS spheroid-rich regions of the biofilm (Fig. 2). These absorption features are well

described for the amide II and amide I vibration modes, respectively, and they are characteristic of polypeptide- and/or protein-derived amino acids (17). Analyses of the spheroid-rich regions of biofilm varied by a few percent in the relative magnitudes of amide I and II absorptions. The SR-FTIR data confirm that the N detected by NanoSIMS analysis of spheroids was organic and support an origin in polypeptides or proteins.

Proteins were directly extracted from density-separated fractions dominated by either organic biofilm components or ZnS spheroids (fig. S6)

(14). Proteins from the biofilm fraction produced faint bands when reacted with protein-specific stains in 4 to 10% polyacrylamide gels at molecular masses of ~ 37 and ~ 48 kD (Fig. 3) (14). In contrast, the ZnS-enriched fraction yielded a strong band at ~ 37 kD, suggesting that the N detected by NanoSIMS and SR-FTIR was associated with protein(s) of this molecular mass. It was not possible to further characterize the protein(s) because of their low concentration and biofilm-sample accessibility (13). However, the observed mass lies within the mass range of bacterial proteins known to bind certain metals (18–20), and genes for these proteins have been reported in some sulfate-reducing bacteria (21–23). We speculate, therefore, that the ZnS-associated protein(s) found in this study may serve a metal-binding function.

In some aggregates, NanoSIMS data indicated overlapping N and S distributions, implying the presence of fine-scale mixtures of ZnS nanoparticles and protein-rich organic matter. Known bacterial metal-binding proteins bind Zn and other potentially toxic metals (e.g., Cd and Cu), primarily at cysteine residues in proximity to OH^- groups (24). Experimental evidence shows that cysteine also binds strongly to ZnS nanoparticles and limits their size to < 5 nm (25) and that thiol groups bind strongly with S-deficient surface Fe(II) atoms in pyrite (16). The conditional stability constant for monoligand cysteine- Zn^{2+} complexation in low-ionic-strength solutions [≤ 0.1 moles of charge (M_c)] at 20° to 25°C is more than four orders of magnitude larger than those of all the other amino acids tested except for lysine, for which

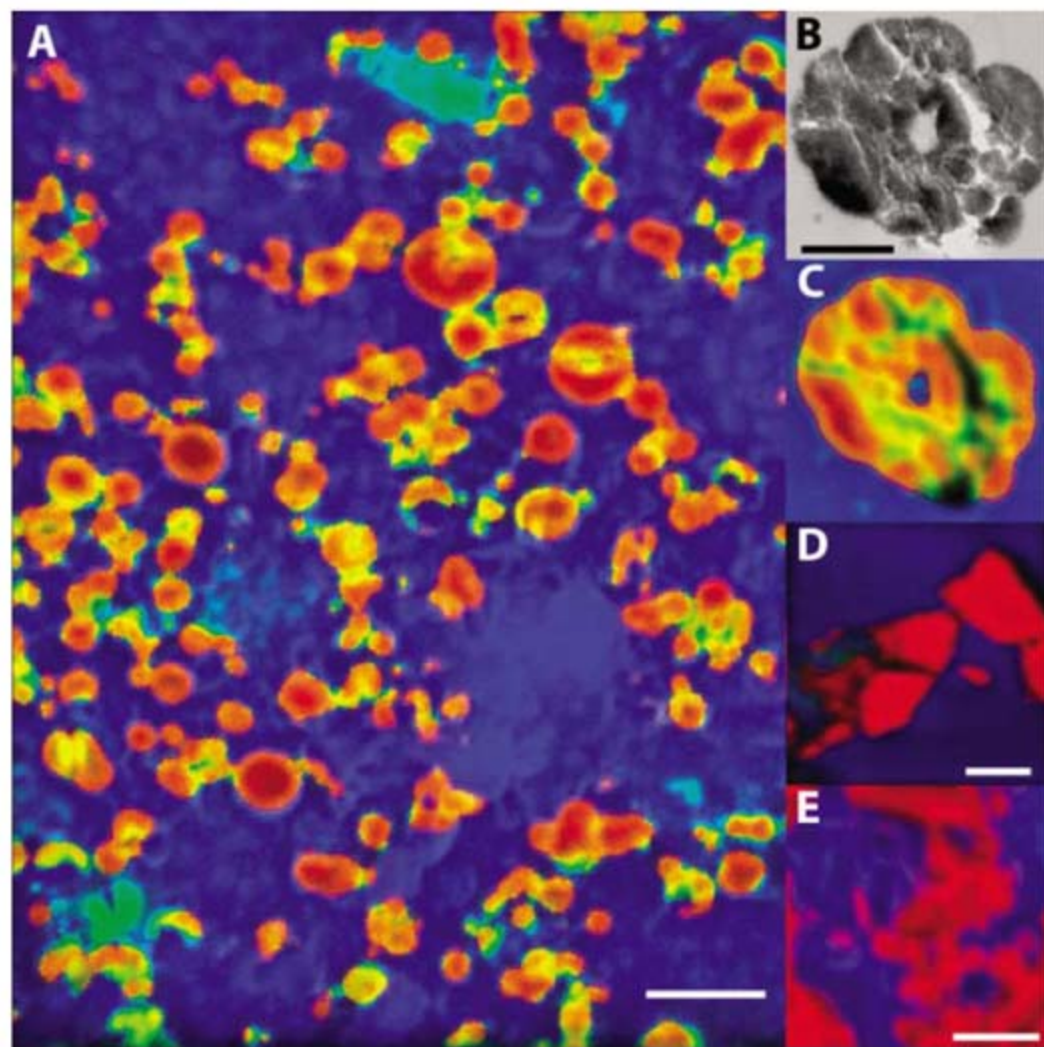


Fig. 1. NanoSIMS secondary-ion images showing C, N, and S distributions in an ultramicrotomed TEM section of biofilm. (A) Composite element distribution map ($\sim 10\ \mu\text{m}$ by $10\ \mu\text{m}$) of ^{12}C (blue), $^{12}\text{C}^{14}\text{N}$ for N (green), and ^{32}S (red). Colors reflect the proportion of each species. Uniformly red regions represent relatively pure S (as ZnS), whereas orange and yellow regions indicate the presence of increased levels of N. Light blue regions indicate the presence of both C and N, with little to no S (no ZnS). (B) TEM image of several conjoined ZnS spheroidal aggregates. (C) NanoSIMS composite element distribution map of (B). (D) NanoSIMS composite element distribution map of ultramicrotomed Balmat ZnS. (E) NanoSIMS composite element distribution map of synthetic nanoparticulate ZnS. (F) Color box plots of the relative ion abundances displayed in (A) and (C) to (E). Primary colors and maximum ion counts are noted for each species along each axis; all axes are linear, with respect to ion counts. In the left box (binary), only binary ion compositions (one or two species) are shown; in the right box (ternary), only primary (the species corresponding to each axis) and ternary ion compositions (three species) are shown. Black and white corners correspond to points of minimum and maximum ion counts, respectively, for all three species. All scale bars are $1\ \mu\text{m}$. Figures S8 to S10 (14) present grayscale versions of (A), (C), and (D), respectively.

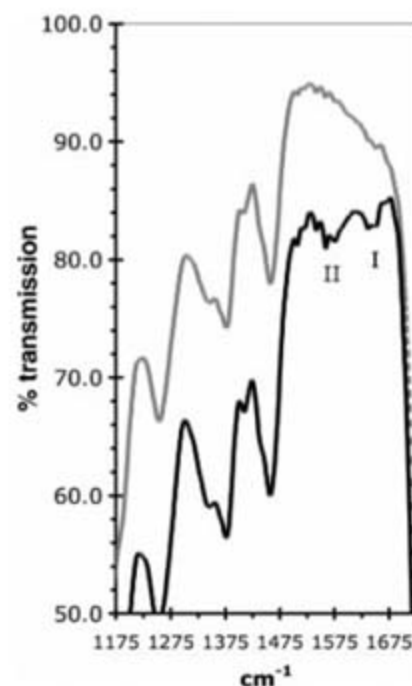


Fig. 2. SR-FTIR transmission spectra of biogenic ZnS aggregates (black) and background biofilm (gray). Amide I ($\sim 1640\text{ cm}^{-1}$) and II ($\sim 1580\text{ cm}^{-1}$) absorption features are diagnostic of amino acid-associated bond vibrations in polypeptides and/or proteins.

the constant is about two orders of magnitude larger (table S1) (14). These observations suggest that cysteine or cysteine-rich polypeptides or proteins could have played a role in determining the ZnS particle size and aggregation state.

We tested the efficacy of individual amino acids (100 μ M) to promote the aggregation of synthetic ZnS particles 3 nm in diameter or smaller (10 μ M) (14). The chosen amino acids (alanine, aspartate, cysteine, lysine, phenylalanine, proline, and serine) possess chemically distinct side-chain functional groups. Aggregation was monitored periodically with dynamic light scattering (DLS) (14), and results showed that the inorganic aggregation of ZnS initially occurred rapidly to form ~100-nm-diameter aggregates, but then slowed greatly or ceased after 1 week (Fig. 4 and fig. S7). In contrast, ZnS nanoparticles in the presence of cysteine exhibited more extensive and prolonged aggregation, ultimately forming 1-to-10- μ m-sized structures. Other amino acids had little (e.g., serine) to no (e.g., proline) detectable effect on nanoparticle aggregation, relative to controls (fig. S7). Cysteine in the absence of ZnS formed no measurable aggregates (Fig. 4), and humic

compounds added to ZnS nanoparticle suspensions did not accelerate aggregation.

The DLS results correlate with earlier studies of the adsorption of amino acids, other organic ligands, and inorganic ions onto the surfaces of metal chalcogenides (16, 26, 27). For example, the sulfhydryl group present in cysteine and mercapto-compounds exhibits strong specific binding to the surfaces of sulfide minerals and nanoparticles. Similarly, serine with a terminal hydroxyl group causes somewhat more aggregation than is observed in control samples, as was expected from both the weaker chemical interaction of this group with sulfide surfaces and the higher pK_a (where K_a is the acid dissociation constant), relative to cysteine (9.15 versus 8.33). Thus, strong specific chemical binding is a necessary prelude to amino acid- or protein-driven ZnS nanoparticle aggregation.

Mineral/protein mixtures with internal organization are typically considered biominerals, and biominerals normally form within organisms. The structures reported here represent an exception to this pattern. Proteins, peptides, and amino acids could be released after cell death and scavenged by hydrophobic ZnS surfaces. Alternatively, bacteria may export Zn-binding

proteins for a physiological reason. Most known bacterial metal-binding proteins are produced for intracellular binding and the subsequent export of toxic metals (24). In the case reported here, biofilm proteins may bind excess aqueous Zn^{2+} or interact with bound Zn(II) and other proteins after ZnS precipitation. In either scenario, the aggregation of metal-sulfide nanoparticles was promoted, preventing incidental uptake by cells (28, 29) or the entombment of cells. From the dense spheroidal morphologies of the aggregates, the rate of aggregation appears to be reaction-limited (30). Similar densely packed aggregates of biogenic metal-bearing nanoparticles have been reported from other metal-contaminated systems (31). Such aggregates in sediments could trap and possibly preserve organic molecules or their degradation products in sediments or rocks.

Microbial and chemical redox transformations of metals can result in the precipitation of metal-bearing nanoparticles across a range of environmental conditions (32). The aggregation state of these particles may have a strong impact on metal mobility and water quality (33). Our results suggest that aggregation induced by extracellular metal-binding polypeptides and proteins plays an important role in limiting nanoparticle dispersal in natural environments.

Fig. 3. Composite SDS-polyacrylamide gel electrophoresis image of biofilm and ZnS protein extractions. SyproOrange and colloidal silver molecular weight standards are shown (far left and right lanes, respectively). (A) Extraction from the biofilm organic fraction stained with SyproOrange. (B) Extraction of the ZnS spheroid fraction stained with SyproOrange. (C and D) Replicate extractions of the biofilm organic fraction stained with silver. (E and F) Replicate extractions of ZnS spheroids fraction stained with silver. Numbers are molecular masses in kilodaltons.

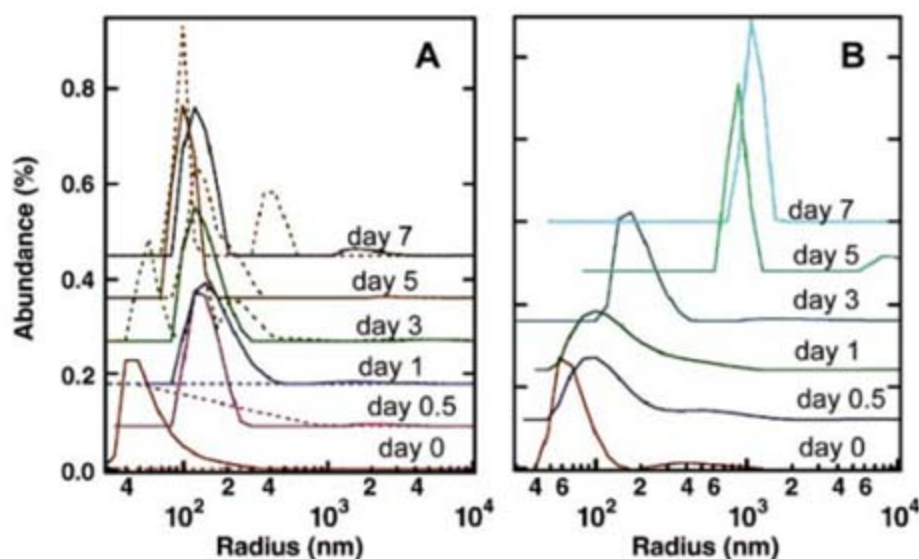


Fig. 4. Size distribution curves from DLS data acquired in ZnS nanoparticle aggregation experiments. (A) Control experiments. 10 μ M ZnS nanoparticles alone (solid lines) aggregate within 1 day to form ~100-nm-radius clusters that exhibit little further growth over a 5-day period. 100 μ M cysteine alone (dashed lines) gives a very weak DLS signal, with no consistent trend in size distribution. (B) In the presence of both 10 μ M ZnS and 100 μ M cysteine, sustained aggregation occurs over the 7-day period, resulting in aggregates that are more than one order of magnitude larger than the initial clusters. DLS correlation functions from which size distributions were derived are shown in fig. S7.

References and Notes

- J. R. Lloyd, A. N. Mabbett, D. R. Williams, L. E. Macaskie, *Hydrometallurgy* **59**, 327 (2001).
- Y. Suzuki, S. D. Kelly, K. M. Kemner, J. F. Banfield, *Nature* **419**, 134 (2002).
- S. L. Hockin, G. M. Gadd, *Appl. Environ. Microbiol.* **69**, 7063 (2003).
- B. D. Honeyman, *Nature* **397**, 23 (1999).
- J. G. Hering, W. Stumm, in *Mineral-Water Interface Geochemistry; Reviews in Mineralogy*, vol. 23, M. F. Hochella Jr., A. F. White, Eds. (Mineralogical Society of America, Washington, DC, 1990), pp. 427-465.
- G. W. Luther, S. M. Theberge, D. T. Rickard, *Geochim. Cosmochim. Acta* **63**, 3159 (1999).
- J. W. Moreau, R. I. Webb, J. F. Banfield, *Am. Mineral.* **89**, 950 (2004).
- C. Allain, M. Cloitre, F. Parisse, *J. Colloid Interface Sci.* **178**, 411 (1996).
- S. A. Bradford, S. R. Yates, M. Bettehar, J. Simunek, *Water Resour. Res.* **38**, 1327 (2002).
- J. W. Zhang, G. H. Nancollas, in *Mineral-Water Interface Geochemistry; Reviews in Mineralogy*, vol. 23, M. F. Hochella Jr., A. F. White, Eds. (Mineralogical Society of America, Washington, DC, 1990), pp. 365-393.
- W. Stumm, J. J. Morgan, *Aquatic Chemistry: Chemical Equilibria and Rates in Natural Waters* (Wiley, New York, 1996), pp. 400-414.
- Q. Lu, F. Gao, D. Zhao, *Nanotechnology* **13**, 741 (2002).
- M. Labrenz et al., *Science* **290**, 1744 (2000).
- Materials and methods are available as supporting material on Science Online.
- E. H. Hauri, J. Wang, D. G. Pearson, G. P. Bulanova, *Chem. Geol.* **185**, 149 (2002).
- J. Bebié, M. A. A. Schoonen, *Geochem. Trans.* **1**, 47 (2000).
- H. H. Mantsch, D. Chapman, *Infrared Spectroscopy of Biomolecules* (Wiley-Liss, New York, 1996).
- M. B. Khazaeli, R. S. Mitra, *Appl. Environ. Microbiol.* **41**, 46 (1981).
- E. Kurek, A. J. Francis, J.-M. Bollag, *Arch. Environ. Contam. Toxicol.* **20**, 106 (1991).
- D. H. Nies, *J. Bacteriol.* **174**, 8102 (1992).
- N. Naz, H. K. Young, N. Ahmed, G. M. Gadd, *Appl. Environ. Microbiol.* **71**, 4610 (2005).

22. T. A. M. Bridge, C. White, G. M. Gadd, *Microbiology* **145**, 2987 (1999).
23. C. A. Blindauer et al., *Proc. Natl. Acad. Sci. U.S.A.* **98**, 9593 (2001).
24. B. P. Rosen, *J. Biol. Inorg. Chem.* **1**, 273 (1996).
25. C. L. Torres-Martinez et al., *Nanotechnology* **10**, 340 (1999).
26. L. Ronngren, S. Sjöberg, Z. Sun, W. Forsling, P. W. Schindler, *J. Colloid Interface Sci.* **145**, 396 (1991).
27. W. Vogel, *Langmuir* **16**, 2032 (2000).
28. T. Barkay, J. Schaefer, *Curr. Opin. Microbiol.* **4**, 318 (2001).
29. J. A. Kloefer, R. E. Mielke, J. L. Nadeau, *Appl. Environ. Microbiol.* **71**, 2548 (2005).
30. G. A. Waychunas, in *Nanoparticles and the Environment; Reviews in Mineralogy and Geochemistry*, vol. 44, J. F. Banfield, A. Navrotsky, Eds. (Mineralogical Society of America, Washington, DC, 1990), pp. 105–166.
31. J. S. Ahn, Y. S. Park, J. Y. Kim, K. W. Kim, *Environ. Geochem. Health* **27**, 147 (2005).
32. M. F. Hochella Jr., *Geochim. Cosmochim. Acta* **66**, 735 (2002).
33. M. S. Diallo, N. Savage, *J. Nanopart. Res.* **7**, 325 (2005).
34. We thank T. Thomsen and colleagues of Diversion SCUBA (Madison, WI) for recovering biofilm samples; Rick and Robyn Webb (University of Queensland, Australia), H. Zhang (University of California, Berkeley), and C. Ramon (LLNL) for assistance in preparing biofilm and synthetic ZnS samples for TEM and NanoSIMS; L. Nittler (Carnegie Institution of Washington, DC) for assistance with processing NanoSIMS data; R. G. Wilson for data on N in ZnS; and M. Thelen and C. Jeans (LLNL) for assistance with protein extractions. The comments of two anonymous reviewers greatly improved the quality and clarity of our manuscript. Work was funded by the U.S. Department of Energy Basic Energy Sciences Program under contract no. DE-FG02-04ER15507, the NASA Astrobiology Institute under contract no. NNA04CC02A (J.W.M. and J.F.B.), and the U.S. Department of Energy Office of Biological and Environmental Research Genomics Genomes to Life research program (P.K.W. and L.D.H.). Work was performed at LLNL under the auspices of the U.S. Department of Energy under contract no. W-7405-Eng-4. The Advanced Light Source is supported by the director of the Office of Science, Office of Basic Energy Sciences, of the U.S. Department of Energy under contract no. DE-AC02-05CH11231.

Supporting Online Material

www.sciencemag.org/cgi/content/full/316/5831/1600/DC1

Materials and Methods

Figs. S1 to S11

Table S1

References

8 February 2007; accepted 4 May 2007

10.1126/science.1141064

Origin of the Low Rigidity of the Earth's Inner Core

Anatoly B. Belonoshko,^{1,2*} Natalia V. Skorodumova,³ Sergio Davis,¹ Alexander N. Osipov,⁴ Anders Rosengren,² Börje Johansson^{1,3,5}

Earth's solid-iron inner core has a low rigidity that manifests itself in the anomalously low velocities of shear waves as compared to shear wave velocities measured in iron alloys. Normally, when estimating the elastic properties of a polycrystal, one calculates an average over different orientations of a single crystal. This approach does not take into account the grain boundaries and defects that are likely to be abundant at high temperatures relevant for the inner core conditions. By using molecular dynamics simulations, we show that, if defects are considered, the calculated shear modulus and shear wave velocity decrease dramatically as compared to those estimates obtained from the averaged single-crystal values. Thus, the low shear wave velocity in the inner core is explained.

Since the discovery of Earth's inner core (IC) by Ingrid Lehmann in 1936 (1), it has been established, on the basis of the equation of state as compared to seismic data and the abundance of iron, that Earth's IC mainly consists of iron (2–5). However, the resistance of iron and its alloys to shear, either measured (6, 7) or calculated (8), does not match the very low resistance to shear of the IC, as follows from the low velocity of the shear signal propagation (4, 9). To explain the low rigidity of the IC, it has been suggested that Earth's IC contains liquid inclusions (10). This suggestion, however, is met with certain difficulties (11, 12), because a liquid is likely to be squeezed out of the IC.

Therefore, a satisfactory explanation of the low rigidity of Earth's IC is still lacking. Computational materials physics has now reached a high degree of sophistication and reliability in the calculations of crystal elastic constants at the conditions relevant for the IC (8). Yet, the shear moduli of relevant iron alloys, obtained by the most advanced computational methods, are systematically higher than the observed shear modulus of the IC (8). This trend makes one question the validity of the procedure currently applied for calculating the elastic constants of materi-

als at high temperature T and pressure P . At present, one calculates the elastic properties of a polycrystalline material by averaging the elastic properties of a single crystal over all possible crystallographic orientations (13). Thus, the elastic properties of a polycrystalline material are completely defined by the properties of the single crystal. Although this approach can be quite legitimate at low temperature, it might fail under conditions when grain boundaries become viscous (14), which is likely at high temperature.

To investigate the impact of defects and grain boundaries on the shear properties of polycrystalline iron under the IC pressure and temperature conditions and to evaluate the applicability of the contemporary approach to calculate shear properties of iron in Earth's IC, we study the elastic behavior of an ideal iron crystal in comparison with that of a "realistic" sample containing several grain boundaries as well as other extensive structural defects.

Among the possible computational methods, the method of molecular dynamics (MD) appears to be very suitable for calculating the elastic properties of a material at finite temperatures. MD simulations of realistic samples require a large number of atoms that prevents the application of pure ab initio methods. Recently, a sufficiently precise embedded-atom model (EAM) of high-pressure iron has been developed (15–17).

Table 1. Calculated properties of bcc iron as compared to the IC data.

Parameter (units)	Ab initio (18)	EAM (15)	Earth's IC (4)
P (GPa)	356.7	360.0	360.0
T (K)	6000.0	6000.0	7400.0
B (GPa)	1486.0	1372.7	1380.0
C_{11} (GPa)	1561.6	1391.0	1415.1
C_{12} (GPa)	1448.1	1363.5	1362.5
C_{44} (GPa)	365.5	448.0	387.0
G (GPa)	242.0	274.3	243.1
ρ (g/cm ³)	13.58	13.90	13.78
V_L (km/sec)	11.54	11.90	11.12
V_S (km/sec)	4.22	4.44	4.20
			176.1
			13.09
			11.26
			3.67

¹Applied Materials Physics, Department of Materials Science and Engineering, The Royal Institute of Technology, SE-100 44 Stockholm, Sweden. ²Condensed Matter Theory, AlbaNova University Center, Department of Theoretical Physics, The Royal Institute of Technology, SE-10691 Stockholm, Sweden. ³Condensed Matter Theory Group, Department of Physics, Uppsala University, Uppsala Box 530, Sweden. ⁴Institute of Mechanics, Moscow State University, 142432 Moscow, Russia. ⁵School of Physics and Optoelectronic Technology and College of Advanced Science and Technology, Dalian University of Technology, Dalian 116024, China.

*To whom correspondence should be addressed. E-mail: anatoly.belonoshko@fysik.uu.se

In this model, the interatomic interaction consists of short-range pair-wise repulsion and a many-body interaction term. The latter represents the energy of embedding an atom into the electron gas. The model was parameterized to reproduce the results of first-principles calculations (15). In the present work, this EAM is further tested by calculating the elastic constants of the body-centered cubic (bcc) iron crystal and comparing those constants to the elastic constants obtained by the projector-augmented wave (PAW) method (18), one of the most precise first-principles methods. Having chosen the model of iron, we now have to decide which phase of iron to consider. Recent theoretical results suggest that the bcc phase of iron (16, 19) [or iron alloyed with silicon (20)] is stable at the pressure and temperature conditions of the IC and, therefore, is appropriate to consider. The elastic moduli of this phase have been calculated by the “stress-strain” approach (21). This approach is based on the generalized Hooke’s law, which states that the stress tensor is proportional to the strain tensor

$$\sigma_i = C_{ij}\epsilon_j \quad (1)$$

where σ_i ($i = 1, \dots, 6$) describes the small stress components caused by the application of a small strain with components ϵ_i . C_{ij} are the components of the stiffness tensor or elastic moduli. Therefore, if one knows the strain and stress tensors, one can derive the elastic constants. This approach has been tested on numerous materials, and it can be applied to crystals at equilibrium as well as under pressure (22, 23). The comparison of the performance of the “stress-strain” method with that of the energy-based approach has shown good agreement between the results obtained by the two methods as well as with experimentally obtained data (22). We consider the bcc phase of iron and, hence, we need to know only three independent constants C_{11} , C_{12} , and C_{44} , which can be extracted from the MD calculations of stresses appearing as a response to small strains applied to the crystals under the constant volume constraint (Table 1). Having obtained these moduli, we can calculate the shear modulus [$G = (C_{11} - C_{12} + 3C_{44})/5$] (13) and, consequently, estimate the longitudinal [$V_L^2 = (B + 4G/3)/\rho$] and shear [$V_S^2 = G/\rho$] velocities (where B and ρ are the bulk modulus and the density of the material at given P and T). We present the elastic moduli and velocities obtained by this method for bcc iron, using the data produced in ab initio (18) and quasi-ab initio (15) EAM MD simulations (Table 1). In all our MD simulations, we used a 0.5-fs time step and periodic boundary conditions. The EAM- and PAW-calculated properties are reasonably close to each other, which allows us to rely on the EAM approach in the MD simulations of polycrystalline iron. The calculated elastic properties (Table 1) agree well with those reported in a recent work that

additionally confirms the validity of our methods (8). Values presented in Table 1 demonstrate once again that calculated shear moduli are substantially higher than the modulus observed for the IC.

A realistic sample can be obtained either by growing a polycrystal from melt (24) (referred to as the M sample) or by performing the Voronoi construction (25, 26) (referred to as the V sample). We prepared iron samples by both methods (Fig. 1). The number of atoms in these cubic samples was close to 1 million. The length of the cube side (L) was about 185 Å. The preparation of the M sample included the following steps.

The bcc sample containing 1,024,000 atoms was heated to 10,000 K to ensure melting. Then, eight bcc crystals were embedded in the eight octants of the box containing the melted iron. These crystals were slightly misplaced from the exact centers of the octants and rotated around randomly chosen axes. This sample was then crystallized at $T = 6800$ K and $P = 3.6$ Mbar for 300,000 time steps (Fig. 1A). The procedure of growing a sample from melt is relevant for the IC case, because the IC is likely formed by crystallization from an iron-rich alloy (27). The V sample originally contained 10 bcc grains, with centers randomly placed in the cube of the same

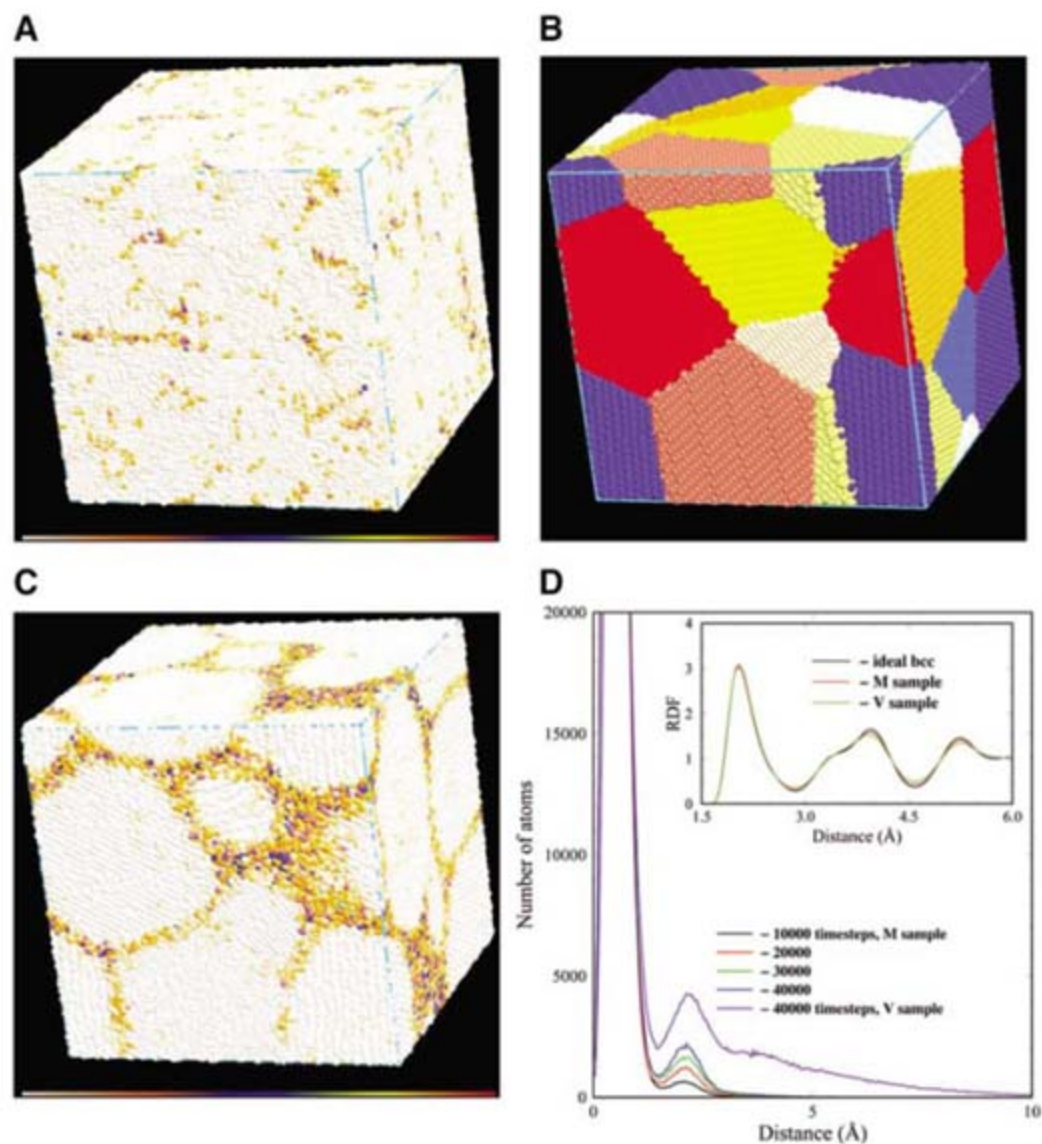


Fig. 1. The structure and atom mobility of the synthesized iron samples (the size is about 200 Å). (A) The sample grown from the M sample. The atoms are colored in accordance with their mobility as shown in (D): Yellow spheres are the most immobile atoms, and blue and red spheres are the most mobile atoms. The color bar shows the exact palette. There are no clear grain boundaries but there is a number of randomly located defects. (B) Initial configuration of atoms in the V sample. Each grain is colored according to its number. (C) The V sample obtained by MD simulations starting from the sample shown in (B). The atoms are colored in accordance with their mobility [with the same palette as for (A)] but in the scale according to their mobility (see the color bar). Grain boundaries are clearly seen. (D) The number of atoms as a function of the traveled distance at the different time steps. The motion of atoms in the V sample (C) is much more intense as compared to that in the M sample (A). The inset shows a comparison of radial distribution functions (RDF) for the ideal bcc crystal, the M sample, and the V sample. Even though there are numerous defects in the M and V samples, their structure is clearly that of the bcc crystal.

size ($L = 185 \text{ \AA}$). Then, a randomly oriented bcc crystal was built around every center. An atom, belonging to a crystal I , was deleted if the distance between the atom and a center of a crystal J was smaller than the distance between the atom and the center of the crystal I . This simple rule allows us to perform the Voronoi construction. If two atoms were spaced by less than 1.5 \AA (this might happen at a grain boundary), one of the atoms was removed. After that, the sample (Fig. 1B) was annealed at $T = 6800 \text{ K}$ and $P = 3.6 \text{ Mbar}$ for 300,000 time steps (Fig. 1C). The atoms are colored in Fig. 1, A and C, according to their mobility (Fig. 1D). All the studied samples retain the bcc structure (28) (inset in Fig. 1D). These crystals contain defects as well as grain boundaries, which are either preset in the sample (V sample) or form as a result of growth from the melt (M sample). The M sample does not contain clear grain boundaries. The diffusion in the M sample (Fig. 1D) is typical of the diffusion in a solid with interstitial and vacancy-like defects. The V sample is rather different from the M sample: It contains clear grain boundaries (Fig. 1C) that result in the presence of atoms with liquid-like mobility (see the tail of the curve in Fig. 1D). Having these two samples, we are now able to distinguish between the relaxation of stress due to the diffusion of defects within a grain and stress relaxation due to the interaction of grain boundaries.

Further, the ideal bcc crystal as well as the M and V samples (Fig. 1, A and C) were subjected to shear. The shear was applied in such a way that the "new" atom coordinates in the deformed sample were obtained from the "old" coordinates according to the formula $u_{\text{new}} = u_{\text{old}} + vd/L$, where u and v were two different (x, y, z) coordinates of an atom, d was shear magnitude, and L was the size of the cubic box. Such a shear corresponds to the strain normally applied to calculate C_{44} . The ideal bcc sample was subjected to the strain $u = x, v = y, d = 5.0 \text{ \AA}$, and $L = 192.0 \text{ \AA}$. We then performed the MD simulation of this sample, keeping constant volume and temperature (6800 K). The resulting shear modulus G , which for this particular shear

coincides with C_{44} , does not change with time (Fig. 2A), and neither does the corresponding shear velocity, calculated as $V_s^2 = G/\rho$ (Fig. 2B). No relaxation of stress is observed. The shear modulus remains constant and higher than that in the IC. Similarly, the M sample (Fig. 1A) was sheared with $u = x, v = y, d = 5.0 \text{ \AA}$, and $L = 188.4 \text{ \AA}$, and the stress was calculated at a constant volume at two temperatures (6000 and 6800 K). Though sample M does not contain grain boundaries, stress relaxation with time is quite different from that in the ideal bcc sample (Fig. 2). The shear modulus decreases from the same value as for the ideal bcc sample to that of the Earth's IC and eventually becomes even lower (which seems to be natural, because it is a matter of time when a stress is released). Changes in the direction of applied strain and moderate variations of temperature (6000 and 6800 K) have little impact on the shear stress behavior.

The V sample was subjected to the shear with $u = x, v = y, d = 1.0 \text{ \AA}$, and $L = 185.8 \text{ \AA}$. We tried out a number of shear magnitudes in order to, on the one hand, resolve the stress as precisely as possible and, on the other hand, remain within the elastic behavior. The temperature was 6800 K during the MD run. We see that the magnitude of the stress (Fig. 2) in the beginning of the run is equal to that averaged over the ideal crystals (Table 1). However, stress relaxation is very fast as a result of a high mobility of atoms at viscous (liquid-like) grain boundaries (Fig. 1, C and D). The very low rigidity of the V polycrystal (Fig. 1C) is likely due to the reverse Hall-Petch effect (29), which consists in the existence of a maximum of crystal strength as a function of a grain size.

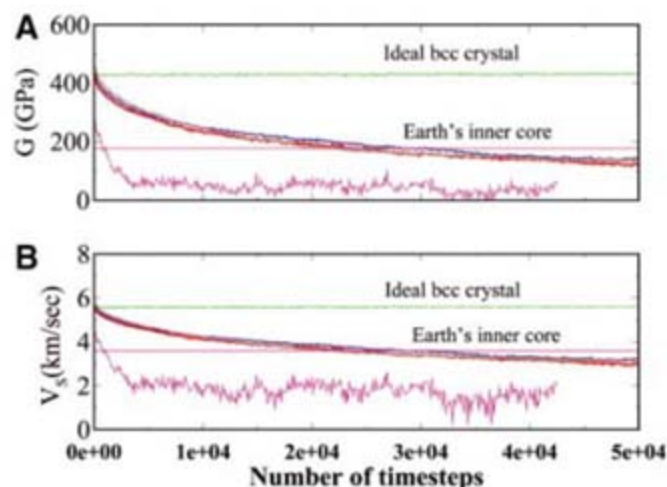
The comparison of relaxation patterns in the V and M samples suggests that even if iron grains in the IC are large, the diffusion within a grain can clearly accommodate the relaxation necessary to attenuate the shear signal and get low seismic shear velocities that are consistent with those observed in seismic studies (4, 9) (Fig. 2B). The impact of introducing defects and grain boundaries consists in depressing the shear

velocity. Evidently, this impact does not depend on the structure of iron: Whatever the phase, the diffusion, either within a grain or at a grain boundary, will decrease the shear resistance. We conclude that the low rigidity of the Earth's IC is due to the viscous grain boundaries and that the high diffusion within iron crystallites is due to high temperature. On a more general note, the calculations of high-temperature elasticity of a material must account for the effects of grain boundaries and diffusion.

References and Notes

1. I. Lehmann, *Publ. Bur. Cent. Assoc. Int. Seismol. A* **14**, 3 (1936).
2. F. Birch, *J. Geophys. Res.* **57**, 227 (1952).
3. L. V. Altshuler, K. K. Krupnikov, B. N. Ledenev, V. I. Zhuchikhin, M. I. Brazhnik, *Zhur. Eksptl. i Teoret. Fiz.* **34**, 874 (1958).
4. A. M. Dziewonski, D. L. Anderson, *Phys. Earth Planet. Inter.* **25**, 297 (1981).
5. R. J. Hemley, H.-K. Mao, *Int. Geol. Rev.* **43**, 1 (2001).
6. D. Antonangeli et al., *Earth Planet. Sci. Lett.* **225**, 243 (2004).
7. H.-K. Mao et al., *Nature* **396**, 741 (1998).
8. L. Vočadlo, *Earth Planet. Sci. Lett.* **254**, 227 (2007).
9. A. Cao, B. Romanowicz, N. Takeuchi, *Science* **308**, 1453 (2005).
10. S. C. Singh, M. A. Taylor, J. P. Montagner, *Science* **287**, 2471 (2000).
11. B. A. Buffett, *Science* **288**, 2007 (2000).
12. I. Sumita, S. Yoshida, M. Kumazawa, Y. Hamano, *Geophys. J. Int.* **124**, 502 (1996).
13. W. Voigt, *Lehrbuch der Kristallographie* (Teubner, Leipzig, Germany, 1928).
14. C. Zener, *Phys. Rev.* **60**, 906 (1941).
15. A. B. Belonoshko, R. Ahuja, B. Johansson, *Phys. Rev. Lett.* **84**, 3638 (2000).
16. A. B. Belonoshko, R. Ahuja, B. Johansson, *Nature* **424**, 1032 (2003).
17. L. Kočič, A. B. Belonoshko, R. Ahuja, *Phys. Rev. B* **73**, 224113 (2006).
18. G. Kresse, J. Furthmüller, *Comput. Mater. Sci.* **6**, 15 (1996).
19. A. B. Belonoshko, E. I. Isaev, N. V. Skorodumova, B. Johansson, *Phys. Rev. B* **74**, 214102 (2006).
20. L. Vočadlo et al., *Nature* **424**, 536 (2003).
21. O. H. Nielsen, R. M. Martin, *Phys. Rev. Lett.* **50**, 697 (1983).
22. Y. Le Page, P. Saxe, *Phys. Rev. B* **65**, 104104 (2002).
23. Y.-S. Seo, Y. Ichikawa, K. Kawamura, *Mater. Sci. Res. Int.* **5**, 13 (1999).
24. S. R. Phillpot, D. Wolf, *J. Appl. Phys.* **78**, 847 (1995).
25. J. Schiøtz, T. Vegge, F. D. Di Tolla, K. W. Jacobsen, *Phys. Rev. B* **60**, 11971 (1999).
26. H. Van Swygenhoven, P. M. Derlet, A. G. Froseth, *Nat. Mater.* **3**, 399 (2004).
27. D. J. Stevenson, *Science* **214**, 611 (1981).
28. A. B. Belonoshko, R. Ahuja, B. Johansson, *Phys. Rev. Lett.* **87**, 165505 (2001).
29. E. O. Hall, *Proc. Phys. Soc. B* **64**, 747 (1951).
30. The authors thank G. Kresse for providing the Vienna Ab Initio Simulation Package, B. Smith and I. Todorov for the DL_POLY package, and K. Kadav for the MD_render package. L. Vočadlo kindly provided her paper before publication. Computations have been performed at the Parallel Computer Center in Stockholm and at the National Supercomputing Center in Linköping. The study was supported by the Swedish Research Council, the Foundation for Strategic Research, and the Royal Swedish Academy of Sciences.

Fig. 2. Relaxation of the sheared iron samples: (A) G and (B) V_s . Different colors are used to distinguish between different samples and ways of the shearing (where d is the shift of the upper side relative to the bottom side): blue, $d = 5.0 \text{ \AA}$ for the M sample (Fig. 1A) and xy plane at $T = 6800 \text{ K}$; brown, $d = 5.0 \text{ \AA}$ for the M sample and xy plane at $T = 6000 \text{ K}$; red, $d = 5.0 \text{ \AA}$ for the M sample and xz plane at $T = 6800 \text{ K}$; green, $d = 5.0 \text{ \AA}$ for the ideal bcc crystal and xy plane at $T = 6800 \text{ K}$; and magenta, $d = 1.0 \text{ \AA}$ for the V sample (Fig. 1C) and xy plane at $T = 6800 \text{ K}$.



15 February 2007; accepted 1 May 2007
10.1126/science.1141374

Frequent Long-Distance Plant Colonization in the Changing Arctic

Inger Greve Alsos,^{1,†} Pernille Bronken Eidesen,¹ Dorothee Ehrich,¹ Inger Skrede,¹ Kristine Westergaard,^{1,2} Gro Hilde Jacobsen,¹ Jon Y. Landvik,³ Pierre Taberlet,⁴ Christian Brochmann¹

The ability of species to track their ecological niche after climate change is a major source of uncertainty in predicting their future distribution. By analyzing DNA fingerprinting (amplified fragment-length polymorphism) of nine plant species, we show that long-distance colonization of a remote arctic archipelago, Svalbard, has occurred repeatedly and from several source regions. Propagules are likely carried by wind and drifting sea ice. The genetic effect of restricted colonization was strongly correlated with the temperature requirements of the species, indicating that establishment limits distribution more than dispersal. Thus, it may be appropriate to assume unlimited dispersal when predicting long-term range shifts in the Arctic.

Climate warming (1) is expected to cause the distribution area of many plant species to shift northward in the Northern Hemisphere (Fig. 1). The composition of future ecosystems will critically depend on the long-distance dispersal capabilities of individual species (2–4). Because long-distance dispersal is supposed to be rare and stochastic, quantification of it poses a considerable challenge (5–8). Models that are used to forecast climate change-induced shifts in species distribution commonly assume that dispersal is unlimited (9, 10), although restricted dispersal may prevent species from filling their climatic niche (11, 12). Thus, it is important to determine whether species will be able to track their climatic niche. In this study, we used genetic data to reconstruct past plant colonization patterns in the Arctic. In particular, we determined the frequency of effective long-distance dispersal events, identified the source areas, and assessed whether dispersal ability is more limiting than establishment in a new area.

The Svalbard Archipelago (Fig. 2) is a good model system in which to study long-distance dispersal in the Arctic because of its remote location and geological history. The islands were almost entirely glaciated during the last glacial maximum 20,000 years before the present (yr B.P.) (13, 14). It has been debated whether any of Svalbard's flora survived in local refugia (15, 16). Recently, genetic studies have indicated that colonization occurred after the glacial retreat (15, 16). This is in accord with recent reconstructions (13), which suggest an

extreme ice cover that excluded glacial survival of most, if not all, species. Paleorecords show a sparse arctic vegetation subsequent to 10,000 yr B.P., and pollen and marine mollusc data indicate that the climate was 1° to 2°C warmer than today from 9500 to 4000 yr B.P. (17). This warm period probably facilitated colonization of the most thermophilous species occurring in Svalbard today.

We analyzed 4439 samples from most of the geographic ranges of nine plant species native to the Arctic, representing the major climatic and dispersal adaptations found in the region, for amplified fragment-length polymorphism (AFLP) (Table 1) (18). To determine the geographic structure of the genetic variation, we used Bayesian clustering analyses, ordination, and tree-building algorithms. The most likely source regions for the plants from Svalbard were determined with multilocus assignment tests. The genetic effect of restricted colonization was quantified by combining six genetic measures. The minimum number of colonizing propagules was estimated as the smallest possible subsample of the source populations needed to bring all observed AFLP markers to Svalbard (18).

We found that colonization of Svalbard has occurred from all possible adjacent source regions (Fig. 2), suggesting that future colonization from the same regions can be expected. We observed a variety of species-specific patterns, as typically found in comparative phylogeography (19). Notably, the predominant source was the most distant region, northwestern Russia. Colonization from Scandinavia was rare; only *Salix herbacea* appears to have derived mainly from this region (Fig. 2). However, the single Russian population of *S. herbacea* that we analyzed belonged to the same genetic group as the northern Scandinavian populations, and colonization from the east could not be excluded even for this species.

In eight of the nine species, multiple propagules were necessary to bring the observed genetic diversity to Svalbard (Table 1; *Arabis alpina* was virtually invariable in the North

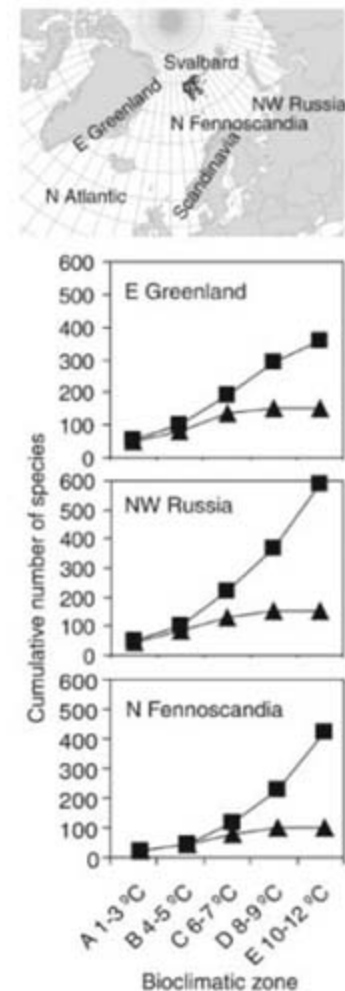


Fig. 1. Number of species that may colonize the geographically isolated Svalbard archipelago (map) from adjacent land masses after climate warming. The graphs show cumulative number of species in successively warmer bioclimatic zones in the source regions (squares) and the cumulative number of these species that are present in Svalbard today (triangles) (18). Mean July temperature is given for each bioclimatic zone. Most of Svalbard's current flora belong to zones A to C. A summer temperature increase of 2° to 4°C (1) could shift Svalbard toward zones D and E. The gap between the lines at bioclimatic zone D and E shows high potential numbers of colonizing species.

Atlantic region). We estimated that a minimum number of 6 to 38 plants of each species must have successfully established and survived in Svalbard, implying that many more propagules actually reached the archipelago (18). In addition to the main source region, the allocation tests (Fig. 2) and the geographic distribution of the AFLP markers (not shown) indicated supplementary source regions for six species. The most hardy species, which are adapted to mean July temperatures of 4° to 5°C or colder (*Dryas octopetala*, *Salix herbacea*, *Cassiope tetragona*, and *Saxifraga rivularis*), were allocated to several source regions and had the highest estimates of colonizing propagules. In these species, the level of genetic diversity in Svalbard was similar to that in the primary source regions (Table 1). More than one source

¹National Centre for Biosystematics, Natural History Museum, University of Oslo, Post Office Box 1172 Blindern, NO-0318 Oslo, Norway. ²Tromsø University Museum, University of Tromsø, NO-9037 Tromsø, Norway. ³Norwegian University of Life Sciences, Post Office Box 5003, NO-1432 Ås, Norway. ⁴Laboratoire d'Ecologie Alpine, CNRS UMR 5553, Université Joseph Fourier, Post Office Box 53, F-38041 Grenoble Cedex 09, France.

[†]To whom correspondence should be addressed. E-mail: ingera@unis.no

[†]Present address: The University Centre in Svalbard, Post Office Box 156, NO-9171 Svalbard, Norway.

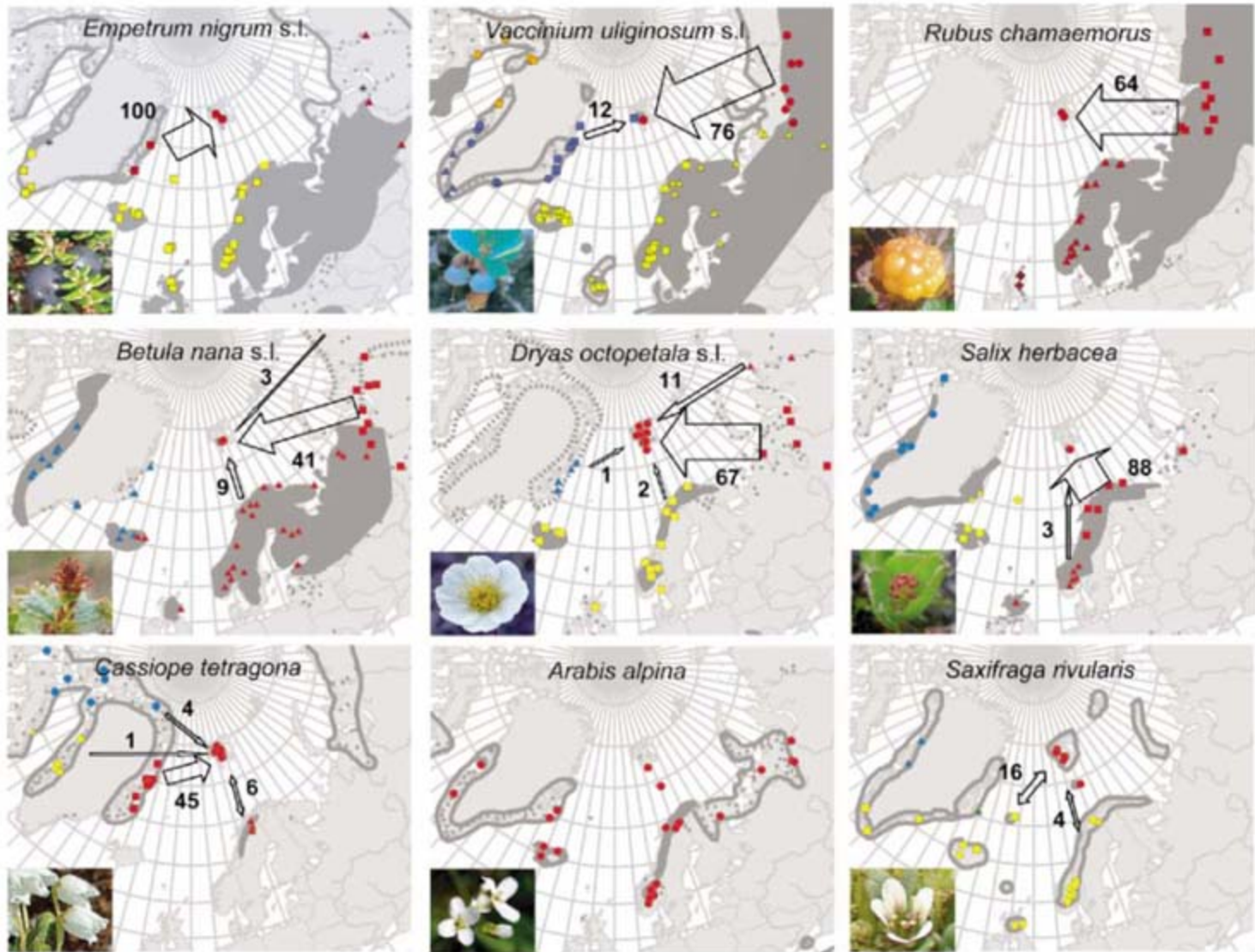


Fig. 2. Source regions for past colonization of Svalbard inferred from genetic data (AFLP). The geographic distribution of the species (23, 24) is shaded, and the distribution of closely related species is indicated by dotted lines (*Betula exilis* and *Dryas integrifolia*). Colors represent main genetic groups and symbols represent subgroups. Asterisks indicate a population that could not be clearly placed into a genetic group (*E. nigrum*). Numbers on the arrows indicate the percentage allocation when a log-likelihood difference of 1 was used (10 times as likely from that source region as from any other source

regions). For *C. tetragona*, the direction of dispersal between Svalbard and Scandinavia is uncertain because of low diversity in Scandinavia. The source for the Svalbard populations of *A. alpina* could not be determined because of lack of genetic variation. In *S. rivularis*, the highest levels of genetic variation and most private markers were observed in the Svalbard populations (Table 1), which also were clearly separated from the two ampho-Atlantic genetic groups. Thus, survival in Svalbard during the last glacial maximum cannot be excluded for this high-arctic species.

region was also found in two of the rarest and most thermophilous species in Svalbard, *Betula nana* and *Vaccinium uliginosum*.

The genetic effect of restricted colonization of Svalbard was negatively correlated with adaptation to the current climate in Svalbard (Fig. 3), suggesting that dispersal itself may not be the limiting factor. The establishment phase—involving germination, survival, and local reproduction—is more likely to be the limiting process. This interpretation is supported by our observation that 80 to 90% of the most cold-adapted species that occur in the potential source regions are currently present in Svalbard, whereas only 40 to 60% of the species limited to bioclimatic zone C (6° to 7° C July temperature) are present in Svalbard (Fig. 1).

Probable dispersal vectors are wind (which may have carried propagules through the air or over snow and sea ice), drift wood and drifting

sea ice, birds, and mammals (3, 5, 8, 20, 21). In contrast to Scandinavia, northwestern Russia and Greenland are frequently connected to Svalbard by way of sea ice during winter. Dispersal from Russia may have been facilitated by drift wood. Bank erosion along the Russian rivers routinely results in logs and other debris finding their way onto drifting sea ice, which reaches Svalbard by means of surface currents (20).

The recurrent glacial cycles have probably selected for a highly mobile arctic flora. In addition, some dispersal vectors may be particularly efficient in the Arctic as a result of the open landscape, strong winds, and extensive snow and ice cover. The high levels of genetic diversity found in several species previously studied in Svalbard are also consistent with multiple dispersals, although the sampling design and genetic methods used did not allow estimation of the frequency or source areas (16, 22). Given that

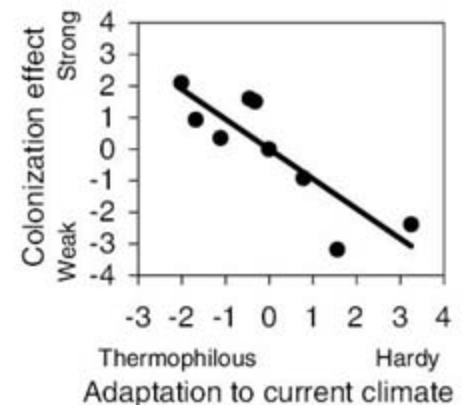


Fig. 3. Index of the genetic effect of restricted colonization of Svalbard for the nine species analyzed compared with an index of adaptation to the current climate in Svalbard. The axes are principal components summarizing three measures of climatic adaptations (Table 1) and six quantities related to the effect of restricted colonization based on genetic data (AFLP) (18).

Table 1. Characteristics of the species analyzed and AFLP data. The northernmost bioclimatic zone where the species is frequent (f) or scattered (s) is given according to the checklist in Elven *et al.* (24). B, Northern Arctic tundra zone; C, Middle Arctic tundra zone; D, Southern Arctic tundra zone. The relative rarity—i.e., how much rarer the species is in Svalbard compared with the abundance reached in its optimal habitat—

is based on our own observations (1 = rare and 6 = abundant). The minimum number of propagules that colonized Svalbard, genetic diversity (D) (\pm standard deviation), and differentiation (Φ_{ST}) within Svalbard and between Svalbard, and the most important source region (compare with Fig. 2) are calculated based on the AFLP data. For *S. rivularis*, two data sets were analyzed (18).

	<i>Empetrum nigrum</i> L. s.l.	<i>Vaccinium uliginosum</i> L. s.l.	<i>Rubus chamaemorus</i> L.	<i>Betula nana</i> L. s.l.	<i>Dryas octopetala</i> L. s.l.	<i>Salix herbacea</i> L.	<i>Cassiope tetragona</i> (L.) D. Don ssp. <i>tetragona</i>	<i>Arabis alpina</i> L.	<i>Saxifraga rivularis</i> L.
Main dispersal vector	Bird	Bird	Bird	Wind	Wind	Wind	Wind?	Wind?	Wind?
Northernmost bioclimatic zone	C (s)	C (s)	D (f)	D (f)	C (f)	C (s)	C (f)	C (f)	B (f)
Minimum mean July temperature (°C) (25)	5 to 6	5 to 6	6 to 7?	6 to 7	3 to 4	4 to 5	4 to 5	5 to 6	<3
Relative rarity in Svalbard	3	1	1	2	5	3	4	2	6
Germinable seeds or seed banks in Svalbard (26)	No data	Not found	No data	Not found	Only in warmest sites	No data	Rare	No data	Abundant
No. of populations analyzed (Svalbard)	46 (4)	131 (3)	45 (2)	71 (5)	72 (21)	41 (3)	58 (12)	36 (2)	32/22 (8)
No. of individuals analyzed (Svalbard individuals/genets)	435 (38/32)	957 (26/17)	398 (15/14)	570 (32/29)	528 (161)	399 (33/32)	579 (132)	305 (10)	268/207(72)
No. of polymorphic markers (private Svalbard)	78 (0)	105 (0)	173 (0)	119 (1)	155 (1)	250 (1)	171 (1)	242 (0)	45 (2) / 78 (8)
AFLP reproducibility % (no. of controls)	97.7 (30)	97.7 (44)	97.8 (63)	98.0 (51)	99.1 (32)	98.0 (41)	99.3 (23)	99.0 (42)	97.3 (104) / 95.0 (40)
Minimum no. of colonizing propagules	7	12	6	11	38	20	14	1	22
D Svalbard (average per population)	0.049 \pm 0.017	0.066 \pm 0.044	0.060 \pm 0.019	0.103 \pm 0.016	0.089 \pm 0.025	0.104 \pm 0.007	0.125 \pm 0.010	0.000	0.122 \pm 0.074
D main source region (average per population)	0.118 \pm 0.032	0.174 \pm 0.020	0.126 \pm 0.011	0.148 \pm 0.013	0.106 \pm 0.017	0.142 \pm 0.015	0.133 \pm 0.011	0.001 \pm 0.002	0.061 \pm 0.024
Φ_{ST} within Svalbard	0.275	0.696	0.272	0.161	0.151	0.188	0.167	—	0.483
Φ_{ST} Svalbard—main source region	0.147	0.049	0.109	0.113	0.157	0.110	0.013	0.000	0.211

the dispersal mechanisms in existence during the early and mid-Holocene are probably still operating today, we can assume that long-distance dispersal still occurs with regularity. Thus, we concluded that arctic species seem to be able to track their potential niche and that unlimited dispersal models (9, 10) may be appropriate to estimate long-term range shifts for arctic regions.

References and Notes

1. ACIA, *Arctic Climate Impact Assessment: Scientific Report* (Cambridge Univ. Press, Cambridge, 2006).
2. M. L. Cain, B. G. Milligan, A. E. Strand, *Am. J. Bot.* **87**, 1217 (2000).
3. S. I. Higgins, R. Nathan, M. L. Cain, *Ecology* **84**, 1945 (2003).
4. T. V. Callaghan *et al.*, *Ambio* **33**, 404 (2004).
5. R. Nathan, *Science* **313**, 786 (2006).

6. R. Nathan, G. Perry, J. T. Cronin, A. E. Strand, M. L. Cain, *Oikos* **103**, 261 (2003).
7. S. I. Higgins *et al.*, *J. Ecol.* **91**, 341 (2003).
8. R. P. Neilson *et al.*, *Bioscience* **55**, 749 (2005).
9. W. Thuiller, S. Lavorel, M. B. Araujo, M. T. Sykes, I. C. Prentice, *Proc. Natl. Acad. Sci. U.S.A.* **102**, 8245 (2005).
10. A. Guisan, W. Thuiller, *Ecol. Lett.* **8**, 993 (2005).
11. J.-C. Svenning, F. Skov, *Ecol. Lett.* **7**, 565 (2004).
12. K. A. Moore, S. C. Elmendorf, *Ecol. Lett.* **9**, 797 (2006).
13. J. Y. Landvik *et al.*, *Quat. Sci. Rev.* **17**, 43 (1998).
14. J. Y. Landvik *et al.*, *Geology* **31**, 905 (2003).
15. O. I. Rønning, in *North Atlantic Biota and Their History*, Å. Löve, D. Löve, Eds. (Pergamon Press, Oxford, 1963), pp. 99–107.
16. C. Brochmann, T. M. Gabrielsen, I. Nordal, J. Y. Landvik, R. Elven, *Taxon* **52**, 417 (2003).
17. H. H. Birks *et al.*, *J. Quat. Sci.* **9**, 133 (1994).
18. Materials and methods are available as supporting material on Science Online.
19. P. Taberlet, L. Fumagalli, A. G. Wust-Saucy, J. F. Cosson, *Mol. Ecol.* **7**, 453 (1998).

20. S. Johansen, H. Hytteborn, *J. Biogeogr.* **28**, 105 (2001).
21. R. Nathan *et al.*, *Nature* **418**, 409 (2002).
22. R. J. Abbott *et al.*, *Science* **289**, 1343 (2000).
23. E. Hultén, M. Fries, *Atlas of North European Vascular Plants North of the Tropic of Cancer* (Koeltz Scientific Books, Königstein, Germany, 1986).
24. R. Elven, D. F. Murray, V. Razzhivin, B. A. Yurtsev, *Checklist of the Panarctic Flora (PAF): Vascular Plants* (Univ. of Oslo, Oslo, Norway, 2005).
25. S. R. Karlsen, A. Elvebakk, *J. Biogeogr.* **30**, 1469 (2003).
26. E. J. Cooper *et al.*, *J. Veg. Sci.* **15**, 115 (2004).
27. We thank our many colleagues and field assistants (table S1) for help with providing plant samples; the authorities in various regions for collection permits and help with field logistics; L. G. Kvernstuen for laboratory assistance; B. E. Sandbakk for photographs; A. Tribsch, P. Schönswetter, R. Elven, and L. Bachmann for discussions; and W. Thuiller, I. Till-Bottraud, K. Kovacs, and three anonymous referees for valuable comments on the manuscript. Part of the material was obtained by means of the Tundra North-West (TNW) 1999 and the

Beringia 2005 expeditions funded by the Polar Research Secretariat at the Royal Swedish Academy of Sciences. The main work was funded by grant 150322/720 to Brochmann from the Research Council of Norway. Additional grants to Westergaard were obtained from K. and H. Jakobsens Fund, King Haakon VII Educational

Fund, Roald Amundsen's Centre for Arctic Research, KOMETEN, and Tromsø University Museum.

Tables S1 and S2
References

Supporting Online Material

www.sciencemag.org/cgi/content/full/316/5831/1606/DC1
Materials and Methods

22 December 2006; accepted 2 May 2007
10.1126/science.1139178

Modulation of Neuronal Interactions Through Neuronal Synchronization

Thilo Womelsdorf,^{1*†} Jan-Mathijs Schoffelen,^{1*†} Robert Oostenveld,¹ Wolf Singer,^{2,3} Robert Desimone,^{4,5} Andreas K. Engel,⁶ Pascal Fries^{1,7}

Brain processing depends on the interactions between neuronal groups. Those interactions are governed by the pattern of anatomical connections and by yet unknown mechanisms that modulate the effective strength of a given connection. We found that the mutual influence among neuronal groups depends on the phase relation between rhythmic activities within the groups. Phase relations supporting interactions between the groups preceded those interactions by a few milliseconds, consistent with a mechanistic role. These effects were specific in time, frequency, and space, and we therefore propose that the pattern of synchronization flexibly determines the pattern of neuronal interactions.

Groups of activated neurons synchronize in the gamma-frequency band (30 to 100 Hz), and previous studies have related gamma-band synchronization to several cognitive functions (1–6). Yet, if gamma-band synchronization subserves those functions, it must have mechanistic consequences for neuronal processing (7). It has been shown that the precise timing of pre- and postsynaptic activation determines long-term changes in synaptic strength (8–10) and that gamma-band synchronization of synaptic inputs directly enhances their effective synaptic strength (11–13).

Synchronization between two groups of neurons is also likely to facilitate interactions between them (Fig. 1A) (6, 14). Gamma-band synchronization entails rhythmic inhibition of the local network (15–17), and the periods between inhibition provide temporal windows for neuronal interaction. Two groups of neurons will therefore probably have a greater influence on each other when their temporal interaction windows open at the same times, i.e., when the

rhythmic synchronization within the groups is also synchronized between the groups. By the same token, the interaction is probably curtailed if the temporal interaction windows open either in an uncorrelated way or consistently out of phase with each other.

We analyzed four data sets: (i) one from awake cat area 17, (ii) one combining awake cat area 18 with area 21a recordings, (iii) one from awake monkey area V1, and (iv) one from monkey area V4. [Data from two of the three area 17 data sets have been used in (18, 19); the V4 data set has been used in (3, 20).] In all cases, we recorded multiunit activity (MUA) and local field potentials (LFPs) simultaneously from four to eight electrodes while the neurons were visually stimulated with moving gratings. From each data set, we used trials with identical visual stimulation and behavioral tasks and based our analysis on the natural fluctuation of neuronal gamma-band synchronization. For each pair of neuronal groups, we quantified synchronization by means of the MUA-MUA phase-coherence spectrum (Fig. 1B) and the MUA-LFP phase-coherence spectrum (Fig. 1C) (21).

Phase-coherence spectra showed a peak in the gamma-frequency band, indicating that phase relations between signals were not random. However, phase coherence was far from perfect (a value of 1.0), but it assumed average peak values of 0.14 and 0.27 for MUA-MUA and MUA-LFP combinations, respectively. The phase relations at 60 Hz in one example MUA-MUA pair are shown for 708 trials of 250-ms length (phase-coherence value of 0.06) (Fig. 1D).

The spread of phase relations around their mean might just be irrelevant noise. Here, however, we used this spread to actually test for its potential physiological consequences. We hypothesized that the mutual influence between two

neuronal groups was a function of their phase relation (Fig. 1A). Phase relations are meaningfully defined per frequency, and we hypothesized that the phase relation at a given frequency should modulate the interaction among the local rhythmic activities specifically at that frequency.

We investigated this hypothesis for the example pair of recordings sites. We sorted the trials into six bins according to the 60-Hz phase relation between the two MUAs (Fig. 1D). For each phase-relation bin separately, we then quantified the two MUAs' mutual influence as the Spearman rank correlation coefficient between the two MUAs' 60-Hz power, across the trials in the bin (Fig. 1E). Fluctuations of 60-Hz power were most strongly correlated when the 60-Hz phase relation was close to its mean across the trials. Specifically, when the gamma-band rhythm in group A led the one in group B by 2.1 ms (mean phase relation at 45.8°), the correlation between each group's gamma-band power was four times as strong as when the rhythms were separated by 10.5 ms (phase relation at 225.8°). The example pair illustrates this for a case with a nonzero mean phase to demonstrate that the effect cannot be ascribed to external artifacts or volume conduction, but the mean phase relations across our sample distributed closely around zero (Fig. 1B).

We performed the same analysis after replacing one of the MUAs by the LFP recorded through the same electrode. The mean MUA-LFP phase relations clustered around 141° (Fig. 1C), and power correlations were again substantially enhanced around the mean phase relation (Fig. 1, F and G). Across our sample, good phase relations mostly distributed close to the respective mean phase relations for both MUA-MUA and MUA-LFP pairs (fig. S1). We correspondingly dubbed the mean phase relation as "good" and the opposite phase relation as "bad," and we aligned the trial binning to the good phase relation.

The observed effect was consistent across the four data sets (Fig. 2 and fig. S2) (140, 86, 111, and 111 MUA-MUA pairs from area 17, areas 18×21a, area V1, and area V4, respectively, and 280, 172, 228, and 237 MUA-LFP pairs from the same areas). MUA-LFP pairs showed qualitatively the same effect as MUA-MUA pairs but with higher signal-to-noise ratios (Fig. 2B). We therefore focused our further analyses on MUA-LFP pairs (recorded from separate electrodes). The effect was also present for pairs of LFP and single-unit recordings (fig. S3). The effect generalized to long-range interactions, because the analysis of the data set combining cat area

¹F. C. Donders Centre for Cognitive Neuroimaging, Radboud University Nijmegen, 6525 EN Nijmegen, Netherlands.

²Department of Neurophysiology, Max Planck Institute for Brain Research, 60528 Frankfurt, Germany. ³Frankfurt Institute for Advanced Studies, Johann Wolfgang Goethe University, 60438 Frankfurt, Germany. ⁴Laboratory of Neuropsychology, National Institute of Mental Health, National Institutes of Health, Bethesda, MD 20892, USA.

⁵McGovern Institute for Brain Research, Massachusetts Institute of Technology, Cambridge, MA 02139, USA.

⁶Department of Neurophysiology and Pathophysiology, University Medical Center Hamburg-Eppendorf, 20246 Hamburg, Germany. ⁷Department of Biophysics, Radboud University Nijmegen, 6525 EZ Nijmegen, Netherlands.

*These authors contributed equally to this work.

†To whom correspondence should be addressed. E-mail: thilo.womelsdorf@fcdonders.ru.nl (T.W.); jan.schoffelen@fcdonders.ru.nl (J.-M.S.)

18 recordings with area 21a recordings was restricted to interareal pairs of recording sites (Fig. 2D).

We did not attempt to relate the two signals' power correlation to their coherence, because

the coherence measure confounds phase synchronization and power correlation. In contrast, we related the correlation between the two signals' power across trials directly to their relative phase. The presence of coherence (Fig. 1H)

does not necessarily result in a phase-relation-dependent power correlation (Fig. 1I) and thus, the demonstration of phase-relation-dependent power correlation goes beyond the demonstration of coherence.

Fig. 1. Precise timing between rhythmic neuronal activities determines the strength of their mutual influence. (A) Sketch of three groups of neurons, each rhythmically active (LFP oscillations with spikes in troughs). Time windows for effective communication are either aligned (red and blue group) or not aligned (red and gray group). (B and C) Average phase-coherence spectrum across all (B) MUA-MUA and (C) MUA-LFP pairs (area 17 data) and corresponding distributions of mean phase relations at 60 Hz. (D) Trialwise phase relations from an example MUA-MUA pair. Phase relations were sorted into bins (light and dark gray ring segments) aligned to the mean phase relation (red line). (E) Spearman rank correlation coefficients between the two MUAs' 60-Hz power as a function of their phase relation. (The solid line indicates a cosine fit.) (F and G) Same as (D) and (E), but with one MUA substituted by the respective LFP. (H and I) Example MUA-LFP pair from the area 17 data set demonstrating that coherence does not necessarily result in phase-relation-dependent power correlations. (H) Coherence with a clear peak around 60 Hz. (I) Power correlations as a function of phase relations, showing no consistent relation.

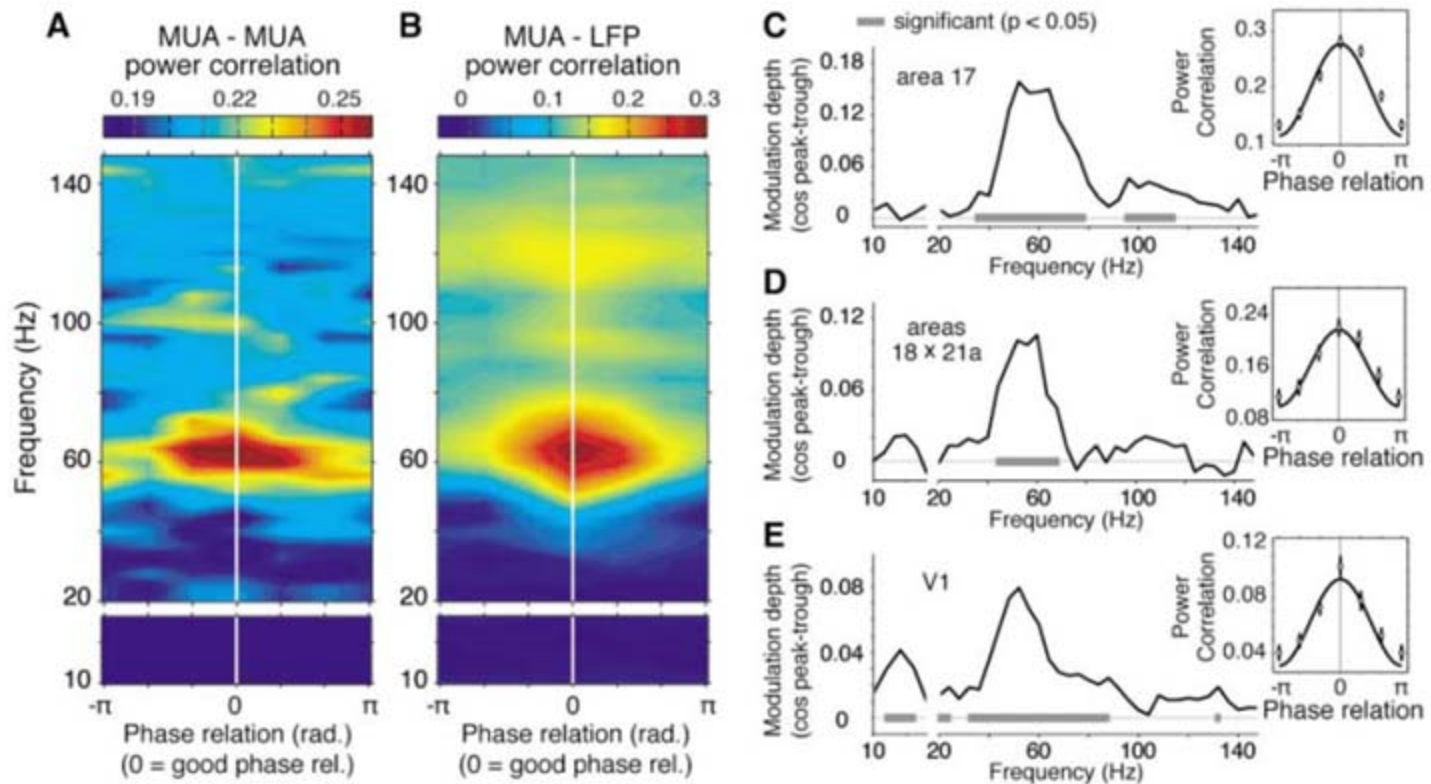
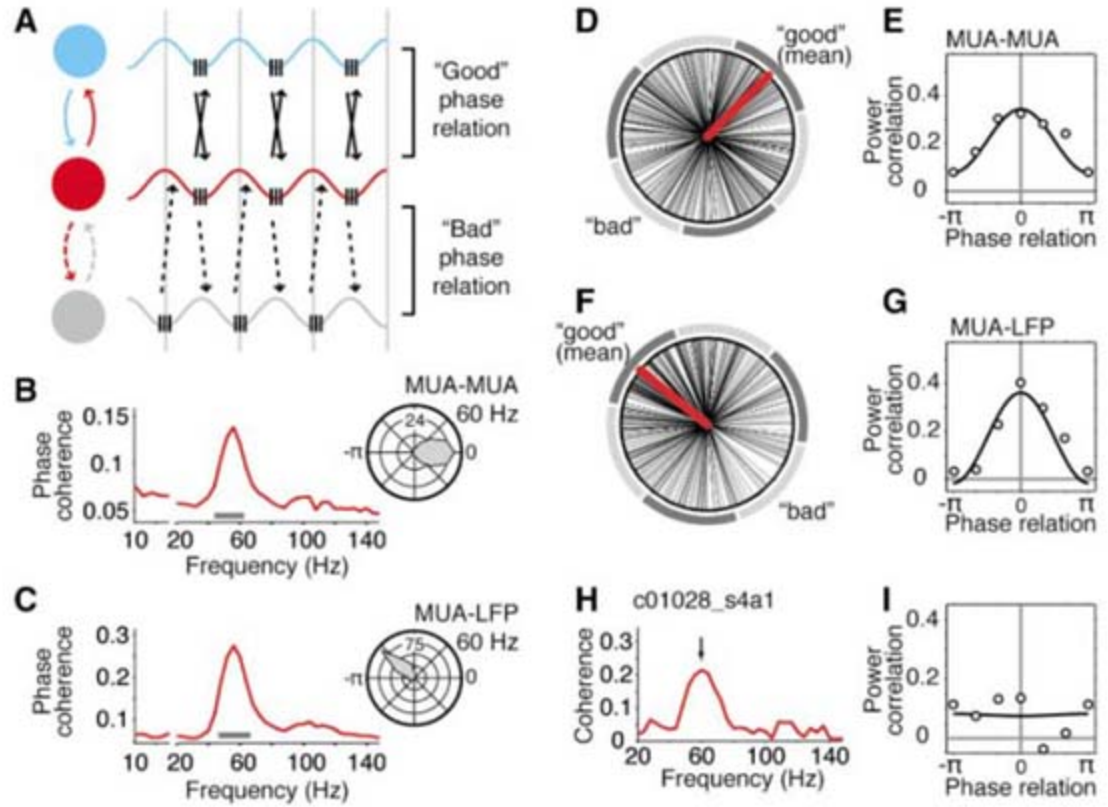


Fig. 2. Phase-relation-dependent modulation of power correlations is frequency specific. (A) Average power correlation as a function of phase relation (x axis) and frequency (y axis) for MUA-MUA pairs recorded in cat area 17. (B) Same as (A), but for MUA-LFP pairs. (C) Modulation depth of the cosine function

fitted to the phase-relation-dependent power correlations. Gray bars indicate significant frequencies ($P < 0.05$, multiple comparisons corrected). (Right) Average phase-relation-dependent power correlation at 60 Hz. (D and E) Same as (C), but for (D) cat area 18x21a and (E) monkey area V1.

One concern is that the effect might be due to rhythmic common input that fluctuates in strength across trials. Common input would bias phase relations and impose correlated power on both groups. Clues about the actual causal chain of events might be gained from the relative timing between phase relation, on one hand, and power correlation, on the other hand. If power correlation covaried with phase relation because of common input, then there should be no delay between the two. However, if good phase relations were actually the mechanistic cause of strong power correlations, then good phase relations should precede strong power correlations by a few milliseconds, incurred by axonal, synaptic, and intracellular delays. We therefore compiled time-resolved estimates of the “goodness” of phase relations and of the strength of power correlations, and then we determined the cross-correlation as a function of time lag between the two time series (21). Figure 3 shows this analysis pooled across all four data sets and demonstrates that good phase relations preceded strong power correlations by 5 ms. We

observed this temporal precedence in each of the four data sets. Additional observations arguing against a common input explanation are given in the supporting online material text.

The modulation of two neuronal groups’ interaction by their phase relation would be particularly interesting if it was spatially specific (Fig. 1A). We therefore investigated recording triplets A, B, and C from three separate electrodes (in which A was an LFP and B and C were MUAs). Figure 4A shows, for one example triplet, a scatter plot in which each dot corresponds to one trial and the *x* and *y* values give the “goodness” of the A-B and A-C phase relations, respectively (22). We sorted the trials according to the quadrants of the plot. In quadrants Q1 and Q2, the phase relation between A and B was good, whereas in Q3 and Q4 it was bad. We contrasted the A-B power correlation for Q1 and Q2 with that for Q3 and Q4 (red line in Fig. 4, B to D). Orthogonally to this, the phase relation between A and C was good in Q1 and Q3, whereas it was bad in Q2 and Q4, and we contrasted the A-B power correlation for Q1

and Q3 with that for Q2 and Q4 (blue line in Fig. 4, B to D). The A-B power correlation depended significantly more on the A-B phase relation than on the A-C phase relation. Thus, the effect had a spatial resolution that was at least as high as the spatial resolution of our recordings (down to 0.65 mm in the monkey data sets).

We provided evidence suggesting that neuronal interactions mechanistically depend on the phase relation between rhythmic activities. The most likely reason for this dependence is that rhythmic activities modulate the gain of incoming synaptic input rhythmically. Effective connectivity can thus be maximized or minimized through synchronization at a good or bad phase relation. The impact of pyramidal cells could be enhanced, for example, if their firing phase relative to interneurons were advanced (15, 23, 24) or if interneuronal firing were delayed through inhibition or reduced excitation (25). Such mechanisms might be invoked directly by cognitive top-down control.

Effective connectivity would diminish when synchronization is less precise, because then synaptic input is more likely to arrive at random phases. This mechanism has the advantage that within a sufficiently wide frequency band, multiple groups can be desynchronized, with respect to a given target group, without being necessarily synchronized to each other. Periods of putative interactions between distant neuronal groups are marked by an increased precision of synchronization (1, 4, 6, 26–30).

We propose that the pattern of synchronization (its precision, phase, or both) weights the anatomical-connection infrastructure with a gain pattern, resulting in an effective interaction pattern (14). Such a mechanism would have several

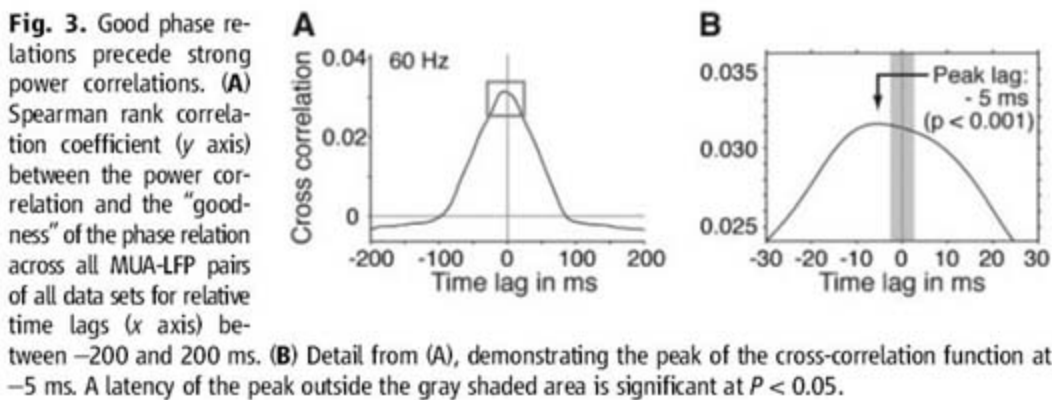


Fig. 3. Good phase relations precede strong power correlations. (A) Spearman rank correlation coefficient (*y* axis) between the power correlation and the “goodness” of the phase relation across all MUA-LFP pairs of all data sets for relative time lags (*x* axis) between –200 and 200 ms. (B) Detail from (A), demonstrating the peak of the cross-correlation function at –5 ms. A latency of the peak outside the gray shaded area is significant at *P* < 0.05.

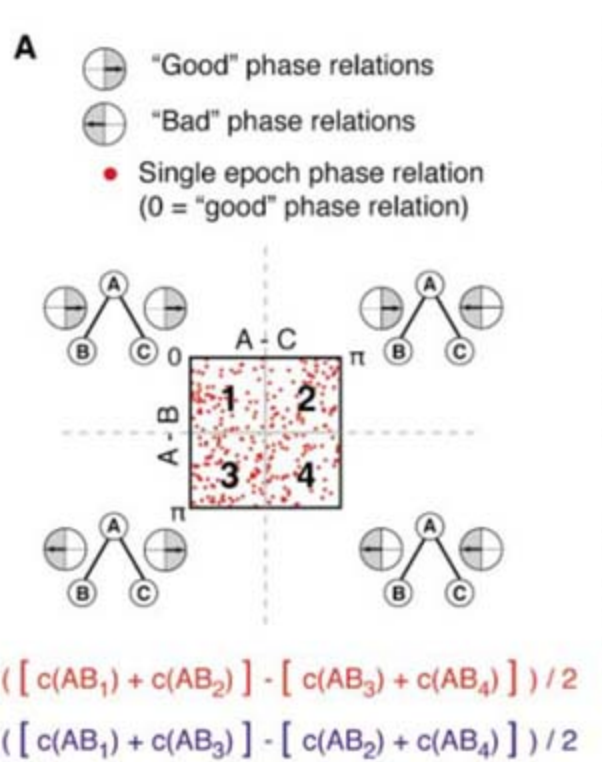
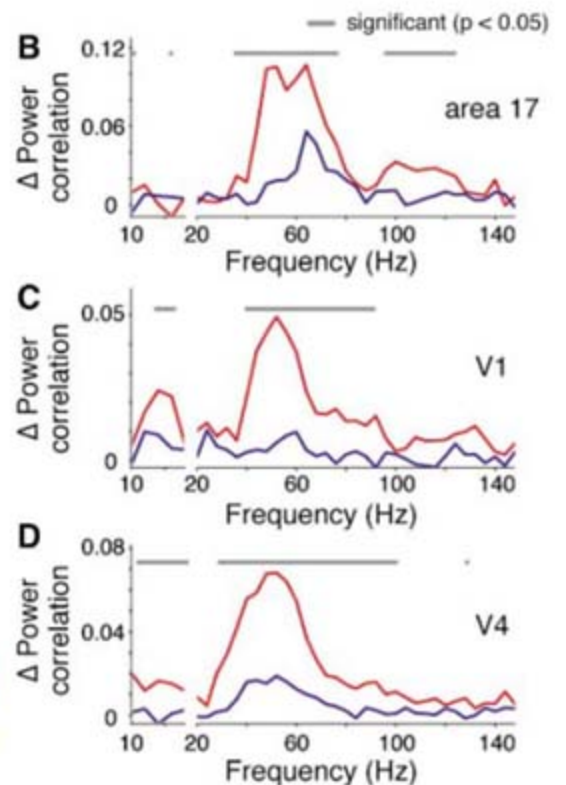


Fig. 4. Spatial selectivity of phase-relation-dependent power correlation. (A) Scatterplot shows the distribution of trialwise phase relations between groups A and B (*y* axis) and between groups A and C (*x* axis) for an example triplet at 60 Hz. Equations define how A-B power correlations from each quadrant were combined for the results shown in (B to D). In the equations, $c(AB_q)$ denotes the A-B power correlation across trials in quadrant *q* (where *q* is 1, 2, 3, or 4). (B) A-B power correlation as a function of the A-B phase relation [irrespective of the A-C phase relation (red line)] and as a function of the A-C phase relation [irrespective of the A-B phase relation (blue line)]. Gray bars indicate frequencies with significant differences (*P* < 0.05, multiple comparisons corrected). The *y* axis denotes the differences in power correlations according to the equations shown in (A). (C and D) Same as (B), but for (C) monkey area V1 and (D) monkey area V4.



interesting features. First, the effective interaction pattern could be modified very dynamically. Second, the mechanism would act connection-wise. Third, a transient interaction would lead to spike-time-dependent plasticity (8–10) and thus, a long-term trace. And fourth, synchronization might emerge in a self-organized manner between “matching” neuronal groups. In the visual cortex, synchronization is stronger among neurons activated by the same visual stimulus (1). This principle might generalize to the handshaking between cognitive top-down control and matching sensory bottom-up information, in which case consecutive synchronization could contribute to the selective routing of sensory information to behavioral control (13, 14, 25). Our results suggest that synchronization has consequences for neuronal interactions, providing a putative mechanism through which synchronization contributes to cognitive functions.

References and Notes

1. C. M. Gray, P. König, A. K. Engel, W. Singer, *Nature* **338**, 334 (1989).
2. A. Bragin et al., *J. Neurosci.* **15**, 47 (1995).
3. P. Fries, J. H. Reynolds, A. E. Rorie, R. Desimone, *Science* **291**, 1560 (2001).
4. J. Fell et al., *Nat. Neurosci.* **4**, 1259 (2001).
5. B. Pesaran, J. S. Pezaris, M. Sahani, P. P. Mitra, R. A. Andersen, *Nat. Neurosci.* **5**, 805 (2002).
6. J.-M. Schoffelen, R. Oostenveld, P. Fries, *Science* **308**, 111 (2005).
7. G. Buzsáki, *Rhythms of the Brain* (Oxford Univ. Press, Oxford, 2006).
8. H. Markram, J. Lübke, M. Frotscher, B. Sakmann, *Science* **275**, 213 (1997).
9. G. Q. Bi, M. M. Poo, *J. Neurosci.* **18**, 10464 (1998).
10. V. Wespapat, F. Tegnigkeit, W. Singer, *J. Neurosci.* **24**, 9067 (2004).
11. P. König, A. K. Engel, W. Singer, *Trends Neurosci.* **19**, 130 (1996).
12. R. Azouz, C. M. Gray, *Neuron* **37**, 513 (2003).
13. E. Salinas, T. J. Sejnowski, *Nat. Rev. Neurosci.* **2**, 539 (2001).
14. P. Fries, *Trends Cognit. Sci.* **9**, 474 (2005).
15. A. Hasenstaub et al., *Neuron* **47**, 423 (2005).
16. I. Vida, M. Bartos, P. Jonas, *Neuron* **49**, 107 (2006).
17. M. Bartos, I. Vida, P. Jonas, *Nat. Rev. Neurosci.* **8**, 45 (2007).
18. P. Fries, P. R. Roelfsema, A. K. Engel, P. König, W. Singer, *Proc. Natl. Acad. Sci. U.S.A.* **94**, 12699 (1997).
19. P. Fries, J. H. Schröder, P. R. Roelfsema, W. Singer, A. K. Engel, *J. Neurosci.* **22**, 3739 (2002).
20. T. Womelsdorf, P. Fries, P. P. Mitra, R. Desimone, *Nature* **439**, 733 (2006).
21. Materials and methods are available as supporting material on Science Online.
22. Positive and negative departures from the good phase relation toward the bad phase relation were pooled because our previous analyses had demonstrated symmetric effects in both directions.
23. P. König, A. K. Engel, P. R. Roelfsema, W. Singer, *Neural Comput.* **7**, 469 (1995).
24. J. Csicsvari, B. Jamieson, K. D. Wise, G. Buzsáki, *Neuron* **37**, 311 (2003).
25. J. Mishra, J. M. Fellous, T. J. Sejnowski, *Neural Networks* **19**, 1329 (2006).
26. A. K. Engel, A. K. Kreiter, P. König, W. Singer, *Proc. Natl. Acad. Sci. U.S.A.* **88**, 6048 (1991).
27. G. Buzsáki, Z. Horváth, R. Urioste, J. Hetke, K. Wise, *Science* **256**, 1025 (1992).
28. P. R. Roelfsema, A. K. Engel, P. König, W. Singer, *Nature* **385**, 157 (1997).
29. C. Tallon-Baudry, S. Mandon, W. A. Freiwald, A. K. Kreiter, *Cereb. Cortex* **14**, 713 (2004).
30. J. Gross et al., *Proc. Natl. Acad. Sci. U.S.A.* **101**, 13050 (2004).
31. We thank P. König, P. R. Roelfsema, and J. H. Schröder for help during the cat experiments and J. H. Reynolds, A. E. Rorie, and A. F. Rossi for help during the monkey experiments. This work was supported by the Human Frontier Science Program and the Netherlands Organization for Scientific Research (P.F.); the Volkswagen Foundation (A.K.E. and P.F.); the Max Planck Society (P.F., A.K.E., and W.S.); European Union grants EU IST-027268 and EU NEST-043457 (A.K.E.); and NIH grant R01EY017292 and the National Institute of Mental Health–Intramural Research Program (R.D.).

Supporting Online Material

www.sciencemag.org/cgi/content/full/316/5831/1609/DC1

Materials and Methods

SOM Text

Figs. S1 to S6

References

5 January 2007; accepted 1 May 2007

10.1126/science.1139597

Neural Mechanisms of Visual Attention: How Top-Down Feedback Highlights Relevant Locations

Yuri B. Saalmann,¹ Ivan N. Pigarev,² Trichur R. Vidyasagar^{1*}

Attention helps us process potentially important objects by selectively increasing the activity of sensory neurons that represent the relevant locations and features of our environment. This selection process requires top-down feedback about what is important in our environment. We investigated how parietal cortical output influences neural activity in early sensory areas. Neural recordings were made simultaneously from the posterior parietal cortex and an earlier area in the visual pathway, the medial temporal area, of macaques performing a visual matching task. When the monkey selectively attended to a location, the timing of activities in the two regions became synchronized, with the parietal cortex leading the medial temporal area. Parietal neurons may thus selectively increase activity in earlier sensory areas to enable focused spatial attention.

Attention allows us to engage with our environment by selecting information relevant for behavior (1–3). This enables preferential processing of particular locations in the visual field or specific features of objects. Attention maintained on a location is usually referred to as spatial attention and that on a

feature as feature-based attention (4, 5). Both types of attention manifest in visual cortical areas as increased activity of neurons representing the attended location or feature and reduced activity of other neurons (6–14). This may require top-down feedback about what is relevant in the environment; however, such feedback has not been empirically demonstrated. There is evidence (6, 11, 15–17) that the posterior parietal cortex (PPC) is critical for spatial attention. The PPC is a higher-order structure along the dorsal stream of visual areas (Fig. 1A), which are particularly concerned with spatial aspects of a scene. It has been suggested that the spatial information about

a scene extracted by the PPC forms the basis for feedback signals to earlier levels of the visual pathway, highlighting spatial locations of potential interest (18, 19) and gating responses depending upon the state of attention.

We simultaneously measured the activity in a part of the macaque PPC called the lateral intraparietal area (LIP), and the immediately earlier stage of the dorsal pathway, the medial temporal area (MT; Fig. 1A). We tested whether LIP feedback increases MT responses to attended visual stimuli. The monkeys performed a delayed match-to-sample (DMS) task, which manipulated both where they were attending and what stimulus feature they were attending to (Fig. 1B) (20). We recorded 29 pairs of neurons from MT and LIP, each pair having overlapping receptive fields (RFs) and the same preferred orientation. Local field potentials (LFPs) from the two sites were also recorded.

We first tested whether our paradigm resulted in increased responses of MT neurons to attended stimuli. Figure 2A shows the effect of spatial attention on a single MT neuron and Fig. 2B, the average population response. For both data sets, the MT response to the second stimulus was significantly increased in the “spatial and feature-based attention” and “spatial attention” conditions, compared to the “neutral” control. When “attention was elsewhere,” the MT response to the second stimulus was significantly reduced (Holm’s controlled Wilcoxon test, $P < 0.05$). These attentional effects on MT neurons are consistent with those reported in other types of cognitive

¹Department of Optometry and Vision Sciences, The University of Melbourne, Parkville 3010, Australia. ²Institute for Information Transmission Problems, Russian Academy of Sciences, Bol’shoy Karetniy 19, 127994 Moscow, Russia.

*To whom correspondence should be addressed. E-mail: trv@unimelb.edu.au

tasks and other cortical areas (2, 6–14) and are not due to simple stimulus repetition (fig. S1).

If LIP neurons code attention priorities, then their activity should differentiate between attention conditions. Figure 2, C and D, show the activity of a single LIP neuron and the population, respectively. Both show a significantly increased response to the second stimulus with “spatial and feature-based attention” compared to the “neutral” first stimulus, but a significantly reduced response when “attention was else-

where” (Holm’s controlled Wilcoxon test, $P < 0.05$). For the “spatial attention” condition, the increased response to the second stimulus was significantly different from the “attention elsewhere” control, though not the “neutral” control. The activity of LIP neurons increased through the delay period after the first stimulus, with the overall delay period activity significantly greater in those cases where attention included the RF location (Holm’s controlled Wilcoxon test, $P < 0.05$). Because LIP activity increased before the

MT response to an attended stimulus, LIP is in a position to provide feedback to MT.

If LIP causes the effect of attention on MT, then the activity in the two areas should be correlated and spikes from LIP neurons should be closely followed by spikes from MT neurons. We calculated the coherence of MT and LIP activities [using multi-taper spectral methods (20–22)], which measures the degree of association between two oscillatory processes (here the spike trains or LFPs in MT and LIP), as a function of oscillation frequency. We generally observed increased coherence between MT and LIP LFPs in the “spatial and feature-based attention” and “spatial attention” conditions (Fig. 3, A and B). The coherence in the 10- to 35-Hz range increased when the first stimulus appeared in the RF. It was also significantly elevated during the delay period (Student’s t test, $P < 0.05$), increasing just before the second stimulus. The coherence peaked around the second stimulus and remained elevated for up to 400 ms around the stimulus. Figure 3C shows the coherence when the first stimulus was flashed outside the RF and thus spatial attention was not drawn to the receptive-field location. The coherence is much weaker in this case, particularly around the second stimulus. Figure 3D shows the average coherence of the population of 29 paired recordings for the two attention conditions and two control states. The coherence was significantly greater (Holm’s controlled Wilcoxon test, $P < 0.05$) when attention was focused on the receptive-field location compared to the “neutral” and “attention elsewhere” controls.

The significant coherence of LFPs in MT and LIP during spatial attention means that there was correlated activity between ensembles of MT and LIP neurons. To determine the relative timing of action potentials between the two areas, we calculated the coherence between simultaneously recorded spike trains from single neurons in MT and LIP (0 to 300 ms after stimulus onset). The coherence between the spikes elicited by MT and LIP neurons was generally low but nonetheless significantly above zero (Student’s t test, $P < 0.1$) in the gamma-frequency range for 34% of neuron pairs. The lower coherence between spike trains than between LFPs is expected, because any particular sampled pair of neurons has a low probability of being strongly connected. Nevertheless, the “spatial and feature-based attention” and “spatial attention” conditions produced significant coherence (Fig. 4A). In contrast, there were no cases of significant coherence in the “neutral” and “attention elsewhere” controls.

If LIP has a top-down influence on MT responses during focal attention, then the phase of the coherence should show LIP leading MT. Figure 4B shows the phase when the coherence was significantly above zero, which occurred only during the two attention conditions. The phase of the peak coherence showed the LIP preceding MT by 4.55 ± 1.04 ms for the “spatial

Fig. 1. The experimental paradigm.

(A) Areas V1, MT, and LIP are connected as shown. We simultaneously recorded from the MT and LIP while the monkey performed the DMS task (B). The monkey is required to match both the orientation and location of two stimulus gratings to obtain a reward. The monkey maintained fixation throughout each trial, while we manipulated his attentional state. Two attention conditions were compared to two controls. When both gratings (S1 and S2) have the neurons’ preferred orientation, and both appear at the RF location (here, the lower left quadrant), the period after onset of S2 is the “spatial and feature-based attention” condition (left cascade). When S1 and S2 are both at the RF, but S1 has the nonpreferred orientation and S2 the preferred, the period after onset of S2 is the “spatial attention” condition (middle cascade). The two controls are the “attention elsewhere” state, which is the period after onset of S2 when S1 is outside the RF and preferred-orientation S2 is at the RF (right cascade); and the “neutral” state, the period after onset of S1 when preferred-orientation S1 is at the RF and S2 has not yet been presented (left cascade). FP, fixation point.

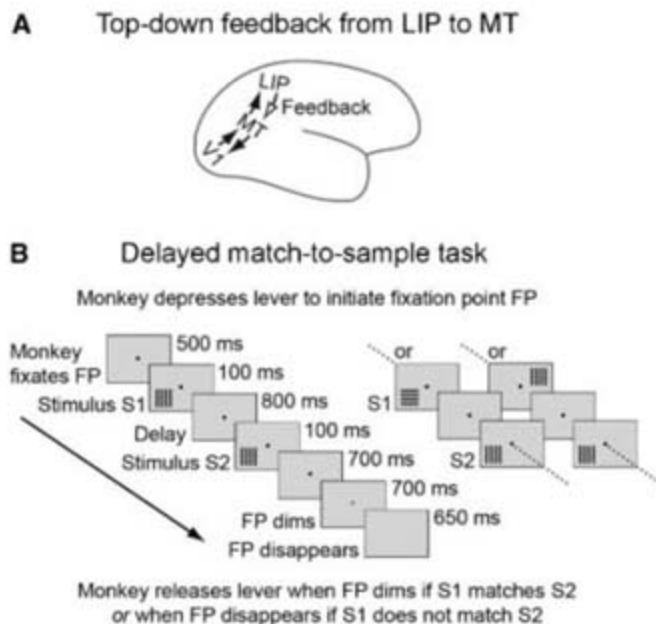
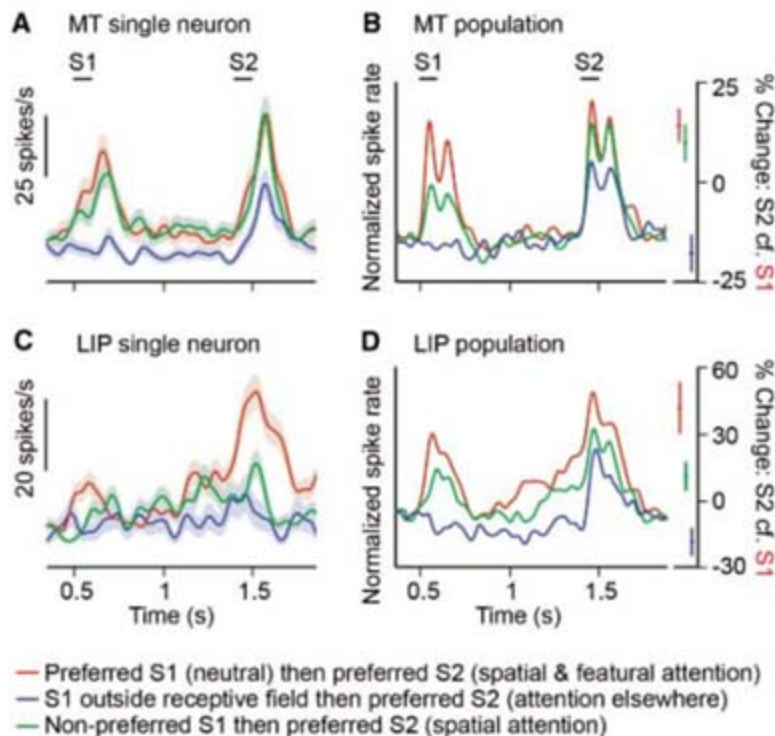


Fig. 2. Attention increased activity in LIP before MT. Examples of single-neuron activity (\pm SE) in the MT (A) and LIP (C) during the DMS task with 800-ms interstimulus delay. Three types of trials are color-coded: red (“neutral” S1, then “spatial and feature-based attention” on S2), green (“spatial attention” on S2), and blue (“attention elsewhere” for S2). Population activity in the MT (B) and LIP (D) represents the average of 24 cells for each area, 12 simultaneously recorded pairs from each of two monkeys, recorded at 800-ms delay. The percentage change (\pm SE) in the population response (0 to 300 ms after stimulus onset) of the MT [(B), right] and LIP [(D), right] evoked by S2 compared to “neutral” S1; shown are the combined data from 24 cells at 800-ms delay and 5 cells at 500-ms delay.



and feature-based attention" condition and by 7.43 ± 2.02 ms for the "spatial attention" condition (mean \pm SE of the 34% of neuron pairs showing significant coherence). This phase relationship is physiologically plausible for feedback from the LIP to MT, assuming a conduction velocity of 1 m/s (23) for intracortical connections. To ensure that the coherence we saw was due to within-trial physiological interactions, we shifted, across time, the LIP spike train relative to the MT train by integer multiples of trials for each recording session and recalculated the coherence (Fig. 4C). This control abolished the attention-enhanced coherence.

We next tested whether LIP spikes preceded enough MT spikes to cause the increased MT activity during spatial attention. We observed a significant increase in the percentage of MT spikes preceded by LIP spikes in the spatial attention conditions compared with the "neutral" and "attention elsewhere" controls (Holm's controlled Wilcoxon test, $P < 0.05$; Fig. 4D). The magnitude of this effect (percentage of MT spikes preceded by LIP spikes within 10 ms: spatial and featural attention, 11.5%; spatial attention, 8.3%) could potentially account for a substantial amount of the increase in MT activity (spatial and featural attention, +14.0%; spatial attention, +9.6%). However, a greater increase in LIP activity, relative to MT activity, could lead to the results in Fig. 4D without LIP feedback to MT. This possibility is discounted by the finding of a significant increase in the percentage of LIP spikes followed by MT spikes with attention (Holm's controlled Wilcoxon test, $P < 0.05$; Fig. 4E). Both increased coherence of oscillatory LFPs and LIP spikes preceding MT spikes in the attention conditions are evident in the raw data from single trials (fig. S2).

Synchronization between LIP neurons may be a fundamental mechanism ensuring that the output from LIP neurons has an increased impact on sensory areas such as MT. We calculated the spike-field coherence in LIP, which indicates the degree of synchronization between spike times and the LFP. The mean spike-field coherence between 25 and 45 Hz was significantly increased in the two spatial attention conditions (Fig. 4F) compared to the "attention elsewhere" control (Holm's controlled Wilcoxon test, $P < 0.05$). This suggests that spike timing, in addition to spike rate, may be important for increased efficacy of attentional feedback.

Our results show that LIP feedback can account for attention-enhanced MT responses. This feedback manifests in the coherent activities of MT and LIP neurons within the gamma-frequency range (25 to 45 Hz), supporting the role of gamma synchronization in information processing (24–26). The phase of the observed coherence is such that LIP feedback can potentially arrive at MT during a depolarizing phase of membrane-potential oscillations, increasing the probability of spike generation. Synchronization of feedback may also increase sensory activity during attention.

The response of LIP neurons to the second stimulus of preferred orientation depended upon whether the first stimulus, though at the same

location, was of the preferred or orthogonal orientation. In MT neurons, however, there was no significant difference in response to the second

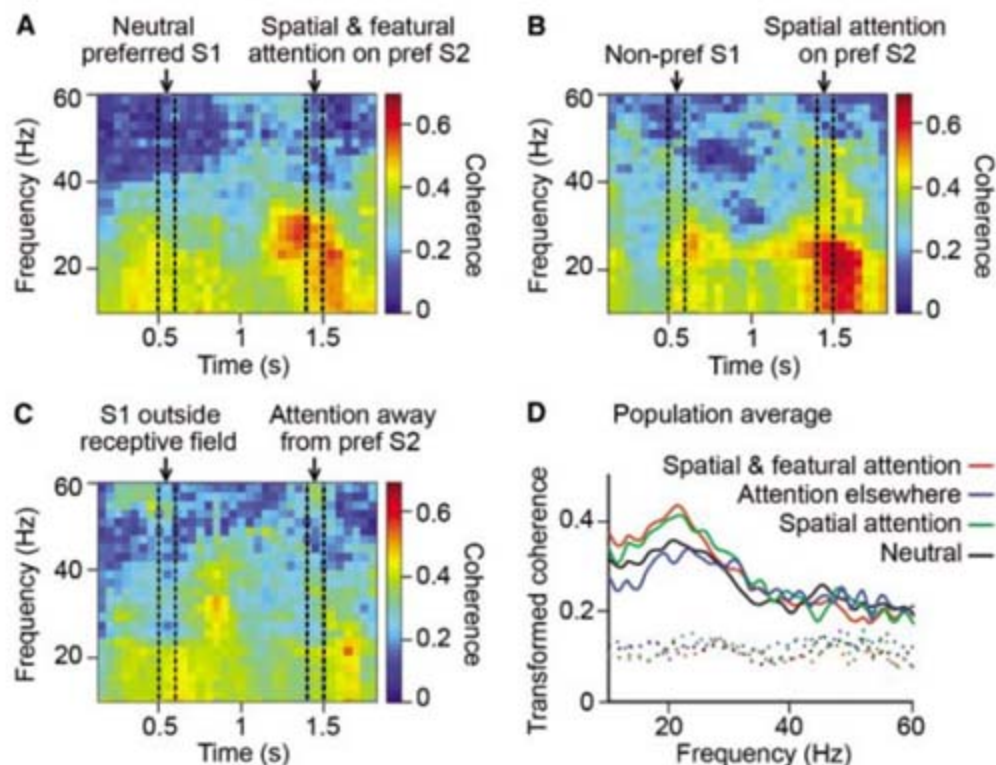


Fig. 3. Coherent neural activity between MT and LIP. The coherence (color-coded) of the MT LFP and LIP LFP from a pair of recording sites during the DMS task. The coherence was calculated in successive 300-ms windows with a step size of 50 ms. S2 is the preferred stimulus in the RF and is the same in each panel. (A) S1 and S2 match for location and orientation; (B) S1 and S2 match for location only; and (C) S1 and S2 differ in location. (D) Population average of the transformed coherence (20) between the MT LFP and LIP LFP, 0 to 300 ms after stimulus onset (solid lines), and the control, where the LIP LFP was shifted relative to the MT LFP (dotted lines).

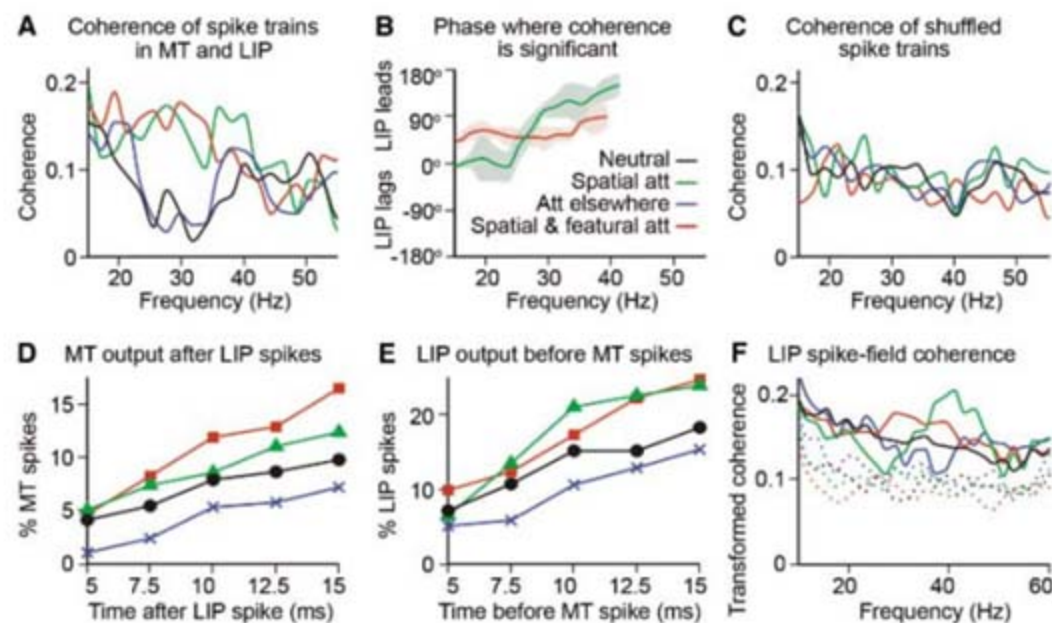


Fig. 4. Synchronized LIP feedback to MT during attention. (A) Coherence of spikes from a pair of LIP and MT neurons, 0 to 300 ms after stimulus onset. Color coding as in Fig. 3D. (B) Phase of significant coherence between the pair of neurons in (A). Only two traces are shown, because neither control showed significant coherence in the gamma range. (C) Relative shifts between spike trains by integer multiples of trials abolished attention-enhanced coherence; compare with (A). (D) Population median of the percentage of MT spikes preceded by LIP spikes, in the 300 ms after stimulus onset. (E) Population median of the percentage of LIP spikes followed by MT spikes, in the 300 ms after stimulus onset. (F) Population average of the transformed spike-field coherence in LIP (solid lines). Increased coherence is seen for the two attention conditions in the gamma range. Shifting spike trains relative to the LFP in LIP abolished attention-enhanced coherence (dotted lines).

stimulus between these two attention conditions. This is consistent with the idea that the parietal cortex uses both spatial and feature-based information to determine purely spatial priorities for its feedback (18). Such a scheme provides a neural framework for "guided search" models of attention (3, 18) and is consistent with feedback to auditory and somatosensory systems (27, 28) being spatial.

The dorsal and ventral cortical pathways are said to represent the spatial and feature-based aspects of a visual scene, respectively, and LIP is part of the dorsal pathway. However, the feature selectivity shown by LIP neurons in our and other studies (29, 30) means that LIP could be involved in processing object features through its direct connections with the ventral pathway (19, 27, 28) or by gating neuronal activity at the level of V1 via MT (18, 19). The attentional modulation of activity in ventral cortical areas (2, 7) and even in V1 (8, 10, 12, 13) may have its origin in LIP as the gain controller.

References and Notes

1. A. M. Treisman, G. Gelade, *Cognit. Psychol.* **12**, 97 (1980).
2. R. Desimone, J. Duncan, *Annu. Rev. Neurosci.* **18**, 193 (1995).
3. J. M. Wolfe, *Psychon. Bull. Rev.* **1**, 202 (1994).
4. S. Yantis, J. T. Serences, *Curr. Opin. Neurobiol.* **13**, 187 (2003).
5. J. H. R. Maunsell, S. Treue, *Trends Neurosci.* **29**, 317 (2006).
6. M. C. Bushnell, M. E. Goldberg, D. L. Robinson, *J. Neurophysiol.* **46**, 755 (1981).
7. J. Moran, R. Desimone, *Science* **229**, 782 (1985).
8. B. C. Motter, *J. Neurophysiol.* **70**, 909 (1993).
9. S. Treue, J. H. R. Maunsell, *Nature* **382**, 539 (1996).
10. T. R. Vidyasagar, *Neuroreport* **9**, 1947 (1998).
11. J. W. Bisley, M. E. Goldberg, *Science* **299**, 81 (2003).
12. J. A. Brefczynski, E. A. DeYoe, *Nat. Neurosci.* **2**, 370 (1999).
13. D. C. Somers, A. M. Dale, A. E. Seiffers, R. B. H. Tootell, *Proc. Natl. Acad. Sci. U.S.A.* **96**, 1663 (1999).
14. S. Kastner, P. De Weerd, R. Desimone, L. G. Ungerleider, *Science* **282**, 108 (1998).
15. M. M. Mesulam, *Ann. Neurol.* **10**, 309 (1981).
16. M. Corbetta, F. M. Miezin, G. L. Shulman, S. E. Petersen, *J. Neurosci.* **13**, 1202 (1993).
17. M. A. Steinmetz, C. Constantinidis, *Cereb. Cortex* **5**, 448 (1995).
18. T. R. Vidyasagar, *Brain Res. Rev.* **30**, 66 (1999).
19. J. Bullier, *Brain Res. Rev.* **36**, 96 (2001).
20. Materials and methods are available as supporting material on Science Online.
21. P. P. Mitra, B. Pesaran, *Biophys. J.* **76**, 691 (1999).
22. M. R. Jarvis, P. P. Mitra, *Neural Comput.* **13**, 717 (2001).
23. J. Bullier, M. E. McCourt, G. H. Henry, *Exp. Brain Res.* **70**, 90 (1988).
24. R. Eckhorn et al., *Biol. Cybern.* **60**, 121 (1988).
25. W. Singer, C. M. Gray, *Annu. Rev. Neurosci.* **18**, 555 (1995).
26. T. J. Sejnowski, O. Paulsen, *J. Neurosci.* **26**, 1673 (2006).
27. G. J. Blatt, R. A. Andersen, G. R. Stoner, *J. Comp. Neurol.* **299**, 421 (1990).
28. J. W. Lewis, D. C. Van Essen, *J. Comp. Neurol.* **428**, 112 (2000).
29. J. Gottlieb, M. Kusunoki, M. E. Goldberg, *Nature* **391**, 481 (1998).
30. P. F. Balan, J. Gottlieb, *J. Neurosci.* **26**, 9239 (2006).
31. We thank P. R. Martin, J. Victor, J. Bisley, and L. Horowitz for useful comments; E. Henry and E. Duff for programming assistance; J. Cappello for help training monkeys; and the Department of Anatomy and Cell Biology, University of Melbourne, for laboratory facilities. Supported by the National Health and Medical Research Council and Australian Research Council.

Supporting Online Material

www.sciencemag.org/cgi/content/full/316/5831/1612/DC1

Materials and Methods

Figs. S1 and S2

References

21 December 2006; accepted 1 May 2007

10.1126/science.1139140

α -Klotho as a Regulator of Calcium Homeostasis

Akihiro Imura,^{1,2,8*} Yoshihito Tsuji,^{1,5*} Miyahiko Murata,^{1,3*} Ryota Maeda,^{1,2} Koji Kubota,^{1,2} Akiko Iwano,^{1,8} Chikashi Obuse,⁹ Kazuya Togashi,¹⁰ Makoto Tominaga,¹⁰ Naoko Kita,¹ Ken-ichi Tomiyama,¹ Junko Iijima,¹ Yoko Nabeshima,¹ Makio Fujioka,⁷ Ryo Asato,⁴ Shinzo Tanaka,⁴ Ken Kojima,⁴ Juichi Ito,⁴ Kazuhiko Nozaki,⁵ Nobuo Hashimoto,⁵ Tetsufumi Ito,¹¹ Takeshi Nishio,³ Takashi Uchiyama,⁶ Toshihiko Fujimori,^{1,8} Yo-ichi Nabeshima^{1,8†}

α -klotho was identified as a gene associated with premature aging-like phenotypes characterized by short lifespan. In mice, we found the molecular association of α -Klotho (α -Kl) and Na⁺,K⁺-adenosine triphosphatase (Na⁺,K⁺-ATPase) and provide evidence for an increase of abundance of Na⁺,K⁺-ATPase at the plasma membrane. Low concentrations of extracellular free calcium ([Ca²⁺]_e) rapidly induce regulated parathyroid hormone (PTH) secretion in an α -Kl- and Na⁺,K⁺-ATPase-dependent manner. The increased Na⁺ gradient created by Na⁺,K⁺-ATPase activity might drive the transepithelial transport of Ca²⁺ in cooperation with ion channels and transporters in the choroid plexus and the kidney. Our findings reveal fundamental roles of α -Kl in the regulation of calcium metabolism.

Klotho mutant mice are short-lived, and the gene responsible for the phenotype is called *klotho* (1). A homolog has also been identified and named β -*klotho* (2, 3). To avoid confusion, we refer to the original gene as *α -klotho*. The *α -klotho* (α -kl) gene encodes a type I membrane protein with considerable similarity to β -glycosidase that is predominantly expressed in tissues that are involved with calcium homeostasis; that is the parathyroid glands, kidney, and choroid plexus (4, 5) (supporting description 1). Although α -Kl has been predicted to be present on the cell surface, large amounts of α -Kl are detectable in the cytoplasm and the cleaved extracellular domain is secreted into the blood and cerebrospinal fluid (CSF) (6). In this paper, we show a

pivotal role of α -Kl in calcium homeostasis (mouse breeding conditions are described in supporting description 2 and fig. S1).

We identified the $\alpha 1$ subunit of Na⁺,K⁺-ATPase ($\alpha 1$ -Na⁺,K⁺-ATPase) as an α -Kl binding protein (7) (supporting description 3) and further confirmed the binding by Western blot analysis and with reciprocal immunoprecipitation (Fig. 1, A and B). α -Kl precipitated by monoclonal antibody to $\alpha 1$ -Na⁺,K⁺-ATPase contained proteins that migrated as two bands of 120 and 135 kD, indicating that Na⁺,K⁺-ATPase binds to α -Kl regardless of its sugar moieties (Fig. 1B) (6). The β subunit of Na⁺,K⁺-ATPase, which has a major role in the regulation of membrane recruitment of Na⁺,K⁺-ATPase (8), was included in the α -Kl-Na⁺,K⁺-ATPase

complex (Fig. 1B). These molecules also associated in mouse kidney and in human parathyroid glands (Fig. 1, C and D).

In these tissues, the majority of α -Kl immunoreactivity was detectable in the cytoplasm, whereas $\alpha 1$ -Na⁺,K⁺-ATPase immunoreactivity was observed at or near the cell surface and diffusely in the cytoplasm (fig. S2). We verified the above histological observations by the surface biotinylation and subcellular fractionation using the choroid plexus and the HeLa cells introduced with both α -Kl and $\alpha 1$ -Na⁺,K⁺-ATPase fused with enhanced green fluorescence protein ($\alpha 1$ -Na⁺,K⁺-ATPase-EGFP), respectively. α -Kl was primarily detected in the nonbiotinylated cyto-

¹Department of Pathology and Tumor Biology, Graduate School of Medicine, Kyoto University, Kyoto 606-8501, Japan. ²Horizontal Medical Research Organization, Graduate School of Medicine, Kyoto University, Kyoto 606-8501, Japan. ³Integrative Brain Science, Graduate School of Medicine, Kyoto University, Kyoto 606-8501, Japan. ⁴Department of Otolaryngology, Head and Neck Surgery, Graduate School of Medicine, Kyoto University, Kyoto 606-8501, Japan. ⁵Department of Neurosurgery, Graduate School of Medicine, Kyoto University, Kyoto 606-8501, Japan. ⁶Department of Hematology and Oncology, Graduate School of Medicine, Kyoto University, Kyoto 606-8501, Japan. ⁷Electron Microscopy Center, Graduate School of Medicine, Kyoto University, Kyoto 606-8501, Japan. ⁸Core Research for Evolutional Science and Technology, Japan Science and Technology Corporation, Saitama 332-0012, Japan. ⁹Laboratory of Functional Networks for Chromosome Inheritance, Graduate School of Life Science, Hokkaido University, Sapporo 001-0021, Japan. ¹⁰Section of Cell Signaling, Okazaki Institute for Integrative Bioscience, National Institutes of Natural Sciences, Aichi 444-8787, Japan. ¹¹Department of Anatomy, Faculty of Medical Sciences, University of Fukui, Fukui 910-1193, Japan.

*These authors contributed equally to this work.

†To whom correspondence should be addressed. E-mail: nabemr@lmls.med.kyoto-u.ac.jp

plasmic fraction and not in the biotinylated cell surface fraction, whereas $\alpha 1$ - and $\beta 1$ - Na^+, K^+ -ATPase were readily detectable in both fractions (Fig. 1E). This demonstrated that α -Kl binds to Na^+, K^+ -ATPase in some intracellular organelle and not at the plasma membrane. The α -Kl and $\alpha 1$ - Na^+, K^+ -ATPase-EGFP complexes were found in the endoplasmic reticulum (ER), Golgi apparatus-plasma membrane (Golgi-PM), and early endosome (EE) fractions (Fig. 1F) (9). The 120-kD premature form of α -Kl was found solely in the ER fraction, whereas the 135-kD mature α -Kl and $\alpha 1$ - Na^+, K^+ -ATPase-EGFP complexes accumulated in the EE and Golgi-PM fractions (6). We conclude that a subset of Na^+, K^+ -ATPase appears to traffic from the ER to the cell surface in conjunction with α -Kl and that α -Kl- Na^+, K^+ -ATPase complexes locate in ER and Golgi apparatus and abundantly accumulate in the EE (including recycling endosome), ready for recruitment to the cell surface.

We hypothesized that α -Kl might directly affect Na^+, K^+ -ATPase activity (supporting description 4 and fig. S3). Because the involvement of α -Kl in calcium homeostasis was strongly suggested, we investigated whether fluctuation of $[\text{Ca}^{2+}]_e$ results in a change in Na^+, K^+ -ATPase activity in the isolated choroid plexus (10, 11). When tissue was incubated in medium containing low Ca^{2+} , the uptake of ^{86}Rb , representing the activity of Na^+, K^+ -ATPase, increased rapidly (within a few minutes), while decreasing in a high Ca^{2+} solution (Fig. 2A). Consistent with the ^{86}Rb uptake data, low Ca^{2+} media significantly increased the surface amount of Na^+, K^+ -ATPase (estimated by tritiated-ouabain labeling) (12, 13),

and conversely were decreased in high Ca^{2+} media (Fig. 2B). This result demonstrates that Na^+, K^+ -ATPase activity is correlated with its amount on the cell surface, both of which respond to $[\text{Ca}^{2+}]_e$ concentrations, leading us to conclude that the shift of $[\text{Ca}^{2+}]_e$ triggers a rapid response that accumulates Na^+, K^+ -ATPase at the plasma membrane. Next, we examined the involvement of α -Kl in this system using α -kl $^{-/-}$ mice. The uptake of ^{86}Rb and levels of surface Na^+, K^+ -ATPase were not affected by the change in $[\text{Ca}^{2+}]_e$ in α -kl $^{-/-}$ mice (Fig. 2, A and B). Notably, the ^{86}Rb uptake in α -kl $^{-/-}$ mice was always comparable to or somewhat lower than that in wild-type (WT) high $[\text{Ca}^{2+}]_e$, the lowest level in WT mice. These indicate that α -Kl is required for the rapid recruitment of Na^+, K^+ -ATPase to the cell surface in response to $[\text{Ca}^{2+}]_e$. The amount of the cell surface Na^+, K^+ -ATPase of the extirpated choroid plexus in α -kl $^{-/-}$ mice was slightly but significantly lower than that in WT mice (Fig. 2C), also indicating the involvement of α -Kl in the transport of Na^+, K^+ -ATPase to the cell surface.

The 130-kD extracellular domain of α -Kl is secreted into serum and cerebrospinal fluid (CSF). Thus, we investigated whether the secretion of α -Kl correlates with surface amounts of Na^+, K^+ -ATPase. Incubation of isolated choroid plexi in buffer containing a low $[\text{Ca}^{2+}]_e$ increased secretion, whereas less secretion was observed in cells exposed to high $[\text{Ca}^{2+}]_e$ (Fig. 2D). In serial infusions with buffers (fig. S4), higher amounts of α -Kl were secreted into the vein of kidney in response to buffer containing a low $[\text{Ca}^{2+}]_e$, and smaller amounts were detected in high Ca^{2+} buffer (Fig. 2E). Secretion of α -Kl was also induced

in response to low $[\text{Ca}^{2+}]_e$ in the isolated parathyroid glands (Fig. 2F). These results suggest that secretion of α -Kl correlates with Ca^{2+} -dependent accumulation of Na^+, K^+ -ATPase at the cell surface.

Because administration of 4 α -phorbol 12,13-didecanoate (4 α -PDD) (14), a specific agonist of transient receptor potential vanilloid-4 (TRPV4), induced a significant increase of the cell surface expression of Na^+, K^+ -ATPase and secretion of α -Kl in the choroid plexi derived from WT, but not in plexi from α -kl $^{-/-}$ mice (Fig. 2, G and H, supporting description 5, and fig. S5A), we transfected HeLa cells with plasmids encoding α -Kl and TRPV4 to explore the possible role of α -Kl in recruiting Na^+, K^+ -ATPase (15, 16). We then verified that both α -Kl and activation of TRPV4 were required for the increase in abundance of Na^+, K^+ -ATPase at the plasma membrane and the correlated secretion of α -Kl in HeLa cell experiments (Fig. 2I) (supporting description 5).

To investigate the response of PTH secretion to low $[\text{Ca}^{2+}]_{\text{serum}}$ (17), we administered a Ca^{2+} chelating gel (Chelex, Biorad, Hercules, CA) to mice through intraperitoneal injection (fig. S6). The decrease in $[\text{Ca}^{2+}]_{\text{serum}}$ caused increased secretion of PTH into serum in WT mice (Fig. 3A). The increase in the serum PTH was much smaller in α -kl $^{-/-}$ mice (Fig. 3A), suggesting that α -Kl has a role in promoting regulated secretion of PTH. Secretion of PTH was also increased in cultured thyroid and parathyroid glands exposed to buffer containing a low $[\text{Ca}^{2+}]_e$ (Fig. 3B). In glands from α -kl $^{-/-}$ mice, PTH secretion induced by low Ca^{2+} was detectable but only about 27% of that observed from WT glands (Fig. 3B). Ouabain, a specific

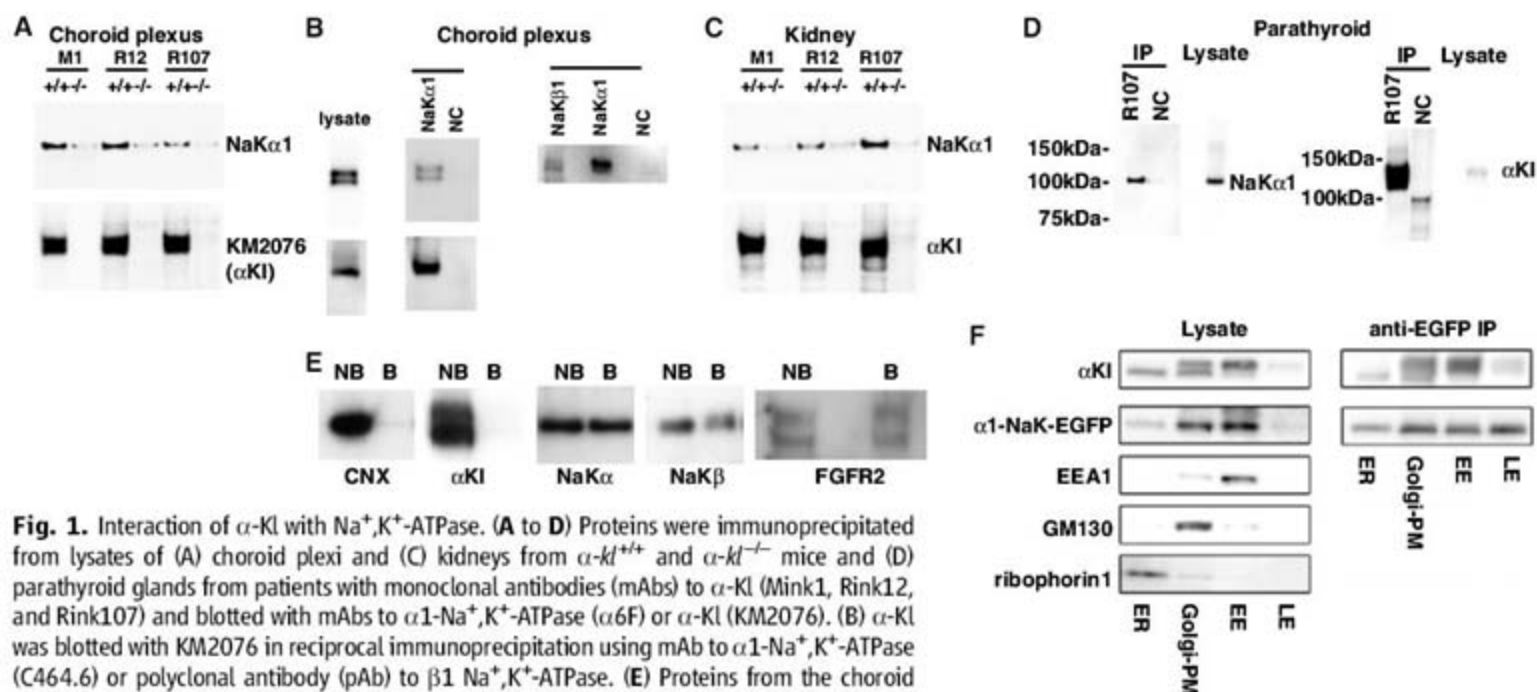


Fig. 1. Interaction of α -Kl with Na^+, K^+ -ATPase. (A to D) Proteins were immunoprecipitated from lysates of (A) choroid plexi and (C) kidneys from α -kl $^{+/+}$ and α -kl $^{-/-}$ mice and (D) parathyroid glands from patients with monoclonal antibodies (mAbs) to α -Kl (Mink1, Rink12, and Rink107) and blotted with mAbs to $\alpha 1$ - Na^+, K^+ -ATPase ($\alpha 6\text{F}$) or α -Kl (KM2076). (B) α -Kl was blotted with KM2076 in reciprocal immunoprecipitation using mAb to $\alpha 1$ - Na^+, K^+ -ATPase (C464.6) or polyclonal antibody (pAb) to $\beta 1$ Na^+, K^+ -ATPase. (E) Proteins from the choroid plexi were surface-biotinylation followed by separation with streptavidin-conjugated resin. Fractions were blotted with one of a series of antibodies (mAbs to calnexin, α -Kl, $\alpha 1$ - Na^+, K^+ -ATPase, and $\beta 1$ - Na^+, K^+ -ATPase, and pAb to FGFR2). (NB, nonbinding fraction; B, fraction binding to streptavidin-conjugated resin). (F) Subcellular localization of α -Kl and Na^+, K^+ -ATPase. (Left) Lysates of HeLa cells were separated into ER, Golgi-PM, EE, and late endosome (LE) fractions on sucrose gradients, and proteins were blotted either with antibody to α -Kl, EGFP, early endosome antigen 1 (EEA1), Golgi matrix 130 (GM130), or ribophorin1 antibodies. (Right) Analysis of α -Kl coimmunoprecipitated with $\alpha 1$ - Na^+, K^+ -ATPase-EGFP.

inhibitor of Na^+, K^+ -ATPase, inhibited the secretion of PTH from WT glands (Fig. 3C). There was no significant effect of ouabain on Ca^{2+} -sensitive PTH secretion from $\alpha\text{-kl}^{-/-}$ glands (Fig. 3C), which suggests that $\alpha\text{-Kl}$ may be required for Na^+, K^+ -ATPase-dependent PTH release. The amount of stored PTH of $\alpha\text{-kl}^{-/-}$ mice was $\sim 53\%$ that of WT mice (fig. S7). However, the amount of responsive PTH secretion during 6 min is validated within 0.33% of stored PTH in $\alpha\text{-kl}^{-/-}$ mice, whereas it is within 0.66% in WT mice. These results suggest that there should be sufficient amounts of stored PTH available for secretion even in $\alpha\text{-kl}^{-/-}$ mice. Taken to-

gether, we suggest that the reduced response of serum PTH in $\alpha\text{-kl}^{-/-}$ mice is largely caused by impairment of Na^+, K^+ -ATPase-dependent secretion of PTH (fig. S7) (supporting description 6).

Since the first report of Brown, it has remained an open question how Na^+, K^+ -ATPase activity responds to low Ca^{2+} in the parathyroid glands (18). When $[\text{Ca}^{2+}]_e$ is lowered, Na^+, K^+ -ATPase is quickly recruited to the plasma membrane in correlation with the secretion of $\alpha\text{-Kl}$ (Fig. 2F). An electrochemical gradient created by increased Na^+, K^+ -ATPase may cause PTH release. If this pathway is disrupted either by $\alpha\text{-kl}$ deficiency or by administration of ouabain,

the regulated secretion of PTH is equivalently suppressed (Fig. 3C). In the choroid plexus, the importance of $\alpha\text{-Kl}$ in Ca^{2+} transport was suggested because (i) surface amounts of Na^+, K^+ -ATPase in $\alpha\text{-kl}^{-/-}$ mice are lower than that of WT (Fig. 2C), (ii) consistent with this, the concentration of total calcium in CSF ($[\text{Ca}]_{\text{CSF}}$) in $\alpha\text{-kl}^{-/-}$ mice was 23.6% lower than that of WT mice (Fig. 3D and fig. S8), and (iii) both surface amounts of Na^+, K^+ -ATPase and secretion of $\alpha\text{-Kl}$ respond to lowering $[\text{Ca}^{2+}]_e$ (Fig. 2, B and D, and fig. S9). These results imply that calcium homeostasis is impaired in the CSF of $\alpha\text{-kl}^{-/-}$ mice and suggest that $\alpha\text{-Kl}$ is involved in regulating

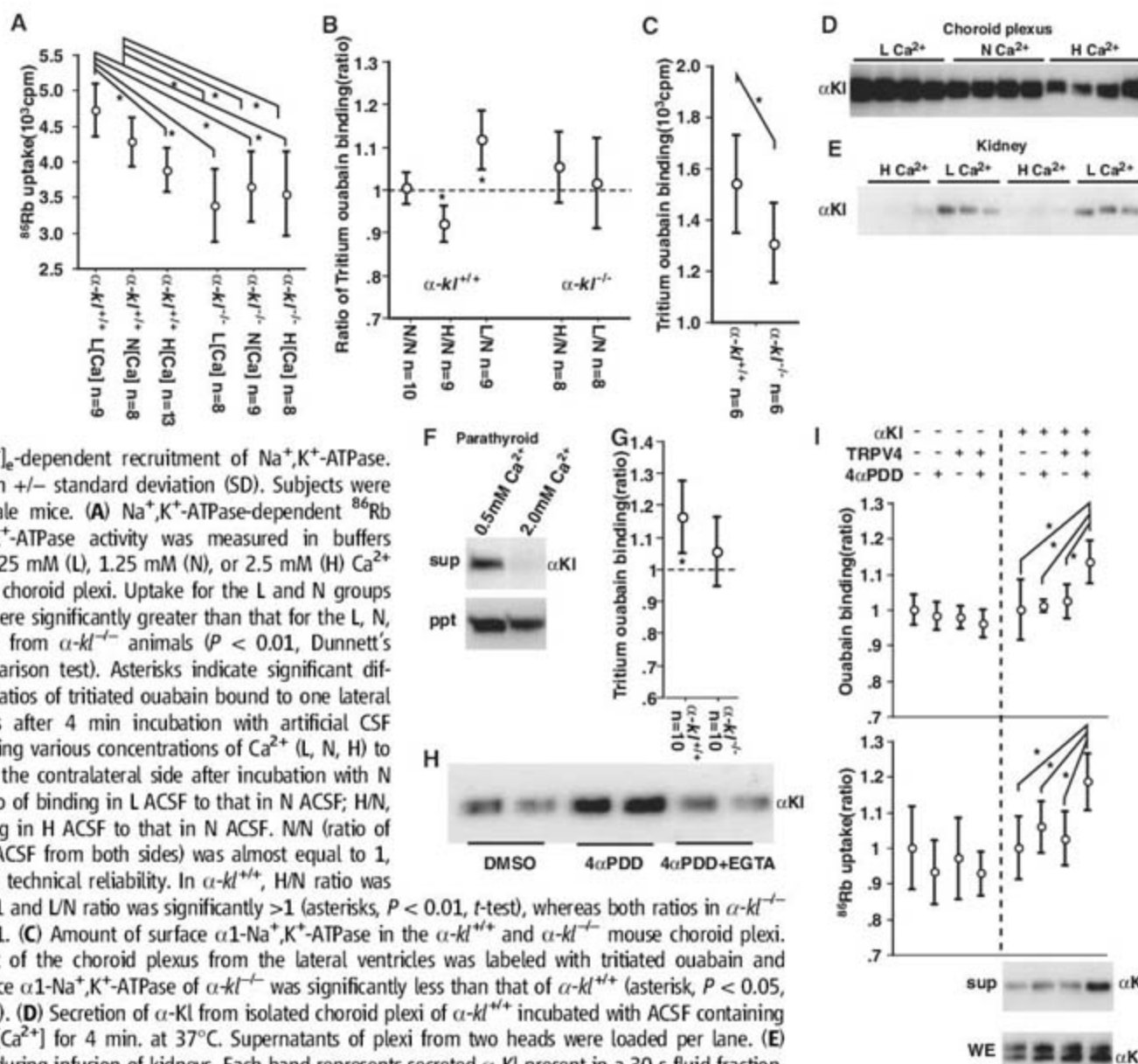


Fig. 2. $[\text{Ca}^{2+}]_e$ -dependent recruitment of Na^+, K^+ -ATPase. Data are mean \pm standard deviation (SD). Subjects were 8-week-old male mice. **(A)** Na^+, K^+ -ATPase-dependent ^{86}Rb uptake. Na^+, K^+ -ATPase activity was measured in buffers containing 0.625 mM (L), 1.25 mM (N), or 2.5 mM (H) Ca^{2+} using bilateral choroid plexi. Uptake for the L and N groups from $\alpha\text{-kl}^{+/+}$ were significantly greater than that for the L, N, and H groups from $\alpha\text{-kl}^{-/-}$ animals ($P < 0.01$, Dunnett's multiple comparison test). Asterisks indicate significant differences. **(B)** Ratios of tritiated ouabain bound to one lateral choroid plexus after 4 min incubation with artificial CSF (ACSF) containing various concentrations of Ca^{2+} (L, N, H) to that bound to the contralateral side after incubation with N ACSF. L/N, ratio of binding in L ACSF to that in N ACSF; H/N, ratio of binding in H ACSF to that in N ACSF. N/N (ratio of binding in N ACSF from both sides) was almost equal to 1, confirming the technical reliability. In $\alpha\text{-kl}^{+/+}$, H/N ratio was significantly < 1 and L/N ratio was significantly > 1 (asterisks, $P < 0.01$, t -test), whereas both ratios in $\alpha\text{-kl}^{-/-}$ were close to 1. **(C)** Amount of surface $\alpha\text{-Kl}$ - Na^+, K^+ -ATPase in the $\alpha\text{-kl}^{+/+}$ and $\alpha\text{-kl}^{-/-}$ mouse choroid plexi. Each fragment of the choroid plexus from the lateral ventricles was labeled with tritiated ouabain and counted. Surface $\alpha\text{-Kl}$ - Na^+, K^+ -ATPase of $\alpha\text{-kl}^{-/-}$ was significantly less than that of $\alpha\text{-kl}^{+/+}$ (asterisk, $P < 0.05$, Student's t -test). **(D)** Secretion of $\alpha\text{-Kl}$ from isolated choroid plexi of $\alpha\text{-kl}^{+/+}$ incubated with ACSF containing the indicated $[\text{Ca}^{2+}]_e$ for 4 min. at 37°C . Supernatants of plexi from two heads were loaded per lane. **(E)** Secreted $\alpha\text{-Kl}$ during infusion of kidneys. Each band represents secreted $\alpha\text{-Kl}$ present in a 30-s fluid fraction. **(F)** Secretion of $\alpha\text{-Kl}$ from the parathyroid gland. Dissected thyroid and parathyroid glands were incubated in low $[\text{Ca}^{2+}]_e$ (0.5 mM Ca^{2+}) and high $[\text{Ca}^{2+}]_e$ (2.0 mM Ca^{2+}) buffers. The supernatants (sup) and precipitates (ppt) were analyzed by Western blotting. **(G)** Agonist for TRPV4 ($4\alpha\text{-PDD}$) induces the Na^+, K^+ -ATPase recruitment. Shown is ratio of ^3H -ouabain-binding of the lateral choroid plexi incubated in ACSF with $4\alpha\text{-PDD}$ (10 μM) for 4 min to that of control plexi incubated without $4\alpha\text{-PDD}$. The ratio of binding in $\alpha\text{-kl}^{+/+}$ was significantly > 1 (asterisk, $P < 0.01$, t -test) but not in $\alpha\text{-kl}^{-/-}$. **(H)** $\alpha\text{-Kl}$ secretion from isolated choroid plexi incubated in the ACSF containing dimethyl sulfoxide (DMSO), 5 μM $4\alpha\text{-PDD}$, or 5 μM $4\alpha\text{-PDD}$ with 2 mM EGTA. Western blots show proteins from $\alpha\text{-kl}^{+/+}$, supernatants of plexi from two heads per lane; $n = 4$; representative samples are shown. **(I)** Requirement of $\alpha\text{-Kl}$ and TRPV4 for regulated accumulation of Na^+, K^+ -ATPase. The activity and the surface amounts of endogenous Na^+, K^+ -ATPase were estimated using HeLa cells introduced with $\alpha\text{-Kl}$ and TRPV4 in various combinations with administration of DMSO or $4\alpha\text{-PDD}$. 96-well study ($n = 12$). Two groups transfected with or without $\alpha\text{-kl}$ were independently normalized as ratios to the average values in the absence of TRPV4 and $4\alpha\text{-PDD}$. Multiple comparisons show that the addition of TRPV4 and its agonist significantly induced accumulation of Na^+, K^+ -ATPase only in $\alpha\text{-kl}$ -transfected groups (asterisks, $P < 0.01$, Dunnett's test). The amounts of secreted $\alpha\text{-Kl}$ from the cells were analyzed by Western blot. WE, whole extract.

the calcium concentration of CSF (supporting description 7) (fig. S10).

The surface expression of Na⁺,K⁺-ATPase is usually controlled by the balance of recruitment to the plasma membrane and internalization of Na⁺,K⁺-ATPase (the conventional recruitment) (19, 20). We presume that, in α-KI expressing cells, Na⁺,K⁺-ATPase is recruited to the cell surface by a combination of the conventional recruitment and the α-KI-dependent recruitment. The latter is characterized by Ca²⁺-dependency and a rapid response (fig. S11). Under normocalcemic conditions, a certain amount of Na⁺,K⁺-ATPase may be additionally recruited by the α-KI-dependent pathway. Therefore, the amount or activity of surface Na⁺,K⁺-ATPase in WT mice is significantly higher than that of α-kl^{-/-} mice (Fig. 2, A and C). Low Ca²⁺ induces an 11.9% increase of the amount of Na⁺,K⁺-ATPase at the plasma membrane. In contrast, high Ca²⁺ led to a 7.8% decrease in the amount of Na⁺,K⁺-ATPase at the plasma membrane (fig. S9). Accordingly, [Ca²⁺]_e regulates this additional

accumulation of Na⁺,K⁺-ATPase at the plasma membrane in correlation with the secretion of α-KI, leading to PTH secretion and Ca²⁺ transport across the epithelium (fig. S11) (supporting description 7) (21). By these means, α-KI participates in the increase of [Ca²⁺]_e in the calcium homeostasis regulatory network. As we reported, α-KI also invokes a negative feedback system to keep [Ca²⁺]_e within normal range (4). α-KI, in combination with fibroblast growth factor 23 (Fgf23), down-regulates the production of 1,25(OH)₂D₃ by negatively regulating the expression of 1α-hydroxylase encoding rate-limiting enzyme of active vitamin D synthesis (4, 22–24). α-KI may be involved in this negative regulation because Urakawa *et al.* reported that (i) α-KI binds to Fgf23 and (ii) α-KI converts canonical FgfR1(IIIc) to specific receptor for Fgf23, enabling the high-affinity binding of Fgf23 to the cell surface of distal convoluted tubule where α-KI is expressed (23) (supporting description 8). α-kl^{-/-} mice show increased production of vitamin D, and altered mineral-ion homeostasis

is suggested to be a cause of premature aging-like phenotypes, because the lowering of vitamin D activity, either by dietary restriction (4) or *fgf23* ablation (23, 25), rescues the premature aging-like phenotypes and prolongs survival in these mutants (26) (supporting description 8). Thus, our results and others indicate that α-KI influences calcium homeostasis. This effect can explain phenotypes observed in α-kl^{-/-} mice and the reason that α-KI is expressed in the tissues related to calcium regulation. The mechanism is different from the previously reported action of α-KI to interfere with the insulin or insulin-like growth factor (IGF) signal transduction (27). The fundamental role of α-KI in a multistep calcium homeostasis is further discussed in supporting description 9.

References and Notes

1. M. Kuro-o *et al.*, *Nature* **390**, 45 (1997).
2. S. Ito *et al.*, *Mech. Dev.* **98**, 115 (2000).
3. S. Ito *et al.*, *J. Clin. Invest.* **115**, 2202 (2005).
4. H. Tsujikawa, Y. Kurotaki, T. Fujimori, K. Fukuda, Y. Nabeshima, *Mol. Endocrinol.* **17**, 2393 (2003).
5. K. Takeshita *et al.*, *Circulation* **109**, 1776 (2004).
6. A. Imura *et al.*, *FEBS Lett.* **565**, 143 (2004).
7. J. C. Skou, M. Esmann, *J. Bioenerg. Biomembr.* **24**, 249 (1992).
8. K. Geering, *FEBS Lett.* **285**, 189 (1991).
9. J. P. Gorvel, P. Chavrier, M. Zerial, J. Gruenberg, *Cell* **64**, 915 (1991).
10. G. G. Somjen, *Neuroscientist* **8**, 254 (2002).
11. V. A. Murphy, Q. R. Smith, S. I. Rapoport, *Brain Res.* **484**, 65 (1989).
12. J. C. Skou, *Methods Enzymol.* **156**, 1 (1988).
13. S. R. Hootman, S. A. Ernst, *Methods Enzymol.* **156**, 213 (1988).
14. H. Watanabe *et al.*, *J. Biol. Chem.* **277**, 13569 (2002).
15. M. Tominaga, M. J. Caterina, *J. Neurobiol.* **61**, 3 (2004).
16. W. Liedtke *et al.*, *Cell* **103**, 525 (2000).
17. J. P. Bilezikian, R. Marcus, M. A. Levine, Eds., *The Parathyroids: Basic and Clinical Concepts* (Academic Press, San Diego, CA, 2005).
18. E. M. Brown *et al.*, *Metabolism* **36**, 36 (1987).
19. J. H. Kaplan, *Annu. Rev. Biochem.* **71**, 511 (2002).
20. M. J. Caplan, B. Forbush III, G. E. Palade, J. D. Jamieson, *J. Biol. Chem.* **265**, 3528 (1990).
21. F. R. Bringhurst, M. B. Demay, H. M. Kronenberg, *William's Textbook of Endocrinology* (Saunders, Philadelphia, ed. 9, 2003).
22. M. S. Razaque, D. Sitara, T. Taguchi, R. St-Arnaud, B. Lanske, *FASEB J.* **20**, 720 (2006).
23. I. Urakawa *et al.*, *Nature* **444**, 770 (2006).
24. T. Yoshida, T. Fujimori, Y. Nabeshima, *Endocrinology* **143**, 683 (2002).
25. T. Shimada *et al.*, *J. Clin. Invest.* **113**, 561 (2004).
26. Y. Nabeshima, *Sci. Aging Knowledge Environ.* **2006**, pe11 (2006).
27. H. Kurosu *et al.*, *Science* **309**, 1829 (2005).
28. We thank Y. Kaziro, G. Yamashita, M. Conner, R. Wang, and R. Yu for editing this manuscript, and H. Kimura, K. Okawa, T. Ishii, and T. Hori for their support in our experiments. Studies presented here were funded by grants from the Ministry of Education, Science, Sports, and Culture of Japan (17109004) and the Ministry of Health and Welfare, and Labor of Japan (H16-genome-005).

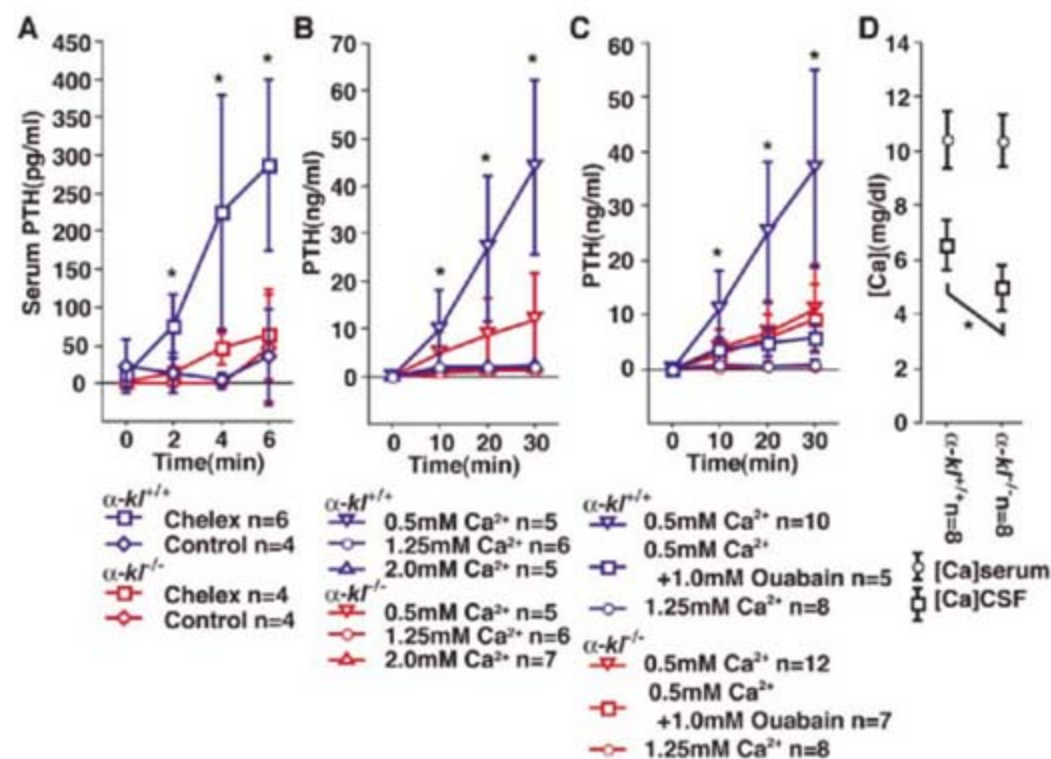


Fig. 3. Role of α-KI-Na⁺,K⁺-ATPase system in regulated PTH secretion and epithelial Ca²⁺ transport. Data are mean ± SD. Dunnett's test was used for multiple comparisons between individual groups. (A) Changes in serum levels of PTH after Chelex injection (1 ml slurry), in α-kl^{+/+} and α-kl^{-/-}. Chelex injection caused significant elevation of PTH from 2 through 6 min in α-kl^{+/+}, compared with control injection in α-kl^{+/+} and both Chelex and control injection in α-kl^{-/-} (asterisks, P < 0.03). (B) PTH secreted from dissected thyroid and parathyroid glands of α-kl^{+/+} and α-kl^{-/-} mice incubated in media containing 0.5 mM, 1.25 mM, or 2.0 mM Ca²⁺. PTH released into 0.5 mM Ca²⁺ by α-kl^{+/+} was significantly greater than that in 1.25 mM or 2 mM Ca²⁺ by α-kl^{+/+} and in all concentrations in α-kl^{-/-} from 10 through 30 min of incubation, except 0.5 mM of α-kl^{-/-} at 10 min (asterisks; P < 0.01). Alternatively, by multiple comparison within each genotype, the accumulation in 0.5 mM Ca²⁺ was significantly greater than that in 1.25 and 2.0 mM Ca²⁺ from 10 through 30 min (P < 0.05). (C) Inhibition of PTH secretion by ouabain under low Ca²⁺ conditions. The accumulation of PTH in 0.5 mM Ca²⁺ of α-kl^{+/+} is significantly greater than that in 1.25 mM Ca²⁺ and 0.5 mM Ca²⁺ with ouabain of α-kl^{+/+} and all conditions of α-kl^{-/-} from 10 through 30 min (P < 0.01). In multiple comparisons within α-kl^{-/-}, there was no significant difference between 0.5 mM Ca²⁺ with and without ouabain from 10 through 30 min (P > 0.50). (D) Calcium concentration in CSF or serum of α-kl^{+/+} and α-kl^{-/-} mice. There was a significant difference between two genotypes in CSF but not in serum (asterisk, P < 0.01, Student's *t* test).

Supporting Online Material

www.sciencemag.org/cgi/content/full/316/5831/1615/DC1
 Materials and Methods
 SOM Text
 Figs. S1 to S11
 References

4 October 2006; accepted 12 April 2007
 10.1126/science.1135901

Wnt Induces LRP6 Signalosomes and Promotes Dishevelled-Dependent LRP6 Phosphorylation

Josipa Bilić,¹ Ya-Lin Huang,¹ Gary Davidson,¹ Timo Zimmermann,² Cristina-Maria Cruciati,¹ Mariann Bienz,³ Christof Niehrs^{1*}

Multiple signaling pathways, including Wnt signaling, participate in animal development, stem cell biology, and human cancer. Although many components of the Wnt pathway have been identified, unresolved questions remain as to the mechanism by which Wnt binding to its receptors Frizzled and Low-density lipoprotein receptor-related protein 6 (LRP6) triggers downstream signaling events. With live imaging of vertebrate cells, we show that Wnt treatment quickly induces plasma membrane-associated LRP6 aggregates. LRP6 aggregates are phosphorylated and can be detergent-solubilized as ribosome-sized multiprotein complexes. Phospho-LRP6 aggregates contain Wnt-pathway components but no common vesicular traffic markers except caveolin. The scaffold protein Dishevelled (Dvl) is required for LRP6 phosphorylation and aggregation. We propose that Wnts induce coclustering of receptors and Dvl in LRP6-signalosomes, which in turn triggers LRP6 phosphorylation to promote Axin recruitment and β -catenin stabilization.

Wnt signaling plays diverse roles during embryonic development such as axis formation and nervous system patterning, and it is implicated in human disease, including cancer (1–4). Wnt ligands are thought to form a ternary

complex with low-density lipoprotein receptor-related proteins 5 and 6 (LRP5/6) and Frizzled (Fz) receptors (5). A key step after Wnt stimulation is the phosphorylation of the LRP6 intracellular domain by Casein kinase 1 γ (CK1 γ). This phosphorylation event activates LRP6 and promotes recruitment of the negative regulator Axin (6–8), which, in turn, stabilizes the Wnt signaling transducer β -catenin (5). Many aspects of Wnt signal transduction at the plasma membrane remain elusive. For example, the mechanism that triggers LRP6 phosphorylation by CK1 γ is unknown, and it is unclear how Fz and the scaffold protein Dishevelled (Dvl) (9–11) fit in.

To analyze LRP6 activation upon Wnt stimulation, we used real-time confocal microscopy. Live cell imaging allows a dynamic view of receptor activation to reveal spatiotemporal aspects that can not be visualized by methods such as biochemical analysis or immunofluorescence of fixed samples. The negative Wnt regulator Axin is recruited to the phosphorylated cytoplasmic domain of LRP6 (12). We therefore transfected HeLa cells with enhanced cyan fluorescent protein (ECFP)-Axin (green signal) and LRP6-enhanced yellow fluorescent protein (EYFP) (red signal) and monitored their localization simultaneously. When the proteins overlap, yellow signals appear (Fig. 1A and movie S1). In unstimulated cells, Axin was localized in intracellular punctae, and LRP6 showed continuous staining at the plasma membrane. No yellow signals were visible, indicating that the two proteins resided in different compartments. However, within 15 min of Wnt treatment, a small fraction of LRP6 protein started coalescing into punctate structures at or below the plasma membrane (fig. S1A), which colocalized with Axin and were therefore yellow. As soon as yellow signals were observed, they were punctate in nature, without transiting through a continuous plasma membrane staining. This suggests that Axin is recruited to LRP6 when the receptor is aggregated. This is supported by biochemical analyses (see below). The number of the LRP6-Axin aggregates plateaued after 1 to 2 hours, and once they formed they were quite stable over the course of 30 min. As seen in time-space plots, neither LRP6 nor Axin showed extensive movements or further coalescence into higher-order structures (fig. S1, B and C).

¹Division of Molecular Embryology, Deutsches Krebsforschungszentrum, Im Neuenheimer Feld 280, D-69120 Heidelberg, Germany. ²Advanced Light Microscopy Facility, European Molecular Biology Laboratory (EMBL), Meyerhofstrasse 1, 69117 Heidelberg, Germany. ³MRC Laboratory of Molecular Biology, Hills Road, Cambridge CB2 2QH, UK.

*To whom correspondence should be addressed. E-mail: Niehrs@DKFZ-Heidelberg.DE

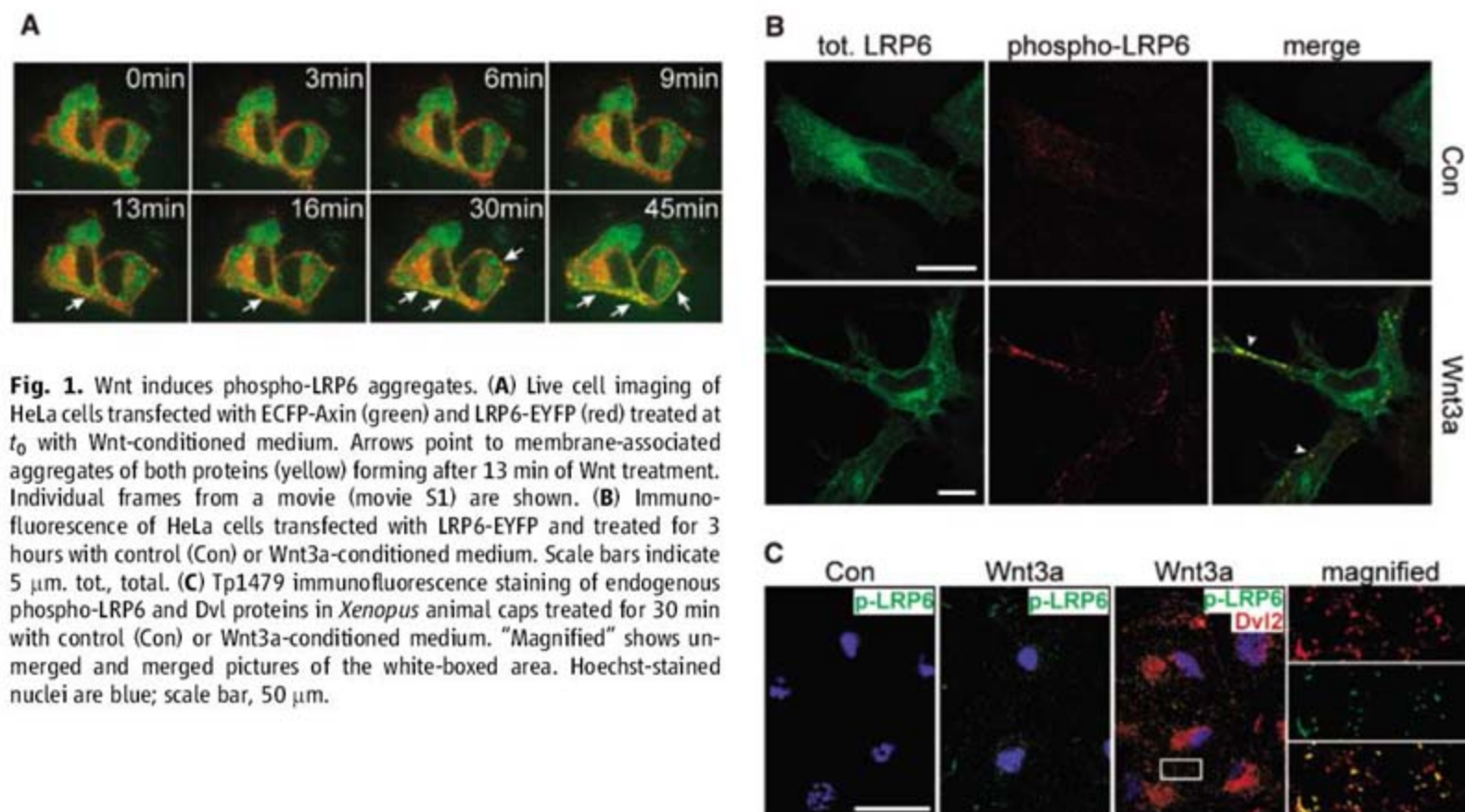


Fig. 1. Wnt induces phospho-LRP6 aggregates. **(A)** Live cell imaging of HeLa cells transfected with ECFP-Axin (green) and LRP6-EYFP (red) treated at t_0 with Wnt-conditioned medium. Arrows point to membrane-associated aggregates of both proteins (yellow) forming after 13 min of Wnt treatment. Individual frames from a movie (movie S1) are shown. **(B)** Immunofluorescence of HeLa cells transfected with LRP6-EYFP and treated for 3 hours with control (Con) or Wnt3a-conditioned medium. Scale bars indicate 5 μ m. tot., total. **(C)** Tp1479 immunofluorescence staining of endogenous phospho-LRP6 and Dvl proteins in *Xenopus* animal caps treated for 30 min with control (Con) or Wnt3a-conditioned medium. "Magnified" shows unmerged and merged pictures of the white-boxed area. Hoechst-stained nuclei are blue; scale bar, 50 μ m.

Because Axin recruitment requires CK1 γ -mediated phosphorylation of LRP6, we carried out immunofluorescence with a phosphospecific antibody recognizing phosphothreonine 1479 (Ab-Tp1479) in the intracellular domain (7) of LRP6. Ab-Tp1479 detected LRP6 phosphorylation within 10 min of Wnt stimulation in Western blots, indicating that this is an immediate response (7). In unstimulated cells, Ab-Tp1479 immunoreactivity was undetectable (Fig. 1B top). In contrast, after Wnt3a treatment, Ab-Tp1479

detected discrete punctate signals at the plasma membrane, which colocalized with a small fraction of total LRP6 (Fig. 1B bottom).

To test whether phospho-LRP6 aggregates are also observed under physiological conditions in untransfected cells and in vivo, we analyzed animal caps of *Xenopus* embryos, which are Wnt-responsive. Robust LRP6-Tp1479 immunoreactivity was reproducibly induced within 30 min of Wnt treatment in the form of punctate structures (Fig. 1C). These phospho-LRP6 ag-

gregates colocalized with Dvl2 (see below). We conclude that phospho-LRP6 aggregates occur under physiological conditions as a rapid response to Wnt stimulation.

The results indicated that Wnt signaling induces large plasma membrane-associated aggregates enriched in phosphorylated LRP6, Axin, and Dvl. To further characterize phospho-LRP6 aggregates, we performed colocalization analyses with markers for vesicular traffic compartments. Occasional colocalization of Wnt-induced phospho-LRP6 aggregates was observed with the fluid phase marker dextran Texas red (fig. S2A), whereas no colocalization was seen with other markers of vesicular transport: TGN 38 (Golgi), Calnexin (endoplasmic reticulum), EEA1 (early endosome), or Clathrin (endocytic vesicles) (fig. S2). Partial colocalization of phospho-LRP6 aggregates was observed with Caveolin within 1 hour but not with 3.5-hour Wnt treatment (Fig. 2A and fig. S2, F and G). Caveolin—which is a marker of caveolae, cholesterol-rich invaginations of the plasma membrane—was recently shown to colocalize with LRP6 and to be required for Wnt-mediated LRP6 endocytosis (13).

In contrast to most trafficking markers, colocalization of phospho-LRP6 aggregates was observed with other components of the Wnt/ β -catenin network, including Fz8, glycogen synthase kinase 3 β (GSK3 β), Dvl, and Axin (Fig. 2, B to E). Furthermore, very pronounced phosphorylated aggregates were observed in the cytoplasm of cells transfected with constitutively active LRP6 (LRP6 Δ E1-4, lacking the ligand binding domain)

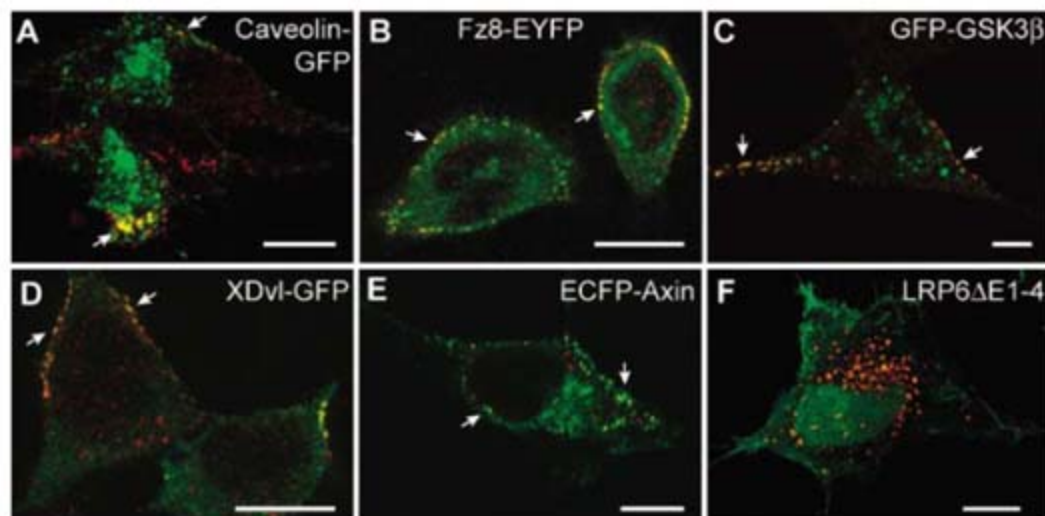


Fig. 2. Colocalization of phospho-LRP6 aggregates with Caveolin and Wnt pathway members. (A to E) HeLa cells were transfected with LRP6 and the indicated protein (green) and stained for phospho-LRP6 (red). Cells were treated with Wnt3a-conditioned medium for 1 hour (A) or 3 hours (B to E). (F) HeLa cells transfected with membrane-bound EYFP (green) and constitutively active LRP6(Δ E1-4) and stained for phospho-LRP6 (red). Note large cytoplasmic aggregates. Scale bar, 10 μ m.

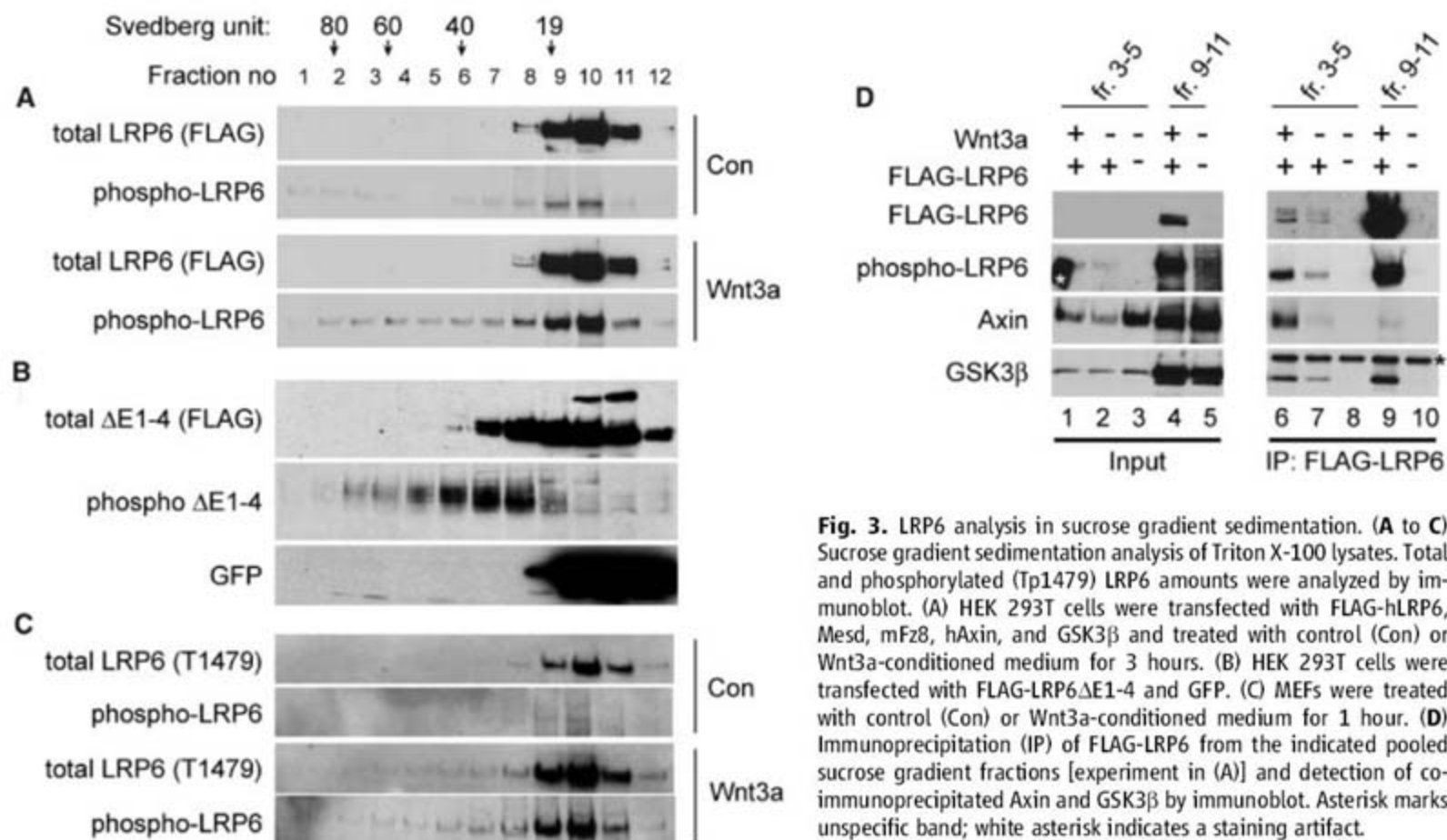


Fig. 3. LRP6 analysis in sucrose gradient sedimentation. (A to C) Sucrose gradient sedimentation analysis of Triton X-100 lysates. Total and phosphorylated (Tp1479) LRP6 amounts were analyzed by immunoblot. (A) HEK 293T cells were transfected with FLAG-hLRP6, Mesd, mFz8, hAxin, and GSK3 β and treated with control (Con) or Wnt3a-conditioned medium for 3 hours. (B) HEK 293T cells were transfected with FLAG-LRP6 Δ E1-4 and GFP. (C) MEFs were treated with control (Con) or Wnt3a-conditioned medium for 1 hour. (D) Immunoprecipitation (IP) of FLAG-LRP6 from the indicated pooled sucrose gradient fractions [experiment in (A)] and detection of co-immunoprecipitated Axin and GSK3 β by immunoblot. Asterisk marks unspecific band; white asterisk indicates a staining artifact.

(fig. S2H) without Wnt stimulation (Fig. 2F). This suggests that LRP6 Δ E1-4 clusters even without Wnt. Wnt-dependent colocalization was also observed for endogenous LRP6 and Dvl2 and Axin in P19 cells (fig. S3A), thus corroborating co-aggregation observed for *Xenopus* LRP6 and Dvl2 (Fig. 1C). We conclude that phospho-LRP6 aggregates represent specialized compartments that assemble components of the Wnt and β -catenin pathway. This compartment is associated with the plasma membrane, partially positive for Caveolin, and largely devoid of fluid-phase marker.

To analyze phospho-LRP6 aggregates biochemically, we solubilized the complexes in detergent and separated them by sucrose density gradient centrifugation (Fig. 3). In Wnt-stimulated and unstimulated cells, total LRP6 showed a relatively discrete peak, cosedimenting approximately with thyroglobulin (670 kD, 19S) (Fig. 3A). In contrast, in Wnt-stimulated cells about half of phospho-LRP6 was "tailing" into much heavier fractions (fractions 1 to 7), overlapping the ribosome peaks, whereas only little phospho-LRP6 was detectable in unstimulated cell lysates. Constitutively active LRP6 Δ E1-4 showed even greater high-molecular weight (MW) enrichment than phospho-LRP6, despite its four times lower MW (Fig. 3B). This indicates that LRP6 Δ E1-4 undergoes strong self-aggregation without Wnt stimulation. In contrast, cotransfected green fluorescent protein (GFP) was never detected in high MW fractions, even in a deliberately overexposed immunoblot (Fig. 3B).

Endogenous phospho-LRP6 in nontransfected mouse embryonic fibroblasts (MEFs) was also detectable in fractions 3 to 7 in a Wnt-dependent manner (Fig. 3C), corroborating that this is not an overexpression artifact. The weaker signal in this case, as well as the observed heterogeneity of phospho-LRP6 aggregates, may be due to their instability, for example, because of partial dephosphorylation and/or degradation during the biochemical analysis.

Axin and GSK3 β were cosedimenting with phospho-LRP6 in heavy fractions independent of Wnt treatment (fig. S4). Dvl2, despite its ability to readily form large intracellular polymers (14, 15), was found in the light fractions (fig. S4), supporting the idea that these polymers are highly dynamic, short-lived, and hence unstable in lysates [see below and (16)].

To confirm that LRP6, Axin, and GSK3 β not only cosediment but are in a complex, we carried out immunoprecipitations from pooled fractions of the sucrose gradient (Fig. 3D). This analysis showed that, whereas Axin is present in all phospho-LRP6-containing fractions (fig. S4), it is complexed only to the aggregated LRP6 form (fractions 3 to 5) and only after Wnt stimulation (compare lane 6 to lane 7). Also, GSK3 β is bound preferentially to aggregated LRP6.

These data with detergent-solubilized cell lysates indicate (i) that LRP6 aggregation is accompanied by its phosphorylation at T1479, (ii) that the microscopically observed phospho-LRP6 aggregates are not the result of cotrapping of

Wnt pathway components in a cargo vesicle (17, 18, 13) but that they represent high-MW protein complexes, (iii) that constitutive activation of LRP6 (Δ E1-4) is accompanied by spontaneous aggregation, and (iv) that Axin and GSK3 β are preferentially associated with aggregated LRP6.

Dvl is a component of the Wnt pathway that is also known to oligomerize and to occur in punctate structures (14, 19, 15). Recent studies (20, 16) demonstrated that Dvl can polymerize and form large protein assemblies that are highly dynamic, short-lived, and reversible, reminiscent of the LRP6 aggregates described here. We observed that endogenous Dvl2 forms membrane-associated aggregates in response to Wnt stimulation (fig. S3B), similar to LRP6. This is an important observation, because Dvl punctae tend to be dismissed as an unphysiological response due to overexpression (21).

In light of these and previous findings (22) and our observation that endogenous Dvl2 and activated LRP6 reside in a common protein assembly, we asked whether Dvl may be required for LRP6 phosphorylation and aggregation. Indeed, knockdown of *dsh/dvl* by RNA interference (RNAi) in *Drosophila* and small interfering RNAs (siRNAs) in MEFs, respectively, inhibited Wnt-induced LRP6 phosphorylation at the CK1 γ site T1479 (Fig. 4A). Similarly, dominant negative Dvl mutants M1 and M2, which block both self-aggregation and signaling of wild-type Dvl (16), also blocked LRP6 phosphorylation (fig. S5A). Concomitantly, phospho-LRP6 aggregates were reduced, as determined by immunofluorescence (Fig. 4B).

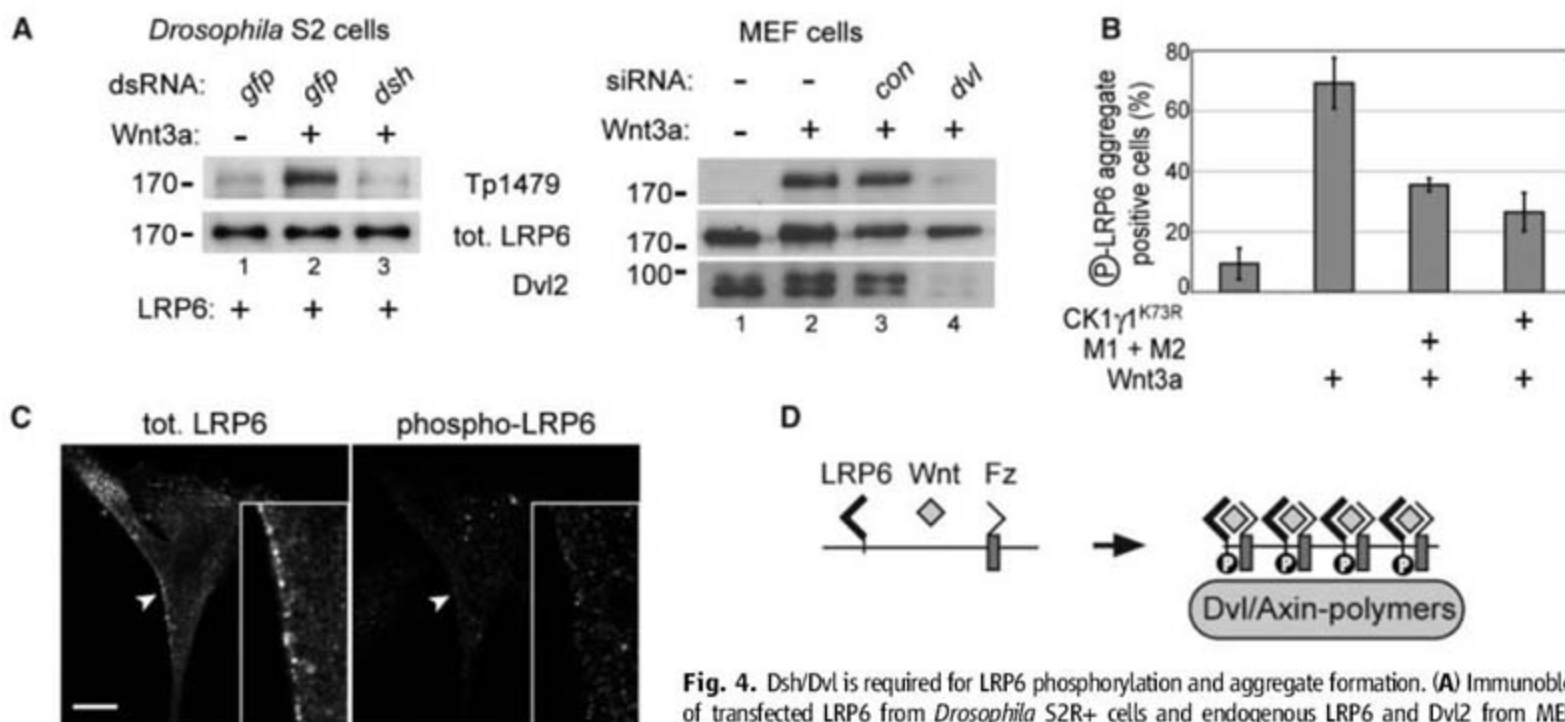


Fig. 4. Dsh/Dvl is required for LRP6 phosphorylation and aggregate formation. (A) Immunoblot of transfected LRP6 from *Drosophila* S2R+ cells and endogenous LRP6 and Dvl2 from MEF, treated with *dsh* dsRNA and *dvl2/3* siRNAs, respectively. (B) HeLa cells were transfected with CK1 γ 1^{K73R} and analyzed by immunofluorescence microscopy for phospho-LRP6 aggregates. Cells positive for EYFP were scored for phospho-LRP6 staining. Error bars indicate standard deviation of the mean; $n = 3$ experiments. (C) Immunofluorescence of HeLa cells transfected with LRP6-EYFP and dominant negative CK1 γ 1^{K73R}, treated with Wnt3a-conditioned medium and stained with Ab Tp1479. LRP6-EYFP (tot. LRP6) and phospho-LRP6 are shown. Note Wnt-induced LRP6 aggregates (arrowheads and higher-magnification insets), which are nonphosphorylated. (D) LRP6-signalosome model. Wnts bridge LRP6 and Fz transmembrane receptors and promote recruitment of polymers of Dvl, which binds Fz. Dvl and Axin co-polymerize LRP6, which induces receptor phosphorylation by CK1 γ . Axin sequestration in LRP6-signalosomes may block GSK3 β phosphorylation of β -catenin, leading to β -catenin accumulation. Other components of the Wnt pathway, such as GSK3 β and adenomatous polyposis coli (APC), are likely components of the LRP6-signalosome but not shown for clarity.

LRP6-EYFP, dominant negative *dvl* mutants M1 and M2, or dominant negative CK1 γ 1^{K73R} and analyzed by immunofluorescence microscopy for phospho-LRP6 aggregates. Cells positive for EYFP were scored for phospho-LRP6 staining. Error bars indicate standard deviation of the mean; $n = 3$ experiments. (C) Immunofluorescence of HeLa cells transfected with LRP6-EYFP and dominant negative CK1 γ 1^{K73R}, treated with Wnt3a-conditioned medium and stained with Ab Tp1479. LRP6-EYFP (tot. LRP6) and phospho-LRP6 are shown. Note Wnt-induced LRP6 aggregates (arrowheads and higher-magnification insets), which are nonphosphorylated. (D) LRP6-signalosome model. Wnts bridge LRP6 and Fz transmembrane receptors and promote recruitment of polymers of Dvl, which binds Fz. Dvl and Axin co-polymerize LRP6, which induces receptor phosphorylation by CK1 γ . Axin sequestration in LRP6-signalosomes may block GSK3 β phosphorylation of β -catenin, leading to β -catenin accumulation. Other components of the Wnt pathway, such as GSK3 β and adenomatous polyposis coli (APC), are likely components of the LRP6-signalosome but not shown for clarity.

The scaffold protein Dvl was previously thought to act downstream of LRP6 because *dsh* overexpression activates β -catenin signaling in *Drosophila* LRP6 (*arrow*) mutants (23) and because the constitutively active Dfz2-Arrow fusion protein is inactive in *dsh* mutants (24). The explanation for this discrepancy may be that overexpressing Dsh/Dvl leads to artificial sequestration of Axin or that the protein has multiple functions in the Wnt pathway.

Taken together, the results suggest that Dvl-mediated co-aggregation triggers LRP6 phosphorylation by CK1 γ . In this model (Fig. 4D), upon Wnt signaling Dvl aggregates form at the plasma membrane, where they co-cluster LRP6 with other pathway components including Fz, Axin, and GSK3 β , in a "LRP6-signalosome." The role of Wnt would be to bridge LRP6 and Fz (25, 5), which copolymerize on a Dvl platform. Clustering of LRP6 then provides a high local receptor concentration that triggers phosphorylation by CK1 γ and Axin recruitment.

Predictions of this model are as follows: (i) artificial oligomerization of LRP6 should activate the receptor and (ii) oligomerized LRP6 should signal independent of Dvl. Indeed, forced oligomerization of LRP6 using a synthetic multimerizer is sufficient to induce Wnt signaling, and this oligomerization bypasses the need for Dvl (25). (iii) Constitutively active LRP6 should signal independently of Dvl because its self-aggregation should bypass the need for Dvl polymers. This is

also the case as shown in reporter assays with Dvl siRNA knockdown (fig. S5, B and C), which supports previous findings (26, 25). (iv) If LRP6 aggregation is a prerequisite for phosphorylation by CK1 γ rather than its consequence, LRP6 aggregates should form even when the kinase is blocked. This is the case: Nonphosphorylated LRP6 aggregates were observed in response to Wnt treatment in cells transfected with dominant-negative CK1 γ (Fig. 4C). The model of LRP6-signalosomes not only provides a mechanism for Wnt signal transduction but may also be relevant for the understanding of intracellular transport of maternal Wnt determinants in the fertilized *Xenopus* egg (27).

References and Notes

1. P. Polakis, *Genes Dev.* **14**, 1837 (2000).
2. R. T. Moon, B. Bowerman, M. Boutros, N. Perrimon, *Science* **296**, 1644 (2002).
3. C. Y. Logan, R. Nusse, *Annu. Rev. Cell Dev. Biol.* **20**, 781 (2004).
4. R. T. Moon, A. D. Kohn, G. V. De Ferrari, A. Kaykas, *Nat. Rev. Genet.* **5**, 691 (2004).
5. X. He, M. Semenov, K. Tamai, X. Zeng, *Development* **131**, 1663 (2004).
6. N. S. Tolwinski, E. Wieschaus, *Trends Genet.* **20**, 177 (2004).
7. G. Davidson et al., *Nature* **438**, 867 (2005).
8. X. Zeng et al., *Nature* **438**, 873 (2005).
9. J. Klingensmith, R. Nusse, N. Perrimon, *Genes Dev.* **8**, 118 (1994).
10. K. Itoh, B. K. Brott, G. U. Bae, M. J. Ratcliffe, S. Y. Sokol, *J. Biol.* **4**, 3 (2005).
11. C. C. Malbon, H. Y. Wang, *Curr. Top. Dev. Biol.* **72**, 153 (2006).
12. J. Mao et al., *Mol. Cell* **7**, 801 (2001).

13. H. Yamamoto, H. Komekado, A. Kikuchi, *Dev. Cell* **11**, 213 (2006).
14. J. D. Axelrod, J. R. Miller, J. M. Shulman, R. T. Moon, N. Perrimon, *Genes Dev.* **12**, 2610 (1998).
15. U. Rothbacher et al., *EMBO J.* **19**, 1010 (2000).
16. T. Schwarz-Romond et al., *Nat. Struct. Mol. Biol.* **14**, 484 (2007).
17. D. G. Capelluto et al., *Nature* **419**, 726 (2002).
18. J. T. Blitzer, R. Nusse, *BMC Cell Biol.* **7**, 28 (2006).
19. S. Kishida et al., *Mol. Cell. Biol.* **19**, 4414 (1999).
20. T. Schwarz-Romond, C. Merrifield, B. J. Nichols, M. Bienz, *J. Cell Sci.* **118**, 5269 (2005).
21. M. J. Smalley et al., *J. Cell Sci.* **118**, 5279 (2005).
22. A. Cliffe, F. Hamada, M. Bienz, *Curr. Biol.* **13**, 960 (2003).
23. M. Wehrli et al., *Nature* **407**, 527 (2000).
24. N. S. Tolwinski et al., *Dev. Cell* **4**, 407 (2003).
25. F. Cong, L. Schweizer, H. Varmus, *Development* **131**, 5103 (2004).
26. L. Li, J. Mao, L. Sun, W. Liu, D. Wu, *J. Biol. Chem.* **277**, 5977 (2002).
27. C. Weaver, D. Kimelman, *Development* **131**, 3491 (2004).
28. We thank R. Pepperkok for support in the EMBL Advanced Light Microscopy Facility; the Nikon Imaging Center at the University of Heidelberg and M. Boutros and D. Ingelfinger for help with siRNA experiments; A. Glinka for advice; N. Maltry for technical help; and J. Axelrod, A. Helenius, J. Nathans, R. Nusse, T. Schwarz-Romond, and M. Semenov for reagents. This work was supported by the European Union (Endotrack) and the Deutsche Forschungsgemeinschaft.

Supporting Online Material

www.sciencemag.org/cgi/content/full/316/5831/1619/DC1
Materials and Methods

Figs. S1 to S5
Movie S1

1 November 2006; accepted 11 May 2007
10.1126/science.1137065

Neural Responses to Taxation and Voluntary Giving Reveal Motives for Charitable Donations

William T. Harbaugh,^{1,2*} Ulrich Mayr,^{3*} Daniel R. Burghart¹

Civil societies function because people pay taxes and make charitable contributions to provide public goods. One possible motive for charitable contributions, called "pure altruism," is satisfied by increases in the public good no matter the source or intent. Another possible motive, "warm glow," is only fulfilled by an individual's own voluntary donations. Consistent with pure altruism, we find that even mandatory, tax-like transfers to a charity elicit neural activity in areas linked to reward processing. Moreover, neural responses to the charity's financial gains predict voluntary giving. However, consistent with warm glow, neural activity further increases when people make transfers voluntarily. Both pure altruism and warm-glow motives appear to determine the hedonic consequences of financial transfers to the public good.

Every society needs public goods, but the mechanisms used to fund them vary. For example, taxation and government spending are lower in the United States than in most European countries, but philanthropy is higher (1). To economists, this charitable giving is a puzzle: Money is a good, so why are people willing to give

it away? One possible explanation is in terms of a "pure altruism" motive (2). Individuals with such a motive receive satisfaction from increases in a public good, such as the provision of basic services to the needy. This altruistic concern provides a motive to give, but there is also an incentive to keep money for oneself, because the cost of such charity is entirely paid by the giver, whereas the benefits are spread out over all those people who care about the needy. Only those people with a very large pure altruism motive would give voluntarily, and taxation is the normal social solution to the resulting free-riding. Pure altruism implies that people should get

some satisfaction even when public goods are supplied through mandatory taxation, because, by this account, people care only about how much of the public good is provided and not about the process by which the transfer occurs. A second possible motive for charitable giving is the sense of agency associated with the act of voluntary giving. This reward from giving has been termed "warm glow" (3, 4). If givers were driven exclusively by the warm-glow motive, they should derive satisfaction from making a voluntary gift, rather than from the increase in the level of the public good itself. On the other hand, taxation should not produce a warm glow, because paying taxes typically does not involve a voluntary choice.

The distinction between pure altruism and warm-glow motives for giving is important for several reasons. First, if giving is motivated by pure altruism, tax-funded government expenditures to provide a public good will reduce private giving, potentially dollar for dollar, as people cut their voluntary contributions in response to these higher taxes (5). There should be no similar effect with warm-glow givers, as their benefit derives from the amount of their gift. Second, a warm-glow motive for altruism provides an argument in favor of policies that encourage voluntary giving, because the warm-glow benefit provides a reward to the giver that exceeds the benefit from paying an equivalent amount in taxes (6).

Neural evidence may help clarify the relative importance of pure altruism and warm-glow motives for charitable giving. Although there is

¹Department of Economics, University of Oregon, Eugene, OR 97403-1285, USA. ²National Bureau of Economic Research (NBER), Cambridge, MA 02138-5398, USA. ³Department of Psychology, University of Oregon, Eugene, OR 97403-1227, USA.

*To whom correspondence should be addressed. E-mail: mayr@uoregon.edu (U.M.) or harbaugh@uoregon.edu (W.T.H.)

considerable evidence linking neural activity in the ventral striatum and the insulae to the processing of concrete rewards such as money, food, and drugs, less is known about how the brain processes more abstract rewards such as those often provided by public goods. For money, activity in the ventral striatum increases as people anticipate increases in payoffs and when they receive unexpected increases in payoffs (7, 8).

Neural responses in the ventral striatum and insulae to information about products and their prices also predict purchase decisions (9). This work supports the theory that these areas provide information on the relative rewards of different outcomes, which serve as an input to decisions about consumption and tradeoffs regarding risk and money (10). Other studies have shown that activity in the ventral striatum and the insulae is

correlated with more abstract rewards, including social rewards such as punishing unfair players in sharing games (11), voluntary contributions to charities (12, 13), and decisions to trust others (14, 15). These results motivate our focus on the ventral striatum and the insulae.

To test for the pure altruism and warm-glow motives, we used functional magnetic resonance imaging while subjects played a dictator game. Subjects received \$100 and then made decisions about whether or not to give money to a local food bank. They also observed mandatory, tax-like transfers of their money to the food bank (Fig. 1, A and B) (16). The behavioral results in this experiment are consistent with economic theory and are similar to those reported in earlier economic experiments (17–19). As shown in Fig. 2A, increases in the amounts going to the charity and decreases in the cost to the giver both increased the likelihood that a voluntary transfer was accepted. Self-reported satisfaction with the transaction followed the same pattern in both the voluntary and the mandatory conditions (Fig. 2B).

To investigate the neural activity associated with pure altruism, we used data from the mandatory treatments, which involved exogenous changes in subject and charity payoffs. Contrasts of parameter estimates (Fig. 3) show that activation in very similar areas of the ventral striatum increased with the monetary payoff to both the subject and to the charity. Regression analyses to explain activation data extracted from anatomical regions of interest (ROIs) show the same result (table S4) (16). This is the first evidence we know of demonstrating that mandatory taxation for a good cause can produce activation in specific brain areas that have been tied to concrete, individualistic rewards.

The pure altruism model predicts that people who highly value increases in the charity's payoff, relative to the value they place on getting money for themselves, will be more likely to give. The evidence economists have typically used to support this model has been indirect: Relative values have been inferred from observed decisions (20). Our experiment allowed us to observe brain activation, in areas known to respond to rewards, as we varied the money the subject received and the money the charity received. This provides a direct test of the model: Do across-subject differences in neural responses to subject and charity payoffs predict who is more likely to give to the charity?

We are able to address this question out of treatment by using neural responses in those "pure" mandatory conditions where only the subject or only the charity got money (orange and green cells, respectively, in Fig. 1B). These responses potentially serve as an indicator of how much subjects valued money for themselves and for the charity. In fact, regression coefficients show that subjects with larger activation responses to money for themselves were less likely to give to the charity (black columns in Fig. 4A), and subjects with larger activation responses to money for the charity were more likely to give (gray columns in Fig. 4A). To illustrate this rela-



Fig. 1. (A) Study protocol. We scanned 19 females using functional magnetic resonance imaging (fMRI) while they were presented with transfers that affected their own account (starting amount, \$100) and the account of a local charity. Half the transfers were mandatory, to resemble taxation; the other half were voluntary. We explained that the experimenters would not know their choices and that one mandatory and one voluntary transfer would be randomly chosen and implemented after the experiment. Events for each trial occurred as presented in the time line, details are in the supporting online material (16). After a 1-s fixation dot, the screen revealed whether this trial's transfer was mandatory or voluntary, as well as the dollar amount change to the accounts of the subject and the charity. After 9 s, two vertically aligned labels were added in the lower portion of the screen, specifying the vertically aligned buttons on a response box. For mandatory transfers, one of the labels read "acknowledge" and the other "invalid button." For voluntary transfers, one of the labels read "accept" and the other "reject." Label positions varied randomly from trial to trial. Immediately after the subject's response, a four-point satisfaction rating scale was shown, to which subjects responded by pressing one of four laterally oriented keys on the button box. The rating scale disappeared after 6 s, and there was a blank screen for an intertrial period that was randomly jittered between 6, 7, and 8 s. **(B)** Study design. The cells show the dollar transfers. Each design cell was implemented three times as a mandatory transfer and three times as a voluntary decision. Orange cells indicate pure gains to the subject; green cells indicate pure gains to the charity. These pure-gain design cells from the mandatory condition were used to predict voluntary giving in the purple cells, where there was a tradeoff between the subject and the charity (see Fig. 4, A and B).

B Key:

Subject \$	-45	-45	-45	-45
Charity \$	0	15	30	45
45	-30	-30	-30	-30
30	-15	-15	-15	-15
15	0	0	0	0
0	0	15	30	45

Fig. 2. (A) Subjects' choices during voluntary transfers as a function of payoffs to the subject and the charity. Many transfers that were costly to the subject but benefited the charity were accepted, and the rate of acceptance increased as the cost of making a given transfer declined. **(B)** Subjective satisfaction ratings as a function of payoffs to the subject and the charity, as well as the voluntary-mandatory factor. Subjective satisfaction increased as transfers increased and costs decreased and was higher in the voluntary (solid lines) than in the mandatory conditions (dashed lines).

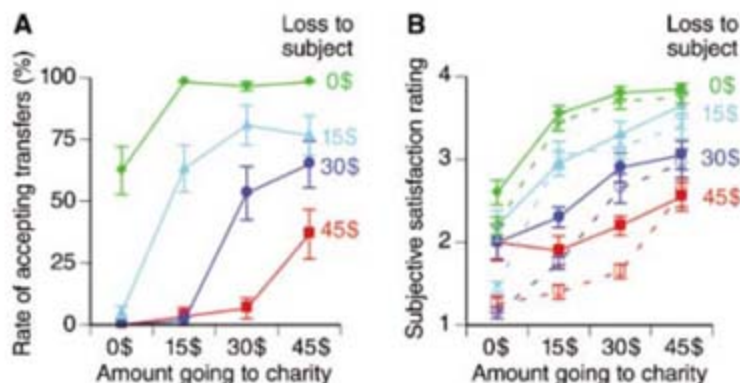


Fig. 3. Neural response in the ventral striatum to mandatory payoffs for the subject (yellow), the charity (blue), and both (green).



relationship graphically, in Fig. 4B we plotted individual acceptance rates against the difference between the neural response to pure charity gains and pure subject gains, pooled over all the regions in Fig. 4A. We also split the sample into “altruists” ($n = 10$) and “egoists” ($n = 9$) depending on whether they had a larger neural response to the charity’s payoff or to their own payoff. Altruists gave money nearly twice as often as egoists (58% versus 31%, $P = 0.015$). This supports the existence of a purely altruistic motive: The larger a person’s neural response to increases in the public good, no matter the source, the more likely they will give voluntarily.

How then is voluntary giving different from tax-like transfers? Reported satisfaction ratings were about 10% higher for voluntary than for the mandatory transfers ($P < 0.01$, see Fig. 2B and table S2) (16). The neural evidence shows a similar result; t tests indicate higher activation in the caudate (left, $P = 0.015$; right, $P = 0.004$); the right nucleus accumbens ($P = 0.01$); and the insulae (left, $P = 0.063$; right, 0.075) in the case of voluntary transfers (table S4) (16).

Of course, these results might simply reflect the basic economic principle that adding choices cannot make the decision-maker worse off. This follows because a person who likes the payoffs in a given mandatory transfer can always obtain that same result in the corresponding voluntary condition by accepting the transfer. However, if the subject does not like the proposed transfer, only the voluntary conditions give them the option of rejecting it and keeping the money. Overall, 55% of the voluntary transfers that involved a subject’s giving up money to the charity (purple cells in Fig. 1B) were rejected. This led to an increase in the expected payoff to the individual of \$13 or 33%, and a decrease in the expected payoff to the charity of \$7 or 10%, relative to the mandatory condition. So, although the opportunity for free

choice means higher activation in the caudate, the left nucleus accumbens, and the insulae, as well as higher payoffs to the individual, it reduced the level of funding for the public good.

An important question, then, is to what degree the observed higher activation comes from the ability to make a choice and to what extent it results from the differences in payoffs from that choice. We looked again at the differences in activation and satisfaction ratings between the mandatory and voluntary conditions, but this time controlling for the consequences of rejection by replacing those payoff changes with \$0. The voluntary-mandatory activation difference remained reliable for the caudate (left, $P = 0.023$; right, $P = 0.011$) and the right nucleus accumbens ($P = 0.042$), even after we controlled for payoffs (table S6) (16). Also, reported satisfaction was higher for voluntary than for mandatory transfers after controlling for payoffs ($P < 0.065$ for the complete design; $P < 0.001$ using the cells involving tradeoffs, purple in Fig. 1B). The pure altruism motive for giving, along with the story about adding choices described above, would imply that there should be no mandatory-voluntary differences after controlling for the payoff effects. Thus, our results suggest that both the increased payoffs and the ability to choose lead to increased neural activity and satisfaction.

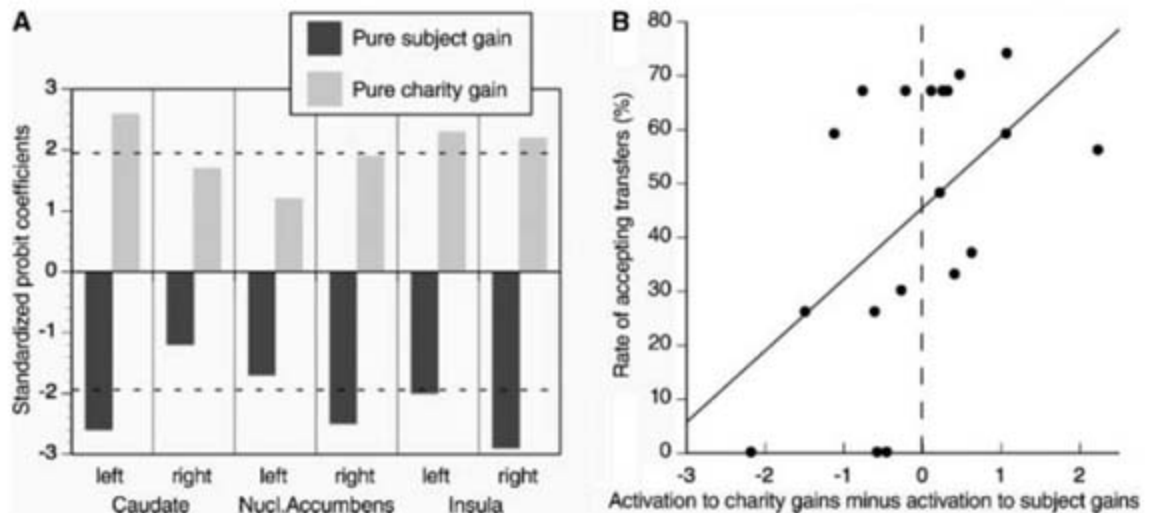
Previous results have demonstrated that activity in the areas we examined is larger when reward can be linked to one’s own actions rather than to extraneous factors (21–24). Our results extend these findings about the role of agency in reward-processing to the important situation involving a choice between the subject’s private payoff and the public good. What is not clear from earlier reports is whether agency-linked modulation of reward activity is actually associated with a modulation of hedonic value. Our study shows that neural activity in the caudate and right nucleus accumbens, as well as subjective

satisfaction, is larger in the voluntary than in the mandatory situation. The fact that this effect persists even after controlling for payoffs supports the warm-glow theory of giving (3).

In summary, we find that three very different things—monetary payoffs to oneself, observing a charity get money, and a warm-glow effect related to free choice—all activate similar neural substrates. This result supports arguments for a common “neural currency” of reward (25–29) and shows that this model can be applied not just to choice over money, risk, and private consumption goods, but also to more abstract policy choices involving taxation and charitable giving (12). Our results are also important for understanding why people give money to charitable organizations. First, these transfers are associated with neural activation similar to that which comes from receiving money for oneself. The fact that mandatory transfers to a charity elicit activity in reward-related areas suggests that even mandatory taxation can produce satisfaction for taxpayers. A better understanding of the conditions under which taxation elicits “neural rewards” could prove useful for evaluating the desirability of different tax policies. Second, we show that the opportunity for free choice is associated with increased activity in regions implicated in processing rewards, as well as with higher reported satisfaction. Furthermore, this effect is not entirely accounted for by increased payoffs. In the context of charitable giving, this choice-related benefit is consistent with a warm-glow motive for giving.

In combination, these results suggest that both pure altruism and warm glow are important motives for charitable giving. Future work may reveal whether the free-choice effect found here extends to other situations, and under which conditions taxation elicits “neural” rewards. A related question is whether people who vote for a tax to provide a public good get a warm-glow benefit.

Fig. 4. (A) Predicting giving from activations in mandatory “pure-gain” conditions. We created measures of neural activation in response to “pure subject gain” and “pure charity gain” by averaging activation from the mandatory conditions where the subject received money at no cost to the charity and where the charity received money at no cost to the subject (orange and green cells, respectively, in Fig. 1B). We used these two sets of activations as independent predictors of the average acceptance rate in the nine design cells involving a tradeoff (purple cells in Fig. 1B). The figure shows standardized probit regression coefficients from models including subject and charity stakes as control variables and neural response to pure subject gains and pure charity gains as independent predictors. The dashed lines indicate $P = 0.05$ significance. Higher response to pure subject gain was consistently associated with less giving. Higher response to pure charity gains was consistently associated with more giving. Coefficients for individual predictors were reliable in seven out of 12 cases. **(B)** Differences in activation predict giving. As an overall measure, we



averaged the neural activation measures across all six brain areas and computed the difference between neural responses to the charity’s pure gains and the neural responses to the subject’s pure gains (orange and green cells in Fig. 2B). Giving increased as the neural response to pure charity gains outweighed the neural response to pure subject gains ($R^2 = 27\%$, $P = 0.02$).

Last, public goods by their very nature are seldom traded in markets, and so we cannot observe the prices people will pay and then use these to measure value. The finding that neural activity predicts voluntary donations suggests that such activity could eventually help measure values and determine optimal levels of public goods.

References and Notes

- Center for Civil Society Studies, www.jhu.edu/cnsp/research/compdata.html.
- S. C. Kolm, in *Public Economics*, J. Margolis and H. Guitton, Eds. (Macmillan, London, 1969), pp. 145–200.
- J. Andreoni, *Econ. J.* **100**, 464 (1990).
- W. T. Harbaugh, *J. Pub. Econ.* **67**, 269 (1998).
- T. Bergstrom, L. Blume, H. Varian, *J. Pub. Econ.* **29**, 25 (1986).
- P. Diamond, *J. Pub. Econ.* **90**, 897 (2006).
- W. Schultz, P. Dayan, P. R. Montague, *Science* **275**, 1593 (1997).
- C. M. Kuhnen, B. Knutson, *Neuron* **47**, 763 (2005).
- B. Knutson, S. Rick, G. E. Wimmer, D. Prelec, G. Loewenstein, *Neuron* **53**, 147 (2007).
- P. W. Glimcher, A. Rustichini, *Science* **306**, 447 (2004).
- D. J. F. de Quervain *et al.*, *Science* **305**, 1254 (2004).
- J. Moll *et al.*, *Proc. Natl. Acad. Sci. U.S.A.* **103**, 15623 (2006).
- D. Tankersley, C. J. Stowe, S. A. Huettel, *Nat. Neurosci.* **10**, 150 (2007).
- J. K. Rilling *et al.*, *Neuron* **35**, 395 (2002).
- T. Singer, S. J. Kiebel, S. W. Joel, J. D. Dolan, C. Frith, *Neuron* **41**, 653 (2004).
- Materials and methods are available as supporting material in Science Online.
- R. Forsythe, J. L. Horowitz, N. E. Savin, M. Sefton, *Games Econ. Behav.* **6**, 347 (1994).
- C. C. Eckel, P. J. Grossman, *J. Pub. Econ.* **87**, 681 (2003).
- J. Andreoni, J. H. Miller, *Econometrica* **70**, 737 (2002).
- T. R. Palfrey, J. E. Prisbrey, *Am. Econ. Rev.* **87**, 829 (1997).
- R. Elliott, J. L. Neuman, O. A. Longe, J. F. Deakin, *Neuroimage* **21**, 984 (2004).
- J. O'Doherty *et al.*, *Science* **304**, 452 (2004).
- E. M. Tricomi, M. R. Delgado, J. A. Fiez, *Neuron* **41**, 281 (2004).
- C. F. Zink, G. Pagnoni, M. E. Martin-Skurski, J. G. Chappelow, G. S. Berns, *Neuron* **42**, 509 (2004).
- P. R. Montague, G. S. Berns, *Neuron* **36**, 265 (2002).
- B. King-Casas *et al.*, *Science* **308**, 78 (2005).
- M. R. Delgado, L. E. Nyström, C. Fissell, D. C. Noll, J. A. Fiez, *J. Neurophysiol.* **84**, 3072 (2000).
- B. Knutson, G. W. Fong, C. M. Adams, J. L. Varner, D. Hommer, *Neuroreport* **12**, 3683 (2001).
- B. Knutson, C. M. Adams, G. W. Fong, D. Hommer, *J. Neurosci.* **21**, RC159 (2001).
- Author contributions: Lead authorship was determined by a coin flip between the first two authors. Supported by the National Institute of Aging R01 AG1929601A1 and NSF SES-0112157. We would like to thank J. Andreoni, R. Bryck, T. Cameron, J. Chalmers, C. Rode, M. Taylor, and S. Frey, as well as the staff at the Lewis Center for Neuroimaging at the University of Oregon.

Supporting Online Material

www.sciencemag.org/cgi/content/full/316/5831/1622/DC1

Materials and Methods

Fig. S1

Tables S1 to S7

References

2 February 2007; accepted 9 May 2007

10.1126/science.1140738

Sequence Finishing and Mapping of *Drosophila melanogaster* Heterochromatin

Roger A. Hoskins,^{1*} Joseph W. Carlson,^{1*} Cameron Kennedy,¹ David Acevedo,¹ Martha Evans-Holm,¹ Erwin Frise,¹ Kenneth H. Wan,¹ Soo Park,¹ Maria Mendez-Lago,² Fabrizio Rossi,³ Alfredo Villasante,² Patrizio Dimitri,³ Gary H. Karpen,^{1,4} Susan E. Celniker^{1†}

Genome sequences for most metazoans and plants are incomplete because of the presence of repeated DNA in the heterochromatin. The heterochromatic regions of *Drosophila melanogaster* contain 20 million bases (Mb) of sequence amenable to mapping, sequence assembly, and finishing. We describe the generation of 15 Mb of finished or improved heterochromatic sequence with the use of available clone resources and assembly methods. We also constructed a bacterial artificial chromosome–based physical map that spans 13 Mb of the pericentromeric heterochromatin and a cytogenetic map that positions 11 Mb in specific chromosomal locations. We have approached a complete assembly and mapping of the nonsatellite component of *Drosophila* heterochromatin. The strategy we describe is also applicable to generating substantially more information about heterochromatin in other species, including humans.

Heterochromatin is a major component of metazoan and plant genomes (e.g., ~20% of the human genome) that regulates chromosome segregation, nuclear organization, and gene expression (1–4). A thorough description of the sequence and organization of heterochromatin is necessary for understanding the essential functions encoded within this region of the genome. However, difficulties in cloning, mapping, and assembling regions rich in repetitive elements have hindered the genomic analysis

of heterochromatin (5–7). The fruit fly *Drosophila melanogaster* is a model for heterochromatin studies. About one-third of the genome is considered heterochromatic and is concentrated in the pericentromeric and telomeric regions of the chromosomes (X, 2, 3, 4, and Y) (5, 8). The heterochromatin contains tandemly repeated simple sequences (including satellite DNAs) (9), middle repetitive elements [such as transposable elements (TEs) and ribosomal DNA], and some single-copy DNA (10).

The whole-genome shotgun sequence (WGS3) was the foundation for finishing and mapping heterochromatic sequences and for elucidating the organization and composition of the nonsatellite DNA in *Drosophila* heterochromatin (5, 6). WGS3 is an excellent assembly of the *Drosophila* euchromatic sequence, but it has lower contiguity and quality in the repeat-rich heterochromatin. We undertook a retrospective analysis of these WGS3 scaffolds (11). Moderately repetitive sequences, such as transposable elements,

are well represented in WGS clones and sequence reads, but they tend to be assembled into shorter scaffolds with many gaps and low-quality regions because of the difficulty of accurately assigning data to a specific copy of a repeat. The typical WGS heterochromatic scaffold is smaller [for scaffolds mapped to an arm, N50 ranged from 4 to 35 kb (11)] than a typical WGS euchromatic scaffold (N50 = 13.9 Mb) (5). Relative to the euchromatic scaffolds, the WGS3 heterochromatic scaffolds have 5.8 times as many sequence gaps per Mb, as well as lower sequence quality.

To produce the Release 5 sequence, we identified a set of 10-kb genomic clones from a library representing 15× clone coverage by paired end reads (mate pairs) and used this set as templates to fill small gaps and improve low-quality regions (11). Higher-level sequence assembly into Mb-sized linked scaffolds used relationships determined from bacterial artificial chromosome (BAC)–based sequence tag site (STS) physical mapping (see below) and BAC end sequences. In addition to the WGS data, we incorporated data from 30 BACs (3.4 Mb; 15 BACs finished since Release 3) that were originally sequenced as part of the euchromatin sequencing effort (5, 10).

Sequence finishing resulted in fewer gaps, longer scaffolds, and higher-quality sequence relative to WGS3 (fig. S1). About 15 Mb of this sequence has been finished or improved, and 50% of the sequence is now in scaffolds greater than 378 kb (N50). Table 1 summarizes the Release 5 sequence statistics by chromosome arm. Improved sequence was generated for 145 WGS3 scaffolds, and a set of 90 new scaffolds were produced by joining or filling 694 gaps of previously unknown size between WGS3 scaffolds. The relationships between the initial WGS scaffolds and the Release 5 scaffolds can be complex (Fig. 1 and figs. S2 to S7); for example, there were eight cases in which small scaffolds were used to fill gaps within larger scaffolds, and two scaffolds whose gaps interdigitated. As expected, the sequence consists largely of nests of frag-

¹Department of Genome and Computational Biology, Lawrence Berkeley National Laboratory, Berkeley, CA 94720, USA. ²Centro de Biología Molecular Severo Ochoa, CSIC-UAM, Cantoblanco 28049, Madrid, Spain. ³Dipartimento di Genetica e Biologia Molecolare "Charles Darwin," Università "La Sapienza," 00185 Roma, Italy. ⁴Department of Molecular and Cell Biology, University of California, Berkeley, CA 94720, USA.

*These authors contributed equally to this work.

†To whom correspondence should be addressed. E-mail: celniker@fruitfly.org

mented TEs, and most remaining gaps are bounded by TEs or simple sequence repeats, including simple repeats not previously described (Fig. 2). The quality of the improved sequence was measured by calculating the estimated error rates within 10-kb sliding windows (overlapping

by 5 kb) on the consensus sequences (11). For all but 11 of 1832 10-kb regions not overlapping one of the known TEs, the estimated error rate is less than 1 per 17,986 base pairs (bp), well below the accepted standard for finished genomic sequence of 1 error per 10,000 bp.

Concurrent with the sequence-finishing effort, we constructed an integrated physical and cytogenetic map to describe the overall structure of the pericentromeric heterochromatin. This map was essential for ordering, orienting, and linking WGS sequence scaffolds into larger BAC contigs and Release 5 scaffolds. Heterochromatic sequences at the centric ends of the Release 3 arm sequences were represented in BAC-based physical maps of the euchromatic and telomeric portions of the chromosomes (12, 13), but most heterochromatic scaffolds had not been mapped in large-insert clones or localized to specific sites on the chromosomes.

BAC-based STS content mapping of WGS3 scaffolds, using 354 probes designed from genomic sequence and five BAC libraries (11), extended and linked many scaffolds into larger

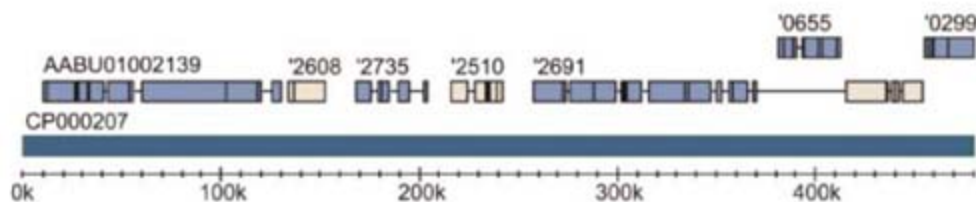


Fig. 1. Comparison of WGS scaffolds to the corresponding Release 5 scaffold. WGS scaffolds (gray, same orientation; tan, opposite orientation) are diagrammed above the Release 5 scaffold (blue). Sequence gaps (thin horizontal lines) in WGS scaffolds are indicated.

Table 1. Status of Release 5. Sequence statistics for the chromosomes are divided into regions contiguous with the euchromatic arm sequences (e.g., Xh) and regions mapped cytologically to those chromosome arms but not

currently connected (e.g., XHet). Bac-Based Rel. 5 refers to the amount of heterochromatin finished in BACs. N50 is the contig length such that 50% of all base pairs are contained in contigs of this length or larger.

Region	Size (bp)	BAC-Based Rel. 5	Rel. 5 without N's	N50	Sized gaps	Total gap size	Unsize gaps
Xh	392,502	312,439	392,502	392,502	0	0	0
XHet	204,112	—	204,112	204,112	0	0	0
2Lh	1,010,570	1,010,470	1,010,470	591,203	0	0	1
2LHet	368,872	—	297,872	99,162	2	71,000	0
2Rh	1,285,689	973,874	1,285,689	1,285,689	0	0	0
2RHet*	3,288,761	—	2,721,941	244,298	17	566,020	8
3Lh	1,587,982	1,020,114	1,587,982	1,587,982	0	0	0
3LHet*	2,555,491	—	2,416,308	366,456	12	138,483	7
3Rh	378,656	378,656	378,656	378,656	0	0	0
3RHet	2,517,507	—	2,264,306	252,624	10	252,801	4
YHet	347,038	—	242,806	9,129	30	101,632	26
Unmapped modified	2,419,890	—	2,222,443	73,591	15	194,247	32
Total for modified sequence	16,357,070	—	15,025,087	378,616	86	1,324,183	78
Unmapped unmodified	7,629,047	—	6,145,805	2,521	439	1,239,942	2,433
Total	23,986,117	3,383,114	21,170,892	—	525	2,564,125	2,511

*Statistics reflect the sequence distributed as Release 5 of the genome and do not account for the scaffold CP000217 moved from 2RHet to 3LHet and the scaffold CP000206 moved from 3RHet to ArmU subsequent to the release.

Fig. 2. Sequenced regions of *D. melanogaster* pericentromeric heterochromatin. The heterochromatin extends proximally from the euchromatin (black) and includes sequenced and assembled regions (aqua) and unsequenced regions (gray). The actual gap sizes between sequence scaffolds are unknown and are presented with an arbitrary 0.5-Mb separation. Finished or improved scaffolds, which end in known or novel simple repeats, are shown with the terminal repeat sequence indicated. The scaffold CP000217, originally identified as part of 2RHet but subsequently mapped to 3LHet, is shown here at its updated location (see text).

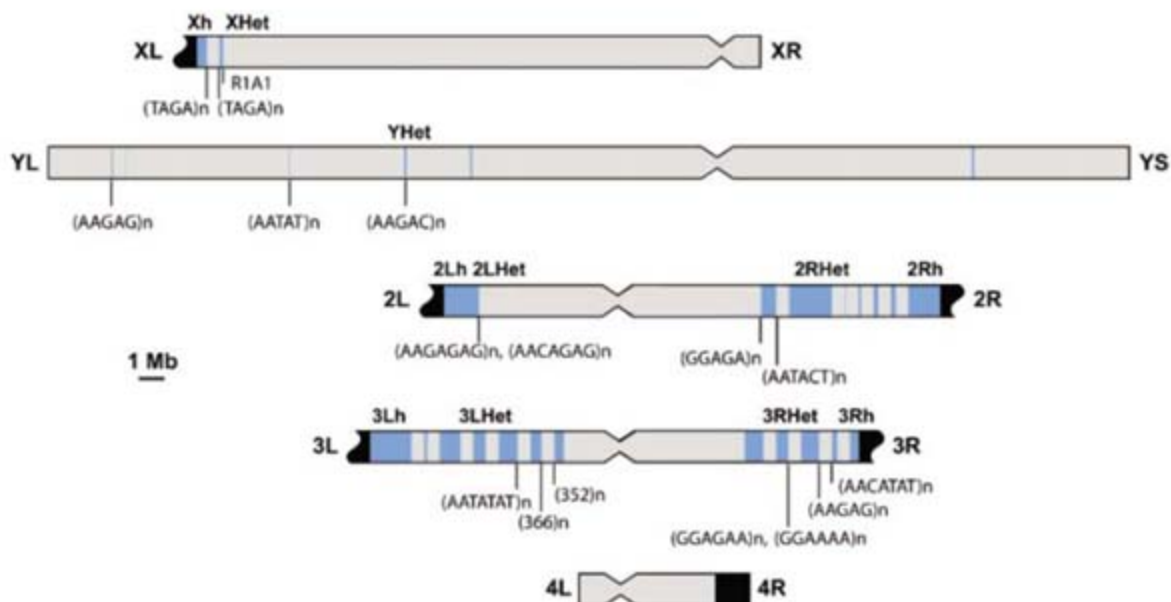


Table 2. Summary of the integrated physical and cytogenetic map assembly. N/A, not applicable.

Chromosome arm	STSs in BAC map	Failed STSs in mapped contigs	WGS3 scaffolds linked to chr. arm	WGS3 scaffolds in Het contigs	Het contigs	Sum of WGS3 lengths in mapped scaffolds (kb)
XL	16	0	3	2	1	498
2L	28	1	2	5	1	1,018
2R	91	1	5	29	3	3,517
3L	91	1	3	24	6	4,039
3R	51	0	0	20	4	2,101
4R	8	2	1	0	0	65
Y	1	4	N/A	0	0	0
Subtotal (Localized)	286	9	14	80	15	11,238
U	68	N/A	N/A	50	31	2,177
Total	354	9	14	130	46	13,415

BAC contigs. The BAC map incorporates scaffolds spanning 13.4 Mb of the WGS3 assembly and links 14 WGS3 scaffolds to the Release 3 arm assemblies (Table 2). In regions proximal to the arm assemblies, it links 130 WGS3 scaffolds into 25 multiscaffold BAC contigs and yields 21 single-scaffold BAC contigs (Table 2) (11). The largest BAC contig links 20 WGS3 scaffolds spanning 1.7 Mb.

We used fluorescence in situ hybridization (FISH) to map BAC contigs and sequence scaffolds to specific cytogenetic locations in mitotic chromosomes (11, 14). The high repeat content of heterochromatin required the use of single-copy probes [P-element insertions (15, 16) and cDNA clones (17, 18)] that could be assigned to specific sequence scaffolds. We also used BAC probes that had sufficient single-copy sequences to provide unambiguous localizations (11) (fig. S8). The

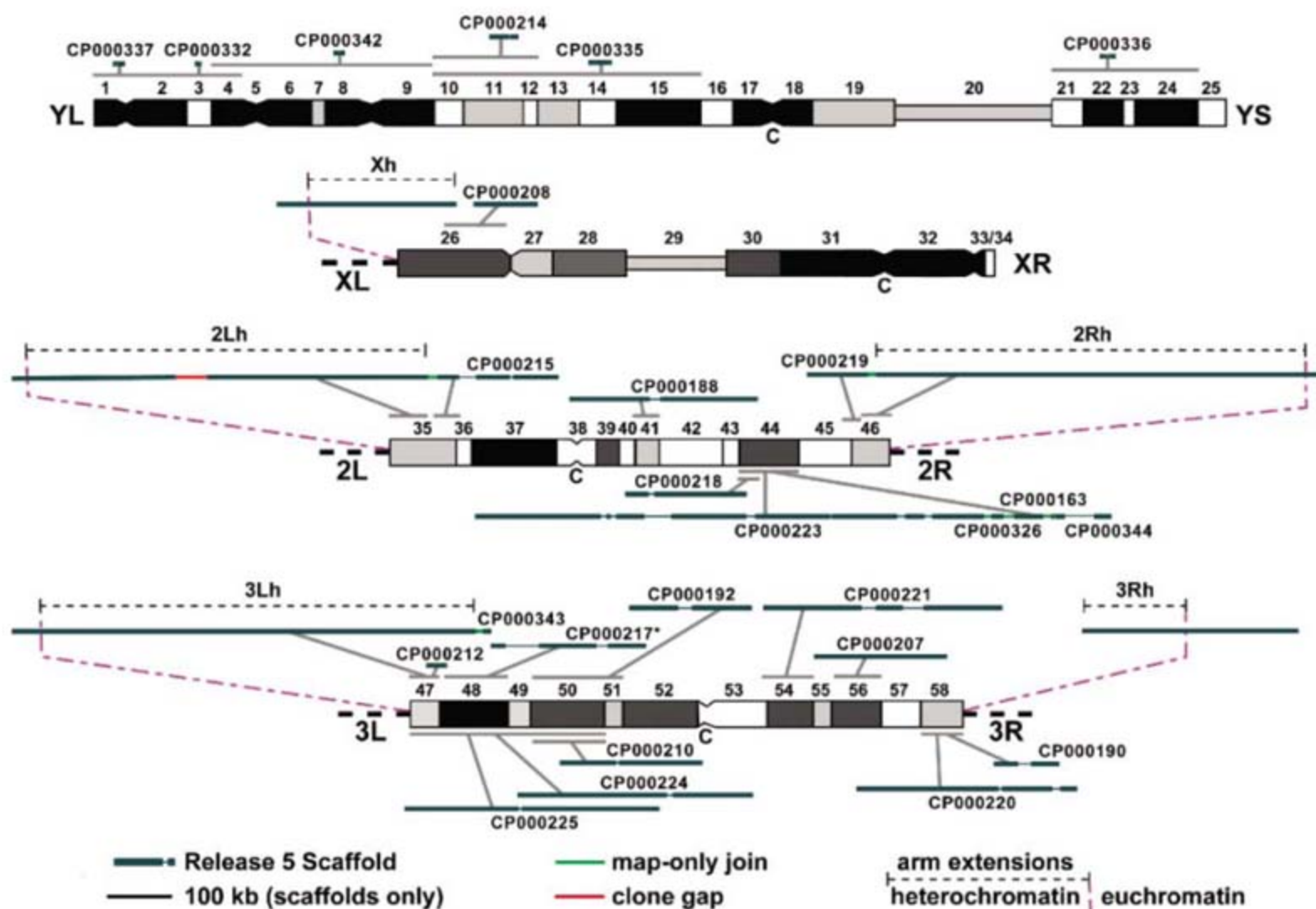


Fig. 3. Integrated map of *D. melanogaster* pericentromeric heterochromatin. The cytogenetic reference map of the heterochromatic regions of the chromosomes with numbered divisions (h1 to h58) and centromeres (C) is shown (22). The fourth chromosome (h58 to h61) is not shown. Release 5 sequence scaffolds are indicated at their cytogenetic map locations, and Het scaffolds are labeled with their GenBank accession numbers. Scaffolds (13.9 Mb in total; see scale bar) and the heterochromatin (100 Mb in total) are represented at different scales. Sequence contigs (thick bars) and sequence gaps (thin bars) within scaffolds are shown. Some sequence gaps are too small to be represented at this scale. A clone gap in the 2Lh sequence is indicated.

Joins between Release 5 scaffolds present in the BAC map assembly but not yet incorporated in the sequence assembly are shown. Cytogenetic locations are indicated by lines connecting scaffolds to cytogenetic ranges. The heterochromatin-euchromatin boundaries within the sequence of the chromosome arms, based on BAC FISH (6), are indicated by dashed magenta lines. The orientations of Het scaffolds are not necessarily known (11, 23). CP000217, originally identified as part of 2RHet but subsequently mapped to 3LHet, is shown here at its updated location; CP000206, originally identified as part of 3RHet but subsequently removed to the unlocalized scaffolds, is not shown (11).

physical and cytogenetic mapping results and previously published data were used to produce an integrated map of pericentromeric heterochromatin (11). We present cytogenetic locations for 15 BAC contigs linking 80 scaffolds and an additional 14 scaffolds that were linked to chromosome arms; these localized scaffolds span 11.2 Mb of pericentromeric heterochromatin in the WGS3 assembly (Table 2). Currently unlocalized are 50 WGS3 scaffolds in 31 BAC contigs, as well as an additional 63 WGS3 scaffolds larger than 15 kb that are not represented in the BAC map. Four scaffolds larger than 15 kb and not represented in the BAC map were incorporated into Release 5 by sequence finishing (11).

Integration of the map and sequence-finishing information led us to define three classes of Release 5 heterochromatic scaffolds: (i) contiguous with the assembled euchromatic arms and extending them farther into pericentromeric heterochromatin (chromosome arm "h"); (ii) mapped to specific chromosome arms with partial information on order and orientation and concatenated into "arm" files (arm "Het"); and (iii) unmapped and concatenated into a single file (arm "U"). The improved, mapped Release 5 scaffolds are diagrammed relative to the chromosome arms in Fig. 3; see (11) for analysis of sequences and maps by chromosome.

We have demonstrated substantial progress toward our goal of assembling and mapping the components of heterochromatin that are not simple repeats, and have shown that heterochromatic regions containing single-copy genes and a high density of transposable elements can be assembled into high-quality, contiguous sequence. How can we generate an even more complete genomic understanding of *Drosophila* heterochromatin? The tiling path of overlapping BACs spanning the Release 5 sequence (11) provides templates for gap closure and scaffold extension in the regions that contain middle-repetitive elements and single-copy genes. Progress can also be made in localizing more sequences by performing FISH with additional cDNAs, BACs, and transposon insertions from other collections (19, 20). Restriction fingerprints of tiling path BACs will also provide an independent benchmark to evaluate the accuracy of finished sequence assemblies (21). The apparent absence of BACs covering various remaining gaps likely reflects the presence of extensive simple sequence arrays, which are unlikely to be completely closed as the map and sequence are improved. New technologies will be required to determine the sequence and structure of these highly repetitive regions. However, an achievable goal using current technologies is to produce complete maps and sequence assemblies for the single-copy and middle-repetitive components of the heterochromatin, combined with cytological definition of the locations and structures of large blocks of tandemly repeated simple-sequence DNA.

Our results suggest that elucidating the organization and composition of heterochromatic regions in other organisms is a practical goal.

However, our ability to substantially improve the sequence and maps required three critical components: (i) a high-quality WGS sequence assembly; (ii) a high-depth collection of precisely sized and aligned genomic clones for sequence finishing and gap closure; and (iii) physical and cytogenetic mapping to deduce relationships between WGS scaffolds. The STS content-mapping experiments benefited greatly from the availability of large-insert BAC libraries produced by fragmenting genomic DNA with three different restriction enzymes and with physical shearing. Analysis of heterochromatin in other genomes would also benefit from improved algorithms that can successfully and accurately assemble sequence of regions rich in repeated DNA.

References and Notes

1. A. F. Dernburg *et al.*, *Cell* **85**, 745 (1996).
2. G. H. Karpen, M.-H. Le, H. Le, *Science* **273**, 118 (1996).
3. P. B. Talbert, S. Henikoff, *Nat. Rev. Genet.* **7**, 793 (2006).
4. L. L. Wallrath, *Curr. Opin. Genet. Dev.* **8**, 147 (1998).
5. S. E. Celniker *et al.*, *Genome Biol.* **3**, RESEARCH0079 (2002).
6. R. A. Hoskins *et al.*, *Genome Biol.* **3**, RESEARCH0085 (2002).
7. E. E. Eichler, R. A. Clark, X. She, *Nat. Rev. Genet.* **5**, 345 (2004).
8. B. John, G. L. G. Miklos, *The Eukaryote Genome in Development and Evolution* (Allen & Unwin, London, 1988), p. 416.
9. A. R. Lohe, D. L. Brutlag, *Proc. Natl. Acad. Sci. U.S.A.* **83**, 696 (1986).
10. M. D. Adams *et al.*, *Science* **287**, 2185 (2000).

11. See supporting material on Science Online.
12. R. A. Hoskins *et al.*, *Science* **287**, 2271 (2000).
13. J. P. Abad *et al.*, *Mol. Biol. Evol.* **21**, 1613 (2004).
14. M. Gatti, S. Pimpinelli, *Annu. Rev. Genet.* **26**, 239 (1992).
15. A. Y. Konev *et al.*, *Genetics* **165**, 2039 (2003).
16. C. M. Yan, K. W. Dobie, H. D. Le, A. Y. Konev, G. H. Karpen, *Genetics* **161**, 217 (2002).
17. The *Drosophila* Gene Collection (www.fruitfly.org/EST/index.shtml).
18. M. Stapleton *et al.*, *Genome Res.* **12**, 1294 (2002).
19. H. J. Bellen *et al.*, *Genetics* **167**, 761 (2004).
20. S. T. Thibault *et al.*, *Nat. Genet.* **36**, 283 (2004).
21. M. A. Marra *et al.*, *Genome Res.* **7**, 1072 (1997).
22. M. Gatti, S. Bonaccorsi, S. Pimpinelli, *Methods Cell Biol.* **44**, 371 (1994).
23. S. E. Celniker *et al.*, BDGP: Release 5 Genomic Sequence Download (March 2006) (www.bdgp.org/sequence/release5genomic.shtml).
24. We thank Celera Genomics Inc. for the 10-kb genomic clones that we used as sequencing templates, A. B. de Carvalho for discussions of Y chromosome sequences, and R. Svirskas, A. M. Ryles, E. Kym, R. Chetty, and S. Galle for technical assistance. Supported by NIH grant R01 HG00747 (G.H.K.); BAC-based sequencing was supported by NIH grant P50-HG00750 (G. M. Rubin) and U.S. Department of Energy contract DE-AC03765F00098 (S.E.C.).

Supporting Online Material

www.sciencemag.org/cgi/content/full/316/5831/1625/DC1
Materials and Methods
SOM Text
Figs. S1 to S8
References

11 January 2007; accepted 7 May 2007
10.1126/science.1139816

The Vaccine Adjuvant Monophosphoryl Lipid A as a TRIF-Biased Agonist of TLR4

Verónica Mata-Haro,^{1,2*} Caglar Cekic,^{1,2} Michael Martin,³ Paula M. Chilton,¹ Carolyn R. Casella,¹ Thomas C. Mitchell^{1,2†}

The inflammatory toxicity of lipopolysaccharide (LPS), a component of bacterial cell walls, is driven by the adaptor proteins myeloid differentiation factor 88 (MyD88) and Toll-interleukin 1 receptor domain-containing adapter inducing interferon- β (TRIF), which together mediate signaling by the endotoxin receptor Toll-like receptor 4 (TLR4). Monophosphoryl lipid A (MPLA) is a low-toxicity derivative of LPS with useful immunostimulatory properties, which is nearing regulatory approval for use as a human vaccine adjuvant. We report here that, in mice, the low toxicity of MPLA's adjuvant function is associated with a bias toward TRIF signaling, which we suggest is likely caused by the active suppression, rather than passive loss, of proinflammatory activity of this LPS derivative. This finding may have important implications for the development of future vaccine adjuvants.

Immunological adjuvants are combined with noninfectious vaccine antigens to generate antibody responses that are faster, stronger, and longer lasting than responses achieved through immunization with antigen alone. Aluminum hydroxide (alum) is currently the only human vaccine adjuvant approved for use in the United States, and although it is effective at boosting antibody responses, these responses require repeated administration and tend to generate antiparasitic T helper 2 (T_H2), rather than antiviral and antibacterial T_H1, T cell immunity

(1). As a consequence, there is much effort devoted to developing prospective adjuvants that can establish protective immunity with fewer vaccinations with less injected material, through durable antibody and T_H1-dependent cytotoxic T cell activity. One of these, MPLA, is likely to be the first vaccine adjuvant to be approved for widespread use since alum because it generates clinically useful immune responses (2–5), and it has ~0.1% of the inflammatory toxicity of its parent molecule, LPS (6, 7). The adjuvant effects of MPLA require TLR4 (6, 8), and although TLR

signaling may not be critical for enhanced antibody responses under all conditions (9), TLR agonists do show particular promise as adjuvants of cytotoxic T cell activity. Because TLR4 is also the receptor for endotoxin, it is important to understand the mechanism(s) by which MPLA can boost T and B cell immunity, without the damaging inflammatory outcomes associated with its parent molecule.

We compared the effects of MPLA versus LPS in T cell priming using an adoptive transfer system in which ovalbumin (OVA) peptide-specific CD8⁺ and CD4⁺ T cells from OT-I (10) and OT-II (11) T cell receptor transgenic mice (C57BL/6 background, CD45.2⁺) were infused into major histocompatibility complex-matched recipients (B6.SJL, CD45.1⁺) before immunization with adjuvant plus OVA peptides 323-339 and 257-264 [SIINFEKL (Ser-Ile-Ile-Asn-Phe-Glu-Lys-Leu)] (12). Adjuvant doses, 30 μ g of MPLA or 10 μ g of LPS, were selected on the basis of similar induction of T cell clonal expansion in pilot experiments (fig. S1) and were used in all subsequent in vivo experiments. From 2.5 to 7 days after immunization, cells harvested from spleens and lymph nodes of treated animals revealed that MPLA and LPS had equivalent adjuvant effects on T cells, with indistinguishable patterns of clonal expansion and contraction (Fig. 1A and fig. S2). In terms of cytokine responses, interleukin-10 (IL-10) production was strong in both MPLA- and LPS-adjuvanted mice (fig. S3), although differences emerged when responses were grouped according to dependence on either of two TLR4 signaling pathways, MyD88 or TRIF, based on previous studies of genetically deficient mice (13–15). Thus, MPLA appeared to be as efficient as LPS at inducing TRIF-dependent factors [Fig. 1C; $P = 0.604, 0.051, \text{ and } 0.058$ for differences in granulocyte colony-stimulating factor (G-CSF), interferon-induced protein 10 (IP-10), and monocyte chemoattractant protein 1 (MCP-1) production respectively] while only weakly stimulating MyD88-associated responses [Fig. 1B; $P < 0.0005$ for interferon- γ (IFN- γ), IL-1 β , IL-6, and macrophage inflammatory protein 1 α (MIP-1 α)].

We next performed microarray analysis of splenocytes from mice that had been immunized as described above (Fig. 1A), which again showed that MPLA had induced strong TRIF-associated but weak MyD88-associated responses when compared with those of LPS. Some of the results from this in vivo analysis of MPLA function

reproduced those previously reported (8) in that IL-1 β transcription was strongly induced (fig. S4), whereas mature protein secretion was not (Fig. 1B). In the earlier study, it appeared that MPLA had failed to activate IL-1 β converting enzyme (8). However, because IL-1 receptor-deficient mice remain susceptible to endotoxic shock (16),

we concluded that this difference in activity was not sufficient to explain the low toxicity of MPLA.

Given the number of MyD88-associated genes that were not strongly induced by MPLA (Fig. 1, B to D), we next tested for generalized defects in MyD88 signaling. Because macrophages are necessary for LPS endotoxicity (17),

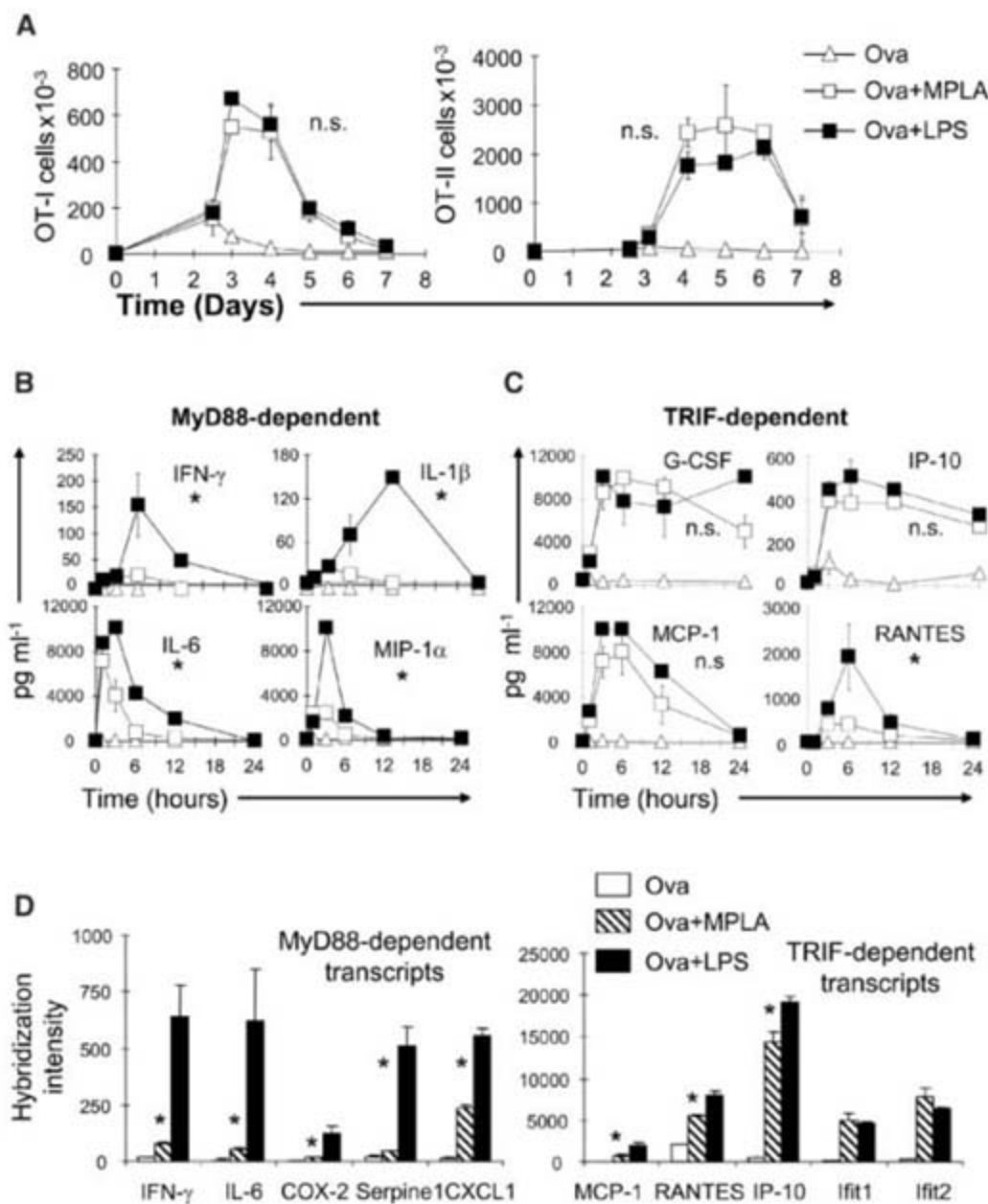


Fig. 1. MPLA induces similar T cell clonal expansion kinetics as compared to LPS but shows TRIF-biased gene expression. In all experiments, OT-I (1×10^5) and OT-II (1.5×10^5) cells were adoptively transferred into B6.SJL mice. After 24 hours, mice were either untreated or immunized with SIINFEKL and OVA_{323–339} alone (OVA; triangles), with OVA and 10 μ g of LPS (OVA+LPS; solid squares), or with OVA and 30 μ g of MPLA (OVA+MPLA; open squares). * $P < 0.05$; n.s., not statistically significant by analysis of variance (ANOVA) and post-hoc Tukey analysis (12). (A) Every day after immunization (from days 2 to 7), cells from spleen and lymph nodes (fig. S2) were harvested; stained for CD4, CD8, CD45.1, and CD45.2; and enumerated by means of flow cytometry. Results are mean values \pm SEM of triplicate mice from one of two representative experiments. (B and C) Serum samples were obtained at the indicated times and analyzed by means of multiplex analysis for cytokines and chemokines. Data were grouped as representative products of the MyD88-dependent (B) or TRIF-dependent (C) signaling pathways and plotted as mean values \pm SEM. (D) Six hours after immunization, spleens were harvested and RNA was isolated. Affymetrix genechip analysis was then performed (12). Selected transcript products from the microarray data were grouped by MyD88-dependent (left) or TRIF-dependent (right) genes. COX-2, cyclooxygenase-2; Serpine1, serine protease inhibitor 1; CXCL1, chemokine (CXC motif) ligand 1; Ifit1, interferon-induced protein with tetratricopeptide repeats. Results are shown as mean hybridization intensity \pm SEM from triplicate mice.

¹Institute for Cellular Therapeutics, University of Louisville, 570 South Preston Street, Louisville, KY 40202, USA.

²Department of Microbiology and Immunology, University of Louisville, 319 Abraham Flexner Way, Louisville, KY 40202, USA. ³Oral Health and Systemic Disease Research Group, University of Louisville, 501 South Preston Street, Louisville, KY 40202, USA.

*Present address: Centro de Investigación en Alimentación y Desarrollo, Hermosillo, Sonora, Mexico.

†To whom correspondence should be addressed. E-mail: tom.mitchell@louisville.edu

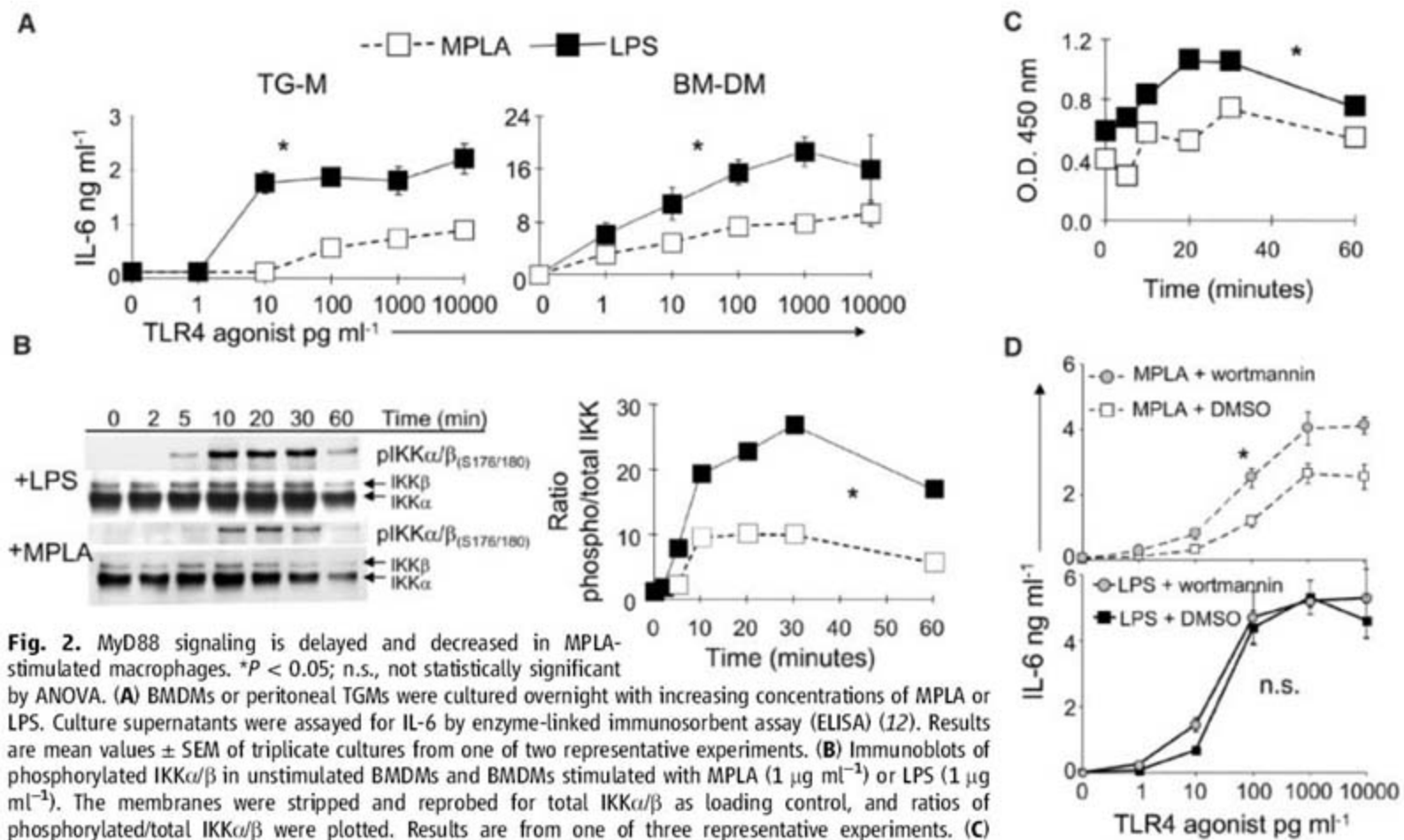


Fig. 2. MyD88 signaling is delayed and decreased in MPLA-stimulated macrophages. * $P < 0.05$; n.s., not statistically significant by ANOVA. **(A)** BMDMs or peritoneal TGMs were cultured overnight with increasing concentrations of MPLA or LPS. Culture supernatants were assayed for IL-6 by enzyme-linked immunosorbent assay (ELISA) (12). Results are mean values \pm SEM of triplicate cultures from one of two representative experiments. **(B)** Immunoblots of phosphorylated IKK α/β in unstimulated BMDMs and BMDMs stimulated with MPLA ($1 \mu\text{g ml}^{-1}$) or LPS ($1 \mu\text{g ml}^{-1}$). The membranes were stripped and reprobed for total IKK α/β as loading control, and ratios of phosphorylated/total IKK α/β were plotted. Results are from one of three representative experiments. **(C)** BMDMs were cultured for the indicated times with MPLA ($1 \mu\text{g ml}^{-1}$) or LPS ($1 \mu\text{g ml}^{-1}$). Nuclear extracts were analyzed for NF κ B-binding activity; data are expressed in optical density (O.D.) units obtained with the TransAM ELISA NF κ B assay performed as described in (12). **(D)** BMDMs were pretreated with dimethyl sulfoxide (DMSO) or with 50 nM freshly prepared wortmannin and then were cultured overnight with increasing concentrations of MPLA or LPS. Culture supernatants were assayed for IL-6 by ELISA (12). Results are mean values \pm SEM of triplicate cultures from one of three representative experiments.

we tested responses to LPS versus MPLA using bone marrow-derived monocytes (BMDMs) and thioglycollate-elicited macrophages (TGMs). Initial tests of cytokine and chemokine production showed that MPLA had the same TRIF-biased activity in BMDMs and TGMs (Fig. 2) as that seen in vivo. Thus, MPLA was two to three orders of magnitude less potent than LPS at inducing MyD88-dependent IL-6 (Fig. 2A) but induced similar TRIF-dependent IP-10, MCP-1, and IFN- β (Fig. 3A). Stimulation of DNA binding activity by the transcription factor nuclear factor κ B (NF κ B) p65 was markedly slower (Fig. 2C) after exposure of wild-type (WT) BMDMs to MPLA, and phosphorylation of a component of its regulatory complex, inhibitor of NF κ B kinase (IKK), was delayed and reduced when compared to phosphorylation after LPS exposure (Fig. 2B). In contrast, MyD88^{-/-} BMDMs showed identical kinetics of IKK phosphorylation upon exposure to LPS or MPLA (fig. S5). These results reveal that MPLA's low potency in inducing IL-6 was correlated with a failure to activate MyD88-dependent events needed for proinflammatory patterns of NF κ B transcriptional activation and were similar to those seen in MyD88^{-/-} mice (13, 14, 18).

In studies looking at TRIF-associated signaling, several events were found to be unimpaired

in BMDMs after exposure to MPLA. The time course and magnitude of phosphorylation of interferon regulatory factor 3 (IRF-3), a defining feature of TRIF-mediated signaling, were identical in both MPLA- and LPS-treated BMDMs (Fig. 3B). Signal transducer and activator of transcription 1 (Stat1) phosphorylation, which is absent in TRIF-deficient cells exposed to LPS (18) and is associated with TLR4-induced autoerine and/or paracrine production of type I interferons (19), was also the same (Fig. 3C).

It has recently been reported that phosphoinositide 5-kinase-generated phosphatidylinositol 4,5-bisphosphate (PIP₂) is required for efficient MyD88 recruitment to TLR4 (20) and that proinflammatory glycogen synthase kinase 3 β (GSK-3 β) is inactivated through phosphoinositide 3-kinase (PI3K)-dependent protein kinase B activity (21). Because PI3K activity would be expected to decrease PIP₂ levels via conversion to phosphatidylinositol 3,4,5-trisphosphate, thereby preventing recruitment of MyD88, as well as to inactivate GSK-3 β , we tested whether PI3K activity might be involved in MPLA's decreased ability to induce IL-6. Pretreatment of BMDMs with the PI3K inhibitor wortmannin increased IL-6 production by MPLA but did not further increase IL-6 production by LPS (Fig. 2D), suggesting that MPLA stimulates more PI3K

activity than LPS. Thus, the inefficient stimulation of MyD88-dependent signaling by MPLA may result from diminished recruitment of MyD88 to TLR4 through loss of PIP₂ species and/or by PI3K-dependent inactivation of proinflammatory GSK-3 β .

Our observation that weak stimulation of MyD88-dependent IL-6 by MPLA was correlated with efficient T cell adjuvant function appears to contradict a previous report concluding that LPS failed to boost T cell priming in MyD88-deficient mice because IL-6 expression was impaired (22). One explanation for this discrepancy might be that MPLA induces low levels of MyD88-mediated signaling that stimulate sufficient production of IL-6 (Fig. 1B). Another explanation is that TRIF, rather than MyD88, may be needed for TLR4-induced adjuvant effects. To distinguish between these possibilities, we returned to the adoptive transfer system to measure T cell priming effects in recipient mice that were either MyD88- or TRIF-deficient. The TLR2 agonist *N*-palmitoyl-S-[2,3-bis(palmitoyloxy)-(2*R*,5*S*)-propyl]-(*R*)-cysteinyl-seryl-(lysyl)(3)-lysine (PAM₃CSK₄), which signals only through MyD88 (23), was used as negative control to demonstrate the absence of MyD88-dependent effects in MyD88-deficient recipients. Four days after immunization,

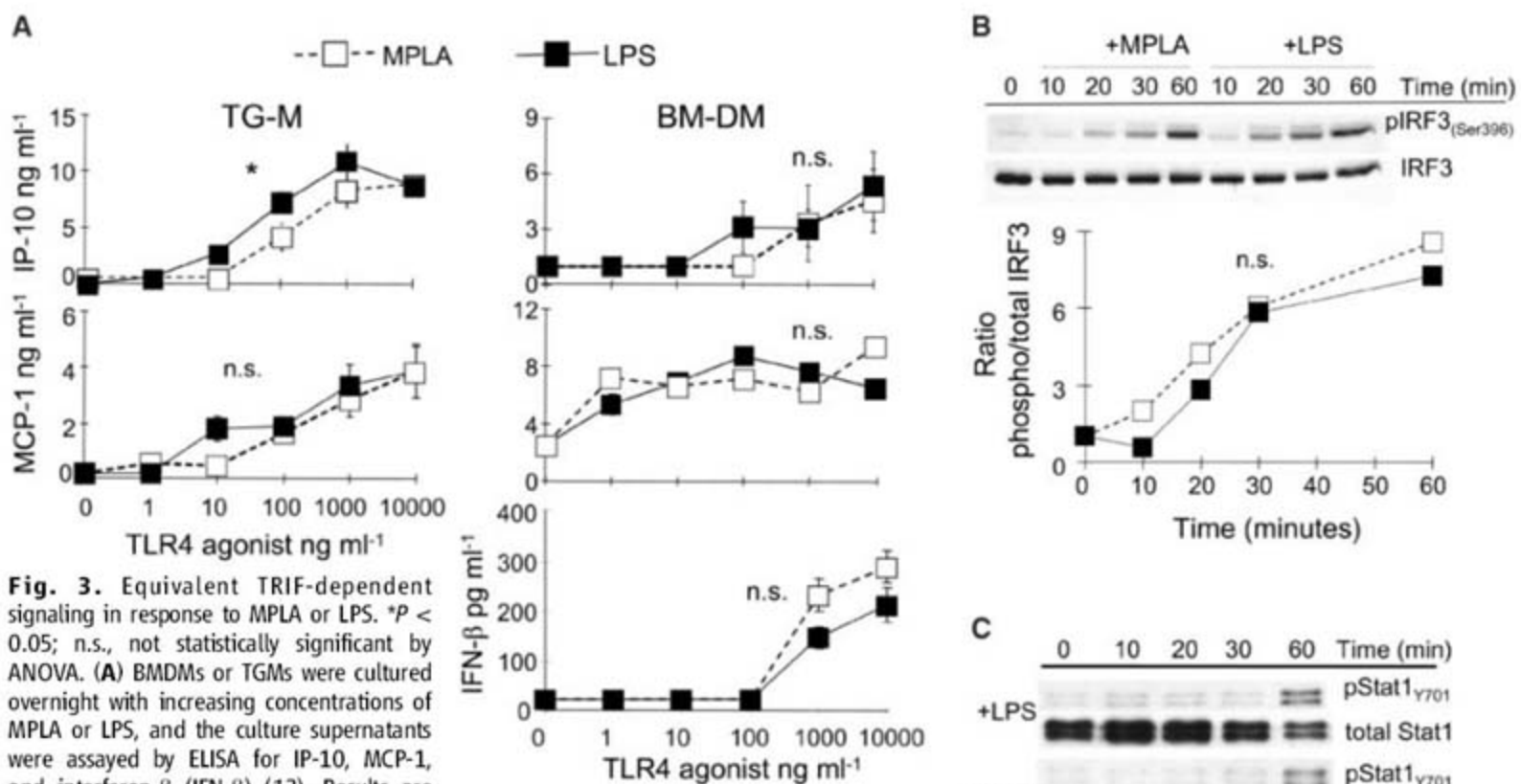


Fig. 3. Equivalent TRIF-dependent signaling in response to MPLA or LPS. **P* < 0.05; n.s., not statistically significant by ANOVA. **(A)** BMDMs or TGMs were cultured overnight with increasing concentrations of MPLA or LPS, and the culture supernatants were assayed by ELISA for IP-10, MCP-1, and interferon-β (IFN-β) (12). Results are mean values ± SEM from one of two representative experiments. **(B and C)** Unstimulated BMDMs or BMDMs stimulated with MPLA (1 μg ml⁻¹) or LPS (1 μg ml⁻¹) were analyzed by Western blot for phosphorylated IRF-3 (Ser³⁹⁶) (B) or phosphorylated Stat1 (Tyr⁷⁰¹ or Y-701) (C). For loading controls, the membranes were stripped and reprobbed for total IRF-3 or total Stat1, respectively. Results are representative of two independent experiments. Parameters were evaluated by ANOVA.

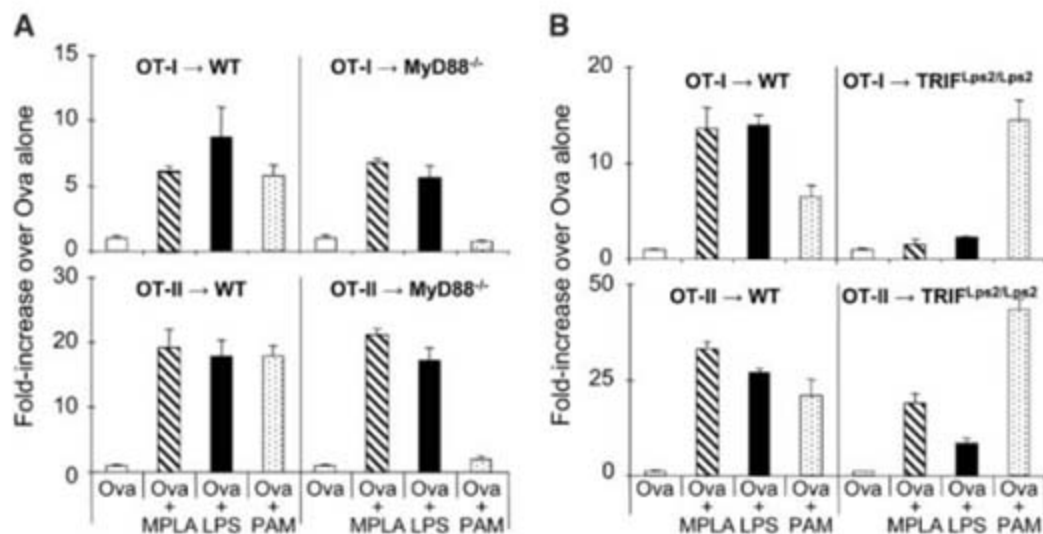


Fig. 4. MyD88 is not required for full adjuvant effects on T cell priming. WT (C57BL/6), MyD88-deficient (MyD88^{-/-}) **(A)**, or TRIF^{Lps2/Lps2} mutant mice **(B)** received 1 × 10⁵ OT-I.SJL and 1.5 × 10⁵ OT-II.SJL cells by adoptive transfer and were treated as in Fig. 1A with the combined OVA peptides in the absence and presence of LPS (10 μg), MPLA (30 μg), or PAM₃CSK₄ (PAM) (50 μg). T cell expansion in the spleens was determined after four days. Results are mean values ± SEM from triplicate mice for fold increases of OVA plus adjuvant-treated mice versus OVA-treated mice and are representative of two experiments. Statistical analysis was performed with the use of the nonparametric Mann-Whitney test; all comparisons between OVA+MPLA and OVA+LPS groups showed statistically insignificant differences (*U* > 0.05).

spleens were harvested and tested for adjuvant effects on T cell proliferation. In these experiments, MyD88 appeared completely dispensable for the MPLA- or LPS-induced adjuvant effects on OT-I and OT-II cells, at least during early

clonal expansion (Fig. 4A). Neither T cell population showed evidence of PAM₃CSK₄-mediated adjuvant effects in MyD88^{-/-} mice. These results confirm that MyD88 was not required for TLR4-mediated adjuvant effects on early T cell priming.

The adjuvant effects of MPLA versus LPS were also compared in TRIF^{Lps2/Lps2} mice, which express a truncated form of TRIF that is inactive (18). These studies revealed that adjuvant-boosted OT-I T cell priming was severely impaired in TRIF^{Lps2/Lps2} hosts, whereas OT-II priming was less strongly affected (Fig. 4B). Responses of TRIF^{Lps2/Lps2} mice to control PAM₃CSK₄ were not diminished, as was expected because TLR2 is known not to require TRIF for its activity (23). Hence, costimulation of OT-I and OT-II T cell proliferation by TLR4 agonists showed substantially greater dependence on TRIF than on MyD88 in this model system. This result indicates that although MPLA is inefficient with respect to stimulation of TLR4/MyD88-induced gene expression, it has fortuitously retained TLR4/TRIF-associated activities, such as induction of type I interferon (Fig. 3A), that may be especially important for T cell clonal expansion (24).

Clinically relevant adjuvants other than MPLA, such as CpG oligonucleotides, also induce type I interferon but in a MyD88-dependent (25), rather than a TRIF-dependent, manner. Thus, different TLRs can reach the same immunostimulatory endpoints without requiring the same signaling adaptors. In the case of the endotoxin receptor TLR4, it is MyD88 that is most associated with proinflammatory outcomes, perhaps because of involvement of the MyD88 coadapter, Mal (MyD88 adapter-like) (26, 27).

The mechanistic basis for MPLA's failure to stimulate full MyD88 signaling, with associated proinflammatory effects, remains to be fully elucidated. However, we propose that an important component is the acquisition, relative to LPS, of an anti-inflammatory function that requires PI3K activity (Fig. 2D). This would be distinct from the loss of a proinflammatory activity, such as a simple failure to recruit Mal and/or MyD88 to TLR4. Discovering the precise mechanism of MPLA's ability to function as a low-toxicity adjuvant may permit improvements in the design of future TLR4-dependent vaccine adjuvants.

References and Notes

1. N. Petrovsky, J. C. Aguilar, *Immunol. Cell Biol.* **82**, 488 (2004).
2. J. R. Baldrige et al., *Expert Opin. Biol. Ther.* **4**, 1129 (2004).
3. L. Vernacchio et al., *Vaccine* **20**, 3658 (2002).

4. S. Thoelen et al., *Vaccine* **16**, 708 (1998).
5. D. M. Harper et al., *Lancet* **367**, 1247 (2006).
6. J. T. Evans et al., *Expert Rev. Vaccines* **2**, 219 (2003).
7. N. Qureshi, K. Takayama, E. Ribí, *J. Biol. Chem.* **257**, 11808 (1982).
8. K. Okemoto, K. Kawasaki, K. Hanada, M. Miura, M. Nishijima, *J. Immunol.* **176**, 1203 (2006).
9. A. L. Gavin et al., *Science* **314**, 1936 (2006).
10. K. A. Hogquist et al., *Cell* **76**, 17 (1994).
11. M. J. Barnden, J. Allison, W. R. Heath, F. R. Carbone, *Immunol. Cell Biol.* **76**, 34 (1998).
12. Materials and methods are available as supporting material on Science Online.
13. M. Yamamoto et al., *Science* **301**, 640 (2003).
14. T. Kawai et al., *J. Immunol.* **167**, 5887 (2001).
15. H. Björkbacka et al., *Physiol. Genomics* **19**, 319 (2004).
16. T. Kawai, O. Adachi, T. Ogawa, K. Takeda, S. Akira, *Immunity* **11**, 115 (1999).
17. B. Beutler, E. T. Rietschel, *Nat. Rev. Immunol.* **3**, 169 (2003).
18. K. Hoebe et al., *Nature* **424**, 743 (2003).
19. K. E. Thomas, C. L. Galligan, R. D. Newman, E. N. Fish, S. N. Vogel, *J. Biol. Chem.* **281**, 31119 (2006).
20. J. C. Kagan, R. Medzhitov, *Cell* **125**, 943 (2006).

21. M. Martin, K. Rehani, R. S. Jope, S. M. Michalek, *Nat. Immunol.* **6**, 777 (2005).
22. C. Pasare, R. Medzhitov, *Immunity* **21**, 733 (2004).
23. A. O. Aliprantis, R. B. Yang, D. S. Weiss, P. Godowski, A. Zychlinsky, *EMBO J.* **19**, 3325 (2000).
24. G. A. Kolumam, S. Thomas, L. J. Thompson, J. Sprent, M. Murali-Krishna, *J. Exp. Med.* **202**, 637 (2005).
25. K. Honda et al., *Nature* **434**, 772 (2005).
26. T. Hornig, G. M. Barton, R. A. Flavell, R. Medzhitov, *Nature* **420**, 329 (2002).
27. K. A. Fitzgerald et al., *Nature* **413**, 78 (2001).
28. This work was supported by the U.S. Public Health Service (grants AI51377 and AI059023), the Commonwealth of Kentucky Research Challenge Trust and Lung Cancer Research Funds, and the Barnstable Brown Foundation.

Supporting Online Material

www.sciencemag.org/cgi/content/full/316/5831/1628/DC1

Materials and Methods

Figs. S1 to S5

References

18 December 2006; accepted 10 May 2007

10.1126/science.1138963

Crystal Structures of Human MD-2 and Its Complex with Antiendotoxic Lipid IVa

Umeharu Ohto,¹ Koichi Fukase,² Kensuke Miyake,^{3,4} Yoshinori Satow^{1*}

Endotoxic lipopolysaccharide (LPS) with potent immunostimulatory activity is recognized by the receptor complex of MD-2 and Toll-like receptor 4. Crystal structures of human MD-2 and its complex with the antiendotoxic tetra-acylated lipid A core of LPS have been determined at 2.0 and 2.2 angstrom resolutions, respectively. MD-2 shows a deep hydrophobic cavity sandwiched by two β sheets, in which four acyl chains of the ligand are fully confined. The phosphorylated glucosamine moieties are located at the entrance to the cavity. These structures suggest that MD-2 plays a principal role in endotoxin recognition and provide a basis for antiseptic drug development.

Innate immunity is the first line of defense against microbial infections (1). Defense responses are activated when microbial components are recognized by a variety of pathogen sensors, including the Toll family of receptors, Nod-like receptors, and double-stranded RNA sensors (2). Among microbial components, lipopolysaccharide (LPS) in the outer membrane of Gram-negative bacteria is a potent stimulant of immune responses, and a small difference in LPS structure has a great influence on host responses against Gram-negative bacteria (3). Excessive responses to the endotoxic LPS frequently result in severe sepsis, a rapidly progressing inflammatory disease with up to 29% mortality, leading to more than 215,000 annual deaths in the United States alone (4). Toll-like receptor 4 (TLR4) and MD-2 form a complex, and both have been implicated

in LPS recognition because mice lacking either molecule are hyporesponsive to LPS (5, 6).

TLR4 is a type I transmembrane protein consisting of extracellular leucine-rich repeats and a cytoplasmic signaling domain similar to the type I interleukin-1 (IL-1) receptor (1). MD-2 is a 160-amino acid glycoprotein with a 16-amino acid secretion signal at the N terminus (7) and represents a class of MD-2-related lipid recognition (ML) proteins that also include mite allergen proteins (8). MD-2 forms a stable complex with TLR4 on the cell surface (9), and MD-2 alone as well as in the complex directly binds to LPS with nanomolar affinity (10). On the other hand, it has also been reported that TLR4 recognizes and binds to LPS (11, 12).

Lipid A, the primary immunostimulatory core of LPS, is diverse in several species (13), and these variations are discriminated by the TLR4-MD-2 complex as endotoxic or as antiendotoxic (14). Lipid A of the *Escherichia coli* type (Fig. 1) acts as a potent agonist in human macrophage cells and in mouse cells. However, its precursor lipid IVa (15), the tetra-acylated form of lipid A, acts as an antagonist in human cells but as an agonist in mouse cells (16). Despite identification of the complex as the LPS receptor, no information is available on the structures of liganded pathogen sensors. Here, we

report crystal structures of human MD-2 and its complex with lipid IVa. The structures suggest that MD-2 plays a principal role in LPS recognition.

We expressed human MD-2 in methylotropic yeast *Pichia pastoris*, as described (17). Polysaccharide moieties of MD-2 were trimmed off by endoglycosidase treatment, which leaves a single *N*-acetylglucosamine (NAG) at each glycosylation site. Monomeric MD-2 was crystallized into space group $P4_12_12$ with $a = 53.1$ Å, $c = 111.5$ Å, and one MD-2 molecule contained in the asymmetric unit. The structure of the native MD-2 crystal was determined at 2.0 Å resolution by multiple isomorphous replacement. A cocrystal with the lipid IVa complex was obtained from a mixture of MD-2 and lipid IVa and is nearly isomorphous to the native crystal. The structure of the complex was refined at 2.2 Å resolution. Details of the crystallographic analyses are given in (17).

Residues from Glu¹⁷ to Asn¹⁶⁰ are defined in the structure with two *N*-linked NAGs at Asn²⁶ and Asn¹¹⁴. MD-2 is folded into a single domain consisting of two β sheets in the immunoglobulin fold conserved among the ML proteins (8): One sheet consists of three antiparallel β strands, and the

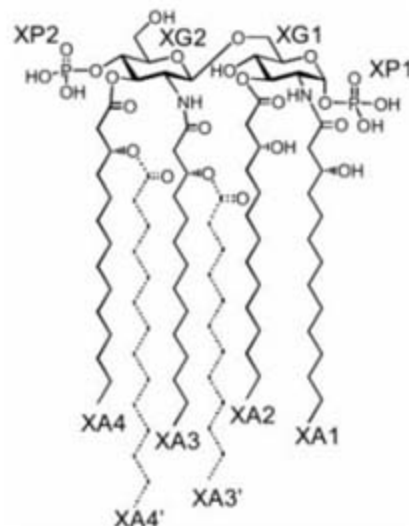


Fig. 1. Chemical structure of lipid IVa. Lipid A has additional XA3' and XA4' acyl chains.

¹Graduate School of Pharmaceutical Sciences, University of Tokyo, 7-3-1 Hongo, Bunkyo-ku, Tokyo 113-0033, Japan.

²Department of Chemistry, Graduate School of Science, Osaka University, 1-1 Machikaneyama, Toyonaka, Osaka 560-0043, Japan. ³Division of Infectious Genetics, Institute of Medical Science, University of Tokyo, 4-6-1 Shirokanedai, Minato-ku, Tokyo 108-8639, Japan. ⁴CREST, Japan Science and Technology Agency, 4-1-8 Honcho, Kawaguchi, Saitama 332-0012, Japan.

*To whom correspondence should be addressed. E-mail: satow@mol.f.u-tokyo.ac.jp

other consists of six antiparallel strands (Fig. 2). Between these sheets is a large and deep hydrophobic cavity. It has a volume of 1710 Å³ with approximate dimensions of 15 Å by 8 Å by 10 Å. The β6 and β7 strands line the entrance to the cavity. The cavity makes the span of the two sheets much wider than that in the previously predicted model of MD-2 (18). Three disulfide bridges are located between Cys²⁵ and Cys⁵¹, between Cys³⁷ and Cys¹⁴⁸, and between Cys⁹⁵ and Cys¹⁰⁵, in contrast to the predicted bridges between Cys²⁵ and Cys¹⁴⁸ and between Cys³⁷ and Cys⁵¹ (18). The sole free Cys¹³³ is located deep in the cavity and seems not to be involved in the oligomerization that has previously been reported (19).

In the native structure, unexpected electron densities were observed in the cavity; these were attributed to bound lipidic molecules that presumably copurified with MD-2 (fig. S1A). Three myristic acid molecules were built into the structure (fig. S2). In the structure of the lipid IVa complex, electron densities in the cavity (fig. S1B) were assigned to the different parts of lipid IVa (Fig. 1): two glucosamine, two phosphate, and four fatty acid chains. The glycosylation sites of both Asn²⁶ and Asn¹¹⁴ are distant from the cavity region, indicating that the glycosylation plays a role not in ligand binding, but (presumably) in the secretion and protection of MD-2.

Root mean square (RMS) positional deviations between the superposed native and complexed structures are 0.3 Å for the main-chain atoms and 0.7 Å for all the protein atoms. Thus, the MD-2 structure is not significantly altered upon lipid IVa binding. A major difference is in the side-chain conformation of Lys¹²² located at the entrance to the cavity: The side chain is shifted toward the second glucosamine moiety XG2 of lipid IVa, with RMS deviations of 0.3 Å for the main-chain atoms and 2.8 Å for the side-chain atoms. Overall *B* factors for the native and complexed structures are 39 Å² and 37 Å², respectively, and a slight decrease (3.3 Å²) in the averaged *B* factor is noticed for β7 upon complexation.

Details of the interactions between lipid IVa and MD-2 are shown in Fig. 3 and fig. S3. The phosphate and sugar groups are aligned in parallel with β7 in the order XP1, XG1, XG2, and XP2, with an XP1-XP2 distance of 12.5 Å, which explains how the peptide fragment from Phe¹¹⁹ to Lys¹³² can bind to LPS (20). Residues Phe¹¹⁹ to Gly¹²³ are important for the LPS recognition, and these residues, with the exception of Lys¹²², are conserved in all the species of MD-2 (21). Three hydrogen bonds to lipid IVa are noticed: Ser¹²⁰ N to XA1 O1' (distance of 2.87 Å), Lys¹²² N to XA3 O1' (3.07 Å), and Ser¹²⁰ O to XA3 O3' (2.66 Å). Water atoms mediating lipid IVa and MD-2 are located at the cavity entrance (Fig. 3). Among a total of 18 lysine and arginine residues of human MD-2, which is highly basic with an isoelectric point value of 8.7, only Lys¹²² and Arg⁹⁰ are located in the vicinities of the entrance, and their side chains cover XG2 and XP2. These interactions tether the hydrophilic moiety of lipid IVa to the cavity. Hydrophobic and electrostatic surface potentials in the vicinities of the entrance indicate that the

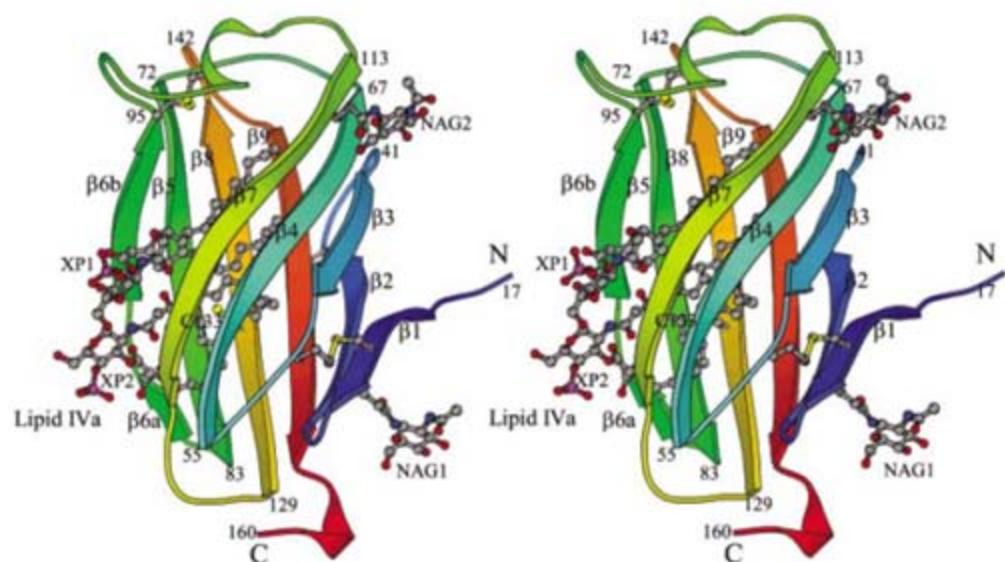


Fig. 2. Stereo ribbon model of human MD-2 in complex with lipid IVa. The N terminus is drawn in blue and the C terminus in red. The β strands are indicated with their labels, and some amino acid residue numbers are shown. Bound lipid IVa and NAGs as well as cysteine residues are drawn as ball-and-stick models. The two β sheets are inclined toward each other by about 45°.

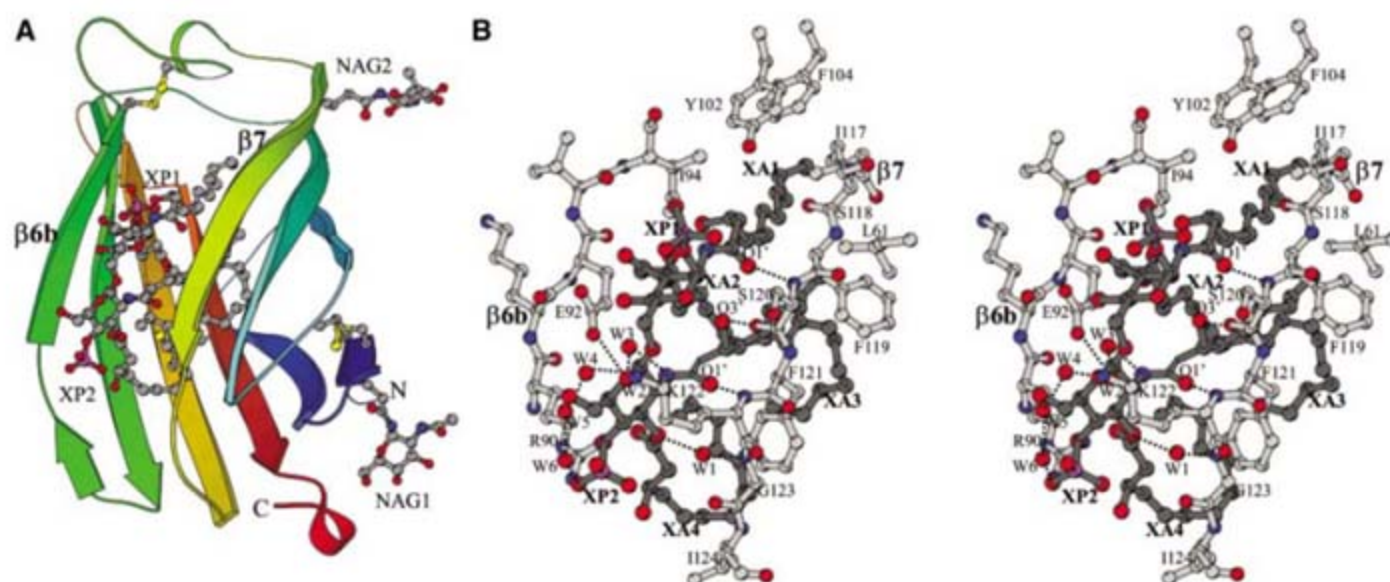


Fig. 3. Binding interface to lipid IVa. (A) Ribbon representation of the lipid IVa complex, as viewed from a 40° rotation with respect to Fig. 2. The representation is similarly drawn as in Fig. 2 so as to show that the entrance to the MD-2 cavity is lined by the β6b and β7 strands. (B) Stereo close-up view of the binding interface. Amino acid residues located in the vicinities of the entrance are drawn as ball-and-stick models with their

residue labels. The structure of the lipid IVa moiety is similarly drawn in darker gray, O atoms in red, N in blue, C in gray, and P in pink. Water O atoms involved in hydrogen bonds (broken lines) are also depicted: W1 between Gly¹²³ N and XG2 O3, as well as a group of W2, W3, W4, W5, and W6, in which W2 is hydrogen-bonded to Glu⁹² O^{e1}, W2 to W3, and W3 to XG2 N2.

entrance is positively charged and the inside of the cavity is highly hydrophobic (Fig. 4). None of the phosphate groups of lipid IVa, which are reported to be essential to the activation of immune responses (13), are involved in direct hydrogen bonds to MD-2 atoms. The lysine and arginine residues mainly contribute to the attraction of negatively charged lipid IVa.

Four fatty acid chains of lipid IVa are all deeply confined in the cavity. The XA1 chain is in an extended linear conformation and is stuck deeply into the cavity: Three of its four sides are surrounded by hydrophobic MD-2 side chains. The XA2 chain is also in the cavity and lined up with XA1. The XA3 and XA4 chains are curved, and the regions of XA3 C10'-11' and XA4 C11'-13' atoms are loosely packed in the cavity. The tip end of XA4 folds back toward the XG2 moiety, and that of XA3 hangs over XA4. The fatty acid chains in the cavity are packed next to each other through van der Waals contacts, as exemplified in the lipid molecules bound to the GM2 activator protein (22). The packed and confined fatty acid structures are distinct from the extended structures of the fatty acid chains of LPS associated with the membrane-embedded region of the FhuA ferri-chrome ion receptor (23). The cavity of MD-2 is divided into four sites on the basis of their interactions to the fatty acid chains: L1 through L4 respectively correspond to XA1 through XA4 (table S3). In the L1, L2, and L3 sites of the native structure, the fatty acid molecules assigned as myristic acids exist in nearly identical configurations to those of XA1, XA2, and XA3, respectively (figs. S2 and S3). The averaged *B* factor for the lipid IVa molecule is 46 Å²; comparable values are obtained for XA1 (33 Å²), XA2 (46 Å²), and XA3 (41 Å²), with a larger one for XA4 (53 Å²). These suggest that the L1, L2, and L3 sites have higher affinities to fatty acid chains. The surface area accommodating lipid IVa is very wide, 890 Å². This large value is comparable to that of ligands bound to the antibodies (24) and explains the nanomolar affinity of MD-2 toward LPS (10).

The MD-2 residues essential to the interaction with TLR4 are reported to be Arg⁹⁰, Lys⁹¹, Asp¹⁰⁰, Tyr¹⁰², Cys⁹⁵, and Cys¹⁰⁵ in the absence of the ligands (25). A synthetic peptide from Cys⁹⁵ to Cys¹⁰⁵, in the oxidized form, exhibits a decrease in LPS-induced activation (18) and is supposed to compete with MD-2 through the interaction with TLR4. These residues are located at the cavity entrance (Fig. 4).

The structure of CD14, which transfers LPS to MD-2, also has a hydrophobic cavity of dimensions nearly equal to those of MD-2 (26); hence, it is presumed to recognize acyl chains of LPS. The only differences between the structures of the antagonist lipid IVa and of the agonist lipid A are two additional acyl chains, XA3' and XA4' (Fig. 1). The MD-2 cavity likely could not accommodate more than four acyl chains. When the additional XA3' chain ester-linked to the XA3 O3' atom is directed toward the inside of the cavity, the hydrogen bonds of the XA3 O3' atom to both Ser¹²⁰ O and to XA1 O1' are disrupted, and hence the XA3 and XA4 portions are rearranged. This rearrangement would displace some portions of XA3 and XA4 toward the region near Val⁸², Leu⁸⁷, and Phe¹²⁶, which is reported to affect ligand-stimulated TLR4 clustering (27).

Binding sites other than L1 through L4 for the additional acyl chains or conformational changes enlarging the cavity are conceivable for lipid A. The additional lipid A acyl chains displaced from the hydrophobic cavity might be involved in activation upon MD-2 complexation with TLR4, and they may induce the reported oligomerization of TLR4 (28). This activation scheme is consistent with the increased MD-2 affinity to lipid A upon association with TLR4 (29). Recombinant human MD-2 in which Ser⁵⁷, Leu⁶¹, and Lys¹²² are replaced with the corresponding mouse residues (Thr⁵⁷, Val⁶¹, and Glu¹²²) is reported to be activated by lipid IVa and lipid A (30). The hydroxy O^γ atom of Ser⁵⁷ in the β4 strand is hydrogen-bonded to Glu⁵³ N, Leu⁶¹ is located deep in the cavity, and Lys¹²² is on the surface of the cavity entrance. The former two replacements

would bring subtle changes in the construction of the cavity, and the replacement with the glutamate side chain would change the electrostatic properties of the cavity entrance.

We hypothesize that the MD-2 structure unaltered by lipid IVa binding might be essential to antagonistic properties in human cells. The complexed structure that confines most of lipid IVa suggests that MD-2 plays a principal role in recognizing LPS. Moreover, it provides a basis for structure-based development of antiseptic drugs that might be effective in preventing endotoxin shock.

References and Notes

- C. A. Janeway Jr., R. Medzhitov, *Annu. Rev. Immunol.* **20**, 197 (2002).
- J. H. Fritz, R. L. Ferrero, D. J. Philpott, S. E. Girardin, *Nat. Immunol.* **7**, 1250 (2006).
- S. W. Montminy et al., *Nat. Immunol.* **7**, 1066 (2006).
- D. C. Angus et al., *Crit. Care Med.* **29**, 1303 (2001).
- Y. Nagai et al., *Nat. Immunol.* **3**, 667 (2002).
- A. Poltorak et al., *Science* **282**, 2085 (1998).
- M. Gangloff, N. J. Gay, *Trends Biochem. Sci.* **29**, 294 (2004).
- M. Inohara, G. Nuñez, *Trends Biochem. Sci.* **27**, 219 (2002).
- K. Miyake, *Semin. Immunol.* **16**, 11 (2004).
- S. Viriyakosol, P. S. Tobias, R. L. Ketchens, T. N. Kirkland, *J. Biol. Chem.* **276**, 38044 (2001).
- A. Poltorak, P. Picciardi-Castagnoli, S. Citterio, B. Beutler, *Proc. Natl. Acad. Sci. U.S.A.* **97**, 2163 (2000).
- E. Lien et al., *J. Clin. Invest.* **105**, 497 (2000).
- C. Alexander, U. Zahring, *Trends Glycosci. Glycotechnol.* **14**, 69 (2002).
- M. Muroi, T. Ohnishi, K. Tanamoto, *Infect. Immun.* **70**, 3546 (2002).
- S. Kusumoto et al., *J. Endotoxin Res.* **9**, 361 (2003).
- T. K. Means, D. T. Golenbock, M. J. Fenton, *Cytokine Growth Factor Rev.* **11**, 219 (2000).
- See supporting material on Science Online.
- A. Gruber, M. Mancek, H. Wagner, R. Kirschning, R. Jerala, *J. Biol. Chem.* **279**, 28475 (2004).
- G. E. Mullen et al., *Proc. Natl. Acad. Sci. U.S.A.* **100**, 3919 (2003).
- M. Mancek, P. Pristovsek, R. Jerala, *Biochem. Biophys. Res. Commun.* **292**, 880 (2002).
- A. Visintin, D. B. Ilijev, B. G. Monks, K. A. Halmen, D. T. Golenbock, *Immunobiology* **211**, 437 (2006).
- C. S. Wright, Q. Zhao, F. Rastinejad, *J. Mol. Biol.* **342**, 585 (2004).
- A. D. Ferguson, E. Hofmann, J. W. Coulton, K. Diederichs, W. Welte, *Science* **282**, 2215 (1998).
- I. A. Wilson, R. L. Stanfield, *Curr. Opin. Struct. Biol.* **4**, 857 (1994).
- F. Re, J. L. Strominger, *J. Immunol.* **171**, 5272 (2003).
- J. I. Kim et al., *J. Biol. Chem.* **280**, 11347 (2005).
- M. Kobayashi et al., *J. Immunol.* **176**, 6211 (2006).
- A. Visintin, E. Latz, B. G. Monks, T. Espevik, D. T. Golenbock, *J. Biol. Chem.* **278**, 48313 (2003).
- S. Akashi et al., *J. Exp. Med.* **198**, 1035 (2003).
- M. Muroi, K. Tanamoto, *J. Biol. Chem.* **281**, 5484 (2006).
- Supported by Japanese Ministry of Education, Culture, Sports, Science and Technology grants-in-aid and a Protein 3000 grant (Y.S.), a JST-CREST grant (K.M.), and the JSPS scholarship and its grant (U.O.). We thank K. Hasegawa for technical assistance in the synchrotron experiment at SPring-8 BL38B1. Coordinates and structure amplitudes have been deposited in the Protein Data Bank with accession numbers 2E56 and 2E59 for the native and complexed structures, respectively.

Supporting Online Material

www.sciencemag.org/cgi/content/full/316/5831/1632/DC1
Materials and Methods

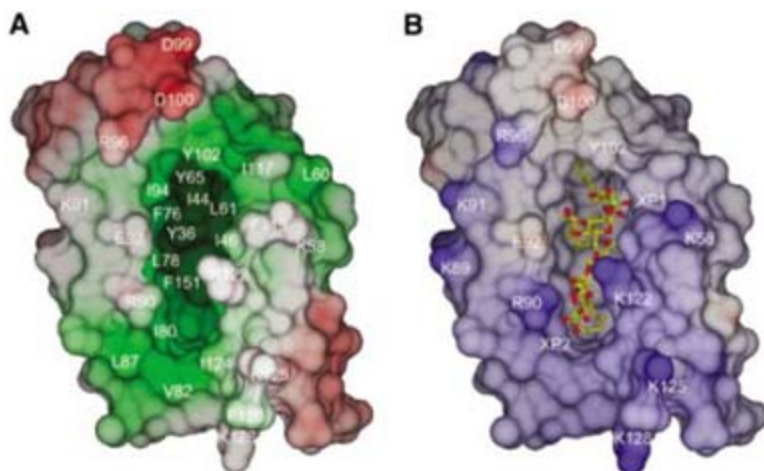
Figs. S1 to S3

Tables S1 to S3

20 December 2006; accepted 18 April 2007

10.1126/science.1139111

Fig. 4. Binding pocket and surface properties of MD-2. MD-2 is viewed from a 90° rotation with respect to Fig. 2, and residues of interest are indicated. (A) Protein surface showing hydrophobic and hydrophilic properties. The lipid IVa structure is removed from the complexed structure. Green and red represent hydrophobicity and hydrophilicity, respectively, and the extent is indicated by color darkness. (B) Electrostatic potential surface. Positive and negative potentials are shown in blue and red, respectively. Bound lipid IVa is drawn as a ball-and-stick representation: O in red, N in blue, C in yellow, and P in green.





Microcentrifuge Pack

The Spectrafuge 24D Microcentrifuge Starter Pack includes all the tools necessary for microsample preparation. The Spectrafuge 24D Microcentrifuge combines innovations such as a unique, easy access rotor design with an exclusive multi-flow air cooling system that keeps samples cool while maintaining quiet operation (less than 55 dBA). A digital microprocessor precisely regulates operation of the high-performance motor drive. The starter pack includes the Spectrafuge 24D digital microcentrifuge, the Spectrafuge mini-centrifuge, the Spectrafuge 24D StripSpin adapter for centrifugation of polymerase chain reaction strips, a 50-place microtube storage box, tube adapters for running 0.5- μ l and 0.2- μ l microtubes, and 500 Labnet 1.5- μ l clear microtubes.

Labnet International For information 732-417-0700 www.labnetlink.com

Peripheral Blood Mononuclear Cells

Cryopreserved human peripheral blood mononuclear cells (PBMC) display greater than 90% viability when thawed. When tested for peptide or protein antigen-induced T-cell recall responses in cytokine enzyme-linked immunospot assays, the frequencies and per-cell cytokine productivities of the thawed cells approximate 100% of fresh PBMC. The cryopreserved PBMC are available either uncharacterized or characterized for HLA-type low/high resolution, antigen reactivity, age, gender, ethnicity, blood type, and vaccination status for vaccinia, tuberculosis, and hepatitis B. Custom orders are also available. The cells can be used for validation and protocol set-up, and for internal controls for clinical trials. They can facilitate human immunological research and assay standardization within and between laboratories. All donors are screened to be negative for a variety of pathogens.

Cellular Technology Ltd For information 888-791-4005 www.immunospot.com

MALDI Spotting System

The NanoLC MALDI Spotting System enables users to use a powerful liquid chromatography (LC) system in matrix-assisted laser-desorption ionization (MALDI) applications. Featuring the new Ekspot spotter, the new system complements the manufacturer's offerings for nanospray mass spectrometry (MS) proteomics analysis. Integration of the Ekspot with the NanoLC provides single-point control from Eksigent software and enables the analysis of complex protein and peptide samples with MALDI MS. The Ekspot spotter/fraction collector deposits fractions eluted from the NanoLC onto a MALDI plate, while a built-in pump automatically adds the matrix. High positioning accuracy ensures consistent spotting with maximum resolution. The high-capacity system stores up to 16 MALDI targets for high-throughput applications. By eliminating flow splitting, Eksigent's proprietary

microfluidic technology improves reproducibility and sensitivity and eliminates solvent waste. The NanoLC's precise microscale flow control runs high performance LC gradients at rates as low as 20 nL per minute.

Eksigent For information 925-560-2627 www.eksigent.com

Human Embryonic Northern Blots

The Human Embryonic message Hunter Northern Blots provide a quick answer to which genes are turned on and off during the human embryonic development stages. Researchers can choose Northern blots at 6, 7, 8, 9, 10, 11, and 12 weeks of development for a variety of tissues. The tissue sources include human embryonic brain, heart, kidney, liver, lung, muscles, and whole embryos.

G-Biosciences/Genotech For information 800-628-7730 www.GBiosciences.com

Real-Time PCR

High-resolution melting (HRM) is a novel, closed-tube, post-polymerase chain reaction (PCR) method that enables researchers to analyze genetic variations (such as single nucleotide polymorphisms, mutations, and methylations) in PCR amplicons prior to or as an alternative to sequencing. It provides high specificity, high sensitivity, and convenience at a significantly higher speed and lower cost than methods such as denaturing high performance liquid chromatography, gels, or gradient-based techniques. The LightCycler 480 Real-Time PCR System now features a new software analysis tool and reagent for PCR and HRM-based mutation scanning, turning it into the first fully integrated, high-throughput platform for this technique. When HRM is used to scan gene fragments, unknown sequence variations in heterozygous samples have melting curves that are shaped differently from those derived from homozygous samples. The LightCycler 480 High Resolution Melting

Master contains a special DNA dye that binds to DNA without preference for sequence or conformation. The dye gives rise to distinct melting signals that, when acquired at high resolution, can reveal subtle differences between wild-type and heterozygous samples.

Roche Diagnostics For information 317-521-2000 www.lightcycler480.com

Systems Toxicology Software

Genedata ToxPedia is computational software offering the opportunity to use systems toxicology for drug safety prediction. Systems toxicology has the potential to reduce costly failures in the late stages of drug development. To use it, scientists need to integrate toxicogenomic data with conventional toxicological end points. This integration enables a systematic search for clinically relevant molecular biomarkers that can be used to predict a compound's toxicity profile before expensive clinical trials are started.

Genedata For information +41 61 697 8510 www.genedata.com

Literature

Ease: Introducing PrepEase Purification Products is a brochure that describes a comprehensive line of purification products for isolation of plasmids, DNA, RNA, and histidine-tagged proteins. The products are based on well-established and reliable methods of purification using anion exchange chromatography and silica membranes.

USB Corporation For information 216-765-5000 www.usbweb.com

Newly offered instrumentation, apparatus, and laboratory materials of interest to researchers in all disciplines in academic, industrial, and government organizations are featured in this space. Emphasis is given to purpose, chief characteristics, and availability of products and materials. Endorsement by *Science* or AAAS of any products or materials mentioned is not implied. Additional information may be obtained from the manufacturer or supplier.

Science Careers

From the journal *Science* AAAS

Classified Advertising



From life on Mars
to life sciences

For full advertising details, go to www.sciencecareers.org and click on **For Advertisers**, or call one of our representatives.

United States & Canada

E-mail: advertise@sciencecareers.org
Fax: 202-289-6742

IAN KING Recruitment Sales Manager
Phone: 202-326-6528

NICHOLAS HINTIBIDZE
West Academic
Phone: 202-326-6533

DARYL ANDERSON
Midwest/Canada Academic
Phone: 202-326-6543

ALLISON MILLAR
Industry/Northeast Academic
Phone: 202-326-6572

TINA BURKS
Southeast Academic
Phone: 202-326-6577

Europe & International

E-mail: ads@science-int.co.uk
Fax: +44 (0) 1223 326532

TRACY HOLMES Sales Manager
Phone: +44 (0) 1223 326525

MARIUM HUDDA
Phone: +44 (0) 1223 326517

ALEX PALMER
Phone: +44 (0) 1223 326527

LOUISE MOORE
Phone: +44 (0) 1223 326528

Japan

JASON HANNAFORD
Phone: +81 (0) 52-757-5360
E-mail: jhannaford@sciencemag.jp
Fax: +81 (0) 52-757-5361

To subscribe to Science:
In U.S./Canada call 202-326-6417 or 1-800-731-4939
In the rest of the world call +44 (0) 1223-326-515

Science makes every effort to screen its ads for offensive and/or discriminatory language in accordance with U.S. and non-U.S. law. Since we are an international journal, you may see ads from non-U.S. countries that request applications from specific demographic groups. Since U.S. law does not apply to other countries we try to accommodate recruiting practices of other countries. However, we encourage our readers to alert us to any ads that they feel are discriminatory or offensive.

POSITIONS OPEN

The Center for Remote Sensing of Ice Sheets (CREGIS) at the University of Kansas seeks a full-time **ASSOCIATE DIRECTOR** in education, outreach, and knowledge transfer. The Associate Director will be expected to plan, implement, manage, and track initiatives of the center's education outreach and knowledge transfer programs. Day-to-day activities include: recurring interaction with the center's graduate and undergraduate students; work with center staff to develop/maintain a compelling web presence of the center; oversight of K-12 outreach; strengthen distance learning efforts; manage summer research experiences for undergraduates and international research experiences programs; and manage graduate student recruitment. Making the center's science and technology development activities and products highly visible, transparent, compelling, and accessible to a broad audience is critical. Seeking additional funding by proposal writing to support new initiatives is also expected. Requires a Master's degree and five years of related experience. Review of applications begins June 28, 2007. Salary range is \$70,000 to \$80,000. For a complete description with complete list of requirements and to apply go to website: <https://jobs.ku.edu> and search for position number 00206340. *Equal Opportunity/Affirmative Action Employer.*

POSTDOCTORAL RESEARCH. Mentored teaching fellowships available: Office for Diversity in Science Training, University of Kansas, NIH-Institutional Research and Academic Career Development Award Program (IRACDA). Postdoctoral fellowships are available through the NIH-IRACDA Program. This comprehensive program offers three years of support to outstanding candidates seeking postdoctoral research training along with an opportunity to obtain mentored teaching experience in a four-year tribal college in preparation for an academic career. Ph.D. in biomedical sciences or related field required. For complete description and application instructions go to website: <https://jobs.ku.edu>, position #00000194. Review of applications will begin July 1, 2007, for appointments beginning shortly thereafter and will continue until positions are filled. *Equal Opportunity/Affirmative Action Employer.*

TEXAS TECH UNIVERSITY HEALTH SCIENCES CENTER, Garrison Institute on Aging department, is accepting applications for a **POSTDOCTORAL FELLOWSHIP** to be available in steroid hormone biosynthesis. Candidate should have a Ph.D. and background in cellular and molecular biology and endocrinology. Experience in gene knockout animal models is preferred. Send curriculum vitae to: Texas Tech University Health Sciences Center, Garrison Institute on Aging, 3601 4th Street, Stop 9424, Lubbock, TX 79430-9424. Fax: 806-743-3636; e-mail: xingjia.wang@ttuhsc.edu. For additional information and to apply, log on to website: <http://jobs.texasstate.edu>. *TTUHSC is an Equal Employment Opportunity/Affirmative Action Employer.*

POSTDOCTORAL POSITION to work on herpes simplex virus latency in an NIH-funded project. Available immediately. Recent Ph.D. Strong background in molecular biology essential. Background in virology, virus latency, or apoptosis desirable. Send curriculum vitae and information for three references to: Steven Wechsler, Ph.D., Professor; Department of Ophthalmology/Department of Microbiology and Molecular Genetics; c/o Alice Lane, Academic Coordinator; Department of Ophthalmology, University of California Irvine; 118 Medical Surge I Building 810; Irvine, CA 92697-4375. Or e-mail: wechsler@uci.edu. *The University of California Irvine is an Equal Opportunity Employer committed to excellence through diversity.*

POSITIONS OPEN

ASSISTANT/ASSOCIATE PROFESSOR Neurophysiology

The College of Veterinary Medicine at North Carolina State University in Raleigh, North Carolina, announces a tenure-track faculty position in neurophysiology with an initial appointment at 70 percent research, 20 to 30 percent teaching, and zero to ten percent service depending upon entering rank. A Ph.D. in neurophysiology or a relevant neuroscience field is required. Candidates also having a D.V.M. or teaching experience in a veterinary professional curriculum are encouraged to apply. To view the full vacancy announcement, with position responsibilities and additional requirements, and to apply, please visit our website: <http://jobs.ncsu.edu> and search by position #B-96-0708. Applications are currently being accepted and the position will be open until August 15, 2007, or until a suitable candidate is identified. Questions about the position can be directed to: **Dr. Lola Hudson, Search Committee Chair, College of Veterinary Medicine, North Carolina State University, 4700 Hillsborough Street, Raleigh, NC 27606, e-mail: lola_hudson@ncsu.edu.** *Affirmative Action/Equal Opportunity Employer. In addition, NC State University welcomes all persons without regard to sexual orientation. For those individuals with disabilities requiring accommodation please contact telephone: 919-515-3148.*

BIOLOGY: POSTDOCTORAL TEACHING FELLOWSHIP Begin August 2007

The Department of Biological Sciences at the University of the Sciences in Philadelphia invites applications for a one-year (renewable) Postdoctoral teaching fellowship. Thirty percent teaching; seventy percent research. Teach an undergrad introductory biology lecture and laboratories. Significant mentoring by experienced educators available. Successful applicant will join a dynamic research group studying Ras/MAP kinase signal transduction in regulating cellular division, growth, and differentiation in *Drosophila melanogaster* retinal development and human cancer cells. (see website: <http://www.usip.edu/biology/marenda.shtml> for more details). A strong background with experience in molecular biology, genetics, and biochemistry, specifically in cloning, immunohistochemistry, and confocal microscopy is highly desired. Applicants should have received their Doctorate within the last two years in a relevant biological science. Please submit cover letter, curriculum vitae, copies of graduate transcripts, and three letters of references to: **D.M. Teaching-Postdoctoral Fellow Search, Department of Biological Sciences, University of the Sciences in Philadelphia, 600 S. 43rd Street, Philadelphia, PA 19104-4495.**

Affirmative Action/Equal Opportunity Employer.

SENIOR RESEARCH TECHNOLOGIST sought by Massachusetts General Hospital to lead a research project that aims to identify the molecular basis of Huntington's disease. Requires M.S. or equivalent in genetics, molecular biology, biochemistry, or neurobiology and two years of industry experience. Must have expertise in each of the combined disciplines above, including genetic manipulation and mouse breeding, brain tissue dissection, culture of neuronal cells, manipulation of nucleic acid in real time polymerase chain reaction analyses, complementary DNA and oligonucleotide microarray analyses; cloning, fusion protein production, immunoprecipitation, sucrose density gradient fractionation, high performance liquid chromatography; development and optimization of cell based assays for high throughput drug screens and expertise in Huntington's disease. If qualified, send resume to: **Cheryl Crowley, Administration Manager, Molecular Neurogenetics Unit, Center for Human Genetic Research, Massachusetts General Hospital, 185 Cambridge Street, Cambridge, MA 02144.**



NIAID Needs You *Because The World Needs Us*

DIRECTOR, DIVISION OF ACQUIRED IMMUNODEFICIENCY SYNDROME (DAIDS), NIAID, NIH, DHHS

The National Institute of Allergy & Infectious Diseases (NIAID) is seeking an exceptional and visionary leader for the position of Director, Division of Acquired Immunodeficiency Syndrome (DAIDS). A \$4.4 billion organization, NIAID supports over 100 major research programs and initiatives in three broad, distinct areas: biodefense, AIDS, and traditional immunologic and infectious diseases.

DAIDS' mission is to increase basic knowledge of the pathogenesis, natural history, and transmission of HIV disease and to support research that promotes progress in its detection, treatment, and prevention. DAIDS accomplishes these goals and objectives through planning, implementing, managing, and evaluating programs in 1) fundamental basic research, 2) discovery and development of therapies for HIV infection and its complications, and 3) discovery and development of vaccines and other prevention strategies.

DAIDS is comprised of 18 Offices, Branches, and Programs with approximately 180 scientific and administrative staff. The Division funds efforts through a comprehensive portfolio of research grants, cooperative agreements, and contracts with a total annual budget of more than \$900M.

The Director, DAIDS reports to the Director, NIAID and provides overall executive direction and scientific leadership for DAIDS. Specifically, develops, directs, and coordinates DAIDS program activities; manages resource allocations to include staff, physical, and financial resources; maintains staff through recruitment, training, mentoring, and workplace diversity; and fosters a productive work environment. In addition, the successful candidate will: serve as an advisor to the Director, NIAID on AIDS and HIV mission and research agenda; liaison with representatives of other major NIH Institutes and Centers, Federal and non-Federal agencies, international research organizations, professional societies, foundations, the media, and patient advocacy groups; establish and maintain research collaborations with industry and public sector organizations; and support and liaison with the AIDS Research Advisory Committee and the AIDS Vaccine Research Committee.

The major thrust of the position is to provide scientific administrative and executive leadership. It may be possible for a candidate to have a laboratory presence in the NIAID Intramural Research Program.

QUALIFICATIONS: Applicants must possess an M.D., Ph.D., or equivalent degree and must demonstrate the following: **1)** Experience working independently in planning, organizing, and conducting biomedical research in fields consistent with the mission of the NIAID and DAIDS (e.g., infectious diseases, HIV); and **2)** Experience serving effectively in research program administration in these fields, which must include managing policies and procedures associated with extramural research administration. This experience may be gained via senior level research experiences as a principal investigator, or may otherwise be gained through active involvement in initiating research projects, developing protocols, conducting studies, documenting findings, interpreting results in a published report (journal), supervising staff, and managing the budget. Preference will be given to those known and respected within their profession, both nationally and internationally, as distinguished individuals of outstanding scientific competence and those that possess a record as a senior scientific administrator/executive leader.

APPLICATION PROCESS: Provide a Curriculum Vitae, bibliography, and a two page summary explaining **1) level of interest in the position and 2) administrative/executive skills in relation to leading change; leading people; producing results/making decisions; administering human, financial, and information resources; and building coalitions/communication.**

Submit package to: Ms. Lisa Poindexter-Steed, Office of Workforce Effectiveness and Resources (OWER), NIAID, 10401 Fernwood Road, Suite 2SE57, Bethesda, Maryland 20817 and reference announcement number **DDAIDS-07-01**. The application review process will begin **August 24, 2007**. Direct inquiries to: Ms. Poindexter-Steed via email: lsteed@niaid.nih.gov or at 301-496-9687. Information regarding the Institute is available on the NIAID website at www.niaid.nih.gov. All information provided by applicants will remain confidential and will only be reviewed by authorized officials of the NIAID. Salary is commensurate with experience and a full package of benefits is available including retirement, health and life insurance, long term care insurance, leave, and savings plan (401K equivalent). This position is subject to a background investigation.



Tenure-Track Positions Liver Diseases Branch

New Research Initiative – Fatty Liver Disease & Obesity - Tenure Track Position:

The Liver Diseases Branch of the National Institute of Diabetes and Digestive and Kidney Diseases (NIDDK), National Institutes of Health (NIH) invites applications for one tenure track position from scientists interested in basic and/or clinical research involving non-alcoholic fatty liver disease and metabolic syndrome. Specific areas of research interest include pathogenesis and mechanism of metabolic derangement in non-alcoholic fatty liver disease and its pathophysiological link to insulin resistance and obesity. Priority will be given to applicants at the Assistant Professor level in traditional universities or those finishing their post-doctoral/fellowship positions.

New Research Initiative – Liver Stem Cells - Tenure Track Position:

The Liver Diseases Branch of the National Institute of Diabetes and Digestive and Kidney Diseases (NIDDK), National Institutes of Health (NIH) invites applications for one tenure track position from scientists interested in basic and/or clinical research involving mammalian adult stem cells. Specific areas of research interest include functional differentiation and mechanism of development of adult tissue-derived stem cells, especially those of the liver, and potential clinical application of stem cell therapy in liver diseases. Priority will be given to applicants at the Assistant Professor level in traditional universities or those finishing their post-doctoral/fellowship positions.

The applicant must have a proven record of accomplishments and will be expected to propose and pursue an independent research program in one of these fields. The position offers unparalleled opportunities for interdisciplinary collaboration within NIDDK and throughout NIH. The Liver Diseases Branch of NIDDK is located on the main intramural campus of the NIH in Bethesda, Maryland, a suburb of Washington, D.C.

Interested applicants should send a Curriculum Vitae and list of publications, copies of three major publications, a summary of research accomplishments, a plan for future research, and three letters of recommendation to **Ms Michelle Brown, Search Committee, Liver Diseases Branch, NIDDK, Building 10-9B16, NIH, Bethesda, MD. 20892-1800.** Application deadline: **September 15, 2007.**



Staff Scientist Laboratory of Infectious Diseases Respiratory Viruses Section

The National Institute of Allergy and Infectious Diseases, a major research component of the NIH and the Department of Health and Human Services, is recruiting a Staff Scientist. The position will be available in the Respiratory Viruses Section of the Laboratory of Infectious Diseases, and scientists with a M.D. or Ph.D. are eligible. The research activity involves (1) the development of live attenuated flavivirus vaccine candidates and their evaluation in rodents and non-human primates as well as in the clinical trials in humans; (2) the use of novel approaches for construction of chimeric viruses to examine basic questions of viral pathogenesis and the molecular basis of attenuation of highly neurovirulent flaviviruses; (3) the evaluation of the immunologic determinants of resistance to infection and illness caused by these flaviviruses. This full-time research position offers a unique opportunity to work on investigations that range from basic molecular biology to applied vaccinology. Staff Scientist applicants should have at least six years of laboratory work experience in molecular virology and immunology; the salary range is \$74,503 - \$162,371. Preference will be given to candidates who have experience working with neurotropic viruses. Applicants should submit their curriculum vitae, a letter of research interests, and names and addresses of three references to:

Alexander Pletnev, NIH/NIAID/LID, 33 North Drive, Room 3W10A, Bethesda, MD 20892-3203, FAX: (301) 496-0501, email: apletnev@niaid.nih.gov. Review of applicants will begin on **September 1, 2007** and continue until a successful candidate is identified.



Staff Scientist Laboratory of Infectious Diseases Respiratory Viruses Section

The National Institute of Allergy and Infectious Diseases, a major research component of the NIH and the Department of Health and Human Services, is recruiting a Staff Scientist. The position will be available in the Respiratory Viruses Section of the Laboratory of Infectious Diseases, and scientists with a M.D., D.V.M. or Ph.D. are eligible. The research activity involves (1) examination of the pathogenesis of pandemic and potential pandemic strains of influenza and their evaluation in vitro and in experimental animals including the 1918 influenza; (2) influenza viral genomics, and examination of viral evolution in fitness and host adaptation; and (3) the development of influenza clinical trials in humans. This full-time research position offers a unique opportunity to work on investigations that range from basic molecular biology to clinical research. Staff Scientist applicants should have at least six years of laboratory work experience in molecular and classical virology research; the salary range is \$74,503 - \$162,371. Preference will be given to candidates who have experience working with influenza viruses especially those with BSL3 experience. Applicants should submit their curriculum vitae, a letter of research interests, and names and addresses of three references to:

Jeffery K. Taubenberger, MD, PhD, Attn: A. LeCointe, NIH/NIAID/LID, Bldg 33/Room 3W02B, MSC 3203, 33 North Drive, Bethesda, MD 20892-3203, FAX: (301) 480-4509, email: lecointe@niaid.nih.gov

Review of applicants will begin on **July 2, 2007** and continue until a successful candidate is identified.



WWW.NIH.GOV



Tenure-Track Position in Molecular Genetics
National Institutes of Diabetes and Digestive and Kidney Diseases

We seek an outstanding scientist to direct a vigorous, innovative research program in Molecular Genetics in the Genetics and Endocrinology Section/Metabolic Diseases Branch. Applicants must have a demonstrated track record of significant publications that address identification and mechanisms of action of tumor genes. The successful candidate is expected to develop an independent, world-class research program complementary to current investigations within the Branch. The position comes with generous start up funds and on-going support.

The Metabolic Diseases Branch of NIDDK is located on the main NIH campus in Bethesda, Maryland, a suburb of Washington DC. The Branch represents interests similar in range to those of an academic department with groups studying G-proteins and hormone-secreting tumors including those mediated by the MEN1 or HRPT2 genes in man. There are strong interactions among the three independent research groups, and the position offers unparalleled opportunities for interdisciplinary collaboration within NIDDK and throughout NIH. Applicants should submit a curriculum vitae, bibliography, copies of three major publications, a summary of research accomplishments, a brief statement of future research goals, and arrange for three letters of reference to be sent to:

Dr. Dan Camerini-Otero, Chair, Search Committee, c/o Linda Robinson, NIDDK, 9000 Rockville Pike, Building 5/Room 201, National Institutes of Health, Bethesda, MD 20892, E-mail: lindar@mail.nih.gov.

Application Deadline: **July 15, 2007.**



Tenure-Track Position in Human Molecular Genetics
National Institute of Diabetes and Digestive and Kidney Diseases

We seek an outstanding scientist to direct a vigorous, innovative research program in the molecular genetics of human type 2 diabetes and/or obesity, in particular as these diseases relate to the Pima Indian population of Arizona. Applicants must be highly motivated and have a demonstrated track record through publications that address significant issues of discovery of genetic susceptibility factors to these conditions in human populations. The successful candidate is expected to develop an independent, world-class research program complementary to current investigations within the Phoenix Epidemiology and Clinical Research Branch (PECRB). The position comes with generous start up funds and on-going support.

The PECRB, NIDDK is located in downtown Phoenix, Arizona. The Branch represents interests similar in range to those of an academic department. There are strong interactions among the independent research groups, and the position offers unparalleled opportunities for interdisciplinary collaboration within NIDDK and throughout NIH. Applicants should submit a curriculum vitae, bibliography, copies of three major publications, a summary of research accomplishments, a brief statement of future research goals, and arrange for three letters of reference to be sent to:

Dr. Dan Camerini-Otero, Chair, Search Committee, c/o Linda Robinson, NIDDK, 9000 Rockville Pike, Building 5/Room 201, National Institutes of Health, Bethesda, MD 20892, e-mail: lindar@mail.nih.gov.

Application Deadline: **July 15, 2007.**

Opportunities with Howard Hughes Medical Institute

The **Howard Hughes Medical Institute (HHMI)**, a national and international philanthropy devoted to biomedical research and science education, is seeking experienced professionals to join our new Science Education Alliance (SEA) program at our **Janelia Farm Research Campus in Ashburn, VA**. For the first several months, these positions will be located at our **headquarters in Chevy Chase, MD**.

The SEA program is an exciting new initiative that promises to become a national resource for science education. SEA's first major project will be to develop a national genomics experiment implemented as a research-based laboratory course for freshmen- and sophomore-level undergraduate students. This program is an opportunity to infuse undergraduate curricula with tested innovative methods to train students for 21st-century science. This research course will begin with techniques used in microbiology, advance through molecular biology, and end in bioinformatics.

Program Officer

In this key position, the Program Officer will help develop and coordinate the national experiment. The Program Officer will assist in developing guidelines for participation in SEA and appropriate training workshops for participating faculty; identify potential participants; identify, assemble, and assess protocols and other resource materials; assist in development of assessment tools; and make site visits to participating institutions once the course is running. During the first year of program development, the Program Officer will be required to spend one day a week traveling out of state. Additionally, the Program Officer will be responsible for helping to identify emerging trends in science education and help develop programs to disseminate science education-related activities, methodologies, and resources.

The ideal candidate must possess a Ph.D. in the biological sciences or related fields with academic experience, excellent communication skills, excellent critical thinking skills, proficient computer skills, demonstrated skill in managing programs and people, and the capacity for strong and imaginative leadership about the future of biomedical science education.

Research Technician/Program Assistant

In this key position, the Research Technician/Program Assistant will help test, develop, modify, assemble, and distribute protocols, biological and reagent kits to be used in faculty training and in course implementation of the national experiment. Additionally, the Research Technician/Program Assistant will perform general office duties during off-peak times.

The ideal candidate must possess a degree in the biological sciences or related fields with two years or more laboratory research experience, preferably in molecular biology, and be able to travel to the out-of-state pilot site location one day per week during the initial year of the initiative. Excellent record keeping skills, communication skills, proficient computer skills, the ability to work well within a team environment, and ability to work independently are a must.

HHMI is an intellectually demanding, results-oriented organization with excellent salaries and benefits. Responses should include your present position, and a brief summary of your scientific interests and accomplishments. Please send your resumes to Christine Leonhardt-Kimm at jobs@hhmi.org. Please include the job title in the subject line. To learn more about HHMI and these positions, visit our Web site at www.hhmi.org.

The Howard Hughes Medical Institute is an Equal Opportunity Employer.

HHMI
 HOWARD HUGHES MEDICAL INSTITUTE

Biomedical Physics Research and Engineering Multiphoton Microscopy in Medical Endoscopy

Located in Ithaca, N.Y., Cornell University is a bold, innovative, inclusive and dynamic teaching and research university where staff, faculty, and students alike are challenged to make an enduring contribution to the betterment of humanity.

Cornell University, in collaboration with Weill Medical College of Cornell University, has undertaken the incorporation of Multiphoton Microscopy (MPM) into human Medical Endoscopies (US Patent 6,839,586). The integration of the established technology of MPM (US Patents 5,034,613, 6,166,385 and 6,344,653) into Medical Endoscopies utilizes the nonlinear excitation of the intrinsic fluorescence of tissues and their Second Harmonic Generation (SHG) for high-resolution microscopic imaging in situ in real time for "optical biopsies" and during surgery, encompassing microscopy in traditional endoscopies. There are opportunities for optical physicists and engineers, and biophysicists and biomedical engineers to serve in postdoctoral or research associate positions at Cornell in Ithaca, NY.

This research involves basic biophysical optics and instrumentation as well as design, development and testing of instrumentation, and its optimization in applications. It also includes documentation of MPM/SHG endoscopy biopsy image comparisons with pathologists' H&E preparations. Expertise in Engineering and Biomedical Physics is required for this laser and microscopy optics instrument design challenge, preferably including proficiency in photophysics and biophysics.

Send cover letter and curriculum vita to: **Prof. Watt W. Webb, School of Applied & Engineering Physics, Cornell University, 223 Clark Hall, Ithaca, NY 14853-2501. Email: www2@cornell.edu**



Cornell University

Cornell University is an Affirmative Action, Equal Opportunity Employer and Educator.

<http://chronicle.com/jobs/profiles/2377.htm>

Fluidigm

Progressive. Innovative. Flexible.

These three words describe Fluidigm's microfluidic technology. They also describe the highly energetic individuals who make up our team. Fluidigm, located in South San Francisco, seeks bright individuals to complement our team of research, development and business management professionals.

APPLICATIONS DEVELOPMENT SCIENTIST

(Molecular Biology)

Develop novel applications for the Fluidigm Digital Array platform. Requires experience with standard molecular biology techniques, including isolating RNA & DNA, PCR, and homogeneous fluorescent PCR assays, and success developing/designing procedures for commercial customers. **(Job Code: 2007-26-SCI)**

TECHNOLOGY DEVELOPMENT SCIENTIST

(Molecular Biology)

Invent & develop novel applications for use with existing and new Fluidigm technology platforms. Requires experience with standard molecular biology techniques, including nucleic acids, proteins and cells, lab expertise, and experience with device/instrument development. **(Job Code: 2007-25-SCI)**

BOTH positions require a Ph.D. or equivalent in Molecular Biology, Biochemistry or Chemistry, and 2+ years of experience in assay development and commercialization.

Why not consider working for one of Red Herring's Top 100 Private Companies? Fluidigm offers an exciting work environment with excellent compensation & benefits, including pre-IPO stock options. Reference the position title and job code in the subject and email resume to: jobs@fluidigm.com. Fluidigm will not accept resumes from 3rd parties. EOE



For more information on Fluidigm and to view all current job opportunities, please visit:

www.fluidigm.com

Director of NUS/A*STAR Clinical Imaging Research Centre (CIRC), Singapore

The National University of Singapore (NUS) School of Medicine, in conjunction with the government's Agency for Science, Technology & Research (A*STAR), is building a major research centre for *in vivo* imaging for clinical and translational medicine. The NUS/A*STAR Clinical Imaging Research Centre (CIRC) will procure and use state-of-the-art clinical imaging systems for investigations in human subjects, focusing particularly on diseases relevant in the region.

A multi-million dollar investment has been committed to fund research staff, equipment and operational costs and the first phase of procurement is underway. We now wish to appoint the first Director of CIRC to lead and develop this Program. The Director will report to a Management Committee, chaired by Professor Sir George Radda, comprising senior representatives from A*STAR and NUS. He/She will be responsible for devising the overall clinical research strategy, making new scientific appointments and for overseeing the procurement of new equipment (additional MRI and related technologies, PET-CT, SPECT-CT, optical imaging, ultrasound) and the planned relocation in 2009 to a new building at the NUS Yong Loo Lin School of Medicine.

The location and research environment are ideal for interacting with scientists, clinicians, engineers and IT/data processing staff belonging to:

- NUS Faculties of Engineering, Science, Information Technology, Medicine and Radiology.
- The University teaching hospital.
- A*STAR's Singapore Institute for Clinical Sciences.
- Other A*STAR Research Institutes and consortia based in Biopolis including those engaged in Preclinical Imaging Research, Stem Cells, Genomics.
- NUS Faculties of Engineering, Science, Information Technology, Medicine and Radiology.
- The University teaching hospital.
- A*STAR's Singapore Institute for Clinical Sciences.
- Other A*STAR Research Institutes and consortia based in Biopolis including those engaged in Preclinical Imaging Research, Stem Cells, Genomics, Molecular and Cell Biology, and Immunology.
- Equipment suppliers and Pharmaceutical Industry research groups.

The intention is to create one of the largest and best-equipped multi-disciplinary centres for clinical research imaging in Asia that will become a national resource for research and training.

We invite internationally-recognized investigators in the area of clinical imaging research to apply for the Directorship. Qualified to MD, PhD, or MD/PhD level, and from either an academic or industrial background, you must be able to demonstrate your ability to lead and run a major programme in clinical imaging/translational research and be able to link this to preclinical scientific findings. Preference will be given to applicants with a strong track record of publications in major journals, who have led a major research program and have built collaborations with other groups. Candidates will be offered a joint appointment at the National University of Singapore (professorial) and with A*STAR. The remuneration package will be highly competitive to reflect the national (and international) significance of this role.

To discuss your interest, please contact Professor Sir George Radda (george.radda@dpag.ox.ac.uk or george.radda@sbic.a-star.edu.sg) or Dr Kevin Young (Kevin.Young@theRSAGroup.com), preferably enclosing your curriculum vitae. All applications will be treated in strict confidence. remuneration package will be highly competitive to reflect the national (and international) significance of this role.

To discuss your interest, please contact Professor Sir George Radda (george.radda@dpag.ox.ac.uk or george.radda@sbic.a-star.edu.sg) or Dr Kevin Young (Kevin.Young@theRSAGroup.com), preferably enclosing your curriculum vitae. All applications will be treated in strict confidence.

Employment Agency Licence: C87401J.



U.S. Department of Energy
Office of Science
Deputy for Programs
Announcement #SES-SC-HQ-013 (kd)

The U.S. Department of Energy's (DOE) Office of Science is seeking highly qualified candidates with outstanding scientific achievements to fill the Deputy for Programs position. The Office of Science is the single largest supporter of basic research in the physical sciences in the United States, with a 2007 budget of \$3.8 billion. It oversees the Nation's research programs in high-energy and nuclear physics, basic and fusion energy sciences, and biological, environmental and computational sciences. The Office of Science is the Federal Government's largest single funder of materials and chemical sciences, and it supports unique and vital parts of U.S. research in climate change, geophysics, genomics, life sciences, and science education. The Office of Science also manages 10 world-class laboratories and oversees the construction and operation of some of the Nation's most advanced R&D user facilities, located at national laboratories and universities. These include particle and nuclear physics accelerators, synchrotron light sources, nanoscale science research centers, neutron scattering facilities, bio-energy research centers, supercomputers and high-speed computer networks. More information on the Office of Science can be found at <http://science.doe.gov>.

The Deputy for Programs provides scientific and management oversight of the six program offices by ensuring program activities are strategically conceived and executed; formulating and defending the Office of Science budget request; establishing policies, plans, and procedures related to the management of the program offices; ensuring the research portfolio is integrated across the program offices with other DOE program offices and other Federal agencies; and representing the organization and make commitments for the Department in discussions and meetings with high-level government and private sector officials. The position is within the ranks of the U.S. government's Senior Executive Service (SES); members of the SES serve in key positions just below the top Presidential appointees.

To apply for this position, please see the announcement and application instructions at <http://jobsearch.usajobs.opm.gov/ses.asp> under the vacancy announcement of #SES-SC-HQ-013 (kd). Qualified candidates are asked to submit their online applications by **August 29, 2007**.



Leibniz-Institut
für Polymerforschung
Dresden e. V.



The **Technische Universität Dresden** (TU Dresden)
Faculty of Science
Department of Chemistry and Food Chemistry
and the

Leibniz-Institut für Polymerforschung Dresden e.V. (IPF)

establish with regard to the Centre of Excellence „Centre for Regenerative Therapies Dresden“ (CRTD)

a new jointly appointed **W3 full Professorship** (tenure) named

„Biofunctional Polymeric Materials“

and search for suitable candidates. The professorship will involve the scientific leadership of the IPF Research Area „Biofunctional Polymer Materials“ at the Max-Bergmann-Centre for Biomaterials.

The chair has to develop interdisciplinary approaches and will link physical and macromolecular chemistry and biochemistry with cell biology, biophysics and medicine. The research focus of the chair will be the development of new strategies for materials inspired by the increasing knowledge in life science. Particularly, the modulation of specific functions of living tissue by biohybrid and biomimetic polymeric materials and the understanding and control of interface interactions between living and artificial systems shall be scientifically explored. In the frame of the CRTD emphasis will be put on bioactive matrices (matrix engineering) which may contribute to the control of stem and progenitor cells *in vitro* and *in vivo* to enable new therapeutical approaches.

The chair is assigned to the *Department of Chemistry and Food Chemistry* of the TU Dresden (*focus Biochemistry*), is associated to the CRTD and involves active participation in international study and graduate programs related to the CRTD.

The candidate shall be an international expert in interdisciplinary research in biomaterials and bio-interface phenomena. Personal management qualities as well as experience in research management, international co-operations, acquisition and leadership of collaborative research projects and the potential to develop new research structures are desired. The applicants have to fulfill the employment conditions of § 40 Sächsisches Hochschulgesetz in its current version.

Applications from women are particularly welcome. The same applies to the disabled. The Applications will be made available to the involved bodies of the TU Dresden and the IPF.

Please send the application with CV, description of the research concept, publication list, list of third party funding and information about teaching experience till **July 13, 2007** to the **Leibniz-Institut für Polymerforschung Dresden e.V., Frau Prof. Dr. B. Voit, Wissenschaftliche Direktorin, Hohe Strasse 6, D-01069 Dresden (Germany)**.

Endothelial Pathobiology
Program
University of Texas
Medical Branch, Galveston

The Department of Pathology, University of Texas Medical Branch, Galveston, is seeking applications for a full professor to develop and lead the newly established Endothelial Pathobiology Program.

The Endothelial Pathobiology Program will include at least eight full-time faculty members by September 2010. Members of the Program will interact with University scientists whose research is focused on infectious, immunological, metabolic, nutritional, toxicological, gestational, or endocrine diseases in which the endothelium of the microvasculature plays a key role in pathogenesis.

The successful applicant will have an extensive body of influential scientific publications, experience in mentoring successful research careers, an established international reputation in the field of endothelial cell biology or pathobiology, and an active research program which employs cutting-edge technologies and physiologically relevant models of microvasculature dysfunction.

Experience in developing research priorities, defining and pursuing research opportunities, and building collaborative research initiatives is essential, as is familiarity with research-based postgraduate and student research programs.

Applicants should send a letter of interest, statement of current and future research objectives, and *curriculum vitae* to:

David H. Walker, M.D.
Professor and Chair
Department of Pathology
Executive Director
Center for Biodefense and
Emerging Infectious Disease
University of Texas Medical Branch
301 University Blvd.
Galveston, TX 77555-0609 USA
Email: dwalker@utmb.edu

The Search Committee will begin evaluating applications **July 15, 2007** and will continue until a suitable candidate is identified.

The University is an Equal Opportunity, Affirmative Action Employer. All qualified applicants are encouraged to apply.



UNIVERSITY OF THE WITWATERSRAND, JOHANNESBURG OFFICE OF THE DEPUTY VICE-CHANCELLOR (RESEARCH)

Institute for Human Evolution – Professor/Associate Professor/Senior Researcher

The University of the Witwatersrand (Wits) is located in the economic heartland of South Africa and in close proximity to some of the most important hominid fossil-bearing sites anywhere in the world. The University holds extensive fossil collections of international significance and the Institute for Human Evolution (IHE) has been established to create a centralized, sustainable, vibrant centre of research excellence. The IHE is a University Institute which reports directly to Deputy Vice Chancellor (Research). The IHE encourages multi-disciplinary research in palaeoanthropology and national and international scientific collaboration. The IHE currently has approximately 12 associate members, who hold teaching appointments across the University. It is the University's intention to locate the IHE in a building dedicated to the IHE and cognate disciplines.

The University wishes to make one or more senior appointments in the IHE. At the full or Associate Professor level, these would be permanent appointments, subject to the usual three year probation period. At the Senior Researcher level, the appointment would be for three years.

Qualifications, experience and attributes

Professor/Associate Professor

- a PhD and postdoctoral experience in the field, with a strong record of outputs in internationally recognized publications
- other forms of peer recognition, eg awards, invitations to international conferences, holding office in learned societies, advisory roles to Government, etc
- the ability to inspire research excellence and to participate in building a common vision of the IHE, in an ethos of collegiality, openness and mutual support
- the ability to work with top scholars from around the world
- proven success in fundraising
- well developed managerial skills
- initiative and commitment to participate in developing an internationally acclaimed research centre with a strong African focus
- the ability to cultivate multi-disciplinary research projects
- a clearly envisaged research programme

Senior Researcher

- a PhD and postdoctoral experience in the field
- a good research record, as reflected in recognized publications
- fundraising ability
- ability to work collaboratively
- a commitment to research excellence
- a clear research proposal

Directorship of the IHE

The senior successful candidate in the Professor/Associate Professor category may also be asked to assume the position of Director of the IHE. The major functions of this position would be:

- to develop and lead the IHE in accordance with the Business Plan of the Institute
- to create a supportive environment for researchers and postgraduate students
- to develop and direct an Institute that enjoys an international reputation for research excellence
- to bear responsibility, together with the University's Collections Curator, for all hominid fossils and associated faunal and floral fossils
- to raise funds, in particular endowment funds, for the sustainable growth and development of the IHE
- to work with the South African Heritage Resource Agency and Government departments or agencies to help shape the legislative and regulatory environment in ways that might benefit the science of palaeoanthropology
- to promote public awareness of the work of the IHE
- to direct and be accountable for the financial management and general administration of the IHE

Remuneration and conditions of service

A competitive salary package is on offer, together with generous leave and a relocation and settling-in allowance. The salary of a successful candidate who was also appointed to the Directorship would be supplemented.

Applications and further information

Fuller details of the Directorship and the IHE are available at <http://www.wits.ac.za/research> Personal enquiries may be directed to Professor B Bozzoli, Deputy Vice-Chancellor (Research) on tel. no. +27 11 717 1151 (GMT+1 hour), or belinda.bozzoli@wits.ac.za


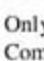
Applications may be made electronically or by conventional mail to:

Mr S Harduth
HR Manager
University of the Witwatersrand
Johannesburg Private Bag 3
PO Wits 2050
Republic of South Africa
sudesh.harduth@wits.ac.za

Applicants should indicate whether they would be interested in assuming the Directorship role and should include a statement in support of the application, full *curriculum vitae* (including a publication list) and the names of four referees who may be contacted by Wits.

Applicants not based in Johannesburg will be expected to make themselves available for interview, preferably in person, but in default by video or telephone conference.

The closing date for applications will be **Friday 29 June 2007**.

-  Only applicants who are short-listed will be contacted
-  Committed to excellence and equity





CHAIR OF PHARMACOLOGY POSITION AVAILABLE

The Ohio State University College of Medicine Department of Pharmacology seeks an energetic and dynamic leader for the position of Chair of Pharmacology.

The Ohio State University Medical Center leads the region with nine specialties named as among the best in America in the latest U.S. News & World Report magazine, and the OSU College of Medicine is ranked 32nd by USNWR, making it one of the best public academic medical centers in the US. The OSU Medical Center has seen dramatic growth in its research programs in recent years, both in funding and in impact. Faculty at Ohio State today hold more than \$182 million in external research funding, all focused on finding the causes of disease and injury, their progression, optimum treatment and – wherever possible – their prevention. The completion of the Biomedical Research Tower has added 10 floors and 180,000 square feet of lab space needed for continued growth. The cancer program has a NCI sponsored phase I U101 and phase II NO1 early trials grant which links closely clinician scientists to the Department of Pharmacology. Additionally, there is a close collaboration between the College of Pharmacy and Department of Pharmacology.

The Department of Pharmacology consists of 15 faculty members, serving as the home for the OSU program in Pharmacogenomics, and a clinical trials division. Faculty research targets CNS pharmacology, cancer, and cardiovascular disease, with a strong group of investigators focusing on drug addiction.

The candidate for Chair should have an excellent scholarly track record in basic biomedical sciences and/or translational research, demonstrated ability to attract extramural funding, and administrative experience.

The candidate will be expected to provide strong leadership in building an outstanding pharmacology department, integrating basic and clinical research. The successful candidate will be expected to lead or foster collaborative programs in support of strategic priorities of the medical center, including neuroscience, heart, cancer, critical care, transplantation, and imaging. OSUMC is continuing to invest heavily in the growth of the biomedical departments within the SOM and is willing to commit significant resources towards a visionary Chair's efforts to develop the Department of Pharmacology

This is a full-time tenure track position. Applicants should submit a C.V. and a description of their accomplishments and current focus and goals to: **Michael Ostrowski, PhD Chair, Search Committee for Chair of Pharmacology, 333 Hamilton Hall, 1645 Neil Avenue, Columbus, OH 43210; E-mail: michael.ostrowski@osumc.edu.**

The Ohio State University is an Equal Opportunity Employer.



Faculty Positions in Cardiovascular Medicine and Research

The University of Massachusetts School of Medicine and The UMass Memorial Medical Center Heart and Vascular Center of Excellence announce a major investment in Cardiovascular Research. We are seeking candidates at the Assistant, Associate, and Full Professor levels for faculty positions that will involve substantial independent research in a newly renovated, state-of-the-art facility. Successful candidates will be expected to either establish or expand an independently funded research program and contribute to the clinical and/or education missions of UMass Medical Center. Successful applicants will have demonstrated expertise in research relevant to cardiovascular disease, a record of high-quality publication, and possess either an M.D or Ph.D. degree. Salary, start-up funds, and space will be commensurate with experience and academic achievement.

Please submit a cover letter, CV, and three references to:

John F. Keaney, Jr., MD
Chief of Cardiovascular Medicine
UMass Memorial Medical Center
55 Lake Avenue North, Room S3-866
Worcester, MA, 01655
or by email to ChaseL@umhc.org

*The University of Massachusetts and UMass
Memorial Healthcare are
Equal Opportunity Employers.*

Buck Institute for Age Research

The Buck Institute brings together scientists from multiple disciplines in innovative research programs concerned with two fundamental issues:

1. The Nature of the Aging Process
2. The Development of Age-Associated Disease

As the nation's only independent research facility focused solely on these topics, the Buck Institute supports a highly collaborative research environment. The National Institute on Aging has designated the Buck Institute as a "Nathan Shock Center of Excellence in the Basic Biology of Aging," one of five in the U.S.

Faculty Positions – Areas of Focus Processes of Aging

Mechanisms of normal aging including lifespan determination, cell aging and cell fate. Genetic, biochemical and physiological mechanisms. Evolution of aging and population genetic and biodemographic approaches.

Research Focus Code F-PA

Diseases of Aging

Mechanisms involved in age-related diseases and therapeutic interventions in areas such as neurodegenerative and cerebrovascular disease, cancer, diabetes or other metabolic disorders, osteoporosis, arthritis, and cardiovascular disease utilizing either in vitro or in vivo invertebrate or vertebrate model systems.

Research Focus Code F-DA

Technological Approaches

State-of-the-art methodological approaches to biological problems relevant to aging or age-related disease. Target areas include computational biology, structural biophysics, mass spectrometry, chemistry, cell biology and bioenergetics.

Research Focus Code F-TEC

Interested Applicants must hold a PhD and/or MD degree and should submit their curriculum vitae, a statement of research interests and the names of three references to: **Faculty Search Committee, Buck Institute for Age Research, Human Resources, 8001 Redwood Blvd., Novato, CA, 94945** or by email to HR@buckinstitute.org

Indicate **Research Focus Code** on CV, cover letter or email. No phone calls please. Review of applications will begin on **July 15, 2007** and continue until the positions are filled. *The Buck Institute is an Affirmative Action, Equal Opportunity Employer. Women and minorities are especially encouraged to apply.*

www.buckinstitute.org

You got
the offer
you always
dreamed of.
Now what?

www.sciencecareers.org

ScienceCareers.org

We know science





THE NOVO NORDISK FOUNDATION CENTER FOR PROTEIN RESEARCH



Are you the next to join us ?

"With a donation of DKK 600 million from the Novo Nordisk Foundation we will build a new centre for protein research – profiling Denmark's capital as a global hot spot for Health Science" says the Dean of the Faculty of Health Sciences, Professor Ulla Wewer.

"The Novo Nordisk Foundation Center for Protein Research" opens by the fall 2008 and will have a staff of about 100 constituting 5 internationally strong and frontline research groups. A particular attraction is the Center's core facility, where researchers can have proteins designed, produced and purified.

The managing director will be Michael Sundström, who will also be in charge of the core facility

Two of the research teams will be headed by two international leading and highly profiled researchers, Professor Matthias Mann who will focus on MS-based proteomics in cell signalling, differentiation and disease and Professor Søren Brunak who will focus on disease systems biology.

Within the next 1-2 years the Center will be recruiting 3 more excellent PI's focusing on protein research in disease and therapeutics – favourable start up packages will be provided. We will advertise later this year. For more details see our home page:

<http://healthscience.ku.dk/research/proteincenter>

Any questions to the Dean: SUNDdekan@adm.ku.dk

The European Molecular Biology Laboratory (EMBL) is an international research organisation with its Headquarters Laboratory in Heidelberg, Germany and four additional Units in Hinxton (the European Bioinformatics Institute, EBI), Grenoble, Hamburg, and Monterotondo. For our Outstation in Grenoble we have a vacancy for a

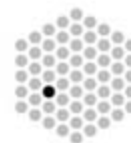
Staff Scientist

New SAXS Beamline at the ESRF at EMBL, France

A scientist is required to join a team within the Partnership for Structural Biology (<http://psb.esrf.fr>) which is establishing a unique and integrated SAXS-SANS platform, making use of the intense synchrotron X-ray and neutron beams of respectively the ERSF and ILL. The successful candidate will be responsible for construction, commissioning and user support of a new state-of-the-art SAXS beamline, dedicated to biology, to be built on undulator beamline ID14-EH3 at the ESRF. The beamline will cater to the growing needs of the European structural biology community who wish to combine SAXS studies with crystallography and other techniques. He/She will benefit from strong technical support from the ESRF MX and Soft Condensed Matter groups and other ESRF services as well as the EMBL Grenoble diffraction instrumentation group. In addition there will be a strong collaboration with the SAXS scientists from the EMBL Hamburg Outstation both to transfer expertise and to provide test facilities during the conception and construction phase of the future SAXS beamline at Petra III in Hamburg.

Applicants are expected to hold a PhD in a related specialisation and have postdoctoral experience in instrumentation and software for small-angle scattering in physics, chemistry or biology, preferably at a synchrotron. At least some knowledge of, and demonstrable interest in, biology is required. Candidates must demonstrate organisational and communication skills, as well as the ability to work in a complex, international environment. Finally, the incumbent will be strong in the use of computers (MS Office) and fluent in English, and will preferably speak basic French or better.

EMBL



EMBL is an inclusive, equal opportunity employer offering attractive conditions and benefits appropriate to an international research organisation.

To apply, please send an English CV (including names and addresses of referees) and covering letter, by email, quoting ref. no. S/07/069 in the subject line, to: application@embl.de

www.embl.org



Cancer Immunology or Immunotherapy (Assistant Professor/Associate Professor/Professor)

Rochester, Minnesota

The Mayo Clinic Comprehensive Cancer Center seeks two independent, cancer immunology and/or immunotherapy investigators to develop internationally competitive and extramurally funded research programs on the Rochester, MN campus. The Immunology/Immunotherapy Program of the Cancer Center includes 34 independent investigators, conducting basic discovery and translational research relating to the immunology of cancer and cancer therapy on the Rochester, Arizona, and Jacksonville campuses. We are seeking colleagues who share our commitment to advance basic understanding of immunobiology and to translate these advances into novel treatments of cancer. Investigators focusing on the biology of reconstitution of the immune system or the use of system biology strategies for the evaluation of the human immune responses are particularly encouraged to apply. Very competitive levels of start-up and sustained intramural funding will be provided to support these new research programs.

To learn more about the Mayo Clinic Comprehensive Cancer Center, Mayo Clinic, and Rochester, MN, please visit www.mayoclinic.org, www.mayo.edu, and <http://cancercenter.mayo.edu/>

Applicants should send their curriculum vitae, a description of research focus, and the names of five references to:

Larry R. Pease, Ph.D.

Professor and Chair, Department of Immunology, Mayo Clinic College of Medicine and Co-Director, Immunology and Immunotherapy Program, Mayo Clinic Comprehensive Cancer Center

Mayo Clinic

200 1st Street SW, Rochester, MN 55905

Mayo Foundation is an affirmative action and equal opportunity educator and employer. Post offer/pre-employment drug screening is required.



YALE UNIVERSITY
School of Forestry & Environmental Studies
School of Architecture

Junior Faculty Position in Sustainable Design and Development

Yale University's School of Forestry & Environmental Studies and School of Architecture seek applicants for an unprecedented joint ladder level Assistant Professorship in Sustainable Design and Development, with an emphasis on the urban environment. More specifically, we seek individuals who have expertise, or the potential to establish this expertise, in the management and design of urban environmental systems and urban ecological infrastructures with a focus on the neighborhood and community scale rather than the building and site scale. Candidates should not only demonstrate an interest in minimizing adverse environmental impacts of urban development but also in enhancing beneficial human connections to natural systems in urban areas. The successful candidate will be expected to advise, supervise and instruct both environmental studies and architecture students, offering lecture, seminar and/or project-based courses in areas such as sustainable design and development, urban design, urban ecology, landscape ecology and design, and restoration of urban environmental systems. This person will be expected to assume a leadership role in the recently established School of Forestry & Environmental Studies and School of Architecture joint Master's Degree program. We prefer a candidate with advanced training in any of the following fields: sustainable design and development, urban design, landscape ecology and design, urban ecology, architecture, or allied fields.

Applicants should send a curriculum vitae; statement of research, teaching, and/or professional practice interests; two representative examples of research or professional publications and/or design work; and a list of three references to: **Professor Stephen R. Kellert, Yale University, School of Forestry & Environmental Studies, 205 Prospect Street, New Haven, CT 06511, USA.** and **Professor James Axley, Yale University, School of Architecture, 180 York Street, New Haven, CT 06511, USA.** The deadline for applications is **July 15, 2007.**

*Yale University is an Affirmative Action/Equal Opportunity Employer.
Men and women of diverse racial/ethnic backgrounds and cultures
are encouraged to apply.*



Chief, Endocrinology and Director, of the Diabetes Center

The Department of Medicine at Case Western Reserve University School of Medicine and University Hospitals Case Medical Center is seeking applicants for Chief, Division of Endocrinology and Director of the Diabetes and Obesity Center. The Division has 15 full-time faculty members providing patient care at University Hospitals Case Medical Center, the Cleveland Wade Park Veterans Administration Hospital, and outpatient satellite centers. The Division has current, robust basic, translational and clinical research programs. Its educational program includes University Hospitals Case Medical Center and the Wade Park Veterans Administration Hospital, with 5 fellows. The successful candidate will have an outstanding record of scholarly achievements, sustained extramural research funding, along with proven leadership, mentoring and administrative abilities. He/she should qualify for the rank of Professor with tenure at Case. A strong commitment to continuing to lead the Division in national prominence through building interdisciplinary programs as Diabetes and Obesity Center Director is expected.

Interested candidates should submit their curriculum vitae and a letter describing their research, teaching, service and administrative experience to: **Robert A. Salata, MD, Chair, Endocrinology Division and Director of the Diabetes and Obesity Center Search Committee, Chief, Infectious Diseases, Department of Medicine, Case Western Reserve University, University Hospitals Case Medical Center, 11100 Euclid Ave., Cleveland, OH, 44106-5083.** Electronic format preferred to: robert.salata@case.edu.

Case Western Reserve University/University Hospitals Case Medical Center are Equal Opportunity/Affirmative Action Employers.



International Max Planck Research School PhD Program in Structure and Function of Biological Membranes

**Max Planck Institute of Biophysics
Max Planck Institute of Brain Research
Goethe University
Frankfurt am Main, Germany**

Several PhD fellowships are available in the International Max Planck Research School in Frankfurt. The two Max Planck Institutes and research groups at Frankfurt University offer a unique environment for the study of biological membranes and membrane proteins. PhD opportunities exist in internationally leading laboratories in the areas of membrane protein structure determination, membrane biochemistry, molecular biology, and functional studies by electrophysiological and spectroscopic methods, computational biophysics and structural bioinformatics, as well as studies of whole membranes, cells and organelles.

Highly qualified candidates with degrees in biochemistry, chemistry, physics, biology, medicine or related subjects are invited to apply for the next round of admission in November 2007. Application forms can be downloaded from the website of the Research School at www.mpibp-frankfurt.mpg.de/research-school. Completed application forms and two letters of reference should arrive no later than **31 July 2007.**

For further details please contact:

Dr. Janet Vonck

MPI of Biophysics

Max-von-Laue-Str. 3

D-60438 Frankfurt am Main

Germany

Tel. +49 (0)69-6303-3004/3001 Fax: +49 (0)69-6303 3002

E-mail: Research.School@mpibp-frankfurt.mpg.de

Inserm hosting
European Research Council
laureates

Inserm

Institut national
de la santé et de la recherche médicale

In the frame of the ERC's Starting and Advanced grants of the FP7 of the European union, Inserm, the only French biomedical research organization, offers an attractive and stimulating environment including:

- attractive salary (up to € 7,000 monthly) with a potential tenure career track;
- research centers with critical mass and multidisciplinary dimension for innovative research, in close relationship with university hospitals;
- full range of performing research infrastructures to support leading edge research activities;
- strong partnerships with both French academic and industrial partners providing fruitful interfaces;
- a tradition of innovation and technology transfer with the support of its private subsidiary Inserm Transfert;
- a strong experience in European and international projects, including recognized know-how in administrative and financial management.

For more information about Inserm for your ERC submission, please contact:

- Department of Regional and European Strategic policies:
philippe.arhets@tolbiac.inserm.fr
- Department of Human Resources:
richard.salives@tolbiac.inserm.fr
- Website of Inserm:
www.inserm.fr/en/inserm

**Imperial College
London**

100 years of living science

100

Division of Cell & Molecular Biology

Lecturer/Senior Lecturer in Bacterial Infection

Lecturer £37,740 to £42,150

Senior Lecturer Starting Salary £46,560

We are seeking to strengthen our portfolio in bacterial infection by making an academic appointment at Lecturer/Senior Lecturer level to join the Centre for Molecular Microbiology & Infection (CMMI; <http://www3.imperial.ac.uk/cmmi>) within the Division of Cell & Molecular Biology <http://www3.imperial.ac.uk/lifesciences/divisions/cellandmolecularbiology>

You should have a strong publication record and have demonstrable ability/potential to direct a competitive independent research programme in any field of bacterial infection. This should ideally complement and enhance our existing activities in bacterial pathogenesis, secretion and virulence, regulation of gene expression, toxins, biofilms and imaging of infection. You would also contribute to our undergraduate teaching programme.

Biological Sciences at Imperial College was graded 5* in the 2001 RAE exercise, and the South Kensington Campus has newly refurbished laboratories with access to state of the art facilities for modern biological research. Further details and an application form can be obtained from the college employment website:

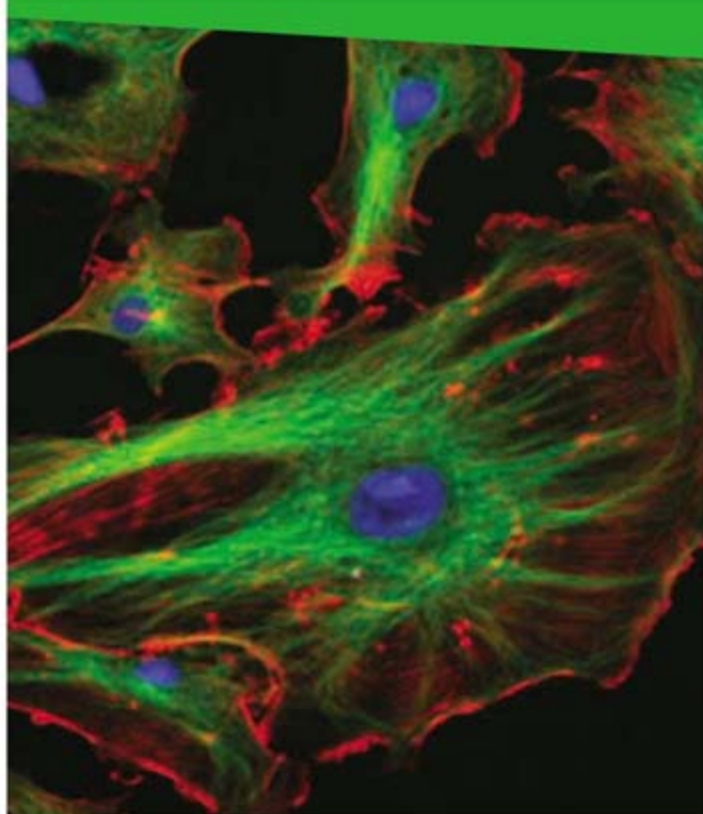
<http://www3.imperial.ac.uk/employment/academic>

Candidates should submit the completed application form with a curriculum vitae, statement of research interests and names and addresses of three referees to Patricia Evans, Division of Cell & Molecular Biology, Biochemistry building, Imperial College London, London, SW7 2AZ (pat.evans@imperial.ac.uk). Informal enquiries can be made to Prof. Gadi Frankel (g.frankel@imperial.ac.uk), Prof. Alain Filloux (filloux@ibsm.cnrs-mrs.fr) or Prof. Murray Selkirk (m.selkirk@imperial.ac.uk).

Closing date: 6 July 2007.

Valuing diversity and committed to equality of opportunity

LIFE SCIENCE TECHNOLOGIES



If it's the **latest technologies** and **newest reagents** you're after, don't miss the life science technology features in *Science*.

UPCOMING FEATURES:

June 22 – Cell Signaling 2

August 24 – Microarray Technologies

October 19 – Genomics 2



Teaching Assistant Professor Positions in Genetics, Cell Biology, and Development

The Department of Genetics, Cell Biology and Development at the College of Biological Sciences (CBS) at the University of Minnesota - Twin Cities invites applications for two new Teaching Assistant Professor positions. CBS is committed to excellence in undergraduate education and the successful applicants will join a dynamic team whose primary focus is quality instruction and the scholarship of teaching and learning in the biological sciences. These are regular positions that emphasize teaching, course development, and scholarship associated with college teaching. The successful applicants will teach genetics and other courses, work with a team of colleagues to develop innovative methods for undergraduate instruction, and engage in research and publication related to teaching and curriculum development. Opportunities also exist for conducting bench research in collaboration with existing laboratories in the department. Both positions involve teaching a genetics laboratory course, as well as upper division genetics lecture-based courses. One position also emphasizes cell biology and the other emphasizes developmental biology. This latter position involves the design and implementation of a developmental biology laboratory. Essential qualifications for both positions include a Ph.D. in the biological sciences, or a related discipline, and at least two years of post-doctoral experience.

A significant background in undergraduate teaching is required, with strong oral and written communication skills, a clear interest in teaching and the scientific study of teaching, and the ability to work as part of a team to develop course content. For more information about the department and the College of Biological Sciences, go to <http://www.gcd.med.umn.edu/> and <http://www.cbs.umn.edu>.

Please apply on-line at: <https://employment.umn.edu> and search for Job Requisition #148390. Attach a cover letter, curriculum vitae, three letters of recommendation, and a statement of your teaching philosophy. Review of completed applications will begin on **October 15, 2007** and will continue until the positions are filled. We welcome applications from women and under-represented groups in the biological sciences. Preferred starting date: June 1, 2008 (beginning of 2008 Summer Semester).

*The University of Minnesota is an Equal Opportunity
Educator and Employer.*

Faculty Position Mitochondrial Biology Interdisciplinary Age Research

The Buck Institute seeks to recruit a Faculty member working in the area of Mitochondrial Biology and/or Function. Outstanding junior or senior scientists are encouraged to apply. The appointment can be made at the Assistant/Associate or Full Professor level. Candidates with an interest in Mitochondrial Physiology and those using imaging approaches are particularly encouraged to apply. The successful candidate will play a leadership role in developing collaborative interdisciplinary programs with other Institute Faculty in areas including, but not limited to, the biology of aging, cancer and neurodegenerative disease. Research in these areas is supported by advanced technology cores, including a state-of-the-art imaging facility equipped with fluorescence, two-photon confocal and electron microscopy. The Buck Institute is an independent research institute located 20 miles north of San Francisco whose research mission is to understand the mechanisms of aging and age-related disease. The Institute fosters an interdisciplinary and highly collaborative research environment, with expertise in chemistry, biology, proteomics, stem cells and genetics of model systems.

Research Focus Code F-MITP

Interested Applicants must hold a PhD and/or MD degree and should submit their curriculum vitae, a statement of research interests and the names of three references to: **Faculty Search Committee/Mitochondrial Biology, Buck Institute for Age Research, Human Resources, 8001 Redwood Blvd., Novato, CA, 94945** or by email to HR@buckinstitute.org

Indicate Research Focus Code on CV, cover letter or email. No phone calls please. Review of applications will begin on **July 15, 2007** and continue until the positions are filled.

*The Buck Institute is an Affirmative Action, Equal Opportunity
Employer. Women and minorities are especially encouraged to apply.*

www.buckinstitute.org

PHARMACOGENETICS / PHARMACOGENOMICS

The Wadsworth Center is launching a broad new initiative in Pharmacogenomics as part of a multi-institutional research effort to develop pharmacogenomics in the Albany, NY region. Wadsworth Center invites applications from associate or full professor level scientists for a New York State-supported, tenure-track position in Pharmacogenomics. The successful candidate will expand his or her current grant-funded research program in any areas of this developing field, including genome-wide and/or mechanistic studies, with examples being studies on drug transporters and metabolizing enzymes. The candidate will have an opportunity to mentor graduate students through the School of Public Health, University at Albany. The Wadsworth Center provides a rich collaborative environment for pharmacogenomics research, focused on molecular, cellular, and genetic aspects of disease and their impact on human health. A competitive package of salary, benefits, and start-up funds is available.

Wadsworth Center enjoys a century of excellence as a research-intensive institution and is the country's most comprehensive state public health laboratory. With 200 doctoral level scientists, and an array of outstanding core facilities, Wadsworth provides a dynamic research environment. Its location in Albany, NY, offers a wide range of cultural and recreational attractions and proximity to New York City, Boston, and Montreal.

A CV and statement of research interests and future plans should be sent to kaminsky@wadsworth.org by August 1, 2007. AA/EOE

Wadsworth Center

New York State Department of Health

www.wadsworth.org Science in the Pursuit of Health®

2005 Best Places to Work in Academia • 2006 Best Places to Work for Postdocs

Scientific Officers

The **Howard Hughes Medical Institute (HHMI)**, a national and international philanthropy devoted to biomedical research, is seeking a Scientific Officer (or Senior Scientific Officer) at our headquarters in Chevy Chase, MD. Scientific Officers have administrative responsibility for activities associated with HHMI's medical research operations at over 60 institutions across the country. These activities include participating in the management of HHMI's investigator competitions, investigator reviews, and science meetings and workshops.

The Scientific Officer (or Senior Scientific Officer) must possess a Ph.D. and/or M.D. plus at least 10 years research experience in the life sciences or the physical sciences, including experience as a principal investigator of grants, a record of publications in peer-reviewed journals, and some administrative experience. Travel to host institutions is required.

HHMI is an intellectually exciting organization with excellent salaries and benefits. Interested candidates should send curriculum vitae and bibliography, a brief statement of scientific experience and accomplishments **prior to August 15th**, either electronically to glotfelt@hhmi.org or by mail, to:

Jack E. Dixon, Ph.D.

Vice President and Chief Scientific Officer

Howard Hughes Medical Institute

4000 Jones Bridge Road

Chevy Chase, MD 20815-6789

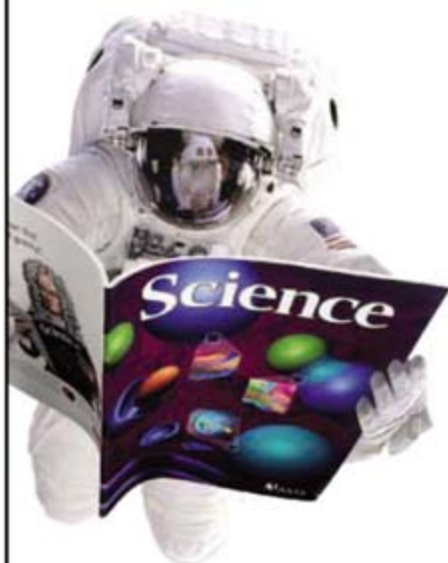
The Howard Hughes Medical Institute is an Equal Opportunity Employer.

HHMI

HOWARD HUGHES MEDICAL INSTITUTE

From
life on Mars
to life sciences

For careers in science,
turn to *Science*



www.ScienceCareers.org

- Search Jobs
- Career Advice
- Job Alerts
- Resume/CV Database
- Career Forum
- Graduate Programs

All of these features
are **FREE** to job seekers.

ScienceCareers.org

We know science



What's your next career move?

Get help
from the
experts.

www.sciencecareers.org

- Job Postings
- Job Alerts
- Resume/CV Database
- Career Advice from Next Wave
- Career Forum
- Graduate Programs
- Meetings and Announcements

ScienceCareers.org

We know science



POSITIONS OPEN

A **POSTDOCTORAL POSITION** is available to study endocytosis and intracellular trafficking of the dopamine transporter. Research will involve various methodological approaches including generation of transgenic mouse models and viral gene transfer into cultured neurons and brain slices. Candidates with training in molecular biology and experience or interest in neuroscience are welcome. Please send curriculum vitae and names of references to: **Alexander Sorkin, Department of Pharmacology, University of Colorado at Denver and Health Sciences Center, Aurora, CO 80045; e-mail: alexander.sorkin@uchsc.edu.** *The University of Colorado is committed to diversity and equality in education and employment.*

POSTDOCTORAL POSITION in CELLULAR IMAGING

We study propagating depolarizations and associated neuronal and astroglial damage during stroke and traumatic brain injury. Experience in whole-cell patch clamp recordings is required. Familiarity with two-photon microscopy, live imaging, models of stroke and traumatic brain injury are a plus. Send application materials to **Dr. Sergei A. Kirov, e-mail: skirov@mcg.edu, Medical College of Georgia.** Details, website: www.mcg.edu/Jobs for position #6128. *Equal Employment Opportunity/Affirmative Action/Equal Access Employer.*

STAFF ASSOCIATE (New York, New York). Research and study of recombinant protein expression, purification, and characterization using optical spectroscopy and study of protein folding employing solution state high resolution nuclear magnetic resonance spectroscopy. Required: Master's in chemistry or biochemistry and one year experience in job. Send resume to: **Jeanie Huang, Human Resources Department, Weill Cornell Medical College, 1300 York Avenue, Olin 211, New York, NY 10021**

MARKETPLACE

science symmetry sculpture



www.bathsheba.com

Widely Recognized Original & Guaranteed	KlenTaq1	8¢/u Truncated Taq DNA Polymerase Withstand 99°C
US Pat #5,436,149 Call: Ab Peptides Fax: 314•968•8988	e-mail: abpeps@msn.com 1•800•383•3362 www.abpeps.com	

EZBiolab www.ezbiolab.com

Custom Peptide 10mg 90%: \$19.59/aa
AB Production \$785 peptide included
Gene Synthesis \$1.20/bp
siRNA 20 nmol PAGE purified: \$285

Oligo Synthesis Columns

↳ Columns For All Synthesizers

↳ Standard and Specialty CPGs

↳ Bulk Column Pricing Available

**BIOSEARCH
TECHNOLOGIES**
Advancing Nucleic Acid Technology™

+1.800.GENOME.1
www.bticolumns.com

HotStart-IT™

Less Heat. No DNA Damage. We couldn't be more specific.

USB's novel hot start PCR method requires no extensive heat denaturation step. The result is no damage to precious samples with increased specificity and yield. HotStart-IT™: highly sensitive to all your critical PCR applications.

HotStart-IT™ Taq DNA Polymerase

- Based on primer sequestration—a novel method developed by USB scientists
- Unique protein binds primers to prevent mispriming
- Primers are released during heat denaturation

Benefits

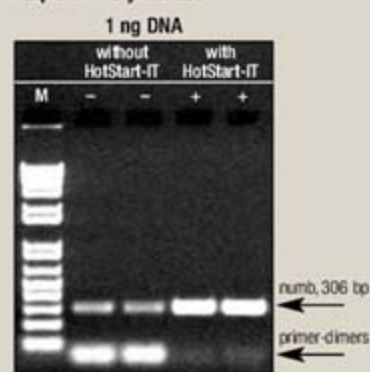
High Sensitivity

- Detects <10 target copies
- Linear dynamic range of 7–8 orders of magnitude, $R^2 \geq 0.95$

Ease of Use

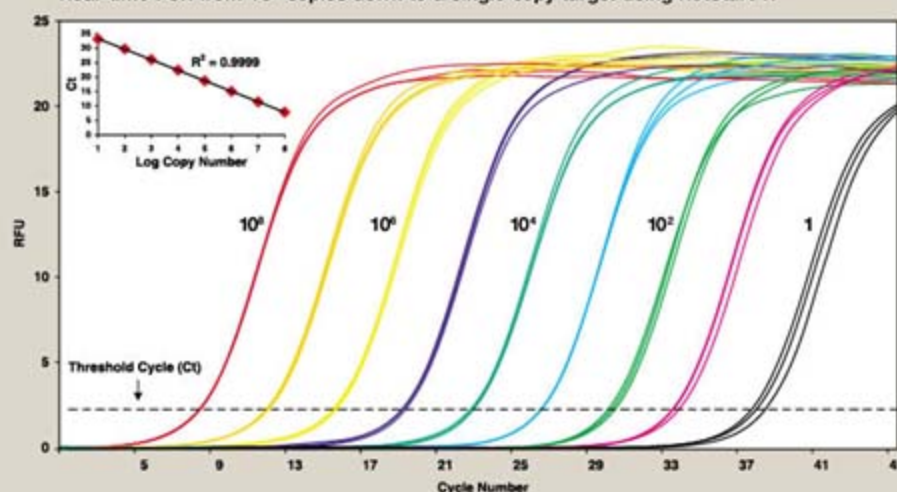
- Multiple instrument compatibility

Increased specificity of HotStart-IT™ Taq DNA Polymerase



Results clearly demonstrate a shift from predominantly primer-dimers to the specific target when HotStart-IT™ is included in the reactions.

Real-time PCR from 10^8 copies down to a single copy target using HotStart-IT™



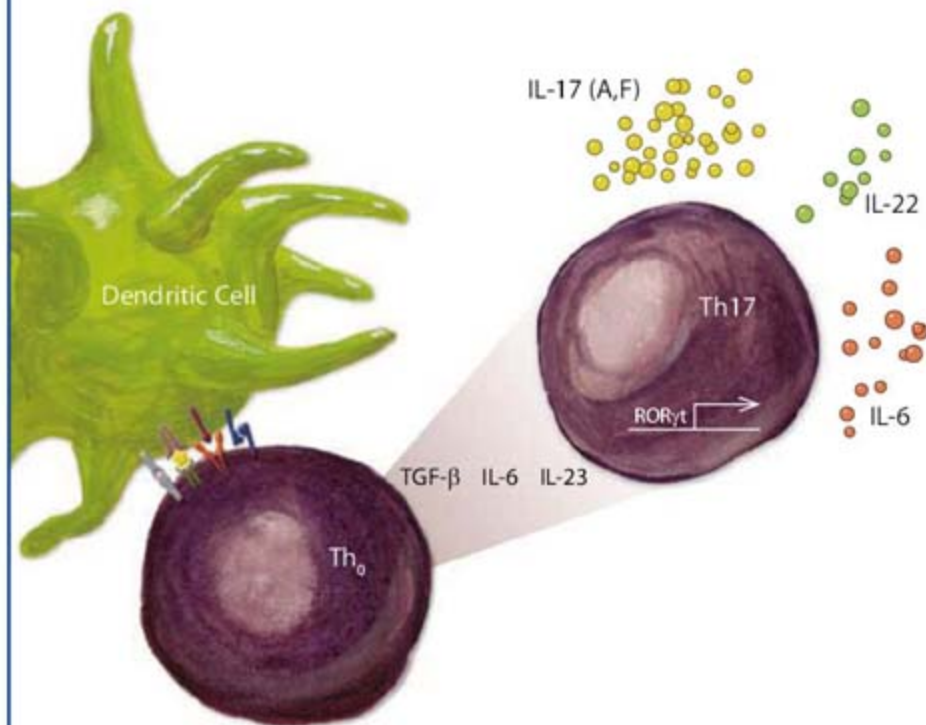
For more information on HotStart-IT™
call 800.321.9322 or visit www.usbweb.com/hotstart
In Europe: +49(0)76 33-933 40 0 or visit www.usbweb.de/hotstart

 **usb**
Fueling Innovation
in Life Science

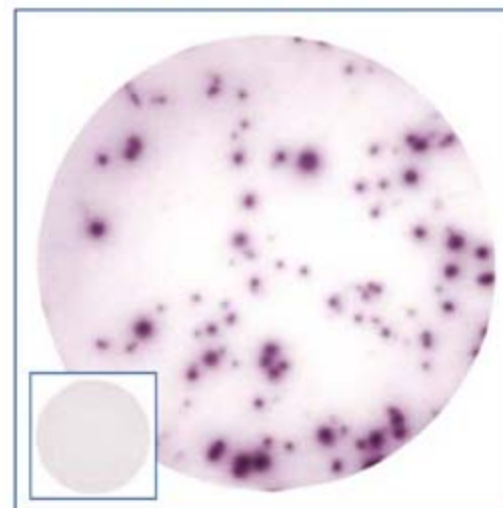
R&D Systems Immunology Reagents

Offering a complete line of Th17-related research tools.

R&D Systems specializes in providing the highest quality reagents for assessing immune system function. These include a wide selection of tools for studying apoptosis, autoimmunity, complement/coagulation pathways, co-stimulation, hematopoiesis, innate/adaptive immunity, infectious diseases, inflammation, & much more.



ELISpot Detection of IL-17-producing Splenocytes



Mouse splenocytes (10^5 cells per well) were cultured in the absence (inset) or presence of PMA and a calcium ionophore. The frequency of IL-17 producing cells was measured with the mouse IL-17 ELISpot Kit (Catalog # EL421).

Th17-RELATED PRODUCTS

Molecule	Antibodies	Proteins	ELISAs/ Assays
CTLA-4	H M	H M	
EDG-1	H		
IL-6	H M R Ca C R E F P	H M R Ca C R E F P	H M R Ca P
IL-17	H M	H M	H M
IL-17 R	H M	H M	
IL-17 F	H M	H M	H M
IL-17 RC	H M	H M	
IL-22	H M	H M R	H M R

Molecule	Antibodies	Proteins	ELISAs/ Assays
IL-22 R	H	H	
IL-23	H M	H M R	
IL-23 R	H M	H M	
IL-27	H M	H M	M
ROR γ	H		
STAT3	H M R		
TGF- β 1	H	H M P	H M R Ca P
TRAF6	H		

Key: Ca Canine CR Cotton Rat E Equine F Feline H Human M Mouse P Porcine R Rat

For a complete listing of immunology-related products visit our website at www.RnDSystems.com/go/Immunology

Tools for Cell Biology Research™



Selection expanding weekly—visit www.RnDSystems.com to sign up for weekly new product updates.

USA & Canada R&D Systems, Inc. Tel: (800) 343-7475 info@RnDSystems.com

Europe R&D Systems Europe, Ltd. Tel: +44 (0)1235 529449 info@RnDSystems.co.uk

For research use only. Not for use in diagnostic procedures.



R&D
SYSTEMS®